

1 **Development of a multi-disciplinary**
2 **toolkit to study time cells in the**
3 **hippocampus**
4

5 A Thesis
6

7 Submitted to the
8 Tata Institute of Fundamental Research,
9 Mumbai
10 for the degree of Doctor of Philosophy
11 in (subject)

12
13 by
14 Kambadur Gundu Ananthamurthy
15
16

17 Tata Institute of Fundamental Research
18 Mumbai
19 [July, 2023]
20 [Final Version Submitted in Month, Year]

22

DECLARATION

23

24 This thesis is a presentation of my original research work.
25 Wherever contributions of others are involved, every effort is
26 made to indicate this clearly, with due reference to the
27 literature, and acknowledgment of collaborative research and
28 discussions.

29

30 The work was done under the guidance of Professor Upinder
31 S. Bhalla, at the Tata Institute of Fundamental Research,
32 Mumbai.

33



Kambadur Gundu Ananthamurthy

35

36 In my capacity as supervisor of the candidate's thesis, I certify
37 that the above statements are true to the best of my
38 knowledge.

39



Prof. Upinder S. Bhalla

41 Date: 24th July, 2023

42 Acknowledgments

43

44 Projects like the ones described in this thesis cannot be accomplished
45 without good, strong leadership. I thank Upi for the opportunity to learn
46 and grow in his lab, and his patience to see me through tough
47 moments.

48 I thank Shona and Mukund for advice and help over the past decade.
49 I thank my seniors Mehrab, Ashesh, Partha, and Subha. I hope I can
50 make them proud, someday.

51 I thank my colleagues Sahil, Dilawar, Oliver, and Aditya for helping me
52 whenever I asked.

53 I thank Sriram, Manoj, Krishna, and Amit for everything I learnt in CIFF.
54 I thank Mohini, Mugdha, Sebastien, Arnab, and Terence, for being my
55 friends for as long as they could.

56 I thank Supriya, Harini, Anupratap, Sohail, and Prabahan, my well-
57 wishers from Shona lab.

58 I thank KS Krishnan for help and advice, in the early days of the
59 programme. His absence cannot be filled with anything else.

60 I thank Sanjay, Axel, Panic, Vatsala, Uma, Madan, and Jitu, for always
61 bringing a breath of inspiration to my life and my work.

62 I thank Dr. Shane Heiney for showing me the way with trace eye-blink
63 conditioning, and Dr. Daniel Dombeck for the chronic hippocampus
64 preparation.

65 I'm indebted to the Animal Care and Resource Center (ACRC), the
66 Central Imaging and Flow Facility (CIFF), Dorababu & the Electronics
67 Workshop, Devakumar & the Mechanical Workshop, for anything and
68 everything I have been able to make or create.

69 I thank Swarna and Nikhila for teaching me Tennis. I also thank the
70 Football group, the Badminton group, the Music group, the Theater
71 group, and the Improv group, for always giving me a chance to
72 explore.

73 I thank Neha Panwar for being there in the end.

74 "Very little" is what I'd have achieved without my parents. I hope to be
75 a good person and live up to the values they have taught me.
76 I thank the canteen, the sports facility and gym, hospitality,
77 instrumentation, and admin, for helping me with everything else.

78

for Archana && Bujju,

Index of Tables

79	Table 1: Summary table of behaviour protocols attempted and essential results.....	105
82	Table 2: Recipe for ready-to-use cortex buffer. The buffer is typically prepared and stored in aliquots to be used each week. The correct pH range of the buffer was often a crucial factor ensuring the success of the hippocampal preparation.....	115

Table of Figures

87	Figure 1: A schematic representation of the Trisynaptic Pathway as observed with coronal slices, along the longitudinal axis of the hippocampus. Image adapted from the webpage for the Neural Circuits and Memory Lab, University of Wisconsin (Milwaukee) [https://sites.lsa.umich.edu/diba-lab/neural-circuits-of-the-hippocampus/]	31
93	Figure 2: Water delivery calibration to reward the animal consistently with the same volume of water.....	72
95	Figure 3: Optoisolator circuit to amplify +5V DC input to +12V DC output	74
97	Figure 4: Lick detector circuit based on a MOSFET design. Whenever the animal performed a lick, a +5V DC Output would be read out.....	75
99	Figure 5: Typical trial structure with the various phases. Each trial was followed by a randomized Inter-Trial Interval (ITI).....	77
101	Figure 6: Performance evaluation for two example mice trained to Protocol 1.1 and 1.2. Percentage of total licks in the various trial phases (Pre-Tone, Tone, CT, and ITI), across all sessions of training (coloured bar plots) for A) Mouse 3, and B) Mouse	78
105	Figure 7: Performance evaluation for two example mice trained to Protocol 2. Percentage of total licks in the various trial phases (Pre-Tone, Tone, CT, and ITI), across all sessions of training (coloured bar plots), for (A) Mouse S1, and (B) Mouse S2	82
109	Figure 8: Schematic representation of the experimental setup for a simple detection task where the animal must perform a lick upon correctly detecting the presence of the conditioned stimulus (CS; from a range of modalities).....	85
113	Figure 9: Typical trial structure with the various phases and lick dependent relationships.....	86
115	Figure 10: (A) Performance traces for all the animals individually shown in dashed grey lines. Mean + SEM in black. (B) Mean Performance (%) and Mean Go Tone Lick Percentage (%) with Session for the Go/No-Go Task, plotted in black and green,	

119	respectively.	87
120	Figure 11: The number of licks in the pre-tone (blue), no-go tone (red),	
121	and go tone (green) phases, in a representative animal, in a session	
122	with maximum Performance (%).	88
123	Figure 12: Schematic representation to showcase the two main	
124	subtypes of Classical Conditioning (Eye-Blink Conditioning, for our	
125	experiments) based on the relative timing and presentation of the CS	
126	and US.	91
127	Figure 13: Trial-by-trial (left) and trial-averaged running speed (right)	
128	for two example animals, (A) M2 Session 12, and (B) M5 Session 12.	
129	94
130	Figure 14: Schematic representation of (A) the behaviour rig with 2-	
131	Photon imaging, to train head-fixed mice on a Trace Eye-Blink	
132	Conditioning (TEC) task, and (B) relative time intervals between the	
133	CS and US.	96
134	Figure 15: A picture of a head-fixed mouse clamped on the behaviour	
135	rig, with key components: 1) Red LED Illumination, 2) Blue LED CS, 3)	
136	Air-puff port directed to the left eye, and 4) Height-adjustable Treadmill.	
137	97
138	Figure 16: Steps from behaviour video frame to Fraction of Eye-	
139	Closed (FEC) analysis	98
140	Figure 17: Conditioned Responses (CRs) are small amplitude eye-	
141	blinks triggered by the CS, and develop with multiple training sessions,	
142	while Unconditioned Responses (URs) are large eye-blanks to the US,	
143	typically consistent across sessions. (A,B) Trial-by-trial FEC traces for	
144	M11 (A) Session 2, and (B) Session 4. (C,D) Trial-averaged FEC	
145	traces for M11 (C) Session 2, and (D) Session 4, with paired (red) and	
146	probe (green) trials.	100
147	Figure 18: Performance in terms of the percentage of Hit Trials to total	
148	trials across sessions, including an ISI switch from 250 ms to 350 ms.	
149	Here, M2 is a strong learner (>60% hit trials/session) and M5 is a weak	
150	learner (30-60 % hit trials/session). M1, M3, and M4 did not learn the	
151	task.....	101
152	Figure 19: Conditioned Responses (CRs) are preserved for previously	
153	learnt ISIs, and switching the ISI to longer intervals results in Complex	
154	(multi-CR) eye-blink responses. (A,B) Trial-by-trial FEC scores for (A)	
155	250 ms ISI (left) and (B) 500 ms ISI. (C,D) Trial-averaged FEC traces	
156	for (C) 250 ms ISI, and (D) 500 ms ISI, with paired (red) and probe	
157	(green) trials.	102
158	Figure 20: Conditioned Response (CR) onset timing is maintained	
159	across ISI switches. Representative examples from a short ISI switch	
160	from (A) 250 ms to (B) 350 ms (right).	103
161	Figure 21: Bar plots for Conditioned Response (CR) onset across	

162	multiple sessions of training after ISI switch from 250 ms to 350 ms,	
163	irrespective of how strongly the animals learnt the task. (A) red, strong	
164	learner, and (B) blue, weak learner.....	103
165	Figure 22: Representative example of mice trained to 550 ms ISI	
166	(Session 6) and 750 ms (Session 4). (A,B) Trial-by-trial FEC responses	
167	for (A) 550 ms ISI (M17 Session 6), and (B) 750 ms ISI (M22 Session	
168	4). (C,D) Trial-averaged FEC responses for (C) 550 ms ISI (M17	
169	Session 6), and (D) 750 ms ISI (M22 Session 4), with paired (red) and	
170	probe trials (green).	104
171	Figure 23: (A) A schematic of the rodent brain, showcasing the two	
172	hippocampi, one in each hemisphere. The hippocampi lie ~1 mm	
173	(mice) below the cortical surface. (B) The hippocampal preparation	
174	allows optical access to the deep lying hippocampal CA1 cells, relative	
175	to the skull/cortex. The CA1 cell bodies arrange in a laminar fashion as	
176	a tight cell body layer that can be visualized by fluorescence (using	
177	either OGB-1 or GCaMP).	112
178	Figure 24: Figure 24: Schematic representation for stereotaxic viral	
179	injection.	117
180	Figure 25: (A) Representative Two-Photon Calcium Image of a plane	
181	of Hippocampal CA1 cells, bolus loaded with Oregon Green Bapta-1	
182	(OGB-1), at an instant in time. Example cells marked out post-hoc as	
183	pink, green, blue and red. Scale bar 20 μ m. (B) Representative dF/F	
184	(%) traces for the calcium activity. Recorded in a single 10s video for	
185	example cells – pink, green, blue, and red. Scale bar 1 sec; 10% dF/F.	
186	120
187	Figure 26: Tissue Degradation over time. Representative Two-Photon	
188	Calcium images of a snapshot in time of the Hippocampal CA1 cell	
189	body layer on (A) Day 1 after the surgery and (B) Day 3, after the	
190	surgery. Scale bar 30 μ m.	122
191	Figure 27: Chronic calcium imaging of the same Hippocampal CA1	
192	cells over weeks. Representative 2-Photon images from (A) Day 20,	
193	and (B) Day 21, after surgery. Landmarks have been marked and were	
194	used to confirm frame registration and identify cells. Scale bar 100 μ m.	
195	123
196	Figure 28: (A) Representative Two-Photon Calcium Image of a plane	
197	of Hippocampal CA1 cells expressing GCaMP6f at an instant in time.	
198	Example cells marked out post-hoc in pink, blue, and green, with no-	
199	cell background in red. Scale bar 20 μ m. (B) Representative dF/F (%)	
200	traces for the calcium activity recorded in a single 10s video for	
201	example cells – pink, blue, and green, with no-cell background in red.	
202	Scale bar 2 sec; 10% dF/F.	124
203	Figure 29: (A) Correlation Coefficients for cell pairs from an example	
204	two-photon recording. (B) Meta-K Means clustering with cell pairs	

205	using the heuristic that within group pairs would be more similar than	
206	between group pairs. In this example, the cells were clustered into two	
207	groups, I (red) and II (yellow). (C) Two-Photon image of the field of	
208	view of cells; same as Figure 25A. (D) Spatial organization of	
209	correlated cell pair groups during spontaneous activity (Modi et al.,	
210	2014).	126
211	Figure 30: (A) Trial-averaged (25 trials) calcium activity from ~100	
212	CA1 cells in trials where a 5000 Hz tone was presented (red bar). (B)	
213	Trial-averaged (18 trials) calcium activity from the same cells in trials	
214	where a 5 LPM air-puff to the ipsilateral whiskers was presented (red	
215	bar). Scale bar 1 sec (black bar).	127
216	Figure 31: (A) Correlation Coefficients for cell pairs from post whisker-	
217	puff stimulation periods. (B) Meta-K Means clustering with cell pairs	
218	using the heuristic that within group pairs would be more similar than	
219	between group pairs. In this example, the cells were clustered into	
220	three groups I (red), II (orange), and III (yellow). (D) No clear spatial	
221	organization of correlated cell pair groups post whisker stimulation.	128
222	Figure 32: (A) Correlation Coefficients for cell pairs from a trial-shuffle	
223	control dataset (B) Meta-K Means clustering revealed that there were	
224	no cell pair groups identified.	129
225	Figure 33: Example Time Cells visualized as event raster plots (A, B,	
226	C), along with the trial-summed activity profiles (D, E, F) suggesting	
227	~50% hit trials, for cells 29 and 72 from Session 1 (session type 5) with	
228	mouse M26, and slightly lower reliability (~25% hit trials) from cell 105.	
229	The Conditioned Stimulus (CS; blue LED) is presented at time 0 ms.	
230	133
231	Figure 34: Example Other Cells visualized as event raster plots (A, B,	
232	C), along with the trial-summed activity profiles (D, E, F) for cells 10,	
233	25, and 120 from Session 1 (session type 5) with mouse M26. The	
234	Conditioned Stimulus (CS; blue LED) is presented at time 0 ms.....	134
235	Figure 35: Event Time Histograms or tuning curves for Identified Time-	
236	Locked Cells with trial-summed peaks in session 4 of training (session	
237	type 5) with mouse M26. (A) Unsorted list of Time cells. (B) Peak-	
238	sorted list of the same cells. Here, 1 bin = 3 frames = ~210 ms	
239	(sampling rate 14.5 Hz without binning; ~5 Hz with binning). As per the	
240	(legacy) session type 5 protocol, the CS (50 ms Blue LED flash) was	
241	presented in frame bin 39, followed by a stimulus-free trace interval	
242	during frame bins 40 and 41, and then the US (50 ms airpuff to	
243	ipsilateral eye) was presented in frame bin 42.....	135
244	Figure 36: Temporal Information (bits) vs Sorted time cell number from	
245	the analytically identified Time Cells in Session 4 (session type 5) with	
246	mouse M26. No clear trend was observed.....	136
247	Figure 37: More time cells observed to attain tuning as training	

248	sessions. Event Time Histograms of the identified set of time cells	
249	between A) Sessions 1 and (B) Session 2, with mouse M26 (session	
250	type 5). 138	
251	Figure 38: Sorted Time Cells form Sequences that develop with	
252	learning. Trial-Averaged calcium activity traces for all recorded cells	
253	across A) Session 1, B) Session 2, and C) Session 4, with mouse M26	
254	(sessiontype 5). Time 0 ms was aligned to the CS. The CS + Trace +	
255	US interval lasted from 0-600 ms, here..... 139	
256	Figure 39: Same/similar tuning across session 1 and session 2 for this	
257	example time cell. Blue Event Time Histograms represent the tuning	
258	curve for the cell for session 1 (date: 20180508) and Red represent the	
259	same but for session 2 (date: 20180509). Pearson's correlation	
260	coefficient between the two session pairs was 0.7011. 140	
261	Figure 40: Three example chronically tracked cell pairs with tuning	
262	peaks arriving earlier with training sessions (rows). Blue Event Time	
263	Histograms represent the tuning curve for any cell for session 1 (date:	
264	20180508) and Red represent the same but for session 2 (date:	
265	20180509). Pearson's correlation coefficient between the session pairs	
266	was 0.6.348, 0.5872 and 0.7027 for A) cell pair 1, B) cell pair 2, and C)	
267	cell pair3, respectively. 141	
268	Figure 41: Example chronically tracked cell pair with de-tuning	
269	between session 1 and 4. Blue Event Time Histograms represent the	
270	tuning curve for the example cell for session 1 (date: 20180508) and	
271	Red represent the same but for session 4 (date: 20180514). Pearson's	
272	correlation coefficient between the two curves was -0.0606. 142	
273	Figure 42: Comparing chronically tracked time cells across sessions	
274	for all matched cell pairs by (A) Correlation Analysis, and (B) Timing of	
275	peaks..... 143	

276 **Table of Contents**

277	DECLARATION 2
278	Acknowledgments 3
279	Index of Tables 6
280	Table of Figures 6
281	Table of Contents 10
282	Abstract 13
283	Chapter 1 – Introduction 15
284	Projects and overall goals 15

285	A toolkit to study time cells: Thesis Objectives	16
286	Engrams associated with Learning and Memory	18
287	Dynamics in the neural code for engrams	20
288	Theories on the function of the hippocampus.....	24
289	A brief introduction to associative learning	27
290	Space and time in the hippocampus	30
291	“Single-cell, multi-trial” vs. “multi-cell, single-trial” approaches in Neuroscience	37
293	Dimensionality reduction in the analysis of physiology.....	39
294	Synthetic benchmarks for pre-hoc development of analytical procedures	40
295	Single-Unit Electrophysiology vs 2-Photon Calcium Imaging to study the	
296	Hippocampus	43
297	Calcium imaging by 2-Photon Microscopy	45
298	Automated ROI detection for large-scale Calcium Imaging datasets	49
299	Short Summaries of the 3 projects.....	50
300	Project I - How do sensory representations transform with learning?.....	50
301	Project II - How does the timing of cellular activity adjust to behavioural task variables?	
302	51
303	Project III - What is the best way to detect and score time-tuned cellular activity?	53
304	Code Availability	54
305	Bibliography	54
306	Chapter 2 – Behaviour.....	68
307	Towards understanding brain activity in a reproducible context.....	68
308	Operant conditioning [Project I]	70
309	Required features	70
310	Water delivery and calibration	72
311	Opto-isolator circuit for solenoid control	72
312	Lick detection circuit.....	74
313	Controlling task details and protocol information.....	75
314	Head-bar implant, Animal Handling, and Water deprivation	76
315	PROTOCOL 1.1: Stimulus Detection Task.....	76
316	PROTOCOL 1.2: Stimulus Detection Task with aversive punishment	77
317	Results – Protocol 1.1 and 1.2	79
318	Protocol 2: Stimulus Detection task with timeout box	79
319	Results – Protocol 2	81
320	Protocol 3: Delayed Non-Match to Sample (DNMS).....	83
321	Results – Protocol 3	84
322	Protocol 4: Go/No-Go Task	84
323	Results – Protocol 4	86

324	Operant conditioning experiments failed to match behavioural requirements.....	89
325	Trace Eye-Blink Conditioning [Project II]	90
326	Tracking eye-blink responses.....	92
327	Treadmill and tracking running speed	93
328	Behaviour rig and protocol control - Software	95
329	Analysis - TEC	98
330	Results - TEC.....	99
331	Bibliography	106
332	Chapter 3 – Imaging.....	108
333	Physiology in the hippocampus	109
334	Methodology – Acute and chronic imaging [Projects I & II]	111
335	Preparation of Cortex Buffer	113
336	Oregon Green Bapta-1 injections for acute imaging.....	115
337	GCaMP and chronic imaging	117
338	Results - Imaging	119
339	2-Photon calcium imaging of hippocampal CA1, <i>in vivo</i>	119
340	Acute Imaging of OGB-1 loaded hippocampal CA1, <i>in vivo</i>	119
341	Chronic imaging of hippocampal CA1 using GCaMP.....	121
342	Spontaneous activity during non-stimulus periods	124
343	Spatial organization of activity correlated cells during spontaneous activity.....	125
344	Stimulus evoked responses	126
345	Spatial organization of activity correlated cells post whisker-puff stimulation.....	128
346	Chronic imaging now possible for weeks with the same mouse	130
347	Preliminary analysis to identify time cells	131
348	Tuning, re-tuning, and de-tuning of time cells across sessions	137
349	Bibliography	145
350	Chapter 4 – Analysis.....	149
351	Chapter 5 – Discussion	155
352	The study of hippocampal CA1 sequences	155
353	Standardizing combined behaviour and recording experiments.....	158
354	Mapping sequences to abstract variables	159
355	Better temporal resolution requires new techniques.....	161
356	Does the brain create or predict?	162
357	Bibliography	164
358	All Bibliography	167

359 **Abstract**

360

361 The mammalian Hippocampus is considered important for the
362 formation of several kinds of memory, one of which is the association
363 between stimuli occurring separately in time. Several studies have
364 shown that small populations of Hippocampal CA1 cells fire in time-
365 locked sequences, "bridging" the time gap in temporal tasks (B. Kraus
366 et al., 2013; MacDonald et al., 2011, 2013; Pastalkova et al., 2008),
367 including a single-session version of Trace Eye-Blink Conditioning or
368 TEC (Modi et al., 2014). Such cells are commonly termed time cells
369 (Eichenbaum, 2017; MacDonald et al., 2011).

370 The main goal of the Thesis was to be able to study time cells under a
371 variety of behavioural tasks and conditions and elucidate several
372 physiological properties. We standardised a multi-day Trace Eye-Blink
373 Conditioning (TEC) protocol to train head-fixed C57Bl6 mice (Siegel et
374 al., 2015). TEC involves an association between a previously neutral
375 Conditioned Stimulus (CS) with an eye-blink inducing Unconditioned
376 Stimulus (US), across an intervening, stimulus-free, Trace Interval. We
377 were able to observe stable, adaptive learning with our protocol. We
378 also standardized an *in vivo* imaging preparation to record calcium
379 activity from Hippocampal CA1 cells, adapted from previously
380 published methods (Dombeck et al., 2010; Modi et al., 2014). We used
381 a custom-built two photon laser-scanning microscope and performed
382 galvo-scans through the imaging window, during TEC acquisition. The
383 behaviour and imaging was conducted simultaneously to record
384 calcium activity as the animal learnt the task. Chronic Calcium Imaging
385 allowed us to track and record the activity of the same cells, confirmed
386 morphologically. We could then identify time cells across sessions, and

387 look for adaptations in tuning curves, along multiple sessions.
388 Furthermore, numerous approaches have been developed to analyse
389 time cells and neuronal activity sequences, but it is not clear if their
390 classifications match, nor how sensitive they are to various sources of
391 data variability. We provide two main contributions to address this: A
392 resource of synthetic 2-photon calcium activity data, and a survey of
393 several methods for analyzing time cell data using our synthetic data
394 as ground truth. The synthetic dataset and its generation code are
395 useful for profiling future methods, testing analysis tool-chains, and as
396 input to computational and experimental models of sequence
397 detection. We characterized strengths and weaknesses of several
398 time-cell analysis methods. Finally, we benchmark how computational
399 requirements scale with large datasets typical of recent recording
400 technologies.

401

402 Chapter 1 – Introduction

403

404 The vertebrate Central Nervous System (CNS), consisting primarily of
405 the central ganglia (brain) and the spinal cord, samples and receives
406 information from the external world offering top-down control over the
407 activity of all parts of the body. Functions like exploration, food
408 acquisition, and danger aversion, all involve complex coordination
409 between,

- 410 ● the Sensory Systems (that integrate information from the
411 environment),
412 ● the Memory Systems (that integrate sensory information with
413 prior experience), and
414 ● the Motor Systems (that integrate motor plans and execute
415 movement).

416

417 Projects and overall goals

418

419 The overall focus of the work and experiments described in this Thesis
420 was to study Memory Systems, specifically, in terms of,

421

422 **Project I:** How do sensory representations transform with
423 learning?

424

425 **Project II:** How does the timing of cellular activity adjust to
426 behavioural task variables?

427

428 **Project III:** What is the best way to detect and score time-tuned
429 cellular activity?

430

431 Narrowing down, we as a lab were interested in the mammalian
432 hippocampus, a brain structure which is important for consolidating
433 information (from Sensory and other Memory Systems) to enable
434 certain kinds of short-term memory and the translation of short-term
435 memory to long-term.

436

437 **A toolkit to study time cells: Thesis 438 Objectives**

439

440 Ramón y Cajal, one of the pioneers of neuroscience around 1900,
441 utilized Camillo Golgi's staining method to conclusively describe
442 neurons in the brain as independent functional units connected to each
443 other in intricate networks made up of many nodes ($\sim 10^6 - 10^9$). These
444 neurons have since been described not just anatomically, but also on
445 the basis of genetics, development, and neurophysiology.

446

447 In the sub-discipline of Learning and Memory an often studied neuron
448 type is the pyramidal neuron, an example of which is the hippocampal
449 CA1 pyramidal neuron. **It has been an important goal to study memory**
450 **and the neural code in terms of finer temporal order, viz., behavioural**
451 **time scales (~ms to s).** Combining

- 452 • stable, adaptable trace eye-blink conditioning behaviour, and,
453 • cellular resolution 2-photon calcium imaging of hippocampal
454 CA1, *in vivo*,
455 • with the goal to study time cell physiology,

456 was the core objective of the toolkit and the thesis as a whole.
457
458 Development in circuit manipulation tools using light-mediated
459 activation or suppression of neuronal excitability (Luo et al., 2018),
460 afford experimenters the ability to control circuits at ms time scales.
461 Concomitant progress in effective physiological models of network
462 activity during bouts of recall of the learnt behavioural trace require
463 standardized behaviour and recording. For us, this mandated the
464 design of a relatively low-cost, end-to-end configurable, combined
465 behavioural and recording technology, to reliably study the neural code
466 at the ms time scale, *in vivo*.
467
468 This thesis describes a toolkit of techniques ranging in a wide, multi-
469 disciplinary scope, assembled with standardized hardware and
470 software routines studying animal behaviour, network neurophysiology,
471 and statistical analyses. The aim of the toolkit was to support the
472 experimental ability to study the hippocampal CA1 pyramidal neuron
473 network, under strictly controlled behavioural contexts designed to train
474 experimental mice on temporal or episodic memory tasks. Specifically,
475 these tasks such as trace eye-blink conditioning (TEC) have previously
476 been described to elicit hippocampal CA1 sequences (B. Kraus et al.,
477 2013; B. J. Kraus et al., 2015; MacDonald et al., 2011, 2013; Modi et
478 al., 2014; Pastalkova et al., 2008). This spatiotemporal network activity
479 sequence is dynamic and built from individual hippocampal CA1
480 pyramidal neurons showcasing time tuned activity through spiking.
481 These cells are called time cells (Eichenbaum, 2017; MacDonald et al.,
482 2011).

483 **Engrams associated with Learning and**
484 **Memory**

485

486 The term "engram" (coined by Richard Semon) refers to the physical
487 substrate of memory in the organism, used for storing and recalling
488 memories (Josselyn & Tonegawa, 2020). Donald Hebb's theory of
489 Hebbian Plasticity (Hebb, 1949) postulated that memory formation was
490 correlated to modulations in synaptic strength and connectivity. The
491 theory critically emphasized that the pair of neurons connected through
492 the synapse undergoing plasticity to strengthen efficacy, required the
493 spiking activity of both neurons. In subsequent decades, research into
494 the idea led to the theory of spike-timing-dependent plasticity
495 (Caporale & Dan, 2008), a mechanism of synaptic plasticity based on
496 the relative timing of activity of the neurons. It is still a matter of debate
497 whether the biophysical manifestation of the engram is the synapse,
498 the activity of the neurons, biophysical or chemical processes, but it is
499 likely that the engram is distributed across several computational
500 scales in the brain.

501

502 Eric Kandel's experiments with the Aplysia sensory neurons studied gill
503 withdrawal - an aversive but stable, adaptive behaviour (Carew et al.,
504 1971). The reliability of this learned response allowed the experiments
505 to include crucial electrophysiological and neurochemical circuit
506 dissections that ultimately lead to the discovery of the entire neural
507 circuit orchestrating the task, even to the level of cellular signaling.
508 This led to decades of research focused on the plasticity of synapses
509 across nervous systems in the animal kingdom.

510

511 Research exploring causal relationships between the physical or
512 functional integrity of various brain regions and overt behaviour has
513 been crucial to mapping many brain regions to specific functions and
514 motor responses. Technological advancements in molecular
515 neuroscience led to the development of a number of fluorescent
516 sensors, conditional tagging, activators and inhibitors that allowed
517 cellular resolution tracing of the engram (Luo et al., 2018).

518

519 Experiments by Sheena Josselyn, Alcino Silva, and colleagues led to
520 the discovery that the intrinsic excitability of a pyramidal neuron in any
521 network positively biased the probability of recruitment to the engram
522 (Han et al., 2009; Rogerson et al., 2014; Silva et al., 2009; Yiu et al.,
523 2014; Y. Zhou et al., 2009), *viz.*, the tagged set of cells were active
524 when memory was learnt and recalled. The engram seemed to be
525 described in terms of the cellular sub-population involved but the
526 experiment could only identify the same over a relatively longer
527 window of time (~mins.). This could lead to only a static list of cells
528 which may even have included False Positives (Type I error).
529 Importantly, any dynamics in the spatiotemporal patterns of activity of
530 the pyramidal neurons were not amenable to study at shorter
531 timescales (~ms.). On the other hand, physiological recordings could
532 describe these dynamics at short timescales, but were rarely translated
533 to chronic measurements of the activity of the same cells across days
534 and sessions, given technical limitations at the time.

535

536

537 **Dynamics in the neural code for engrams**

538

539 We first discuss some important results that help motivate the study of
540 physiological recordings in the context of engrams, *i.e.*, the dynamical
541 nature of the neural code (~ms to s). In later sections we will describe
542 these dynamics in more detail.

543

544 Place cells and their role in spatial navigation have been studied in
545 great detail through decades of research ever since they were first
546 described by John O'Keefe (O'Keefe & Dostrovsky, 1971). We did not
547 explicitly study place cells in this thesis but some key discoveries in
548 literature require mention, with the goal to build a case for a theory of
549 CA1 ensemble sequences (Modi et al., 2014). Briefly, place cells are
550 pyramidal neurons that showcased a higher than baseline probability
551 of firing action potentials whenever animals navigating spatial
552 environments visited specific locations. The tuning curves or firing
553 fields for these cells often map to the real spatial trajectory of the
554 animal and is thought to be an assimilation of both brain external
555 stimuli such as visual cues, as well as brain internal variables such as
556 motivation, goal orientation, memory, and experience(Ferbinteanu et
557 al., 2011; Ferbinteanu & Shapiro, 2003; Foster, 2017; Frank et al.,
558 2000; Wood et al., 2000).

559

560 As the animal enters these landmark locations in any spatial context,
561 these place cells showcase Phase Precession, firing earlier in phase to
562 cycles of Theta a network rhythm clocked at ~4-10 Hz, as the animal's
563 position changes relative to the landmark. These navigation mapped

564 place cell sequences are called Theta Sequences (Foster & Wilson,
565 2007), typically mapped to a few active neurons at a time.

566

567 In very specific contexts, these place cells express activity sequences
568 synchronized to Sharp Wave Ripples, a different network activity
569 phenomenon clocked at ~10-30 Hz, often not tied to the animal's
570 location, called Replay Sequences (Csicsvari et al., 2007; Foster &
571 Wilson, 2006). These sequences have been described to play out
572 typically in reverse temporal order to models of place cell sequences
573 describing known trajectories in space.

574

575 There is variability in the firing of place cells in any spatial context, and
576 studies have mapped specific sequences to very specific trajectory
577 goals (going towards or away from locations) with modulation by both
578 egocentric and allocentric orientations cues(Davidson et al., 2009;
579 Ferbinteanu et al., 2011; Ferbinteanu & Shapiro, 2003; Frank et al.,
580 2000; Wood et al., 2000) and movement speed based estimates of
581 distance (Kropff et al., 2015).

582

583 Place cell and time cell sequences have many similarities and
584 differences in descriptive neurophysiology, but may emerge from the
585 same memory organization principles (Buzsáki & Llinás, 2017). It is
586 argued that there is significance to the exact phrasing of the CA1
587 sequence in any given context. Furthermore, a very interesting feature
588 observed is Time-stamping, *viz.*, time dependent overlap of ensemble
589 responses to different contexts and behavioural parameters (Cai et al.,
590 2016; Mau et al., 2018).

591

592 We developed and standardized a multi-session, adaptable Trace Eye-
593 Blink Conditioning (TEC) paradigm in which head-fixed mice learn to
594 form associations between neutral and high-valence stimuli. We
595 describe associative learning in later sections as well in Chapter 2 –
596 “Behaviour”. TEC has been previously observed to elicit CA1 activity
597 sequences even in a single session of training (Modi et al., 2014). The
598 functional involvement of the hippocampus in the acquisition of
599 Conditioned Responses (CRs) has been studied and implicated by
600 studying acquisition rates to multiple trace intervals. It was found that
601 memory load, inferred in terms of task difficulty with longer trace
602 intervals (300 ms vs 500 ms), was crucial to observing an effect of
603 hippocampal lesions on the behavioural expression of CRs (Moyer et
604 al., 1990).

605
606 Several stimulus modalities have been used as the Unconditioned
607 Stimulus (US) such as periorbital air-puffs and electrical shocks (see
608 Disterhoft & Weiss, 2017 for review). Throughout all our TEC
609 experiments, we chose to use the mildly aversive air-puff to elicit the
610 Unconditioned Response (UR) to the US. Further, we use a flash of a
611 blue LED as the Conditioned Stimulus (CS), expecting to observe
612 reliable Conditioned Responses (CRs) to the CS within 3-7 days, for
613 trace intervals of ~250 ms (Siegel et al., 2015). CRs are observed as a
614 preemptive eye-blink response elicited reliably before the presentation
615 of the US – a reproducible attempt to avoid the discomfort of the
616 aversive air-puff. This is in accordance with the Rescorla-Wagner
617 model of Classical Conditioning, which assumes that association of the
618 CS and US based on repeated pairing depends on how well the
619 presence of the CS predicts the future occurrence of the US, along
620 with other variables such as the relative intensities and modalities of

621 the presented stimuli (Rescorla & Wagner, 1972). Extensions to this
622 model have suggested that there could be negative effects to the
623 associative learning when other CS (CS1, CS2, etc.) are also paired
624 together in within-compound-association tasks such as “backward
625 blocking” (Hamme & Wasserman, 1993). For our experiments we used
626 only one CS for any training session, typically a 50 ms flash of a blue
627 LED. However, our behavioural setup allows for multiple CS types,
628 e.g., CS1 = Blue LED flash and CS2 = auditory tone, to be presented
629 based on the experiment.

630

631 Transient increases in CA1 excitability post acquisition of the task were
632 described up to 4-5 days (Moyer et al., 1996) and could be important to
633 the forging of the task specific spatiotemporal sequences during
634 learning. In an *in vitro* assay, coronal sections of the hippocampus
635 (Figure 1) were stimulated at the Perforant Path to the cells of the
636 Dentate Gyrus in patterns that could be mnemonically mapped to
637 stereotypic, temporal sequences of Excitatory Postsynaptic Potentials
638 (EPSPs) read out at the hilar mossy cell layer ~400-500 ms later (Hyde
639 & Strowbridge, 2012). This suggested the presence of temporal
640 sequences even at the Dentate Granule cell layer, many synapses
641 before the hippocampal CA1.

642

643 On a longer timescale, hippocampal lesion based experiments on mice
644 have been used to describe the role of the hippocampus to within 4
645 weeks of TEC, with deficits in Conditioned Responses (CRs) as a
646 readout of the effect of the lesion (Takehara et al., 2002). We aimed to
647 examine the processes that underlie this time-dependent role of the
648 hippocampus by chronically tracking the same cohort of hippocampal
649 CA1 cells across the sessions of TEC, at cellular resolution, using

650 galvo-scanning 2-photon calcium imaging. We were specifically
651 interested in studying the emergence and long-term activity dynamics
652 of time cells, touted to be the behavioural time scale ($\sim 10\text{-}10^3$ ms)
653 expression of the memory engram during associative learning, as
654 described in later sections. Preliminary results and additional details on
655 our TEC paradigm may be found in Chapter 2 – “Behaviour”.

656 **Theories on the function of the**
657 **hippocampus**

658

659 Four main ideas of hippocampal function studied over the past few
660 decades are,

661 A) Response Inhibition - Studied mostly in the 1960's, this
662 perspective described the Hippocampus as important to the
663 ability of animals to inhibit their impulses and natural, habitual,
664 or dominant behavioral responses to stimuli, in order to select
665 more appropriate responses. This perspective was justified by
666 two observations with regard to animals with hippocampal
667 damage - 1) these animals tended to be hyperactive, and 2)
668 were unable to withhold previously learnt responses. British
669 psychologist Jeffrey Alan Gray developed this perspective to
670 link hippocampal activity with anxiety (McNaughton & Gray,
671 2000). Studies have now implicated the hippocampus in the
672 facilitation of correct responses and inhibition of incorrect
673 responses during contextual memory tasks, though not for
674 visual discrimination of contexts (Kim & Lee, 2012).

675

676 B) Episodic Memory – a form of declarative or explicit memory that
677 refers to the ability and mechanistic paradigms that allow for the
678 behavioural recall of a collection of past personal experiences,
679 occurring at particular places and times to the subject. The term
680 was coined by Endel Tulving in 1972 (see Clayton et al., 2007),
681 although the perspective was popularized many decades prior,
682 by the psychological studies on Patient H. M. (Henry Molaison),
683 who had been suffering from epileptic seizures and had to
684 undergo extensive hippocampectomy (surgical destruction of
685 the hippocampi), as treatment. American neurosurgeon William
686 Beecher Scoville and British-Canadian neuropsychologist
687 Brenda Milner were pioneers of this study and were able to
688 describe severe anterograde and partial retrograde amnesia in
689 the patient post surgery (Scoville & Milner, 1957). Since the late
690 2000's, the discovery and description of time cells (B. Kraus et
691 al., 2013; B. J. Kraus et al., 2015; MacDonald et al., 2011, 2013;
692 Modi et al., 2014; Pastalkova et al., 2008), has reinvigorated this
693 perspective.

694

695 C) Spatial Cognition – is the ability of experimental animals to
696 locate and ascribe valence to points in space, during navigation
697 of environments. Originally popularized by the remarkable work
698 of American-British neuroscientist John O'Keefe and American
699 psychologist Lynn Nadel, the link between hippocampal function
700 and spatial navigation was solidified with the discovery and
701 subsequent descriptions of place cells (Morris et al., 1982;
702 O'Keefe & Dostrovsky, 1971; O'Keefe & Recce, 1993). This
703 perspective is the most popular amongst the known and studied
704 functions of the Hippocampus and has been the subject of a

705 large body of work. Indeed, the Nobel Prize in Physiology or
706 Medicine 2014 was awarded to John O’Keefe, May-Britt Moser,
707 and Edvard I. Moser, for “The Brain’s Navigational Place and
708 Grid Cell System”.

709

710 D) Contextual Mapping – An emerging consensus in the field is
711 that the hippocampus actually builds contextual maps of the
712 environment or perceived events, with expansions to the neural
713 activity code along any relevant dimension of stimuli. Stimuli or
714 events cuing any modality, e.g., spatial, temporal, frequency,
715 etc., may be assimilated, along with more brain internal
716 variables such as (but not limited to) motivation, expected
717 reward status, prior experience in related tasks, and goal-
718 orientation (task specific). Furthermore, this allows the
719 hippocampus to make predictive models that bind new
720 information streams to collectively update predictions (M. R.
721 Cohen & Kohn, 2011; Eichenbaum, 2017; Miller et al., 2023;
722 O’Keefe & Nadel, 1978). **Pattern separation and conjunctive
723 representation of the combined multi-modal experience in the
724 hippocampus, has been implicated in reinforcement learning**
725 (Ballard et al., 2019). **Contextual mapping considers the
726 hippocampal-entorhinal as a Tolman-Eichenbaum machine
727 (TEM) with the medial entorhinal cortex (MEC) cells thought to
728 describe important aspects of past experience and the
729 hippocampal cells implicated in binding the current sensory
730 experience with prior experience** (Ballard et al., 2019;
731 Eichenbaum, 2017), **with the goal to develop a functional model
732 of the subjective experience of animals and flexibly selecting
733 appropriate responses.**

734
735 Episodic memory forms the central function of study for all of the
736 hippocampus related experiments described in the thesis. Trace Eye-
737 Blink Conditioning (TEC) is an example of a task used to study
738 episodic recall (Thompson, 2004). The behavioural acquisition and
739 expression of CRs correlate well with the neuronal expression of
740 spatiotemporal sequences of time cells (Modi et al., 2014). Our
741 experiments aimed to describe finer details such as how the animals
742 assign valence to the neutral Conditioned Stimulus (CS) and how time
743 cell population codes adapt to changes in the trace interval. Some
744 characteristic features of the engram at behavioural time scales, *viz.*,
745 time cell activation sequences, have been described as preliminary
746 results (Chapter 3 – “Imaging”), under the behavioural context of TEC.
747

748 **A brief introduction to associative learning**

749
750 The ability to physiologically record cells is insufficient without placing
751 the experimental animals in precisely defined, stable behavioural
752 contexts. Only in this way can neural activity be checked for
753 correlations or mapping to distinct changes in external behaviour
754 variables and the decisions that the animal makes, accordingly.
755 Combining behaviour and recording was considered an important
756 guiding principle in all our experiments. **Associative learning** is the
757 overall process by which animals develop behavioural valence to
758 neutral stimuli that occur in temporal conjunction to other potent,
759 behaviour eliciting stimuli. We wished to study the network level
760 responses in the hippocampus, *in vivo*, especially during early learning

761 of associated stimuli, *i.e.*, behavioural acquisition, combining stable,
762 adaptable associative learning paradigms such as Trace Eye-Blink
763 Conditioning (TEC) with cellular resolution, behaviour time scale, high-
764 yield recordings of neurophysiology.

765

766 Prior to the early 20th century, Structuralism was a dominant
767 perspective in Psychology, insisting on introspection - the observation
768 and report of one's own mind and thoughts. Experiments and
769 discoveries by Ivan Pavlov at the Military Medical Academy in
770 Petrograd (St. Petersburg), eventually led to a dramatic shift in
771 perspective, with the birth of Classical Conditioning, a type of
772 associative learning. Following the very same methodology advocated
773 by Francis Bacon (early 17th century), quantitative data from carefully
774 conducted animal experiments were recorded, with the idea to narrow
775 down on a small number of hypotheses that could explain experimental
776 observations.

777

778 Ivan Pavlov provided essential demonstrations of anticipation and
779 made tremendous progress in understanding the circumstances on
780 which anticipation depends, and this is why Classical Conditioning is
781 also often referred to as Pavlovian Conditioning. Following Pavlov's
782 studies (Pavlov, 1927), it was proposed that Classical Conditioning
783 was a prototypical example of Association. While it does have caveats
784 such as covert learning when observable behaviour may be blocked
785 (Dickinson et al., 1983; Krupa & Thompson, 2003), Associative
786 learning is rich with a variety of animals and association tasks that
787 have been crucial to study memory and learning over the past century.
788

789 Typically, animals require no prior training to elicit a behavioural or
790 motor movement to biologically potent stimulus (appetitive or aversive),
791 called an Unconditioned Stimulus (US). Examples include food, water,
792 electrical shock, temperature shock, etc.. Without pairing with a US, a
793 neutral stimulus elicits no observable response from an animal, and
794 such a stimulus is called a Conditioned Stimulus (CS). Examples
795 include simple auditory tones, flashes of light, among others.

796

797 Classical Conditioning is both the behavioural procedure as well as the
798 learning process that results from the pairing of a previously neutral
799 stimulus (CS) with a biologically potent stimulus (US). Repeated
800 pairing allows animals to make implicit associations between the CS
801 and US, and essentially anticipate the occurrence of the US, once the
802 CS is observed. Animals report this forecasting feat by producing the
803 same response that they would to a US, albeit often a milder version.

804 Typical protocols for Classical Conditioning, follow the regime of
805 Forward pairing, *viz.*, - the CS is presented before the US, and this
806 temporal structure will be followed unanimously across all behaviour
807 experiments described in this thesis.

808

809 The standardization of the behavioural task, physiological recording
810 (imaging) preparation, as well as the custom analysis routines to look
811 for various physiological features are described in this thesis.

812 Combining these multi-disciplinary approaches allowed us to develop a
813 toolkit to study time cells in the hippocampus, under strict behavioural
814 contexts. It is important to note, however, that spatiotemporal
815 sequences of activity as measured by calcium imaging based
816 simultaneous recordings of a large number of cells, are not limited to
817 the hippocampus, being studied even in the visual cortex (Pachitariu et

818 al., 2017; Poort et al., 2015), somatosensory cortex (Petersen, 2019),
819 entorhinal cortex (Heys et al., 2014), and even in the cerebellum
820 (Giovannucci et al., 2017). Essentially, the analytical methods
821 developed (Ananthamurthy & Bhalla, 2023) can easily be adapted to
822 other neuronal network recordings where time-tuning may be
823 applicable. **Experimental protocols for associative learning have been**
824 **standardized for a variety of animals, in a variety of experimental**
825 **conditions. The specific issue is of developing an experimental system**
826 **that can run simultaneous TEC behaviour and 2-photon imaging, in**
827 **concert, and provide the context for time cell physiology to be studied,**
828 ***in vivo*. It was important to design both aspects of the experiments**
829 **(behaviour and imaging), since these were the most suitable conditions**
830 **for studies on time cells.**

831 **Space and time in the hippocampus**

832
833 Damage to the hippocampal system has been shown to cause the
834 impairment of long-term memory or amnesia, in human patients,
835 rodents, and non-human primates. Interestingly, such damage to the
836 Hippocampus seems to have no observable effect on the capacity for
837 acquisition and expression of skilled performance. These two results
838 suggest the role of the Hippocampus in certain kinds of memory, but
839 not all.

840
841 Anatomically, the hippocampal system receives input from, and in turn,
842 projects to the neocortical brain regions that serve as the site to
843 process higher order categories and modalities of information. **The**
844 **hippocampal circuit is anatomically >3-4 synapses away from the**

845 peripheral nervous system, and information typically arrives after many
846 layers of intervening processing and computation. It is thus suggested
847 that the hippocampus holds a privileged position in the brain, receiving
848 the outcomes of the computation of the brain's various modules, and
849 relating to them (Baudry & Lynch, 1981; Ekstrom & Ranganath, 2018;
850 Moscovitch et al., 2016; Poppenk et al., 2013; Tao et al., 2021). A
851 large majority of the cortical information is sent to the Hippocampus via
852 the Entorhinal Cortex (EC). This information is processed in roughly
853 three stereotactically and molecularly separable layers of cells in the
854 following order: EC → Dentate Gyrus → CA3 → CA1. This pathway
855 from the EC to the CA1 has three separate synaptic connections
856 (across the layers) and is also known as the Trisynaptic Pathway
857 (Figure 1). The output of the CA1 is then sent to other cortical areas.
858

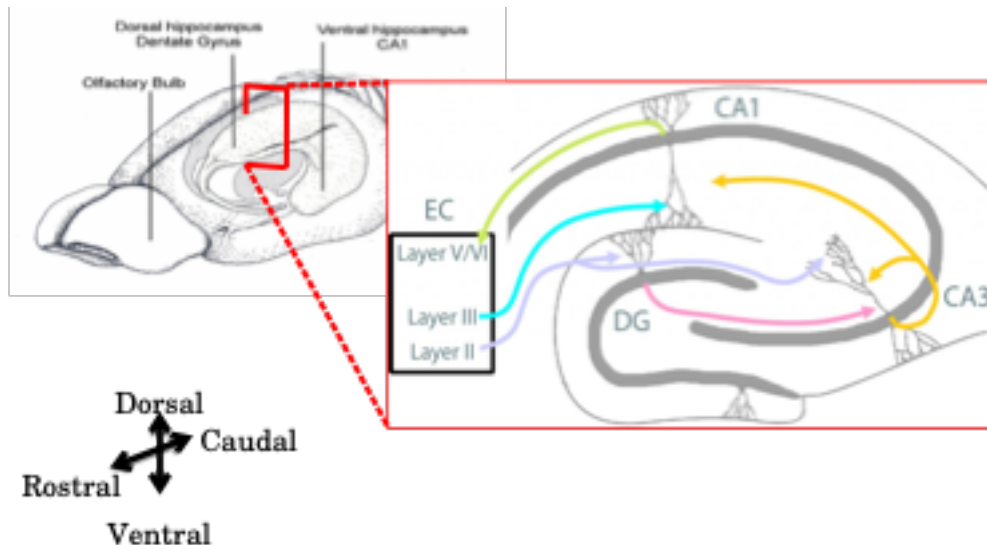


Figure 1: A schematic representation of the Trisynaptic Pathway as observed with coronal slices, along the longitudinal axis of the hippocampus. Image adapted from the webpage for the Neural Circuits and Memory Lab, University of Wisconsin (Milwaukee) [<https://sites.lsa.umich.edu/diba-lab/neural-circuits-of-the-hippocampus/>]

859 One of the most significant discoveries in the hippocampal system and
860 surrounding brain structures was the role played in spatial cognition.
861 An enormous corpus of research has conclusively described,
862 • head-direction cells: with tuning curves tied to the direction that
863 experimental animals were oriented to. These cells respond to
864 egocentric vestibular cues as well as allocentric sensory cues
865 (Ranck, 1973; Taube et al., 1990), in the dorsal presubiculum,
866 retrosplenial cortex, entorhinal cortex, thalamus, and striatum,
867 among others.
868 • grid cells: with multi-modal tuning curves at regular spatial
869 positions as a lattice, across the environment being navigated.
870 These cells assimilate information about location, distance, and
871 direction, and are typically found in the entorhinal cortex (Fyhn
872 et al., 2004; Hafting et al., 2005).
873 • boundary vector cells: with tuning curves to the edges of the
874 environment being navigated. These cells are typically found in
875 the subiculum, pre- and para-subiculum, and entorhinal cortex
876 (Bjerknes et al., 2014; Lever et al., 2009; O'Keefe & Burgess,
877 1996; Savelli et al., 2008; Solstad et al., 2008).
878 • speed cells: with modulated firing rates based on the actual
879 running or movement speed of the animals. These cells are
880 typically found in the entorhinal cortex (Kropff et al., 2015).
881 • place cells: with tuning curves to specific locations in the
882 environment (O'Keefe & Dostrovsky, 1971; O'Keefe & Recce,
883 1993). These cells may be found in several hippocampal sub-
884 layers but often studied in the CA1.
885

886 The activity of neurons in the hippocampus of awake, behaving
887 animals is modulated by significant stimuli or objects in the
888 environment as well as relationships between temporally discontiguous
889 but relevant, paired stimuli. With the discovery of place cells, it was
890 clear that the CA1 of animals navigating a spatial environment,
891 showcased location specific firing fields. With the discovery of time
892 cells, it was noted that the CA1 of animals could elicit spatiotemporal
893 sequences of activity whenever the animal was required to make a link
894 between stimuli or events, even with a stimulus-free period in between.
895 Together, these results provided an important physiological parallel
896 between the spatial learning and episode learning deficit seen with
897 damage to the Hippocampus. Curiously, both place cells and time
898 cells, as well as the sequences built up with them were non-
899 topographically mapped, *i.e.*, they may be located anywhere in the
900 hippocampus, with no obvious spatial order (Dombeck et al., 2010;
901 Modi et al., 2014)(Dombeck et al., 2010; Modi et al., 2014), in contrast
902 to results from the cortex (Dombeck et al., 2009; Ozden et al., 2008).
903
904 In an experiment published in 2008, Eva Pastalkova and colleagues
905 from Gyorgy Buzsaki's lab had rats navigate a figure 8 maze, with the
906 animal being rewarded with water, in between trials, if they managed to
907 alternate between the left and right arms (Pastalkova et al., 2008). As
908 an added nuance in the task, just before launching into the left or right
909 arms, the animal had to spend a fixed amount of time running a
910 treadmill, held in place. This would allow self-motion cues, but with the
911 absence of any other external stimuli. Impressively, single-units
912 recorded from the hippocampal CA1 cells revealed strong correlation
913 with the time spent on the treadmill, despite the absence of external
914 cues, and that different cells tuned to different time points, forming a

915 spatiotemporal sequence of activation (Pastalkova et al., 2008). In a
916 different experiment published in 2011, Christopher J. MacDonald and
917 colleagues from Howard Eichenbaum's lab had rats had to go around
918 a maze and perform a olfactory task (MacDonald et al., 2011). The
919 animals were first presented with an odour, then made to wait for a
920 delay period in a cordoned off section of the maze, before being
921 allowed to either dig for a reward or continue on the maze, depending
922 on the odour presented. As trials progressed, Hippocampal CA1 cells
923 were recorded (single-units) and found to not only be modulated by the
924 decision to be taken, but also to the amount of time spent in the delay
925 period. Experimentally, the delay period could be elongated or
926 shortened, each having an effect on remapping of the tuning fields of
927 the various CA1 cells, but to different extents (MacDonald et al., 2011).

928

929 In 2013, the Eichenbaum group published their findings with head-fixed
930 rats (no movement in space) performing a Delayed Match-To Sample
931 (DMS) task with pairs of odours, where again time tuned activity could
932 be observed with a sequence of Hippocampal CA1 cell activations, that
933 depended on the identity of the first odour (MacDonald et al., 2013). In
934 2014, Mehrab Modi, Ashesh Dhawale, and Upinder Bhalla published
935 their results with head-fixed mice learning and performing a Trace Eye-
936 Blink Conditioning (TEC), wherein it was observed that Hippocampal
937 CA1 cell activity sequences emerged in close relation to the acquisition
938 of behavioural performance, thus cementing the idea that sub-
939 populations of Hippocampal CA1 cells could bridge temporal gaps
940 between relevant, paired stimuli, and that they did so with the activity
941 of time-tuned cells (Modi et al., 2014).

942

943 Finally, it was important to study if these apparently time-tuned cells
944 were tuned to the actual duration of time in a delay period, or whether
945 it was more important for these cells to track the distance run. In an
946 experiment published in 2013, Benjamin Kraus and colleagues from
947 Howard Eichenbaum's lab again had their rats navigate a figure 8
948 maze, but with a motorized treadmill in the central arm, to
949 experimentally regulate the running speed. With this setup, the study
950 was successful at delineating that both time spent running and
951 distance run were important features, and that different cells could tune
952 to either of the features (B. Kraus et al., 2013; B. J. Kraus et al., 2015).
953 Whenever hippocampal CA1 cells showcased time-tuned activity (as
954 opposed to space/location-tuned activity), such cells were dubbed
955 "Time Cells" (Eichenbaum, 2017; MacDonald et al., 2011).

956

957 Other interesting physiological parallels between the CA1 place cells
958 and time cells are,

- 959 1. Phase Precession: In relation to theta oscillations (6-10 Hz)
960 measured as local field potentials (LFP), individual cells tended
961 to fire action potentials at progressively earlier phases with each
962 successive cycle, described first for place cells (O'Keefe &
963 Recce, 1993), and then also for time cells (Pastalkova et al.,
964 2008).
- 965 2. Temporal Compression: Sequences of place or time cells could
966 be elicited at significantly shorter time scales, with fidelity in the
967 participating cells (Dragoi & Buzsáki, 2006; Foster, 2017).
968 Indeed, with regard to the typically studied regime of ~100-200
969 ms or behaviour time scales, the same sequence may be
970 elicited at ~10 ms as short segments during Sharp Wave
971 Ripples (Dragoi et al., 1999; V. Itskov et al., 2008; Jadhav et al.,

972 2012; O’Keefe & Recce, 1993; Valero et al., 2015) or even as
973 the whole sequences during Replay (Csicsvari et al., 2007; Diba
974 & Buzsáki, 2007; Foster, 2017; Foster & Wilson, 2006; Gupta et
975 al., 2010; Pfeiffer & Foster, 2013) or Pre-play (Dragoi, 2013;
976 Dragoi & Tonegawa, 2011).

977 3. Remapping: Systematic changes in the experimental paradigm,
978 such as those to the size of the experimental arena or in the
979 time interval between stimuli or events, would result in
980 systematic changes in the firing fields of place (Muller & Kubie,
981 1989) and time cells (MacDonald et al., 2011).

982 4. Variable Firing Fields: The width of the firing fields for a set of
983 place or time cells, respectively, may be variable. However, an
984 important distinction here is that there is as yet no clearly
985 identified predictor of the widths for place cells to spatial
986 directions, while time cells tuned to later time points in the inter-
987 stimulus or delay periods usually exhibit a widening of firing
988 fields (B. Kraus et al., 2013; B. J. Kraus et al., 2015; MacDonald
989 et al., 2011, 2013; Mau et al., 2018; Pastalkova et al., 2008).
990 The significance of firing field density and tuning widths is as yet
991 an open line of inquiry.

992

993 Single-units recorded from the medial entorhinal cortex (MEC) as well
994 as the hippocampal CA1 that were found tuned to specific frequency
995 “landmarks” during frequency sweeps self-initiated by rats (Aronov et
996 al., 2017), suggesting that the CA1 could tune to variables other than
997 space and time. This added even more weight to “Contextual Mapping”
998 as an important function of the hippocampus.

999 **“Single-cell, multi-trial” vs. “multi-cell,
1000 **single-trial” approaches in Neuroscience****

1001

1002 A dominant, early perspective in neurophysiology had been to record
1003 activity from a single cell, over many trials, under a variety of
1004 conditions (bath applications in slice physiology, different physiological
1005 conditions like stress and genetic background, etc.). For more than one
1006 recorded cell, the process would be repeated, till the dataset was
1007 complete.

1008

1009 An intermediate perspective was to record from multiple cells
1010 simultaneously, yet treat each cell independently for analysis towards
1011 correlation and mechanism studies, across many repeats of
1012 experimental conditions or trials (same as above).

1013

1014 An important and more modern perspective is to record from multiple
1015 cells simultaneously, and use this network or population activity to
1016 decode single-trial characteristics (position, time, stimulus presence,
1017 etc.) using very powerful numerical and mathematical algorithms
1018 involving (but not limited to) Bayesian Decoding and Information
1019 Theory. The essential idea is that the neuronal code of the brain is not
1020 defined just by the activity of single neurons since they may only
1021 encode very specific fractions of the experience, but rather that the
1022 population encodes the full experience, using a number of distributed
1023 and redundant strategies.

- 1024 • Bayesian Decoding: Using the activity of multiple,
1025 simultaneously recorded neurons to develop a likelihood
1026 estimate of the evidence (firing rate combinations) to the

1027 experimental parameter (spatial position, relative time, etc.)
1028 and combine this with the experimentally determined prior
1029 (probability), to obtain estimates of the conditional or
1030 posterior probability of a parameter value, given evidence.
1031 Bayes' Rule describes

$$1032 P(A|B) = P(B|A).P(A)/P(B)$$

1033 ... where,
1034 A: Parameter value (position, time, etc.)
1035 B: Evidence (cellular firing rate)
1036 P(A): Prior Probability (experimentally defined)
1037 P(B): Probability of evidence (Firing Rate)
1038 P(A|B): Posterior probability of parameter value given
1039 evidence
1040 P(B|A): Likelihood estimate of evidence given parameter
1041 value (based on recordings)

1042 This methodology has been used to not only successfully
1043 predict specific time points in a trial from population activity, but
1044 has also been used to observe that the population activity from
1045 a session of recording is able to predict time points in trials
1046 conducted on subsequent sessions of recording, up unto 3-4
1047 sessions (Mau et al., 2018).

- 1048 • Information Theory: Using recorded cellular activity to
1049 estimate how much information this activity carries about
1050 experimental parameters (position, time, stimuli, etc.) in a
1051 trial-by-trial fashion. Three essential metrics have been
1052 used,
 - 1053 1. Information per activity spike (I_{spike}), in bits/spike
 - 1054 2. Information per unit time (I_{sec}), in bits/sec

1055 3. Mutual Information (MI) between evidence and
1056 parameter value, in bits
1057 William Skaggs, Bruce McNaughton and colleagues published a
1058 series of experiments working out the value of Information Theory
1059 based approaches to deciphering the hippocampal code, reviewed
1060 previously (Skaggs et al., 1996). This idea was later adapted strongly
1061 by the field but focus throughout, remained on place cells.
1062
1063 A major step forward with “multi-cell, single-trial” approaches is the
1064 benefit of resolving how each cell and inter-cell interactions contribute
1065 to stimulus representation, behavioural task variables, and other brain-
1066 intrinsic computation. Technological advances in large-scale
1067 neurophysiology recordings such as the increased density of tetrode
1068 drives, Neuropixels, Optical sectioning and microscopy, Resonant
1069 scanning, etc., have enabled the discovery of well coordinated
1070 sequences of cellular activity such as Sharp Wave Ripples (SWRs),
1071 Replay, and behavioural timescale spatio-temporal sequences, *in vivo*,
1072 among others. This is primarily due to a radical improvement in an
1073 experimenter’s ability to simultaneously record from multiple cells
1074 (Foster, 2017), going from yields of ~10 cells to even ~10⁴ cells, per
1075 animal.
1076

1077 **Dimensionality reduction in the analysis of**
1078 **physiology**
1079
1080 Bayesian and Information theoretic approaches as well as methods
1081 like Principal Component Analysis (PCA) afford the experimenter a
1082 variety of mathematical procedures to examine dimensionality

1083 reduction, viz., the transformation of high-dimensional
1084 neurophysiological activity from recorded cells into low-dimensional
1085 representations that still retain meaningful properties of the original
1086 data (Pudil & Novovičová, 1998; van der Maaten et al., 2009). Claude
1087 Shannon is often credited with development of Information Theory
1088 (Shannon, 1948) yet the field has evolved to also describing how
1089 relevance is assigned to a signal, based on statistical associations
1090 between multiple signals or stimuli in a sensory experience (Bialek et
1091 al., 1996, 2001; Chigirev & Bialek, 2004; Tishby et al., 1999).
1092
1093 In the first *bioRxiv* preprint of our paper – “Synthetic Data Resource
1094 and Benchmarks for Time Cell Analysis and Detection Algorithms”
1095 (<https://www.biorxiv.org/content/10.1101/2022.01.01.474717v1?versioned=true>), we had compared several dimensionality reduction
1096 techniques such as Principal Component Analysis, Temporal
1097 Information, trial-averaging, etc.). In the final version of the paper
1098 (Ananthamurthy & Bhalla, 2023; attached as Chapter 4 – “Analysis”),
1099 we reoriented focus on the most popular of the algorithms, and provide
1100 very well performing Python/C++ implementations, especially of the
1101 Ridge-to-background ratio (Mau et al., 2018) and Temporal Information
1102 (Mau et al., 2018) calculations.

1104 **Synthetic benchmarks for pre-hoc
1105 development of analytical procedures**

1106
1107 An interesting study published in 2018 used synthetic test datasets to
1108 go to the extent of estimating place cell detection algorithm
1109 performance on the basis of I_{spike} , I_{sec} and MI (Souza et al., 2018). They
1110 found,

1111 1. MI could outperform the other two in a variety of scenarios.
1112 2. I_{spike} and I_{sec} may still be useful in identifying unique
1113 subpopulations of place cells.
1114 3. Important algorithmic adjustments could be made to the
1115 calculations of I_{spike} and I_{sec} , to equalize performance between
1116 them and MI.

1117 There is clear nuance in the population code that required such a
1118 perspective during analysis. Eichenbaum and colleagues popularized
1119 the use of such metrics in the context of time cells (Mau et al., 2018),
1120 yet a systematic approach to identifying the best algorithms for time
1121 cells was requisite. We resorted to the use of such surrogate synthetic
1122 datasets acting as a large cohort of user-configurable test datasets to
1123 benchmark and characterize the predictive performance of a variety of
1124 time cell detection algorithms (Ananthamurthy & Bhalla, 2023; attached
1125 as Chapter 4 – “Analysis”). Analysis on real physiology datasets where
1126 categorical labels must be assessed is expected to benefit from this
1127 comparative analysis. Our Python/C++ implementations were
1128 rigorously tested and developed to the extent of excellent predictive
1129 performance. These algorithmic procedures may be used to study the
1130 nuances of time cell sequences with more statistical confidence.

1131

1132 Correlation analysis between pairs of recorded cells is one of the most
1133 important analytical directions taken by neurophysiologists
1134 understanding brain function, and has been reviewed previously (M. R.
1135 Cohen & Kohn, 2011). However, such analysis can be subject to False
1136 Positives, without appropriate significance studies. Specifically, it is
1137 important to look at whether the activity profile or tuning curves for cells
1138 (in relation to task variables) is significant above chance or other
1139 clearly defined cutoffs, using a large number of randomized surrogates

1140 of the recorded activity, generated by adding random timing shifts or
1141 bootstraps. Multiple pairwise correlations may not be sufficient to
1142 identify synchronous sequential activity in the network, without looking
1143 at higher orders of correlation across recorded cells. Ultimately, such
1144 studies benefit from simultaneous high-yield recordings, updated
1145 analytical procedures utilizing surrogate data for significance analysis,
1146 examining repetitions across trials (or trial-to-trial variability), and even
1147 the use of multiple analytical strategies, as reviewed previously
1148 (Foster, 2017; Grün, 2009).

1149

1150 Internally driven as opposed to externally driven network models of
1151 activity sequences have been proposed as the mechanism driving
1152 hippocampal CA1 sequences (Buzsáki & Llinás, 2017; Eichenbaum,
1153 2017). The CA1 neurons participating in any sequence may represent
1154 physiologically mappable attractors in temporally specific contexts. Our
1155 2-photon calcium recordings are expected to shed light on important
1156 correlations between task variables and the spatiotemporal sequence
1157 of activity, measured chronically, at cellular resolution.

1158

1159 Synfire chains (Abeles, 1982, 1991, 2004, 2009; Abeles et al., 2004)
1160 as sequential neuronal activity patterns or motifs have been described
1161 in cortical slices *in vitro* (Reyes, 2003), as well as *in vivo* (Ikegaya et
1162 al., 2004). The 2004 study described these sequences as songs
1163 (Ikegaya et al., 2004) that can incorporate new information as
1164 extensions of the motifs by combining multiple synfire chains
1165 (Bienenstock, 1995). However, an important consideration is that the
1166 original theoretical ideas behind synfire chains assumed feed-forward
1167 connections between layers of neurons, with recognition by

1168 subsequent neurons looking only at waves of synchrony, rather than
1169 specific individual neuronal identities (Abeles, 2004). Another important
1170 perspective is that these cortical sequences could be artifacts elicited
1171 just by chance, given the nature of membrane voltage fluctuations
1172 (McLelland & Paulsen, 2007; Mokeichev et al., 2007). There is thus
1173 some speculation over the significance of “cortical songs”, *in vivo*. The
1174 use of properly developed and benchmarked analytical procedures,
1175 tested and verified on physiology-equivalent test datasets (synthetic),
1176 is expected to help alleviate potential doubts in published physiology
1177 results (real recordings). For proper testing of our time cell detection
1178 algorithms, we incorporated many important user-controllable
1179 parameters for the generation of synthetic datasets, such as (but not
1180 limited to) Noise, Event Widths, Hit Trial Ratio, Trial-pair Imprecision,
1181 and Background Activity.

1182

1183 **Single-Unit Electrophysiology vs 2-Photon 1184 Calcium Imaging to study the Hippocampus**

1185

1186 The most well characterized and studied function of the hippocampus
1187 and surrounding tissue (Entorhinal Cortex, Parasubiculum, etc.) was
1188 the role these tissue systems played in Spatial Navigation and Coding.
1189 Single-Unit Electrophysiology was paramount to being able to isolate
1190 the activity from individual cells, and eventually was used to discover
1191 and describe properties of place cells (O’Keefe & Dostrovsky, 1971),
1192 grid cells (Fyhn et al., 2004; Hafting et al., 2005)(Fyhn et al., 2004;
1193 Hafting et al., 2005), head-direction cells (Taube et al., 1990), along

1194 with numerous other important physiological discoveries, as detailed
1195 previously. However, even with advances in the density of tetrode
1196 recordings, the yield of recorded cells from any given animal was often
1197 limited to <50 cells. It was only with the invention of Neuropixels (Jun
1198 et al., 2017) that this yield could be expanded to ~1000 cells. We had
1199 opted to utilize calcium imaging by 2-Photon Microscopy (Denk et al.,
1200 1990; Stosiek et al., 2003). This methodology, allowed us to record
1201 ~100-150 cells per session with our mice, albeit with significant cost to
1202 the recording frame rate on account of the limitations of the technique.
1203 Electrical recordings may be sampled even >20 kHz, while imaging
1204 based techniques typically cannot be used to record wide fields of
1205 view, sampled at >100 Hz (1-2 orders of magnitude, comparing
1206 sampling rates). Many spike sorting algorithms (see Buccino et al.,
1207 2022 for review) as well as automated ROI detection (see Robbins et
1208 al., 2021 for review) have been suggested for automated cell source
1209 identification, yet challenges remain, such as,
1210 1) scalability - more sources to identify from ever larger datasets force
1211 longer analysis runs.
1212 2) reproducibility – pre-processing analytical steps require manual
1213 curation to clean up the raw datasets, and this often affects the final
1214 result. We discuss details of our technique along with challenges and
1215 preliminary results, in Chapter 3 – “Imaging”.
1216
1217 The hippocampi (one in each hemisphere) of the mouse brain lie ~1
1218 mm below the most superficial layers of cortex (just inside the
1219 cranium), a barrier typically too wide for typical 1-photon fluorescence
1220 imaging systems (Confocal, Spinning Disk, etc.). This poses a very
1221 difficult challenge for imaging preparations since there are hardware
1222 and other technical limits to how long the working distance of

1223 microscope objectives can be made. The use of 2-photon microscopy
1224 combined with combinations of cortical excavations (to aid physical
1225 access), microendoscopes, as well as prisms to guide emitted
1226 fluorescence, have all been used to achieve deep brain imaging based
1227 recordings at cellular resolution, in rodents (Andermann et al., 2013;
1228 Attardo et al., 2015; Barreto et al., 2009; Barreto & Schnitzer, 2012;
1229 Dombeck et al., 2010; Heys et al., 2014; Murray & Levene, 2012;
1230 Velasco & Levene, 2014; Ziv et al., 2013).

1231

1232 All imaging preparation standardizations described in this thesis invoke
1233 2-Photon calcium imaging of hippocampal CA1 cells at cellular
1234 resolution (1 pix = ~1 μ m), following cortical excavations just above the
1235 left hippocampus (Dombeck et al., 2010).

1236 **Calcium imaging by 2-Photon Microscopy**

1237

1238 Typically, as cells become activated and elicit action potentials, there is
1239 often a large concomitant influx of Ca^{2+} ions through voltage gated
1240 calcium channels all around the perisomatic membrane, amongst other
1241 cellular compartments. Several organic dyes have been developed that
1242 reversibly bind Ca^{2+} ions in the cytosol and either become fluorescent
1243 or emit greater fluorescence (often with a red shift) when in this Ca^{2+} -
1244 bound state (Paredes et al., 2008). Additionally tremendous advances
1245 in molecular biology has seen the deployment of Genetically Encoded
1246 Calcium Indicators (GECIs) that may be exogenously incorporated into
1247 the genome of target cells. These GECIs serve the same function as
1248 organic calcium dyes, but may easily be replenished in the cytosol
1249 given the cell's natural machinery for transcription and translation, and

1250 whose Fluorescence properties can be engineered for brightness,
1251 responsivity, Ca^{2+} binding K_d , and fluorescence emission wavelengths.
1252 The number of cells that may be recorded by fluorescence is often only
1253 limited to either the spread of the organic dye or the imaging
1254 magnification settings, allowing for yields of 100-1000 cells.

1255

1256 With any Imaging based neurophysiology, there is always a trade-off
1257 between yield (number of cells recorded simultaneously) and temporal
1258 resolution. Increasing the yield by recording over a larger area of tissue
1259 requires many more pixels per imaging frame, resulting in a loss of
1260 temporal resolution (frame rate). On the other hand, increasing the
1261 frame rate necessitates capturing fewer pixels per frame, decreasing
1262 yield. There is even a limitation of simply zooming out, since stable
1263 fluorescence intensity fluctuations can only be identified when each
1264 cell is defined at least by a certain number of pixels, to allow proper
1265 isolation.

1266

1267 Specifically with calcium imaging, the signal to be recorded
1268 corresponds to Ca^{2+} flux in the cytoplasm as measured by the change
1269 in emitted fluorescence of reporters such as GCaMP, with a $\tau_{\text{rise}} = 10-$
1270 100 ms and $\tau_{\text{fall}} = 100-300$ ms (Chen et al., 2013). This signal is one or
1271 two orders of magnitude slower than the action potential ($\sim 2-5$ ms).
1272 However, this may not necessarily be a limitation since a dominant
1273 idea in the field is to simply consider rate coding, or time-averaged
1274 spiking activity (Abeles, 2004), bringing down the effective temporal
1275 resolution of the electrical record.

1276

1277 Genetically Encoded Voltage Indicators (GEVIs) that fluoresce with
1278 higher emission during membrane voltage dynamics have also been

1279 developed. However, their localization onto the membrane of the cell,
1280 instead of the cytoplasm, diminishes the total emitted photon flux per
1281 unit time, and requires longer bin times to achieve reasonable signal-
1282 to-noise, as reviewed previously (Mollinedo-Gajate et al., 2021). This
1283 unfortunately brings down the frame rate even more than what can be
1284 achieved with GECIs. We avoided GEVIs in the projects described in
1285 this thesis.

1286

1287 A major advancement in Fluorescence Imaging was the invention of
1288 Confocal and Multiphoton (typically 2-Photon) Microscopes, which
1289 allowed for unprecedented recording signal-to-noise by optical
1290 sectioning. 2-Photon Imaging itself was an important development for
1291 the neurophysiology of tissue greater than 300 μm in thickness, typical
1292 of rodent brain tissue, because it avoids wasteful excitation of imaging
1293 planes that are not in focus (out-of-plane). The 2-Photon effect
1294 requires two photons of longer wavelength (lower energy per photon),
1295 to near instantaneously excite a fluorophore. The photon flux is highest
1296 at the focal plane (with an N-squared dependence) of the microscope
1297 so only the section of the tissue corresponding to the focal place is
1298 allowed to achieve fluorescence. Additionally, longer wavelengths of
1299 excitation light can more easily penetrate deeper layers of tissue, due
1300 to comparatively lower scattering or Rayleigh effect (Denk et al., 1990;
1301 Helmchen & Denk, 2005).

1302

1303 The hippocampus (specifically the hippocampal CA1) was the main
1304 brain structure of interest for all our physiology experiments, and lies
1305 under about 1 mm of cortical tissue for mice. This is a depth that is
1306 difficult to image even with 2-Photon Microscopy. The typical
1307 methodology employed in such cases is to perform a cortical

1308 excavation just above the Hippocampus filling the crevice with optically
1309 clearer agarose or silicone elastomer. Even so, the hippocampal CA1
1310 cell body layer (*Stratum Pyramidale*) still lies about 150-300 µm below
1311 the external capsule and corpus callosum fibers (left intact for chronic
1312 imaging). Accordingly, we combined cortical excavation with 2-Photon
1313 microscopy, using a long working distance objective with a wide field of
1314 view, imaging cytosolic Ca²⁺ activity with the help of either an organic
1315 dye (OGB-1; acute imaging) or a GECI (GCaMP6f; chronic imaging).

1316

1317 An important perspective that has motivated the use of Imaging based
1318 physiology recordings (as opposed to Electrophysiological methods)
1319 other than potential yield, is that imaging provides anatomical
1320 confirmation of any particular recorded cell, and this in turn allows for,
1321 A) Unambiguous isolation of the same cell across multiple imaging
1322 sessions (across days and weeks). Single-Units are ultimately
1323 only algorithmically resolved and this can be done only for cells
1324 that are active and are represented in multiple spatially
1325 separated electrodes. However, very recently, Ashesh Dhawale
1326 and colleagues from Bence Olveczky's lab have devised a
1327 solution to track the movement of electrodes in tissue over time
1328 and use this information to ensure chronic recording of the
1329 same units (Dhawale et al., 2017). This technique was not
1330 available at the time when experiments for this thesis were
1331 started.

1332 B) Unambiguous detection of the lack of activity in an otherwise
1333 recorded cell. Since the cell can be anatomically identified
1334 independent of activity, it is possible to observe the absence of
1335 Ca²⁺ activity. Automated cell ROI detection (Francis et al., 2012;
1336 Maruyama et al., 2014; Mukamel et al., 2009; Pachitariu et al.,

1337 2017; Pnevmatikakis et al., 2016) simplifies the pre-processing
1338 step of cell isolation even over large batch sizes. These
1339 procedures inherently require the use of the calcium activity
1340 profiles of recorded cells, viz., inactive cells (though
1341 anatomically visible), may not be isolated.

1342 **Automated ROI detection for large-scale**
1343 **Calcium Imaging datasets**

1344
1345 A number of automated ROI detection algorithms have been cited in
1346 literature that require minimal user intervention, perform relatively fast
1347 identification for a large number of identified sources (putative cells).
1348 Some popular algorithms include PCA/ICA (Mukamel et al., 2009),
1349 Suite2p (Pachitariu et al., 2017), and Non-Negative Matrix
1350 Factorization or NNMF (Pnevmatikakis et al., 2016), which all have
1351 been developed to the extent where comparable or oftentimes much
1352 better ROI detection is achieved than as compared to the more tedious
1353 hand-drawn ROIs which scales very poorly with orders of cells
1354 recorded.
1355 We have strictly followed Suite2p (Pachitariu et al., 2017) for all
1356 physiological ROI (cell sources) described in this thesis.
1357

1358 Short Summaries of the 3 projects

1359 Project I - How do sensory representations transform 1360 with learning?

1361 Sensory Systems Neuroscience is a very popular field spanning
1362 studies looking at numerous brain regions and sub-regions in the
1363 cortex and hippocampus, *in vivo* (R. A. Andersen et al., 1993; Fassihi
1364 et al., 2017; Khan et al., 2010; Meeks et al., 2010; Petersen, 2019;
1365 Poort et al., 2015; Voelcker et al., 2022), among several others. Many
1366 if not most of these studies describe neural activity in animals with
1367 expert levels of behavioural learning and performance to the presented
1368 stimuli. Lacunae still remain as to mechanisms deployed during active
1369 or online learning especially in the early stages of behavioural training.

1370 There are not many published physiological readouts from large CA1
1371 populations, *in vivo*, under behavioural contexts for time cell activation,
1372 during the early, acquisition phases (Sessions 1-7, etc.) in associative
1373 learning. It is unclear what the spatiotemporal pattern of activity would
1374 reveal with a systematic, longitudinal survey.

1375

1376 We deployed our experiments with the intention to study how Calcium
1377 Imaging by 2-Photon could reveal finer population level details of
1378 network activity as the animals were tested on the learning of an
1379 operant conditioning or lick behaviour task. We were able to,
1380 1. Prototype OGB-1 based calcium imaging *in vivo*, from head-
1381 fixed mice in a manner suited to combined behaviour and
1382 recording experiments, and

1383 2. Study preliminary data from animals that correlation based
1384 functional activity clusters of recorded CA1 cells have spatial
1385 organization during bouts of spontaneous activity.

1386

1387 However, we were not satisfied with the level and rate of learning in
1388 our test animals eventually leading to a search for more stable
1389 behaviour paradigms in mice. Additionally, the use of OGB-1 as the
1390 Calcium Indicator also had to be abandoned since this fundamentally
1391 disallowed multi-day tracking of the same cells. We discuss our
1392 prototyping efforts and preliminary data for this project in detail, in the
1393 first few sections each of Chapters 2 (“Behaviour”) and 3 (“Imaging”).

1394

1395 **Project II - How does the timing of cellular activity adjust**
1396 **to behavioural task variables?**

1397

1398 Research on the cerebellum has made substantial progress in the
1399 elucidation of network mechanisms correlating well with external
1400 stimulus timing based variables, as animals learn Trace Eye-Blink
1401 Conditioning and Delay Conditioning (Kalmbach, Davis, et al., 2010;
1402 Kalmbach, Ohyama, et al., 2010; Medina et al., 2000; Ohyama et al.,
1403 2003; Siegel & Mauk, 2013). The preeminent studies on time cells in
1404 the hippocampus have focused on the context of appetitive reinforcing
1405 stimuli (Eichenbaum, 2004, 2017; B. Kraus et al., 2013; B. J. Kraus et
1406 al., 2015; MacDonald et al., 2011, 2013; Mau et al., 2018; Pastalkova
1407 et al., 2008). Time cells in the behavioural context of Trace Eye-Blink
1408 conditioning, an aversive learning paradigm, have been explored (Modi
1409 et al., 2014), but details such as correlations with rates of behavioural

1410 learning, tuning adaptability, and long-term stability (~weeks) of the
1411 time sequences are yet to be studied. **The degree of variability in time**
1412 **cell responses under these conditions is likely to inform mechanistic**
1413 **models of spatiotemporal sequences as observed in the hippocampus.**

1414

1415 We prototyped a GCaMP6f based *in vivo* hippocampal preparation that
1416 allowed for chronic, longitudinal recordings of hippocampal CA1, by 2-
1417 Photon Calcium Imaging (Dombeck et al., 2010) that could be
1418 combined with a stable and adaptable learning protocols of Trace Eye-
1419 Blink Conditioning (Siegel et al., 2015).

1420 From our preliminary set of recordings we were able to,

1421 1. Detect time cells in our population recordings,
1422 2. Observe signs of expansion of the time cell sub-population over
1423 early stages of learning, and
1424 3. Observe shifts in the timing of peak for known, chronically
1425 tracked time cells, typically moving away from the US and
1426 towards the CS.

1427

1428 Technical difficulties prevented us from expanding our experimental
1429 recording datasets to the point where these results could be looked at
1430 more critically and the results may be sufficient for publication. We
1431 discuss our prototyping efforts and preliminary data for this project in
1432 detail, in the last few sections each of Chapters 2 (“Behaviour”) and 3
1433 (“Imaging”).

1434

1435 **Project III - What is the best way to detect and score**
1436 **time-tuned cellular activity?**

1437

1438 Given that we had collected a reasonable sample of multi-day tracked
1439 cells while head-fixed mice were being trained to a Trace Eye-Blink
1440 Conditioning (TEC) task, we wished to move forward to identifying time
1441 cells in the most reliable way, with the aim to drawing quality
1442 conclusions from the physiology recordings.

1443

1444 The paper entitled “Synthetic Data Resource and Benchmarks for Time
1445 Cell Analysis and Detection Algorithms” (Ananthamurthy & Bhalla,
1446 2023) was a consolidation of our progress to analyse physiology data
1447 from real and synthetic cells expressed as calcium activity trials and
1448 sessions.

1449

1450 Here, we used a computational approach and developed categorically
1451 labelled, user definable, large scale synthetic datasets, as a test bed to
1452 compare and benchmark the predictions made by popular time cell
1453 detection algorithms. We were able to test the sensitivity of these
1454 computational algorithms across a wide array of experimental
1455 recording parameters, and could ultimately conclude the best
1456 operational regimes for each of them. All of the code base for this
1457 project is freely available online

1458 (<https://github.com/bhallalab/TimeCellAnalysis>) and is intended to be a
1459 resource to researchers.

1460 The paper is attached as Chapter 4 (“Analysis”).

1461 **Code Availability**

1462

1463 All our code for Synthetic Data generation and time cell Analysis is
1464 available at <https://www.github.com/bhallalab/TimeCellAnalysis>.

1465

1466 All our code for conducting Trace Eye-Blink Conditioning (TEC)
1467 behaviour is available at
<https://www.github.com/ananthamurthy/eyeBlinkBehaviour>.

1469

1470 Analysis scripts for evaluating TEC performance are available at
1471 <https://github.com/ananthamurthy/MATLAB/tree/master/TECAnalysis>.

1472 **Bibliography**

1473

1474 Abeles, M. (1982). *Local Cortical Circuits: An Electrophysiological*
1475 *Study*. Springer-Verlag.

1476 <https://books.google.co.in/books?id=s25lwwEACAAJ>

1477 Abeles, M. (1991). *Corticonics: Neural Circuits of the Cerebral Cortex*.
1478 Cambridge University Press. [https://doi.org/DOI:
1479 10.1017/CBO9780511574566](https://doi.org/DOI:10.1017/CBO9780511574566)

1480 Abeles, M. (2004). Time Is Precious. *Science*, 304(5670), 523–524.
1481 <https://doi.org/10.1126/science.1097725>

1482 Abeles, M. (2009). *Synfire Chains* (L. R. B. T.-E. of N. Squire, Ed.; pp.
1483 829–832). Academic Press.

1484 <https://doi.org/https://doi.org/10.1016/B978-008045046-9.01437-6>

1485 Abeles, M., Hayon, G., & Lehmann, D. (2004). Modeling
1486 compositionality by dynamic binding of synfire chains. *Journal of*
1487 *Computational Neuroscience*, 17(2), 179–201.

1488 <https://doi.org/10.1023/B:JCNS.0000037682.18051.5f>

1489 Ananthamurthy, K. G., & Bhalla, U. S. (2023). Synthetic Data Resource
1490 and Benchmarks for Time Cell Analysis and Detection Algorithms.
1491 *ENeuro*, ENEURO.0007-22.2023.

1492 <https://doi.org/10.1523/ENEURO.0007-22.2023>

1493 Andermann, M. L., Gilfoy, N. B., Goldey, G. J., Sachdev, R. N. S.,
1494 Wölfel, M., McCormick, D. A., Reid, R. C., & Levene, M. J. (2013).
1495 Chronic Cellular Imaging of Entire Cortical Columns in Awake

- 1496 Mice Using Microprisms. *Neuron*, 80(4), 900–913.
1497 <https://doi.org/10.1016/j.neuron.2013.07.052>
- 1498 Andersen, R. A., Snyder, L. H., Li, C.-S., & Stricanne, B. (1993).
1499 Coordinate transformations in the representation of spatial
1500 information. *Current Opinion in Neurobiology*, 3(2), 171–176.
1501 [https://doi.org/https://doi.org/10.1016/0959-4388\(93\)90206-E](https://doi.org/https://doi.org/10.1016/0959-4388(93)90206-E)
- 1502 Aronov, D., Nevers, R., & Tank, D. W. (2017). Mapping of a non-spatial
1503 dimension by the hippocampal-entorhinal circuit. *Nature*,
1504 543(7647), 719–722. <https://doi.org/10.1038/nature21692>
- 1505 Attardo, A., Fitzgerald, J. E., & Schnitzer, M. J. (2015). Impermanence
1506 of dendritic spines in live adult CA1 hippocampus. *Nature*,
1507 523(7562), 592–596. <https://doi.org/10.1038/nature14467>
- 1508 Ballard, I. C., Wagner, A. D., & McClure, S. M. (2019). Hippocampal
1509 pattern separation supports reinforcement learning. *Nature
1510 Communications*, 10(1), 1073. <https://doi.org/10.1038/s41467-019-08998-1>
- 1512 Barretto, R. P. J., Messerschmidt, B., & Schnitzer, M. J. (2009). In vivo
1513 fluorescence imaging with high-resolution microlenses. *Nature
1514 Methods*, 6(7), 511–512. <https://doi.org/10.1038/nmeth.1339>
- 1515 Barretto, R. P. J., & Schnitzer, M. J. (2012). In vivo optical
1516 microendoscopy for imaging cells lying deep within live tissue.
1517 *Cold Spring Harbor Protocols*, 2012(10), 1029–1034.
1518 <https://doi.org/10.1101/pdb.top071464>
- 1519 Baudry, M., & Lynch, G. (1981). Hippocampal glutamate receptors.
1520 *Molecular and Cellular Biochemistry*, 38(1), 5–18.
1521 <https://doi.org/10.1007/BF00235685>
- 1522 Bialek, W., Callan, C. G., & Strong, S. P. (1996). Field Theories for
1523 Learning Probability Distributions. *Physical Review Letters*,
1524 77(23), 4693–4697. <https://doi.org/10.1103/physrevlett.77.4693>
- 1525 Bialek, W., Nemenman, I., & Tishby, N. (2001). Predictability,
1526 Complexity, and Learning. *Neural Comput.*, 13(11), 2409–2463.
1527 <https://doi.org/10.1162/089976601753195969>
- 1528 Bienenstock, E. (1995). A model of neocortex. *Network: Computation
1529 in Neural Systems*, 6(2), 179–224. https://doi.org/10.1088/0954-898X_6_2_004
- 1531 Bjerknes, T. L., Moser, E. I., & Moser, M.-B. (2014). Representation of
1532 Geometric Borders in the Developing Rat. *Neuron*, 82(1), 71–78.
1533 <https://doi.org/10.1016/j.neuron.2014.02.014>
- 1534 Buccino, A. P., Garcia, S., & Yger, P. (2022). Spike sorting: new trends
1535 and challenges of the era of high-density probes. *Progress in
1536 Biomedical Engineering*, 4(2), 022005.
1537 <https://doi.org/10.1088/2516-1091/ac6b96>
- 1538 Buzsáki, G., & Llinás, R. (2017). Space and time in the brain. *Science*

- 1539 (New York, N.Y.), 358(6362), 482–485.
1540 <https://doi.org/10.1126/science.aan8869>
- 1541 Cai, D. J., Aharoni, D., Shuman, T., Shobe, J., Biane, J., Song, W.,
1542 Wei, B., Veshkini, M., La-Vu, M., Lou, J., Flores, S. E., Kim, I.,
1543 Sano, Y., Zhou, M., Baumgaertel, K., Lavi, A., Kamata, M.,
1544 Tuszynski, M., Mayford, M., ... Silva, A. J. (2016). A shared neural
1545 ensemble links distinct contextual memories encoded close in
1546 time. *Nature*, 534(7605), 115–118.
1547 <https://doi.org/10.1038/nature17955>
- 1548 Caporale, N., & Dan, Y. (2008). Spike timing-dependent plasticity: a
1549 Hebbian learning rule. *Annual Review of Neuroscience*, 31, 25–
1550 46. <https://doi.org/10.1146/annurev.neuro.31.060407.125639>
- 1551 Carew, T. J., Castellucci, V. F., & Kandel, E. R. (1971). An Analysis of
1552 Dishabituation and Sensitization of The Gill-Withdrawal Reflex In
1553 Aplysia. *International Journal of Neuroscience*, 2(2), 79–98.
1554 <https://doi.org/10.3109/00207457109146995>
- 1555 Chen, T.-W., Wardill, T. J., Sun, Y., Pulver, S. R., Renninger, S. L.,
1556 Baohan, A., Schreiter, E. R., Kerr, R. A., Orger, M. B., Jayaraman,
1557 V., Looger, L. L., Svoboda, K., & Kim, D. S. (2013). Ultrasensitive
1558 fluorescent proteins for imaging neuronal activity. *Nature*,
1559 499(7458), 295–300. <https://doi.org/10.1038/nature12354>
- 1560 Chigirev, D., & Bialek, W. (2004, January). Optimal manifold
1561 representation of data: An information theoretic approach.
1562 *Advances in Neural Information Processing Systems 16 -*
1563 *Proceedings of the 2003 Conference, NIPS 2003*.
- 1564 Clayton, N. S., Salwiczek, L. H., & Dickinson, A. (2007). Episodic
1565 memory. *Current Biology*, 17(6), R189–R191.
1566 <https://doi.org/10.1016/j.cub.2007.01.011>
- 1567 Cohen, M. R., & Kohn, A. (2011). Measuring and interpreting neuronal
1568 correlations. *Nature Neuroscience*, 14(7), 811–819.
1569 <https://doi.org/10.1038/nn.2842>
- 1570 Csicsvari, J., O'Neill, J., Allen, K., & Senior, T. (2007). Place-selective
1571 firing contributes to the reverse-order reactivation of
1572 CA1 pyramidal cells during sharp waves in open-field exploration.
1573 *The European Journal of Neuroscience*, 26(3), 704–716.
1574 <https://doi.org/10.1111/j.1460-9568.2007.05684.x>
- 1575 Davidson, T. J., Kloosterman, F., & Wilson, M. A. (2009). Hippocampal
1576 replay of extended experience. *Neuron*, 63(4), 497–507.
1577 <https://doi.org/10.1016/j.neuron.2009.07.027>
- 1578 Denk, W., Strickler, J. H., & Webb, W. W. (1990). Two-photon laser
1579 scanning fluorescence microscopy. *Science (New York, N.Y.)*,
1580 248(4951), 73–76. <https://doi.org/10.1126/science.2321027>
- 1581 Dhawale, A. K., Poddar, R., Wolff, S. B. E., Normand, V. A.,

- 1582 Kopelowitz, E., & Ölveczky, B. P. (2017). Automated long-term
1583 recording and analysis of neural activity in behaving animals.
1584 *ELife*, 6, e27702. <https://doi.org/10.7554/eLife.27702>
- 1585 Diba, K., & Buzsáki, G. (2007). Forward and reverse hippocampal
1586 place-cell sequences during ripples. *Nature Neuroscience*, 10(10),
1587 1241–1242. <https://doi.org/10.1038/nn1961>
- 1588 Dickinson, A., Nicholas, D. J., & Mackintosh, N. J. (1983). A re-
1589 examination of one-trial blocking in conditioned suppression. *The
1590 Quarterly Journal of Experimental Psychology B: Comparative and
1591 Physiological Psychology*, 35, 67–79.
1592 <https://doi.org/10.1080/14640748308400914>
- 1593 Disterhoft, J. F., & Weiss, C. (2017). Eyeblink Conditioning – A
1594 Behavioral Model of Procedural and Declarative Learning. In J. H.
1595 Byrne (Ed.), *Learning and Memory: A Comprehensive Reference
1596 (Second Edition)* (pp. 327–355). Academic Press.
1597 <https://doi.org/https://doi.org/10.1016/B978-0-12-809324-5.21087-0>
- 1599 Dombeck, D. A., Graziano, M. S., & Tank, D. W. (2009). Functional
1600 Clustering of Neurons in Motor Cortex Determined by Cellular
1601 Resolution Imaging in Awake Behaving Mice. *The Journal of
1602 Neuroscience*, 29(44), 13751 LP – 13760.
1603 <https://doi.org/10.1523/JNEUROSCI.2985-09.2009>
- 1604 Dombeck, D. A., Harvey, C. D., Tian, L., Looger, L. L., & Tank, D. W.
1605 (2010). Functional imaging of hippocampal place cells at cellular
1606 resolution during virtual navigation. *Nature Neuroscience*, 13(11),
1607 1433–1440. <https://doi.org/10.1038/nn.2648>
- 1608 Dragoi, G. (2013). Internal operations in the hippocampus: single cell
1609 and ensemble temporal coding. *Frontiers in Systems
1610 Neuroscience*, 7, 46. <https://doi.org/10.3389/fnsys.2013.00046>
- 1611 Dragoi, G., & Buzsáki, G. (2006). Temporal encoding of place
1612 sequences by hippocampal cell assemblies. *Neuron*, 50(1), 145–
1613 157. <https://doi.org/10.1016/j.neuron.2006.02.023>
- 1614 Dragoi, G., Carpi, D., Recce, M., Csicsvari, J., & Buzsáki, G. (1999).
1615 Interactions between hippocampus and medial septum during
1616 sharp waves and theta oscillation in the behaving rat. *The Journal
1617 of Neuroscience : The Official Journal of the Society for
1618 Neuroscience*, 19(14), 6191–6199.
1619 <http://www.ncbi.nlm.nih.gov/pubmed/10407055>
- 1620 Dragoi, G., & Tonegawa, S. (2011). Preplay of future place cell
1621 sequences by hippocampal cellular assemblies. *Nature*,
1622 469(7330), 397–401. <https://doi.org/10.1038/nature09633>
- 1623 Eichenbaum, H. (2004). Hippocampus: Cognitive processes and
1624 neural representations that underlie declarative memory. *Neuron*,

- 1625 44(1), 109–120. <https://doi.org/10.1016/j.neuron.2004.08.028>
- 1626 Eichenbaum, H. (2017). On the Integration of Space, Time, and
1627 Memory. *Neuron*, 95(5), 1007–1018.
1628 <https://doi.org/10.1016/j.neuron.2017.06.036>
- 1629 Ekstrom, A. D., & Ranganath, C. (2018). Space, time, and episodic
1630 memory: The hippocampus is all over the cognitive map.
1631 *Hippocampus*, 28(9), 680–687.
1632 <https://doi.org/https://doi.org/10.1002/hipo.22750>
- 1633 Fassihi, A., Akrami, A., Pulecchi, F., Schönfelder, V., & Diamond, M. E.
1634 (2017). Transformation of Perception from Sensory to Motor
1635 Cortex. *Current Biology : CB*, 27(11), 1585-1596.e6.
1636 <https://doi.org/10.1016/j.cub.2017.05.011>
- 1637 Ferbinteanu, J., & Shapiro, M. L. (2003). Prospective and retrospective
1638 memory coding in the hippocampus. *Neuron*, 40(6), 1227–1239.
1639 [https://doi.org/10.1016/s0896-6273\(03\)00752-9](https://doi.org/10.1016/s0896-6273(03)00752-9)
- 1640 Ferbinteanu, J., Shirvalkar, P., & Shapiro, M. L. (2011). Memory
1641 Modulates Journey-Dependent Coding in the Rat Hippocampus.
1642 *The Journal of Neuroscience*, 31(25), 9135 LP – 9146.
1643 <https://doi.org/10.1523/JNEUROSCI.1241-11.2011>
- 1644 Foster, D. J. (2017). Replay Comes of Age. *Annual Review of
1645 Neuroscience*, 40, 581–602. <https://doi.org/10.1146/annurev-neuro-072116-031538>
- 1647 Foster, D. J., & Wilson, M. A. (2006). Reverse replay of behavioural
1648 sequences in hippocampal place cells during the awake state.
1649 *Nature*, 440(7084), 680–683. <https://doi.org/10.1038/nature04587>
- 1650 Foster, D. J., & Wilson, M. A. (2007). Hippocampal theta sequences.
1651 *Hippocampus*, 17(11), 1093–1099.
1652 <https://doi.org/10.1002/hipo.20345>
- 1653 Francis, M., Qian, X., Charbel, C., Ledoux, J., Parker, J. C., & Taylor,
1654 M. S. (2012). Automated region of interest analysis of dynamic
1655 Ca²⁺ signals in image sequences. *American Journal of
1656 Physiology. Cell Physiology*, 303(3), C236-43.
1657 <https://doi.org/10.1152/ajpcell.00016.2012>
- 1658 Frank, L. M., Brown, E. N., & Wilson, M. (2000). Trajectory encoding in
1659 the hippocampus and entorhinal cortex. *Neuron*, 27(1), 169–178.
1660 [https://doi.org/10.1016/s0896-6273\(00\)00018-0](https://doi.org/10.1016/s0896-6273(00)00018-0)
- 1661 Fyhn, M., Molden, S., Witter, M. P., Moser, E. I., & Moser, M.-B.
1662 (2004). Spatial representation in the entorhinal cortex. *Science
1663 (New York, N.Y.)*, 305(5688), 1258–1264.
1664 <https://doi.org/10.1126/science.1099901>
- 1665 Giovannucci, A., Badura, A., Deverett, B., Najafi, F., Pereira, T. D.,
1666 Gao, Z., Ozden, I., Kloth, A. D., Pnevmatikakis, E., Paninski, L.,
1667 De Zeeuw, C. I., Medina, J. F., & Wang, S. S.-H. (2017).

- 1668 Cerebellar granule cells acquire a widespread predictive feedback
1669 signal during motor learning. *Nature Neuroscience*, 20(5), 727–
1670 734. <https://doi.org/10.1038/nn.4531>
- 1671 Grün, S. (2009). Data-Driven Significance Estimation for Precise Spike
1672 Correlation. *Journal of Neurophysiology*, 101(3), 1126–1140.
1673 <https://doi.org/10.1152/jn.00093.2008>
- 1674 Gupta, A. S., van der Meer, M. A. A., Touretzky, D. S., & Redish, A. D.
1675 (2010). Hippocampal Replay Is Not a Simple Function of
1676 Experience. *Neuron*, 65(5), 695–705.
1677 <https://doi.org/https://doi.org/10.1016/j.neuron.2010.01.034>
- 1678 Hafting, T., Fyhn, M., Molden, S., Moser, M.-B., & Moser, E. I. (2005).
1679 Microstructure of a spatial map in the entorhinal cortex. *Nature*,
1680 436(7052), 801–806. <https://doi.org/10.1038/nature03721>
- 1681 Hamme, L. J. Van, & Wasserman, E. A. (1993). Cue Competition in
1682 Causality Judgments: The Role of Manner of Information
1683 Presentation. *Bulletin of the Psychonomic Society*, 31(5), 457–
1684 460. <https://doi.org/10.3758/bf03334962>
- 1685 Han, J.-H., Kushner, S. A., Yiu, A. P., Hsiang, H.-L. L., Buch, T.,
1686 Waisman, A., Bontempi, B., Neve, R. L., Frankland, P. W., &
1687 Josselyn, S. A. (2009). Selective erasure of a fear memory.
1688 *Science (New York, N.Y.)*, 323(5920), 1492–1496.
1689 <https://doi.org/10.1126/science.1164139>
- 1690 Hebb, D. O. (1949). The organization of behavior; a
1691 neuropsychological theory. In *The organization of behavior; a*
1692 *neuropsychological theory*. Wiley.
- 1693 Helmchen, F., & Denk, W. (2005). Deep tissue two-photon microscopy.
1694 2(12), 9. <https://doi.org/10.1038/nmeth818>
- 1695 Heys, J. G., Rangarajan, K. V., & Dombeck, D. A. (2014). The
1696 Functional Micro-organization of Grid Cells Revealed by Cellular-
1697 Resolution Imaging. *Neuron*, 84(5), 1079–1090.
1698 <https://doi.org/10.1016/j.neuron.2014.10.048>
- 1699 Hyde, R. A., & Strowbridge, B. W. (2012). Mnemonic representations
1700 of transient stimuli and temporal sequences in the rodent
1701 hippocampus in vitro. *Nature Neuroscience*, 15(10), 1430–1438.
1702 <https://doi.org/10.1038/nn.3208>
- 1703 Ikegaya, Y., Aaron, G., Cossart, R., Aronov, D., Lampl, I., Ferster, D.,
1704 & Yuste, R. (2004). Synfire chains and cortical songs: temporal
1705 modules of cortical activity. *Science (New York, N.Y.)*, 304(5670),
1706 559–564. <https://doi.org/10.1126/science.1093173>
- 1707 Itskov, V., Pastalkova, E., Mizuseki, K., Buzsaki, G., & Harris, K. D.
1708 (2008). Theta-mediated dynamics of spatial information in
1709 hippocampus. *The Journal of Neuroscience : The Official Journal*
1710 *of the Society for Neuroscience*, 28(23), 5959–5964.

- 1711 https://doi.org/10.1523/JNEUROSCI.5262-07.2008
1712 Jadhav, S. P., Kemere, C., German, P. W., & Frank, L. M. (2012).
1713 Awake hippocampal sharp-wave ripples support spatial memory.
1714 *Science (New York, N.Y.)*, 336(6087), 1454–1458.
1715 https://doi.org/10.1126/science.1217230
1716 Josselyn, S. A., & Tonegawa, S. (2020). Memory engrams: Recalling
1717 the past and imagining the future. *Science (New York, N.Y.)*,
1718 367(6473). https://doi.org/10.1126/science.aaw4325
1719 Jun, J. J., Steinmetz, N. A., Siegle, J. H., Denman, D. J., Bauza, M.,
1720 Barbarits, B., Lee, A. K., Anastassiou, C. A., Andrei, A., Aydin, Ç.,
1721 Barbic, M., Blanche, T. J., Bonin, V., Couto, J., Dutta, B., Gratiy,
1722 S. L., Gutnisky, D. A., Häusser, M., Karsh, B., ... Harris, T. D.
1723 (2017). Fully integrated silicon probes for high-density recording of
1724 neural activity. *Nature*, 551(7679), 232–236.
1725 https://doi.org/10.1038/nature24636
1726 Kalmbach, B. E., Davis, T., Ohyama, T., Riusech, F., Nores, W. L., &
1727 Mauk, M. D. (2010). Cerebellar Cortex Contributions to the
1728 Expression and Timing of Conditioned Eyelid Responses. *Journal
1729 of Neurophysiology*, 103(4), 2039–2049.
1730 https://doi.org/10.1152/jn.00033.2010
1731 Kalmbach, B. E., Ohyama, T., & Mauk, M. D. (2010). Temporal
1732 Patterns of Inputs to Cerebellum Necessary and Sufficient for
1733 Trace Eyelid Conditioning. *Journal of Neurophysiology*, 104(2),
1734 627–640. https://doi.org/10.1152/jn.00169.2010
1735 Khan, A. G., Parthasarathy, K., & Bhalla, U. S. (2010). Odor
1736 representations in the mammalian olfactory bulb. *Wiley
1737 Interdisciplinary Reviews. Systems Biology and Medicine*, 2(5),
1738 603–611. https://doi.org/10.1002/wsbm.85
1739 Kim, S., & Lee, I. (2012). The hippocampus is required for visually
1740 cued contextual response selection, but not for visual
1741 discrimination of contexts. *Frontiers in Behavioral Neuroscience*,
1742 6. https://doi.org/10.3389/fnbeh.2012.00066
1743 Kraus, B. J., Brandon, M. P., Robinson, R. J., Connerney, M. A.,
1744 Hasselmo, M. E., & Eichenbaum, H. (2015). During Running in
1745 Place, Grid Cells Integrate Elapsed Time and Distance Run.
1746 *Neuron*, 88(3), 578–589.
1747 https://doi.org/10.1016/j.neuron.2015.09.031
1748 Kraus, B., Robinson, R., White, J., Eichenbaum, H., & Hasselmo, M.
1749 (2013). Hippocampal “Time Cells”: Time versus Path Integration.
1750 *Neuron*, 78(6), 1090–1101.
1751 https://doi.org/10.1016/j.neuron.2013.04.015
1752 Kropff, E., Carmichael, J. E., Moser, M.-B., & Moser, E. I. (2015).
1753 Speed cells in the medial entorhinal cortex. *Nature*, 523(7561),

- 1754 419–424. <https://doi.org/10.1038/nature14622>
- 1755 Krupa, D., & Thompson, R. (2003). Inhibiting the Expression of a
1756 Classically Conditioned Behavior Prevents Its Extinction. *The
1757 Journal of Neuroscience : The Official Journal of the Society for
1758 Neuroscience*, 23, 10577–10584.
1759 <https://doi.org/10.1523/JNEUROSCI.23-33-10577.2003>
- 1760 Lever, C., Burton, S., Jeewajee, A., O'Keefe, J., & Burgess, N.
1761 (2009). Boundary Vector Cells in the Subiculum of the
1762 Hippocampal Formation. *The Journal of Neuroscience*, 29(31),
1763 9771 LP – 9777. <https://doi.org/10.1523/JNEUROSCI.1319-09.2009>
- 1764 Luo, L., Callaway, E. M., & Svoboda, K. (2018). Genetic Dissection of
1765 Neural Circuits: A Decade of Progress. *Neuron*, 98(2), 256–281.
1766 <https://doi.org/https://doi.org/10.1016/j.neuron.2018.03.040>
- 1767 MacDonald, C. J., Carrow, S., Place, R., & Eichenbaum, H. (2013).
1768 Distinct hippocampal time cell sequences represent odor
1769 memories in immobilized rats. *The Journal of Neuroscience : The
1770 Official Journal of the Society for Neuroscience*, 33(36), 14607–
1771 14616. <https://doi.org/10.1523/JNEUROSCI.1537-13.2013>
- 1772 MacDonald, C. J., Lepage, K. Q., Eden, U. T., & Eichenbaum, H.
1773 (2011). Hippocampal “time cells” bridge the gap in memory for
1774 discontiguous events. *Neuron*, 71(4), 737–749.
1775 <https://doi.org/10.1016/j.neuron.2011.07.012>
- 1776 Maruyama, R., Maeda, K., Moroda, H., Kato, I., Inoue, M., Miyakawa,
1777 H., & Aonishi, T. (2014). Detecting cells using non-negative matrix
1778 factorization on calcium imaging data. *Neural Networks : The
1779 Official Journal of the International Neural Network Society*, 55,
1780 11–19. <https://doi.org/10.1016/j.neunet.2014.03.007>
- 1781 Mau, W., Sullivan, D. W., Kinsky, N. R., Hasselmo, M. E., Howard, M.
1782 W., & Eichenbaum, H. (2018). The Same Hippocampal CA1
1783 Population Simultaneously Codes Temporal Information over
1784 Multiple Timescales. *Current Biology*, 28(10), 1499-1508.e4.
1785 <https://doi.org/10.1016/j.cub.2018.03.051>
- 1786 McLelland, D., & Paulsen, O. (2007). Cortical Songs Revisited: A
1787 Lesson in Statistics. *Neuron*, 53(3), 319–321.
1788 <https://doi.org/https://doi.org/10.1016/j.neuron.2007.01.020>
- 1789 McNaughton, N., & Gray, J. A. (2000). Anxiolytic action on the
1790 behavioural inhibition system implies multiple types of arousal
1791 contribute to anxiety. *Journal of Affective Disorders*, 61(3), 161–
1792 176. [https://doi.org/10.1016/s0165-0327\(00\)00344-x](https://doi.org/10.1016/s0165-0327(00)00344-x)
- 1793 Medina, J. F., Garcia, K. S., Nores, W. L., Taylor, N. M., & Mauk, M. D.
1794 (2000). Timing mechanisms in the cerebellum: testing predictions
1795 of a large-scale computer simulation. *The Journal of*
- 1796

- 1797 *Neuroscience : The Official Journal of the Society*
1798 *for Neuroscience*, 20(14), 5516–5525.
1799 <https://doi.org/10.1523/JNEUROSCI.20-14-05516.2000>
- 1800 Meeks, J. P., Arson, H. A., & Holy, T. E. (2010). Representation and
1801 transformation of sensory information in the mouse
1802 accessory olfactory system. *Nature Neuroscience*, 13(6), 723–
1803 730. <https://doi.org/10.1038/nn.2546>
- 1804 Miller, A. M. P., Jacob, A. D., Ramsaran, A. I., De Snoo, M. L.,
1805 Josselyn, S. A., & Frankland, P. W. (2023). Emergence of a
1806 predictive model in the hippocampus. *Neuron*.
1807 <https://doi.org/10.1016/j.neuron.2023.03.011>
- 1808 Modi, M. N., Dhawale, A. K., & Bhalla, U. S. (2014). CA1 cell activity
1809 sequences emerge after reorganization of network correlation
1810 structure during associative learning. *eLife*, 3, e01982–e01982.
1811 <https://doi.org/10.7554/eLife.01982>
- 1812 Mokeichev, A., Okun, M., Barak, O., Katz, Y., Ben-Shahar, O., &
1813 Lampl, I. (2007). Stochastic Emergence of Repeating Cortical
1814 Motifs in Spontaneous Membrane Potential Fluctuations In Vivo.
1815 *Neuron*, 53, 413–425.
1816 <https://doi.org/10.1016/j.neuron.2007.01.017>
- 1817 Mollinedo-Gajate, I., Song, C., & Knöpfel, T. (2021). Genetically
1818 Encoded Voltage Indicators. *Advances in Experimental Medicine*
1819 and Biology, 1293, 209–224. https://doi.org/10.1007/978-981-15-8763-4_12
- 1821 Morris, R. G. M., Garrud, P., Rawlins, J. N. P., & O'Keefe, J. (1982).
1822 Place navigation impaired in rats with hippocampal lesions.
1823 *Nature*, 297(5868), 681–683. <https://doi.org/10.1038/297681a0>
- 1824 Moscovitch, M., Cabeza, R., Winocur, G., & Nadel, L. (2016). Episodic
1825 Memory and Beyond: The Hippocampus and Neocortex in
1826 Transformation. *Annual Review of Psychology*, 67(1), 105–134.
1827 <https://doi.org/10.1146/annurev-psych-113011-143733>
- 1828 Moyer, J. R. J., Thompson, L. T., & Disterhoft, J. F. (1996). Trace
1829 eyeblink conditioning increases CA1 excitability in a transient
1830 and learning-specific manner. *The Journal of Neuroscience : The*
1831 *Official Journal of the Society for Neuroscience*, 16(17), 5536–
1832 5546. <https://doi.org/10.1523/JNEUROSCI.16-17-05536.1996>
- 1833 Mukamel, E. A., Nimmerjahn, A., & Schnitzer, M. J. (2009). Automated
1834 analysis of cellular signals from large-scale calcium imaging data.
1835 *Neuron*, 63(6), 747–760.
1836 <https://doi.org/10.1016/j.neuron.2009.08.009>
- 1837 Muller, R. U., & Kubie, J. L. (1989). The firing of hippocampal place
1838 cells predicts the future position of freely moving rats. *The Journal*
1839 *of Neuroscience : The Official Journal of the Society*

- 1840 for *Neuroscience*, 9(12), 4101–4110.
1841 <https://doi.org/10.1523/JNEUROSCI.09-12-04101.1989>
- 1842 Murray, T. A., & Levene, M. J. (2012). Singlet gradient index lens for
1843 deep in vivo multiphoton microscopy. *Journal of Biomedical
1844 Optics*, 17(2), 021106. <https://doi.org/10.1117/1.JBO.17.2.021106>
- 1845 Ohyama, T., Nores, W. L., Murphy, M., & Mauk, M. D. (2003). What
1846 the cerebellum computes. *Trends in Neurosciences*, 26(4), 222–
1847 227. [https://doi.org/10.1016/S0166-2236\(03\)00054-7](https://doi.org/10.1016/S0166-2236(03)00054-7)
- 1848 O'Keefe, J., & Burgess, N. (1996). Geometric determinants of the
1849 place fields of hippocampal neurons. *Nature*, 381(6581), 425–428.
1850 <https://doi.org/10.1038/381425a0>
- 1851 O'Keefe, J., & Dostrovsky, J. (1971). The hippocampus as a spatial
1852 map. Preliminary evidence from unit activity in the freely-moving
1853 rat. *Brain Research*, 34(1), 171–175. [https://doi.org/10.1016/0006-8993\(71\)90358-1](https://doi.org/10.1016/0006-8993(71)90358-1)
- 1855 O'Keefe, J., & Nadel, L. (1978). The Hippocampus as a Cognitive Map.
1856 In *Philosophical Studies* (Vol. 27).
1857 <https://doi.org/10.5840/philstudies19802725>
- 1858 O'Keefe, J., & Recce, M. L. (1993). Phase relationship between
1859 hippocampal place units and the EEG theta rhythm.
1860 *Hippocampus*, 3(3), 317–330.
1861 <https://doi.org/10.1002/hipo.450030307>
- 1862 Ozden, I., Lee, H. M., Sullivan, M. R., & Wang, S. S.-H. (2008).
1863 Identification and Clustering of Event Patterns From In Vivo
1864 Multiphoton Optical Recordings of Neuronal Ensembles. *Journal
1865 of Neurophysiology*, 100(1), 495–503.
1866 <https://doi.org/10.1152/jn.01310.2007>
- 1867 Pachitariu, M., Stringer, C., Dipoppa, M., Schröder, S., Rossi, L. F.,
1868 Dagleish, H., Carandini, M., & Harris, K. D. (2017). Suite2p:
1869 beyond 10,000 neurons with standard two-photon microscopy.
1870 *BioRxiv*, 61507. <https://doi.org/10.1101/061507>
- 1871 Paredes, R. M., Etzler, J. C., Watts, L. T., Zheng, W., & Lechleiter, J.
1872 D. (2008). Chemical calcium indicators. *Methods (San Diego,
1873 Calif.)*, 46(3), 143–151.
1874 <https://doi.org/10.1016/j.ymeth.2008.09.025>
- 1875 Pastalkova, E., Itskov, V., Amarasingham, A., & Buzsaki, G. (2008).
1876 Internally Generated Cell Assembly Sequences in the Rat
1877 Hippocampus. *Science*, 321(5894), 1322–1327.
1878 <https://doi.org/10.1126/science.1159775>
- 1879 Pavlov, I. P. (1927). Conditioned reflexes: an investigation of the
1880 physiological activity of the cerebral cortex. In *Conditioned
1881 reflexes: an investigation of the physiological activity of the
1882 cerebral cortex*. Oxford Univ. Press.

- 1883 Petersen, C. C. H. (2019). Sensorimotor processing in the rodent
1884 barrel cortex. *Nature Reviews. Neuroscience*, 20(9), 533–546.
1885 <https://doi.org/10.1038/s41583-019-0200-y>
- 1886 Pfeiffer, B. E., & Foster, D. J. (2013). Hippocampal place-cell
1887 sequences depict future paths to remembered goals. *Nature*,
1888 497(7447), 74–79. <https://doi.org/10.1038/nature12112>
- 1889 Pnevmatikakis, E. A., Soudry, D., Gao, Y., Machado, T. A., Merel, J.,
1890 Pfau, D., Reardon, T., Mu, Y., Lacefield, C., Yang, W., Ahrens, M.,
1891 Bruno, R., Jessell, T. M., Peterka, D. S., Yuste, R., & Paninski, L.
1892 (2016). Simultaneous Denoising, Deconvolution, and Demixing of
1893 Calcium Imaging Data. *Neuron*, 89(2), 285–299.
1894 <https://doi.org/https://doi.org/10.1016/j.neuron.2015.11.037>
- 1895 Poort, J., Khan, A. G., Pachitariu, M., Nemri, A., Orsolic, I., Krupic, J.,
1896 Bauza, M., Sahani, M., Keller, G. B., Mrsic-Flogel, T. D., & Hofer,
1897 S. B. (2015). Learning Enhances Sensory and Multiple Non-
1898 sensory Representations in Primary Visual Cortex. *Neuron*, 86(6),
1899 1478–1490. <https://doi.org/10.1016/j.neuron.2015.05.037>
- 1900 Poppenk, J., Evensmoen, H. R., Moscovitch, M., & Nadel, L. (2013).
1901 Long-axis specialization of the human hippocampus. *Trends in
1902 Cognitive Sciences*, 17(5), 230–240.
1903 <https://doi.org/10.1016/j.tics.2013.03.005>
- 1904 Pudil, P., & Novovičová, J. (1998). Novel Methods for Feature Subset
1905 Selection with Respect to Problem Knowledge. In H. Liu & H.
1906 Motoda (Eds.), *Feature Extraction, Construction and Selection: A
1907 Data Mining Perspective* (pp. 101–116). Springer US.
1908 https://doi.org/10.1007/978-1-4615-5725-8_7
- 1909 Ranck, J. B. (1973). Studies on single neurons in dorsal hippocampal
1910 formation and septum in unrestrained rats: Part I. Behavioral
1911 correlates and firing repertoires. *Experimental Neurology*, 41(2),
1912 462–531. [https://doi.org/https://doi.org/10.1016/0014-4886\(73\)90290-2](https://doi.org/https://doi.org/10.1016/0014-4886(73)90290-2)
- 1913 Rescorla, R. A., & Wagner, A. (1972). A theory of Pavlovian
1914 conditioning: Variations in the effectiveness of reinforcement and
1915 nonreinforcement. In *Classical Conditioning II: Current Research
1916 and Theory: Vol. Vol. 2*.
- 1917 Reyes, A. D. (2003). Synchrony-dependent propagation of firing rate in
1918 iteratively constructed networks in vitro. *Nature Neuroscience*,
1919 6(6), 593–599. <https://doi.org/10.1038/nn1056>
- 1920 Robbins, M., Christensen, C. N., Kaminski, C. F., & Zlatic, M. (2021).
1921 Calcium imaging analysis - how far have we come?
1922 *F1000Research*, 10, 258.
- 1923 Rogerson, T., Cai, D. J., Frank, A., Sano, Y., Shobe, J., Lopez-Aranda,
1924 M. F., & Silva, A. J. (2014). Synaptic tagging during memory

- 1926 allocation. *Nature Reviews. Neuroscience*, 15(3), 157–169.
1927 <https://doi.org/10.1038/nrn3667>
- 1928 Savelli, F., Yoganarasimha, D., & Knierim, J. J. (2008). Influence of
1929 boundary removal on the spatial representations of the
1930 medial entorhinal cortex. *Hippocampus*, 18(12), 1270–1282.
1931 <https://doi.org/10.1002/hipo.20511>
- 1932 Scoville, W. B., & Milner, B. (1957). Loss of recent memory after
1933 bilateral hippocampal lesions. In *Journal of Neurology,*
1934 *Neurosurgery & Psychiatry* (Vol. 20, pp. 11–21). BMJ Publishing
1935 Group. <https://doi.org/10.1136/jnnp.20.1.11>
- 1936 Shannon, C. E. (1948). A Mathematical Theory of Communication. *Bell
1937 System Technical Journal*, 27(3), 379–423.
1938 <https://doi.org/https://doi.org/10.1002/j.1538-7305.1948.tb01338.x>
- 1939 Siegel, J. J., & Mauk, M. D. (2013). Persistent Activity in Prefrontal
1940 Cortex during Trace Eyelid Conditioning: Dissociating Responses
1941 That Reflect Cerebellar Output from Those That Do Not. *The
1942 Journal of Neuroscience*, 33(38), 15272 LP – 15284.
1943 <https://doi.org/10.1523/JNEUROSCI.1238-13.2013>
- 1944 Siegel, J. J., Taylor, W., Gray, R., Kalmbach, B., Zemelman, B. V.,
1945 Desai, N. S., Johnston, D., & Chitwood, R. A. (2015). Trace
1946 Eyeblink Conditioning in Mice Is Dependent upon the Dorsal
1947 Medial Prefrontal Cortex, Cerebellum, and Amygdala: Behavioral
1948 Characterization and Functional Circuitry. *ENeuro*, 2(4),
1949 ENEURO.0051-14.2015. <https://doi.org/10.1523/ENEURO.0051-14.2015>
- 1950 Silva, A. J., Zhou, Y., Rogerson, T., Shobe, J., & Balaji, J. (2009).
1951 Molecular and cellular approaches to memory allocation in neural
1952 circuits. *Science (New York, N.Y.)*, 326(5951), 391–395.
1953 <https://doi.org/10.1126/science.1174519>
- 1954 Skaggs, W., McNaughton, B., Gothard, K., & Markus, E. (1996). An
1955 Information-Theoretic Approach to Deciphering the Hippocampal
1956 Code. *Neural Inf. Process Syst.*, 5.
- 1957 Solstad, T., Boccara, C. N., Kropff, E., Moser, M.-B., & Moser, E. I.
1958 (2008). Representation of Geometric Borders in the Entorhinal
1959 Cortex. *Science*, 322(5909), 1865–1868.
1960 <https://doi.org/10.1126/science.1166466>
- 1961 Souza, B. C., Pavão, R., Belchior, H., & Tort, A. B. L. (2018). On
1962 Information Metrics for Spatial Coding. *Neuroscience*, 375, 62–73.
1963 <https://doi.org/10.1016/j.neuroscience.2018.01.066>
- 1964 Stosiek, C., Garaschuk, O., Holthoff, K., & Konnerth, A. (2003). In vivo
1965 two-photon calcium imaging of neuronal networks. *Proceedings of
1966 the National Academy of Sciences of the United States of
1967 America*, 100(12), 7319–7324.
- 1968

- 1969 https://doi.org/10.1073/pnas.1232232100

1970 Takehara, K., Kawahara, S., Takatsuki, K., & Kirino, Y. (2002). Time-
1971 limited role of the hippocampus in the memory for trace eyeblink
1972 conditioning in mice. *Brain Research*, 951(2), 183–190.
1973 https://doi.org/10.1016/s0006-8993(02)03159-1

1974 Tao, S., Wang, Y., Peng, J., Zhao, Y., He, X., Yu, X., Liu, Q., Jin, S., &
1975 Xu, F. (2021). Whole-Brain Mapping the Direct Inputs of Dorsal
1976 and Ventral CA1 Projection Neurons. *Frontiers in Neural Circuits*,
1977 15. https://doi.org/10.3389/fncir.2021.643230

1978 Taube, J. S., Muller, R. U., & Ranck, J. B. J. (1990). Head-direction
1979 cells recorded from the postsubiculum in freely moving rats.
1980 I. Description and quantitative analysis. *The Journal of
1981 Neuroscience : The Official Journal of the Society
1982 for Neuroscience*, 10(2), 420–435.
1983 https://doi.org/10.1523/JNEUROSCI.10-02-00420.1990

1984 Thompson, R. F. (2004). In Search of Memory Traces. *Annual Review
1985 of Psychology*, 56(1), 1–23.
1986 https://doi.org/10.1146/annurev.psych.56.091103.070239

1987 Tishby, N., Pereira, F. C., & Bialek, W. (1999). The information
1988 bottleneck method. *Proc. of the 37-Th Annual Allerton Conference
1989 on Communication, Control and Computing*, 368–377.
1990 https://arxiv.org/abs/physics/0004057

1991 Valero, M., Cid, E., Averkin, R. G., Aguilar, J., Sanchez-Aguilera, A.,
1992 Viney, T. J., Gomez-Dominguez, D., Bellistri, E., & de la Prida, L.
1993 M. (2015). Determinants of different deep and superficial CA1
1994 pyramidal cell dynamics during sharp-wave ripples. *Nature
1995 Neuroscience*. https://doi.org/10.1038/nn.4074

1996 van der Maaten, L., Postma, E., & van den Herik, H. (2009).
1997 Dimensionality reduction: a comparative review. *Journal of
1998 Machine Learning Research*, 66–71.

1999 Velasco, M. G. M., & Levene, M. J. (2014). In vivo two-photon
2000 microscopy of the hippocampus using glass plugs. *Biomedical
2001 Optics Express*, 5(6), 1700–1708.
2002 https://doi.org/10.1364/BOE.5.001700

2003 Voelcker, B., Pancholi, R., & Peron, S. (2022). Transformation of
2004 primary sensory cortical representations from layer 4 to layer 2.
2005 *Nature Communications*, 13(1), 5484.
2006 https://doi.org/10.1038/s41467-022-33249-1

2007 Wood, E. R., Dudchenko, P. A., Robitsek, R. J., & Eichenbaum, H.
2008 (2000). Hippocampal Neurons Encode Information about Different
2009 Types of Memory Episodes Occurring in the Same Location.
2010 *Neuron*, 27(3), 623–633.
2011 https://doi.org/https://doi.org/10.1016/S0896-6273(00)00071-4

- 2012 Yiu, A. P., Mercaldo, V., Yan, C., Richards, B., Rashid, A. J., Hsiang, H.-L. L., Pressey, J., Mahadevan, V., Tran, M. M., Kushner, S. A.,
- 2013 Woodin, M. A., Frankland, P. W., & Josselyn, S. A. (2014). Neurons are recruited to a memory trace based on relative neuronal excitability immediately before training. *Neuron*, 83(3), 722–735. <https://doi.org/10.1016/j.neuron.2014.07.017>
- 2018 Zhou, Y., Won, J., Karlsson, M. G., Zhou, M., Rogerson, T., Balaji, J., Neve, R., Poirazi, P., & Silva, A. J. (2009). CREB regulates excitability and the allocation of memory to subsets of neurons in the amygdala. *Nature Neuroscience*, 12(11), 1438–1443. <https://doi.org/10.1038/nn.2405>
- 2023 Ziv, Y., Burns, L. D., Cocker, E. D., Hamel, E. O., Ghosh, K. K., Kitch, L. J., El Gamal, A., & Schnitzer, M. J. (2013). Long-term dynamics of CA1 hippocampal place codes. *Nature Neuroscience*, 16(3), 264–266. <https://doi.org/10.1038/nn.3329>
- 2027

2028 **Chapter 2 – Behaviour**

2029

2030 **Towards understanding brain activity in a**

2031 **reproducible context**

2032

2033 Our understanding of memory and learning depends upon the type of
2034 learning that is studied (Schreurs, 1989). Two important categories of
2035 memory and learning experiments are,

- 2036 1. Non-associative (Habituation and Sensitization), and
- 2037 2. Associative learning (Classical and Operant Conditioning).

2038

2039 Non-associative learning paradigms provide information about how an
2040 organism responds to repeated presentations of a single stimulus
2041 (Brown, 1998). However, it was of interest to us to study how animals
2042 responded to a number of events and stimuli being associated, and
2043 how the activity of the brain relates to this. **Multi-modal stimulus**
2044 **integration is typical of the sensory experience. We felt it interesting to**
2045 **study how animals learnt to associate each stimulus modality,**
2046 **individually, given no clear *a priori* reason to assume that the**
2047 **physiological response would be identical for each.** Hence, we chose
2048 to design our experiments to incorporate associative learning, which is
2049 a relatively permanent change in behaviour that results from the
2050 temporal conjunction of two or more events or stimuli.

2051

2052 Empirically, reproducible behaviour depends on strong associations
2053 between the events or stimuli being paired, and may often require

2054 many repeated pairings or trials. Additionally, having the animal
2055 engage in the behavioural task and pay attention to the stimuli being
2056 presented, is crucial to look for important correlations between the
2057 experiment conditions (external) and brain activity (internal).
2058

2059 Anaesthetized animals have been previously used to study brain
2060 activity and led to important discoveries, e.g. - visual representation of
2061 moving bars in the visual cortex (Hubel & Wiesel, 1962), habituation in
2062 the Hippocampus (Deshmukh & Bhalla, 2003). However, it was clear
2063 that similar experiments repeated in awake animals did not result in the
2064 same observations. Indeed, animals needed to navigate a known
2065 environment before the discovery of place cells (O'Keefe &
2066 Dostrovsky, 1971), grid cells (Fyhn et al., 2004; Hafting et al., 2005),
2067 and head-direction cells (Ranck, 1973; Taube et al., 1990), among
2068 others, could be made. **We chose to avoid anaesthetized animals for**
2069 **the experiments described in this thesis. It is unclear if deep states of**
2070 **anaesthesia are also conducive to time cell sequence activation.**

2071

2072 The reliability of the overt behavioural responses of the experiment
2073 animals then sets the conditions and parameter list to study physiology
2074 within the confines of reproducible behavioural contexts, and was
2075 considered an important mandate for the standardization of any of the
2076 behavioural tasks described in this chapter. Under the umbrella of
2077 associative learning, we began our experiments with various protocols
2078 related to operant conditioning wherein the reinforcing signal for
2079 learning was a water reward to correctly timed licks. As will be
2080 discussed in the next few sections, we later switched to aversive
2081 conditioning with Trace Eye-Blink Conditioning.

2082 **Operant conditioning [Project I]**

2083

2084 Operant conditioning is both the procedure and a type of associative
2085 learning process through which the strength of a voluntarily performed
2086 behaviour is modified positively (appetitively) by reward (water,
2087 sucrose, food, etc.), or negatively (aversively) by punishment (air-puff
2088 to the eye, electrical shocks, etc.). For example, if the animal responds
2089 to a presented stimulus by performing a lick onto a water spout, then a
2090 water reward would strengthen the behaviour while Lithium Chloride
2091 solution (which is aversive) would weaken it.

2092

2093 We now describe our experiments and results with regard to operant
2094 conditioning, in more detail.

2095

2096 **Required features**

2097

2098 For Project I, the goal was to study how the association of a neutral
2099 stimulus with a water reward modified the neurophysiological activity of
2100 the hippocampal CA1. **We aimed to more systematically study time**
2101 cells with the granularity of well-defined associative learning and ms
2102 resolution, high-yield (~100-150) CA1 recordings using 2-photon
2103 imaging. We believe this is why there is still insufficient clarity on the
2104 network level responses in the CA1, *in vivo*, especially during early
2105 learning of associated stimuli, *i.e.*, behavioural acquisition. We outline
2106 our set of core objectives required as features for the behavioural task:
2107 1. An assortment of different stimuli and modalities (light, tone, etc.)
2108 to be presented to the animal.

2109 2. The animal must withhold any motor movement during the
2110 presentation of the stimuli, to study pure stimulus responses.

2111 3. The animal must perform a lick for a water reward after the end of
2112 the stimulus presentation.

2113 4. The animal must be able to make the association between stimuli
2114 and water reward within 7-14 days of training (given technical
2115 limitations of chronic recording from tissue).

2116

2117 The behavioural state of the animal, in terms of anxiety, motivation,
2118 attention, etc., may be variable when a naïve animal is presented with
2119 different stimuli. This may cause a large variability in the activity of
2120 cells, since the animal may not be paying attention to it. Also, if the
2121 animal were rewarded for performing the task it is expected that there
2122 would be motivation to pay attention to the stimuli presented. Finally,
2123 such a task would involve the animal associating the stimuli that it is
2124 trained to with a behavioural task and this would provide an apt context
2125 to study association related changes in stimulus responses.

2126

2127 In **the following** sections, we discuss some important protocols that we
2128 tried and tested and a list of the various kinds of behavioural tasks we
2129 employed for head-fixed mice.

2130

2131 For Project I, we tried several variations of operant conditioning
2132 including Stimulus Detection tasks, Delayed Non-Match to Sample
2133 (DNMS), as well as Go/No-Go tasks. Each of these tasks requires
2134 animals to perform licks to the Conditioned Stimuli and for them to be
2135 rewarded (2-3 µL water) or punished based on the task demands and
2136 protocol design.

2137 **Water delivery and calibration**

2138 The lick port was made from a trimmed and smoothed 16 gauge
2139 syringe, connected to a water reservoir with small diameter tubing. A
2140 solenoid valve clamped onto this tubing, gated by a 12V DC signal.
2141 When this gate was opened, the volume of water could be regulated by
2142 the duration of the 12V DC signal. We calibrated the duration of gate
2143 opening to achieve ~2 μ L per pulse or spurt (Jaramillo & Zador, 2014).
2144 The weight of 100 spurts was measured and then divided by 100 to get
2145 the weight of 1 spurt. 65 ms was found corresponding to 2.5 μ L (this
2146 value is going to be used for behaviour). In the figure below (Figure 2),
2147 the measured volumes/weights are plotted as blue filled diamonds,
2148 error bars are presented as Standard Error and the linear trendline is
2149 shown in black.

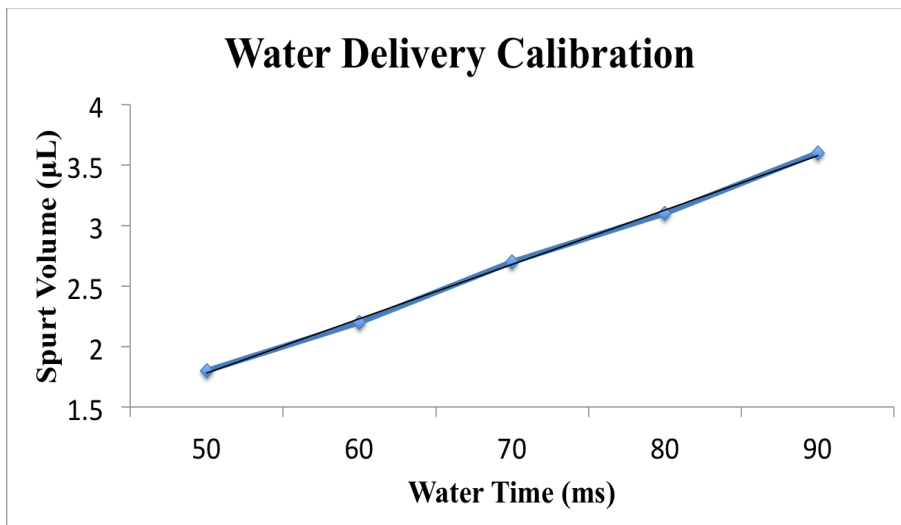


Figure 2: Water delivery calibration to reward the animal consistently with the same volume of water

2150 **Opto-isolator circuit for solenoid control**

2151

2152 To be able to programmatically control the 12V DC line to the solenoid
2153 valve, we used the following circuit (Figure 3), which accepted a 5V
2154 digital input from the DAQ (NI USB-6001) interfacing the lab computer
2155 to the behaviour rig.

2156

2157 **Parts list**

- 2158 1. 470 ohm resistor
- 2159 2. 15 kohm resistor
- 2160 3. MCT2e
- 2161 4. ULN2003
- 2162 5. Bases (adaptors for MCT2e and ULN2003)
- 2163 6. +5V and +12V DC inputs from a Power Supply)
- 2164 7. Source of +5V DC input (DAQ, etc.)
- 2165 8. Connecting wires
- 2166 9. Load Resistance (Solenoid, etc.)

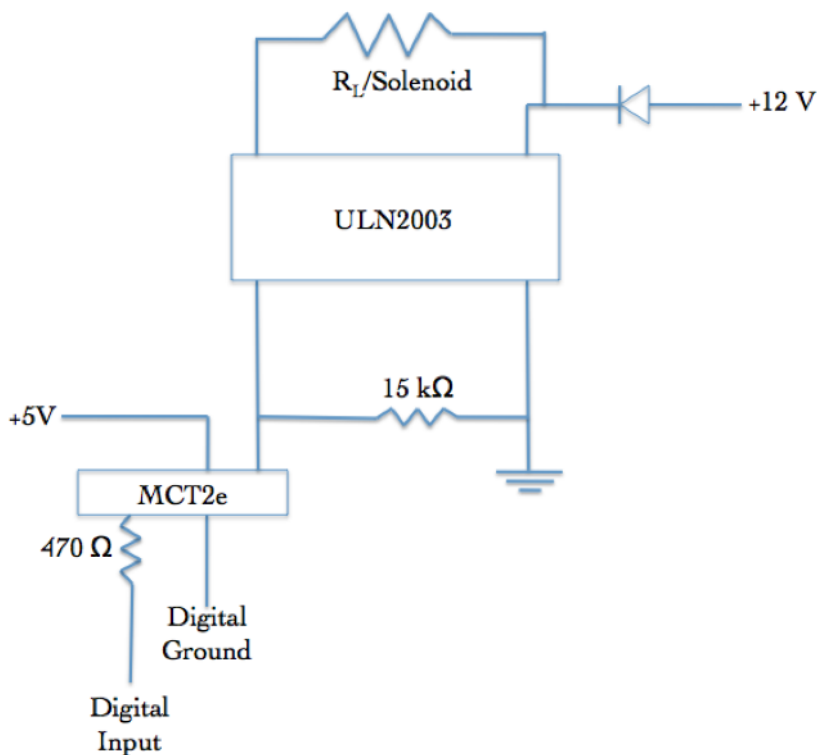


Figure 3: Optoisolator circuit to amplify +5V DC input to +12V DC output.

2168

2169 **Lick detection circuit**

2170

2171 To be able to monitor the presence or absence of licks to the port, the
 2172 conductive part (metal) of the lick port syringe was connected to a
 2173 MOSFET such that a 5V DC voltage could be read out, whenever the
 2174 animal would make contact with the port. This was designed as a
 2175 readout to Stimulus Detection by the animal. The circuit diagram is
 2176 shown below (Figure 4):

2177

2178 **Parts list**

2179 1. +5V Power Supply

2180 2. 4.7 kohm resistor
2181 3. 22 Mohm resistor
2182 4. IN4007 Diode
2183 5. NPN Transistor IRF540N (MOSFET)
2184

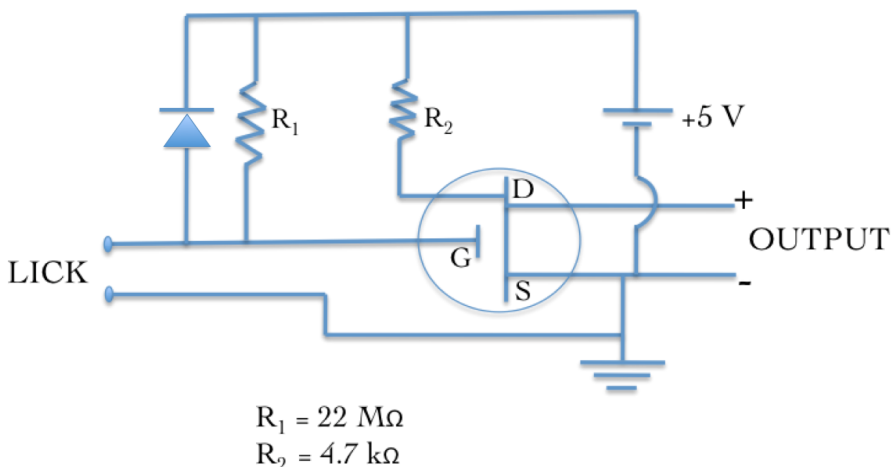


Figure 4: Lick detector circuit based on a MOSFET design.
Whenever the animal performed a lick, a +5V DC Output would be read out.

2186 Controlling task details and protocol information

2187
2188 All protocols were controlled using custom scripts written in NI
2189 LabVIEW 8. These scripts were run on a lab desktop which interfaced
2190 with the DAQ (NI USB-6001) via USB. The DAQ,
2191 1. Sent the 5V digital input to switch on the solenoid valve
2192 regulating water delivery, and
2193 2. Received the 5V digital output of the lick detection circuit
2194 whenever a lick was produced by the animal.
2195

2196 **Head-bar implant, Animal Handling, and Water**
2197 **deprivation**

2198

2199 All experiments were planned to be conducted on head-fixed C57Bl/6
2200 mice, with the eventual intention to perform in vivo imaging on these
2201 animals. For this, we surgically implanted metal head-bars on the skull
2202 of the animals while they were maintained on 1-2% Isoflurane, above a
2203 heating pad (35°C). Surgeries would last no longer than 30 mins per
2204 animal.

2205

2206 After 1-7 days of recovery after surgery, we handled the animals gently
2207 for 2 days till the animals would appear comfortable with lifting and
2208 gentle collar grabbing. Next, for 3-4 days, we kept the animals head-
2209 clamped. We restricted our animals to ~1ml of water per day, keeping
2210 check that their body weight did not fall to below 80% of the weight on
2211 day 1.

2212

2213 **PROTOCOL 1.1: Stimulus Detection Task**

2214

2215 We first tried the simplest version of the lick task wherein an auditory
2216 tone was followed by a water reward. The animal would have to
2217 withhold licking till the end of the stimulus presentation, and then
2218 perform the lick for the reward (Figure 5).

2219

2220 **Total number of trials:** 600/session; 1 session/day

2221 **Trial phases:**

2222 1. Stimulus free pre-tone (PT): 1 s

- 2223 2. Tone: 5 kHz for 1 s
2224 3. Critical timeout (CT): 100 ms
2225 4. Inter-trial Interval (ITI): randomized between 2 s to 5
2226



Figure 5: Typical trial structure with the various phases. Each trial was followed by a randomized Inter-Trial Interval (ITI).

2231

- 2232 Only licks during the critical timeout (CT) phase immediately after the
2233 Tone phase were rewarded while licks in other phases resulted in a
2234 phase restart. **No aversive stimuli were presented in this particular
2235 protocol.**

2236

2237 **PROTOCOL 1.2: Stimulus Detection Task with aversive
2238 punishment**

2239

2240 **Total number of trials:** 600/session; 1 session/day

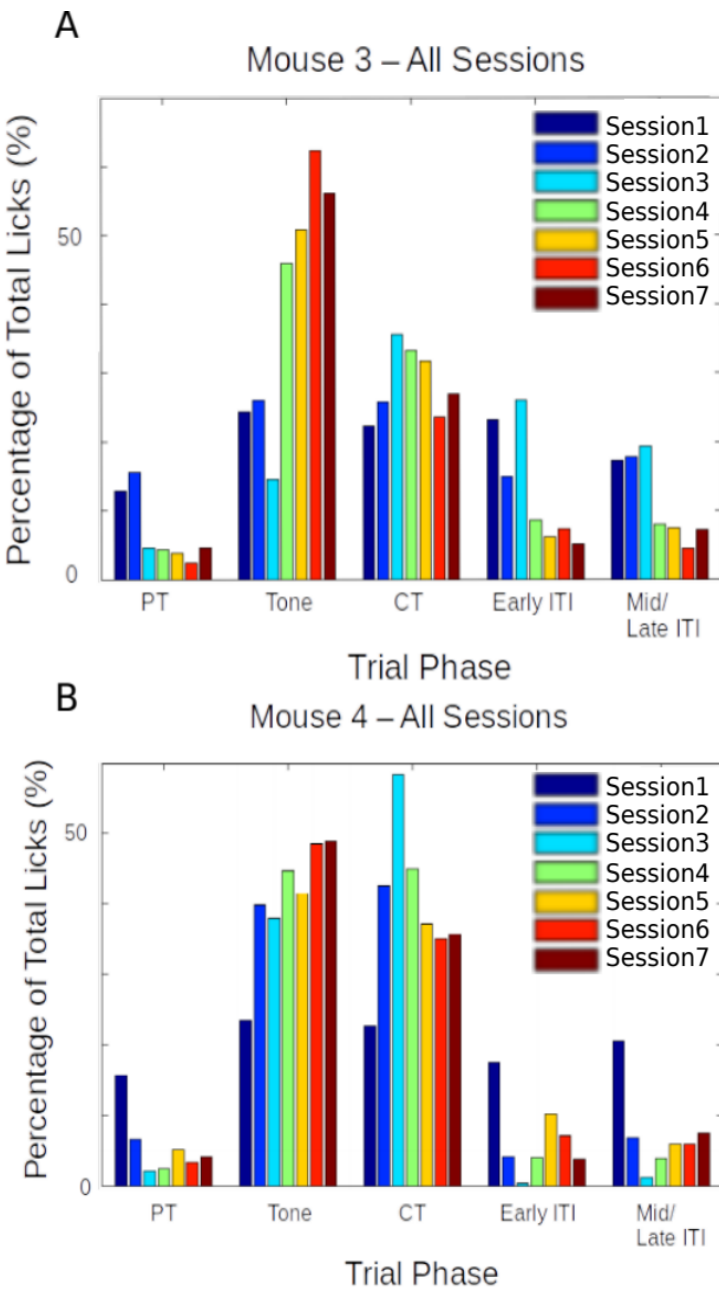


Figure 6: Performance evaluation for two example mice trained to Protocol 1.1 and 1.2. Percentage of total licks in the various trial phases (Pre-Tone, Tone, CT, and ITI), across all sessions of training (coloured bar plots) for A) Mouse 3, and B) Mouse

2245 Only licks during the critical timeout (CT) phase immediately after the
2246 Tone phase were rewarded while licks in other phases resulted in an
2247 aversive punishment, *viz.*, 100 ms air-puff to the body of the animal,
2248 before a phase restart. For Mouse 3 we started Protocol 1.2 from
2249 Session 3 while for Mouse 4 we started Protocol 1.2 from Session 2.

2250 **Results – Protocol 1.1 and 1.2**

2251
2252 The behavioural performance for each of the experiment animals was
2253 evaluated using custom analysis scripts written in MATLAB 2011. Here
2254 are the results from two mice trained based on Protocols 1.1 and 1.2
2255 (Figure 6). In both the examples shown, animals would typically
2256 produce a great percentage of total licks even during the Tone period.
2257 **Each animal was presented with 600 training trials/day (1 session/day).**
2258 **The inability to behaviourally discriminate or withhold incorrect or**
2259 **unrewarded licks even for 7-14 sessions, was considered and the task**
2260 **was ultimately unsuccessful.**

2261
2262 **Total animals trained:** 2
2263 **Conclusion:** Fail
2264

2265 **Protocol 2: Stimulus Detection task with timeout box**

2266
2267 We also tried the same Stimulus Detection protocol, without an air-puff
2268 punishment, but with incorrect licks punished by a trial abort and a
2269 stimulus-free timeout phase, which the animal could escape from if it
2270 withheld licking. We decided to train the animals in blocks, each with a
2271 specific goal that the animal had to achieve.

2272

2273 **Trial phases:**

2274 1 Stimulus-free pre-tone (PT): 1 s

2275 2 Tone: 5 kHz for a variable duration (based on Block)

2276 3 Critical timeout (CT): 1000 ms

2277 4 Inter-trial Interval (ITI): randomized between 2 s to 5 s

2278

2279 Only licks during the critical timeout (CT) phase immediately after the

2280 Tone phase were rewarded while licks in other phases resulted in a

2281 phase restart.

2282

2283 **Block 1:** Unconditional Water to get the animal to associate the tone

2284 - ~20 trials

2285 - 100 or 200 ms Tone duration

2286 - Unconditional water provided at the end of the tone, irrespective of

2287 lick

2288

2289 **Block 2:** Conditional Water to get the animal to learn that licking

2290 with/after tone is going to be rewarded

2291 - 100 or 200 ms Tone duration

2292 - 1000 ms Reward phase

2293 - Lick during/after tone (Reward phase) = reward

2294 - No lick = no reward

2295 - Lick during pre-tone = no reward/abortion of trial

2296 - Lick during ITI = no reward/abortion of trial

2297 - Animals graduate to the next Block of training only after achieving at

2298 least 70-80% success rates

2299

2300 **Block 3:** Training the animal to learn "when" to lick

2301 - 1000 ms pre-tone, 100 or 200 ms Tone, 1000 ms Reward phase, 3-5
2302 s randomized ITI
2303 - Lick during Reward phase = reward
2304 - Any lick during the pre-tone or the tone, aborts the trial and sends the
2305 program to a Timeout phase (lasting, 2-3 s)
2306 - The timeout phase ends only when there is a 2-3 s (specified) interval
2307 of no licking
2308 - If the timeout phase ends, a new trial begins
2309 - Licks during ITI are also "punished" accordingly
2310 - Animals graduate to the next Block of training only after achieving 70-
2311 80% success rates
2312
2313 **Block 4:** Same as Block 3, but with a gradually increasing tone
2314 duration in steps of 50/100 ms
2315 - The tone duration is gradually increased, the increase being tailored
2316 to the performance of the animal
2317 - It will be attempted to get the animals to learn to wait for 500-700 ms
2318 - Animals graduate to the next Block of the experiment only after
2319 achieving 70-80% success rates

2320

2321 **Results – Protocol 2**

2322
2323 The behavioural performance for each of the experiment animals was
2324 evaluated using custom analysis scripts written in MATLAB. Here are
2325 two representative examples of mice trained based on Protocol 2 –
2326 Block 3 (Figure 7).

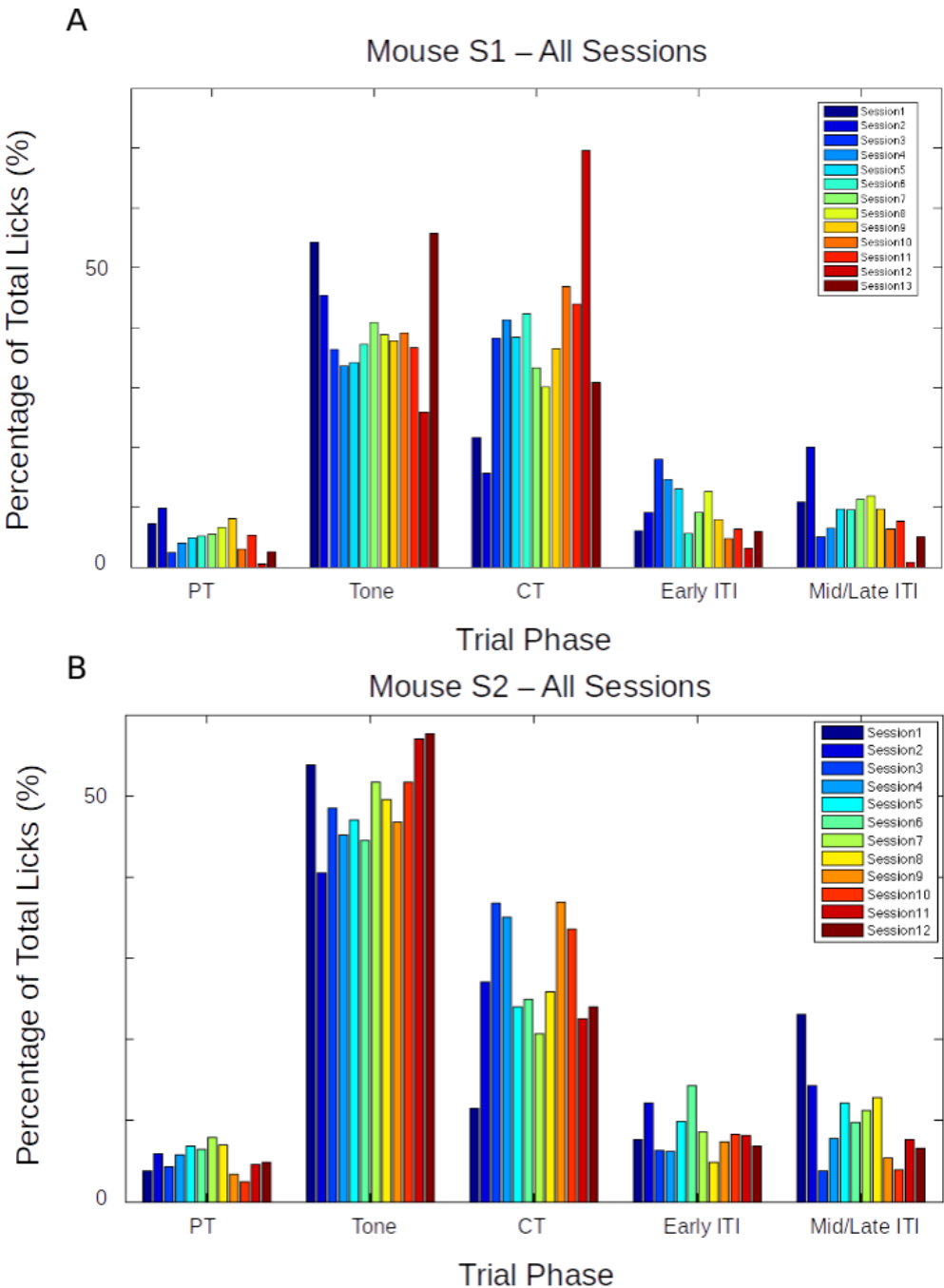


Figure 7: Performance evaluation for two example mice trained to Protocol 2. Percentage of total licks in the various trial phases (Pre-Tone, Tone, CT, and ITI), across all sessions of training (coloured bar plots), for (A) Mouse S1, and (B) Mouse S2.

2328 Again, as is clear from the examples above, that while the mice
2329 eventually produced a decent percentage of total licks in the critical
2330 timeout (CT) phase to get a water reward, they did not learn to
2331 withhold licks during the Tone phase, even after >10 sessions. The
2332 task was ultimately unsuccessful.

2333

2334 **Total animals trained:** 4

2335 **Conclusion:** Fail

2336

2337 **Protocol 3: Delayed Non-Match to Sample (DNMS)**

2338

2339 Delayed Non-Match to Sample (DNMS) is a task that is ideally suited
2340 to study working memory and recognition (Chudasama, 2010), but we
2341 decided to try it. This task involves trial-by-trial presentation of two
2342 stimuli separated by a stimulus-free delay interval. For any given trial,
2343 If the two pseudorandomly chosen pairs of stimuli were identical, then
2344 licks would not be rewarded. However, if the pair of stimuli were
2345 different, then licks would be rewarded with 2 μ L water.

2346

2347 We referenced previously published protocols (Jaramillo & Zador,
2348 2014) for their selection of auditory tone frequencies (3 kHz - 16.3 kHz)
2349 to select frequencies in the audible range. We had designed the
2350 experiment in such a way that the animal could behaviourally express
2351 a response to the perception of the various stimuli presented, as well
2352 as having learnt the overall task. We tried to incorporate more tones, in
2353 the hope that this may improve the chances of the animals focusing on
2354 the task specifics, instead of producing licks to just any stimulus.

2355

2356 **Tones used:** 6000 Hz, 8500 Hz, 10000 Hz, and 11500 Hz

2357 **Trial phases:**

2358 1. Pre-Tone duration (ms): 1000 ms

2359 2. CS 1 duration (ms): 350 ms

2360 3. Delay Interval duration (ms): 250 ms

2361 4. CS 2 duration (ms): 350 ms (unless a correct lick is
2362 elicited)

2363 5. ITI duration (s): randomized from 1 s to 3 s

2364 **Punishment:** Timeout Box (minimum of 3s of no licks to escape)

2365 **Reward:** 2 µL of water

2366

2367 **Results – Protocol 3**

2368

2369 >70-80% of the trials had to be aborted because the animals would not
2370 withhold licking after the 1st of the pair of tones was presented. This
2371 did not change even after 7 days (sessions) of training.

2372

2373 **Total animals trained:** 6

2374 **Conclusion:** Fail

2375

2376 **Protocol 4: Go/No-Go Task**

2377

2378 In an attempt to simplify the behavioural task, we decided to
2379 reconfigure the DNMS task to a simpler Go/No-Go task. Here, we
2380 would again present the animal with two stimuli, but with the only

2381 condition being that the animal would have to lick after the second
2382 stimulus, and not before. This simplifies the behaviour to a certain
2383 extent, because the animals need only use the first stimulus as a cue
2384 for the second. Failure to perform this task could more easily then be
2385 attributed to a lack of attention in that trial. Only the data from the trials
2386 where the animal succeeds to do the task would be considered for
2387 analysis. Training related changes in actual stimulus representations
2388 would be carefully dissected out. Furthermore, such a task would
2389 control for the behavioural state of the animal and help provide
2390 important datasets.

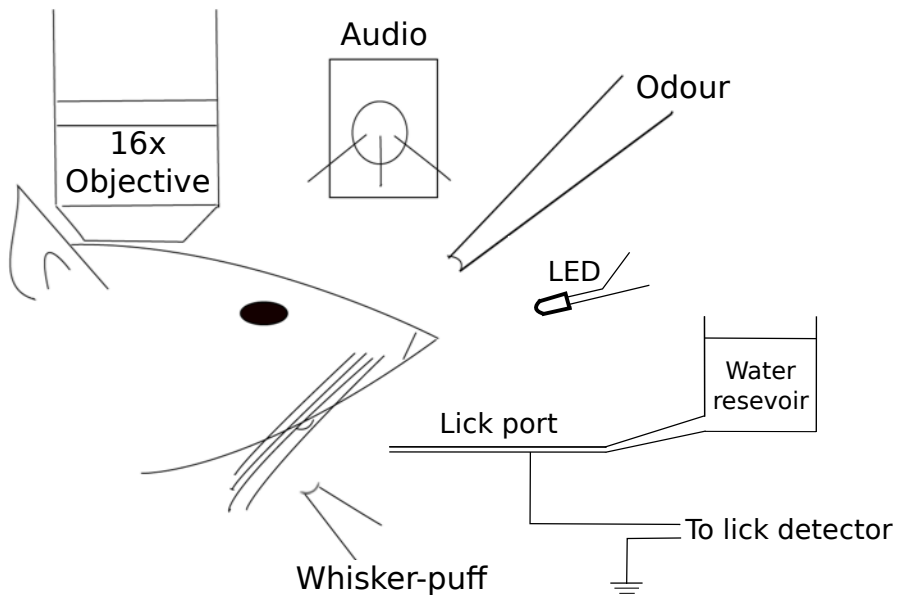


Figure 8: Schematic representation of the experimental setup for a simple detection task where the animal must perform a lick upon correctly detecting the presence of the conditioned stimulus (CS; from a range of modalities).

2395 In terms of imaging, we hoped to use the no-go stimulus to record a
2396 clean stimulus response without the possible contamination of
2397 movement (licking behaviour), and the go stimulus to verify attention
2398 (Figure 8).
2399 Trials were designed to go through the following phases and have the
2400 animal graduate to subsequent phases, only after correctly performing
2401 the behaviour:
2402 1. Pre-tone: Stimulus-free period; no lick
2403 2. No-go tone: 7kHz tone period; no lick
2404 3. Go tone: 10kHz tone period; lick for reward
2405 If the animal would perform an incorrect lick, the particular phase
2406 currently occurring was restarted. Only licks to the Go tone were
2407 rewarded (Figure 9).

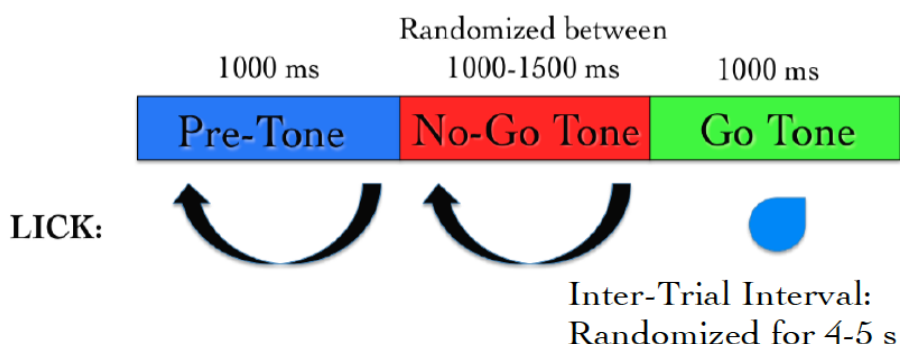


Figure 9: Typical trial structure with the various phases and lick dependent relationships.

2408

2409 **Results – Protocol 4**

2410

2411 The behavioural performance improves only after ~3-4 sessions of
2412 training (Figure 10A). This is primarily due to an increase in the
2413 percentage of trials with a correct Go tone lick, as shown (Figure 10B).

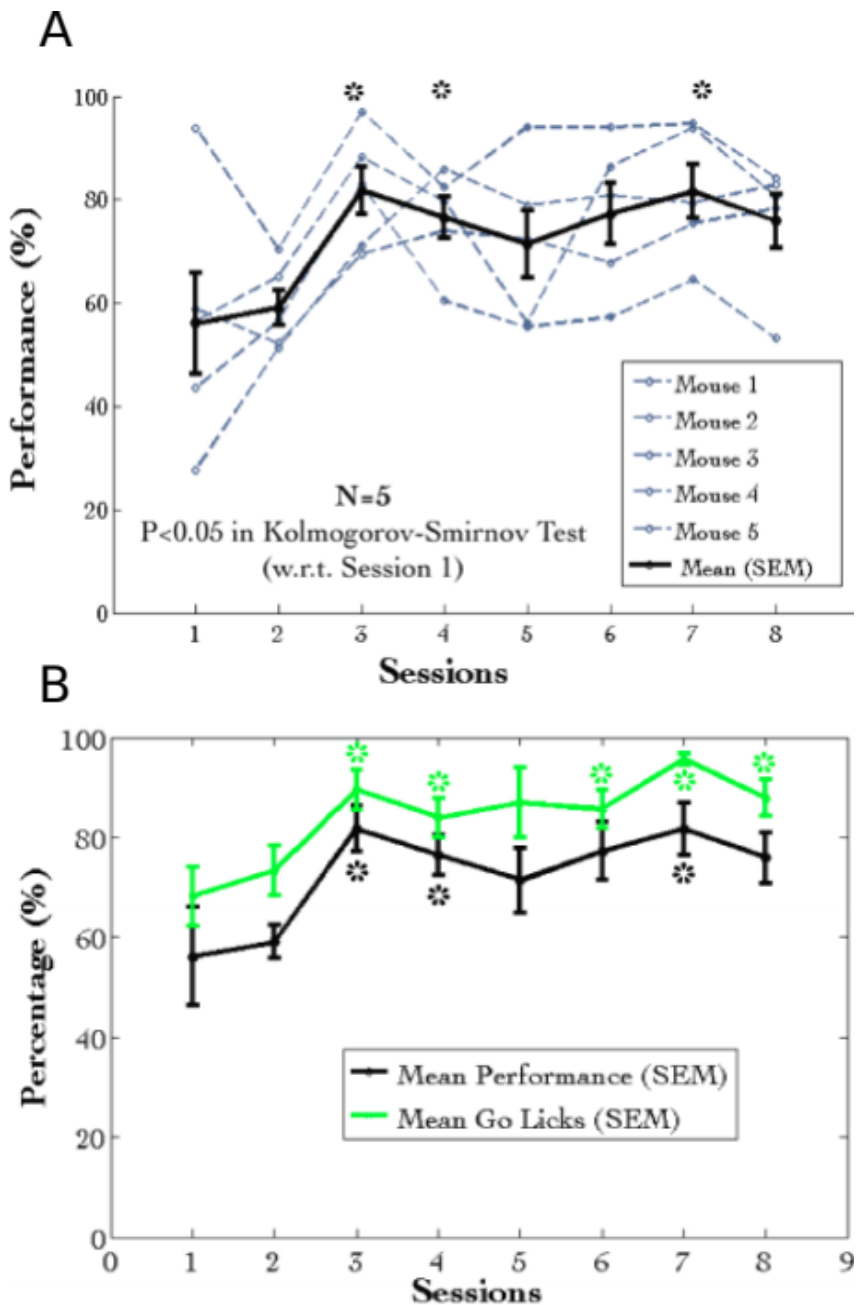


Figure 10: (A) Performance traces for all the animals individually shown in dashed grey lines. Mean + SEM in black. (B) Mean Performance (%) and Mean Go Tone Lick Percentage (%) with Session for the Go/No-Go Task, plotted in black and green, respectively.

2416 A plot of the lick histogram for the various trial phases revealed that
2417 despite reaching the maximum success rate, the animals continued to
2418 lick during the no-go tone phase (incorrect lick) for a long duration of
2419 time (Figure 11). There was no difference in the amounts of time spent
2420 in the pre-tone or no-go tone phases. This suggested that the animals
2421 did not discriminate between the Go and no-go tones. Accordingly, the
2422 current protocol was not being learnt as expected.

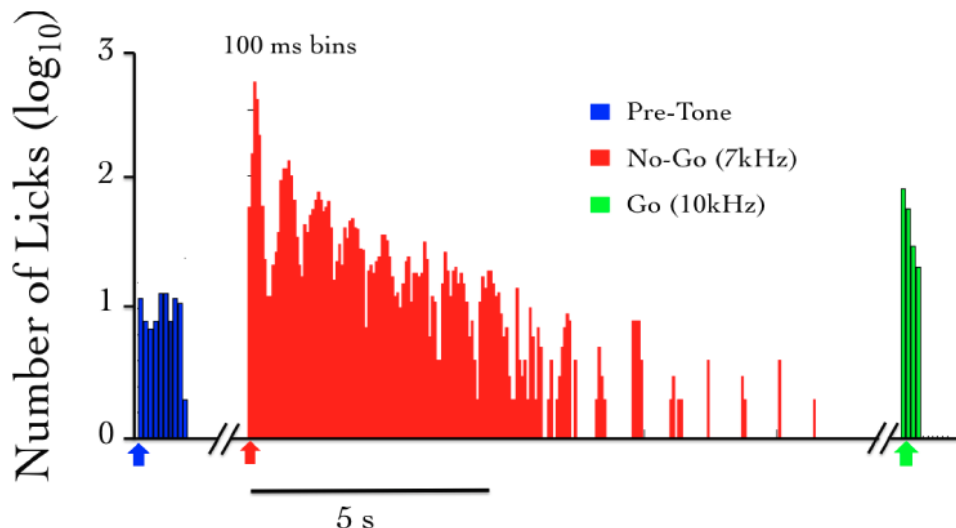


Figure 11: The number of licks in the pre-tone (blue), no-go tone (red), and go tone (green) phases, in a representative animal, in a session with maximum Performance (%).

2423
2424 We were not able to get discriminatory detection. Animals would resort
2425 to performing licks continuously and agnostically, to the go and no-go
2426 stimulus. In a study published many years later, it was determined that
2427 discriminatory tasks such as the one described above, could often
2428 require 3-4 weeks of training (Guo et al., 2014), since the animal was
2429 not punished with anything more than a delay or phase restart.

2430

2431 **Total animals trained:** 5

2432 **Conclusion:** Fail

2433 **Operant conditioning experiments failed to match**
2434 **behavioural requirements**

2435

2436 Operant conditioning tasks have been extensively and successfully
2437 modeled in a variety of laboratories. For our specific experiments, we
2438 required a task that could be learnt within 1-2 weeks. This was
2439 because we were not confident on how many simultaneous days of
2440 chronic imaging, we could achieve with the *in vivo* chronic 2-photon
2441 calcium imaging preparation (see Chapter 3 – “Imaging”). Additionally,
2442 it takes typically 3-4 weeks for rodents to acquire sufficient expertise in
2443 behavioural performance for Operant Conditioning tasks (Guo et al.,
2444 2014).

2445

2446 One alternative that we could have tried was to train the animals to
2447 expert levels of performance, and subsequently performed the
2448 hippocampus prep. The issue(s) with this is that,
2449 a) We wanted to study the hippocampal CA1 network during the
2450 learning or acquisition phase of behavioural training, as a distinct
2451 experiment from those published in literature.
2452 b) In such a protocol, we would require two separate surgeries, viz., i)
2453 Head-bar implant, and, ii) hippocampus preparations. This, we
2454 believed would increase the technical difficulty of the overall
2455 experiment and could be more stressful for the experiment animals.
2456 c) We suspected that there could be unknown effects on behavioural
2457 performance, post-surgery, complicating the analysis and insights we
2458 aimed to study.

2459

2460 Across all Operant Conditioning protocols attempted, we could not
2461 observe behavioural discrimination (not licking to incorrect phases)
2462 within 1-2 weeks of training. On this basis, we considered the
2463 experiments as failures.

2464

2465 Eventually, we had to abandon these experiments, to switch to an
2466 aversive conditioning task, *viz.*, Trace Eye-Blink Conditioning (TEC).
2467 With the change in the main behavioural task we also changed the
2468 project goals. The TEC task was standardized with the intention to
2469 work on Project II which is to study how animals make complex
2470 associations between different types of stimuli and how they adapt to
2471 changes to the inter-stimulus interval (ISI).

2472 **Trace Eye-Blink Conditioning [Project II]**

2473

2474 We have introduced the Trace Eye-Blink conditioning paradigm in
2475 Chapter 1 – “Introduction”, but some key definitions and results require
2476 mention. Eye-blink Conditioning is a class of Classical Conditioning
2477 and requires the presentation of a neutral stimulus (Conditioned
2478 Stimulus, CS) along with an eye-blink eliciting, mildly aversive stimulus
2479 (Unconditioned Stimulus, US). Depending on whether the CS
2480 presentation overlaps with the US presentation or if the two stimuli are
2481 separated by a stimulus free interval in between (Trace interval), the
2482 concomitant procedure is called Delay Conditioning or Trace
2483 Conditioning, respectively (Figure 12). In either case, precise timing of
2484 the CS and US is mandated.

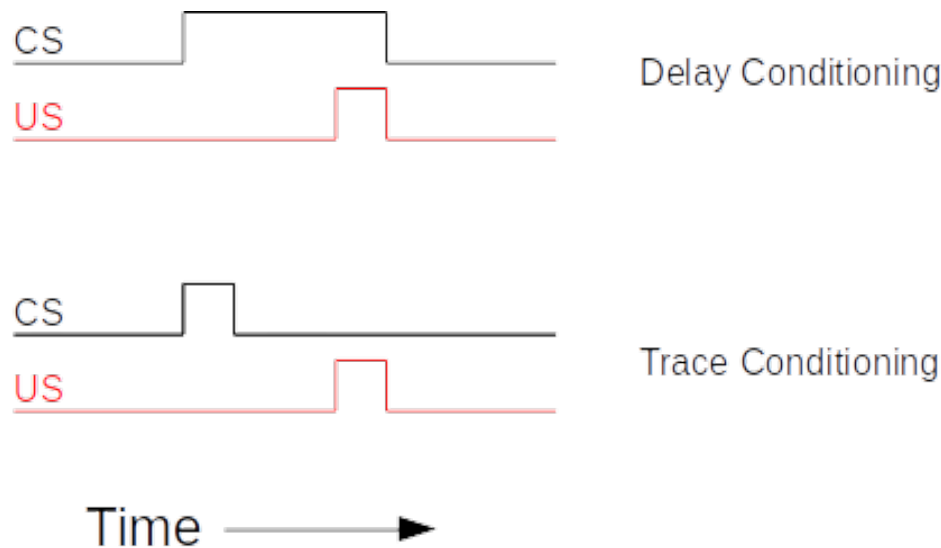


Figure 12: Schematic representation to showcase the two main subtypes of Classical Conditioning (Eye-Blink Conditioning, for our experiments) based on the relative timing and presentation of the CS and US.

2485

2486 The CS is usually an auditory tone or a visual stimulus (e.g.- LED
 2487 Flash), while the US is typically a mild air-puff to the cornea, or a
 2488 gentle electric shock to the eye-lid. Naive animals (rabbits, rodents,
 2489 monkeys, etc.) produce a robust, reflexive eye-blink to the US
 2490 (Unconditioned Response or UR) and ignore the CS, in early trials.
 2491 However, with repeated pairing of CS and US, the animals are able to
 2492 associate the two, and use the CS as a cue to predict the US,
 2493 producing a partial, preemptive eye-blink just before the expected time
 2494 of the US (Conditioned Response or CR). The CR develops in
 2495 amplitude over multiple pairings or training sessions. In well trained
 2496 animals, the CR begins at a time point closer and closer to the CS
 2497 onset, and usually merges with the UR. The animals produce this CR
 2498 in an attempt to avoid the US.
 2499

2500 Traditionally, Trace Eye-Blink Conditioning has been an important
2501 hippocampus-dependent behavioural task, and has been adapted to a
2502 variety of different species, spanning rabbits, rats, and mice.

2503

2504 Damage or inhibition of the hippocampus has been shown to limit task
2505 acquisition without affecting other non-hippocampus dependent tasks
2506 such as Delay Conditioning. In an experiment, Ibotenic Acid was used
2507 in a session dependent fashion, to observe both limitations in first
2508 acquiring the Trace Conditioning task, as well as detriments to
2509 behavioural recall, even after animals learn the task to a high degree of
2510 proficiency, suggesting the pivotal role that the hippocampus plays in
2511 temporal tasks of this nature (Tseng et al., 2004).

2512

2513 A single session of Trace Eye-Blink Conditioning, with strong stimuli
2514 (CS and US), has been previously employed (Modi et al., 2014), but
2515 with only upto 50% of the animals learning the task. Typically animals
2516 require around 3-7 sessions (~200-600 trials) to robustly learn the task.
2517 Accordingly, we designed and standardized a multi-session version of
2518 TEC, to allow more animals to learn and acquire the task, based on
2519 previously published work (Siegel et al., 2015).

2520

2521 **Tracking eye-blink responses**

2522

2523 The most foolproof way to track eye-blink responses (especially with
2524 head-fixed animals) chronically (for multiple sessions across days), is
2525 to use a video camera. We used a Point Grey Chameleon3 1.3 MP
2526 Monochrome USB3.0 camera) for this purpose. It is cost effective and
2527 with proper scaling of the resolution and field of view, can achieve

2528 recording rates of >200 frames per second (FPS). An important criteria
2529 for getting faster frame rates is to have better illumination, so that the
2530 camera may be set to lower exposure settings. We used a set of 5-10
2531 Red colour LEDs as the light source, and these are run using a 12V
2532 DC line, with current limited resistors in series. Additionally, we used
2533 an IR-blocking filter to avoid capturing the 2-Photon excitation light
2534 (910-920 nm) when conduction behaviour and imaging experiments
2535 simultaneously. Finally, to focus the light from the eye of the animal
2536 onto the camera sensor, we used a Tamron M118FM16 lens (1/1.8,
2537 16mm F/1.4).

2538 **Treadmill and tracking running speed**

2539

2540 Allowing the head-fixed animals to run on a treadmill was an important
2541 behaviour rig consideration, as this allows the animals to be more
2542 engaged and less stressed **during experiments**. We considered
2543 **treadmill tracking as a relevant variable to keep track of**, despite the
2544 **potential complications this could provide to imaging**, viz., z-axis drift
2545 **owing to relative motion between the brain tissue and microscope**
2546 **objective as the head-fixed animals run**. We used a 6 inch cylindrical
2547 massage roller with a stainless steel axle running along the length.
2548 This axle had ball bearings on the two ends, to allow for free rotation
2549 against clamps. Additionally, we used linear actuators to be able to
2550 adjust the height of the treadmill relative to the head-fixing clamps.

2551

2552 On one side of the treadmill, we used a printed pattern of black
2553 squares (side length: 1 cm) along the circumference. This allowed an
2554 IR LED - Photodetector pair to catch the edges of the black printed
2555 squares. The number of edges detected per unit time, then gave us the

2556 run speed of the animals being trained. We followed previously
2557 published routines and protocols (Siegel et al., 2015) for setting up the
2558 treadmill and run speed tracking (Figure 13), **over 50 ms sized bins**,
2559 across each trial.

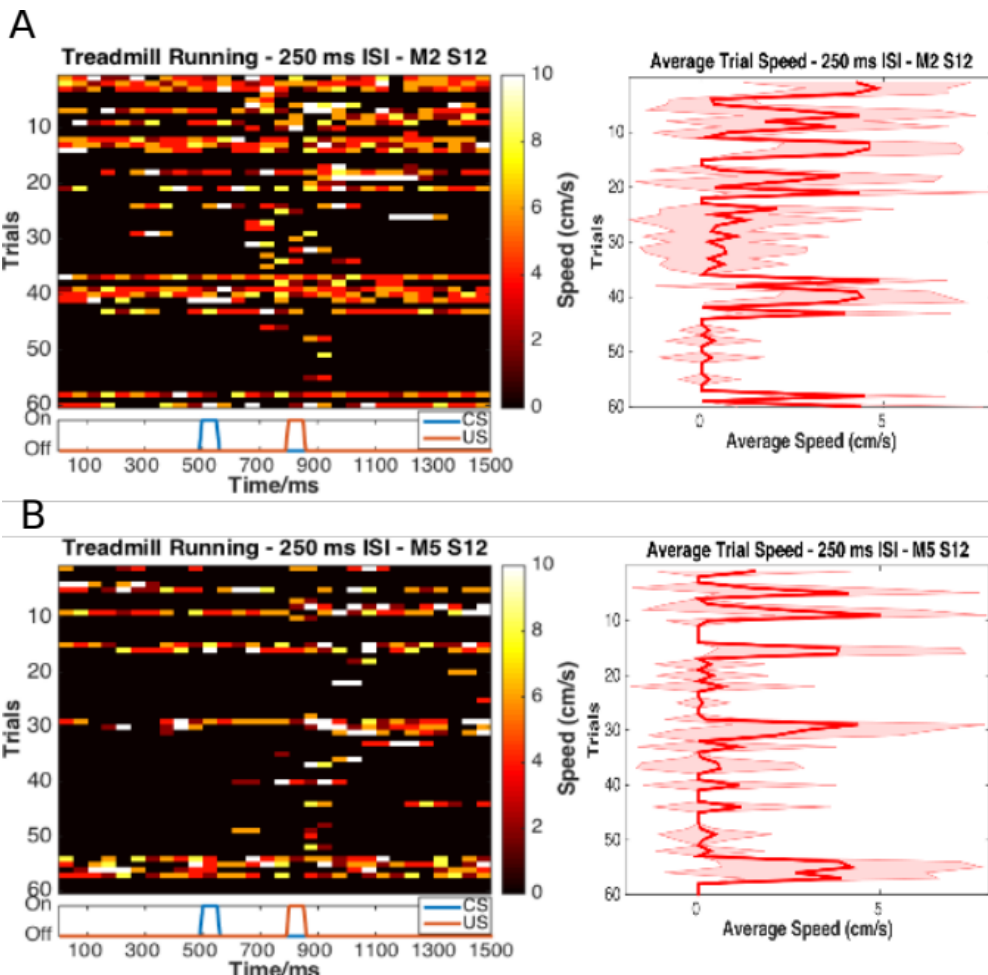


Figure 13: Trial-by-trial (left) and trial-averaged running speed (right) for two example animals, (A) M2 Session 12, and (B) M5 Session 12.

2560

2561

2562 **Behaviour rig and protocol control - Software**

2563

2564 For our initial experiments we used the open-source behaviour

2565 controlling software suite Bonsai (Windows version). Later on, we were

2566 able to implement our own custom codes that allowed integration of

2567 the video camera, Arduino for stimulus delivery and treadmill tracking,

2568 and the software side of the protocols. Dilawar S. Rajput was

2569 instrumental in setting up the camera pipeline and integrating it into the

2570 Arduino code. The Camera server was implemented in C++ with

2571 Spinnaker API (Point Grey) and this fetched frames from the camera.

2572 The camera client was written in Python, and this read the frames to

2573 produce a copy to monitor the video feed live, as well as write the

2574 video frames to disk as .tif files.

2575 With this setup, the maximum memory usage was ~1.3 GB RAM, and

2576 the code (available at <https://github.com/BhallaLab/PointGreyCamera>)

2577 had the following dependencies:

2578 • libopencv-dev, python-opencv

2579 • cmake, g++, gnu-make

2580 • libtiff-dev, python-tifffile, python-numpy

2581 • python-gnuplotlib, gnuplot-x11

2582

2583 An important requirement for our behaviour experiment design was to

2584 be able to train the animals systematically under reproducible

2585 conditions, with the aim to have stable behavioural training and animal

2586 performance. We used a blue LED as the Conditioned Stimulus (CS,

2587 50 ms flash) with an air-puff to the eye serving as the Unconditioned

2588 Stimulus (US, 50 ms pulse). We used an Arduino to orchestrate

2589 stimulus delivery and protocol design. All experiments were performed

2590 on head-fixed C57Bl6 mice, since we planned to use a stationary,

2591 custom-built two-microscope to image hippocampal CA1 activity during
2592 task acquisition and recall (Figure 14; Figure 15).

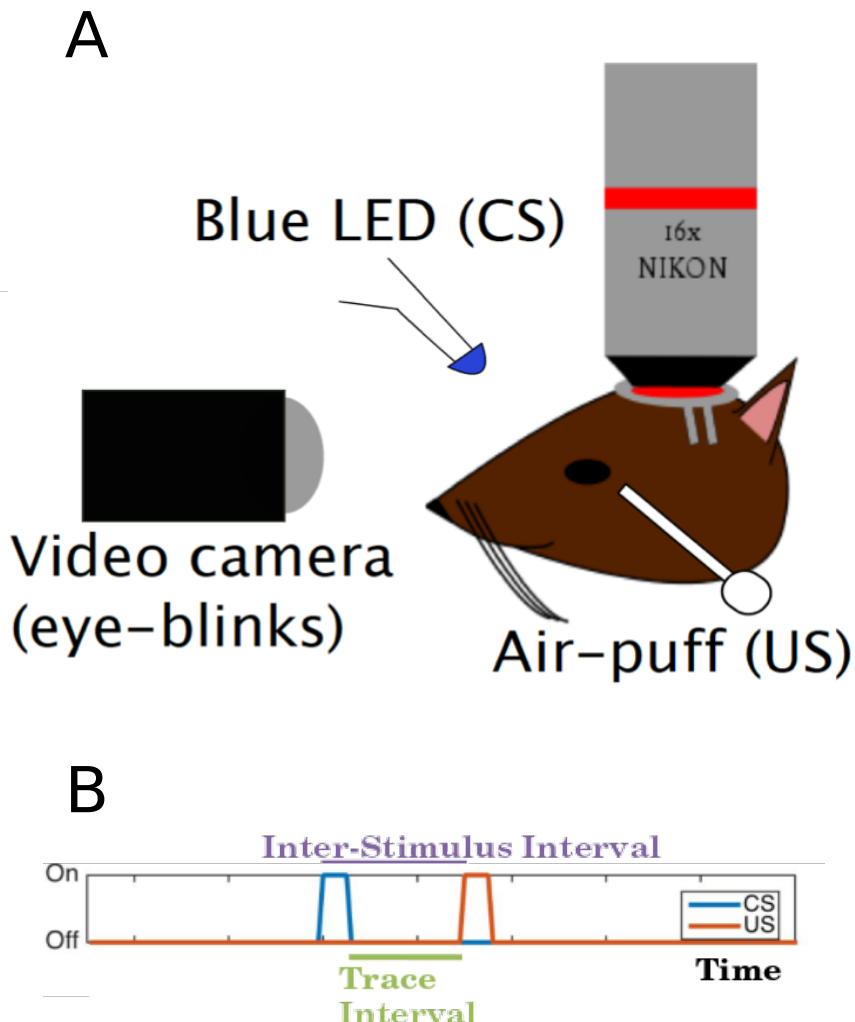


Figure 14: Schematic representation of (A) the behaviour rig with 2-Photon imaging, to train head-fixed mice on a Trace Eye-Blink Conditioning (TEC) task, and (B) relative time intervals between the CS and US.

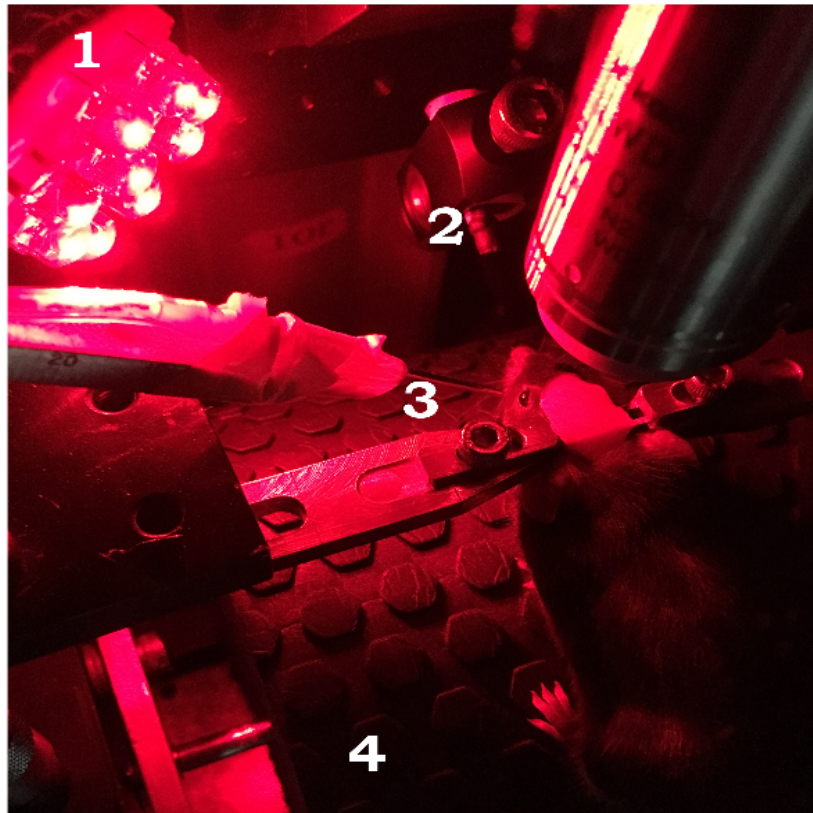


Figure 15: A picture of a head-fixed mouse clamped on the behaviour rig, with key components: 1) Red LED Illumination, 2) Blue LED CS, 3) Air-puff port directed to the left eye, and 4) Height-adjustable Treadmill.

2609 **Analysis - TEC**

2610

2611 Once the .tif movies of the eye of the animal being trained were saved,
2612 they were analyzed by a custom script written in MATLAB, wherein for
2613 every frame we (Figure 16),

2614 Adjust contrast (optional)

2615 Apply a median filter (optional)

2616 Crop out the pixels defining the eye and surrounding (identical number
2617 of pixels for all trials and animals)

2618 Binarize the image of the eye to get black pixels defining the visible
2619 (opened) portion of the eye

2620 Count the relative proportion of open vs closed eye pixels in the
2621 cropped image, and

2622 Assign each frame with a Fraction of Eye Closure (FEC) score.

2623

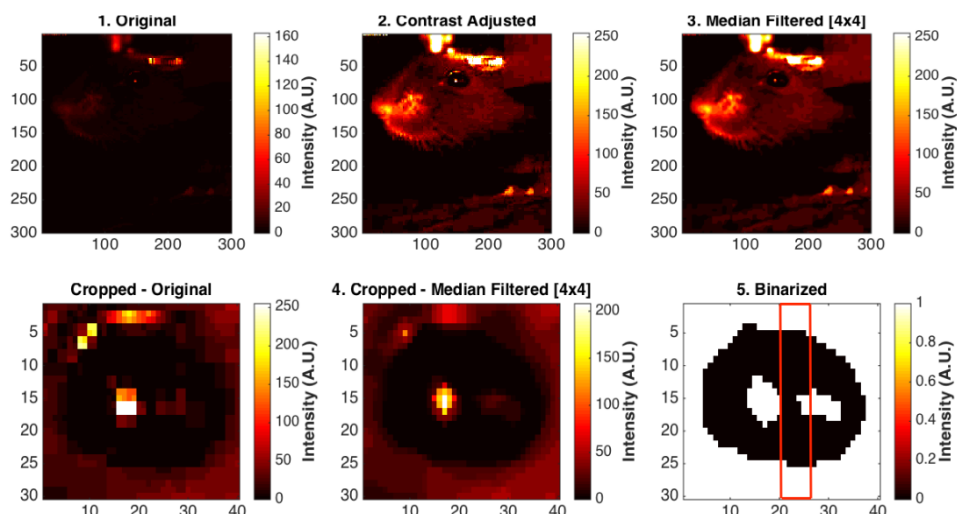


Figure 16: Steps from behaviour video frame to Fraction of Eye-Closed (FEC) analysis

2624

2625 The FEC score then allowed us to analyse each trial's worth of frames
2626 for eye-blanks. There are many features of the eye-blink that could be
2627 used to gauge the overall performance of the animal in terms of both
2628 the Conditioned Response (CR) as well as the Unconditioned
2629 Response (UR), but for our experiments, we chose to use Eye-Blink
2630 Amplitude (Siegel et al., 2015). Additionally, we studied whether the

2631 animals could produce CRs in the absence of the US, by
2632 pseudorandomly selecting 10% trials to skip the US (Probe Trials).

2633

2634 **Results - TEC**

2635

2636 1. Animals showcase task acquisition by performing Conditioned
2637 Responses (CRs), observed as pre-emptive blinks timed to
2638 avoid the aversive US. The kinetics of the CR (timing,
2639 amplitude, etc.) are dependent on the amount of training, but
2640 are identical across paired and probe trials (Figure 17).

2641

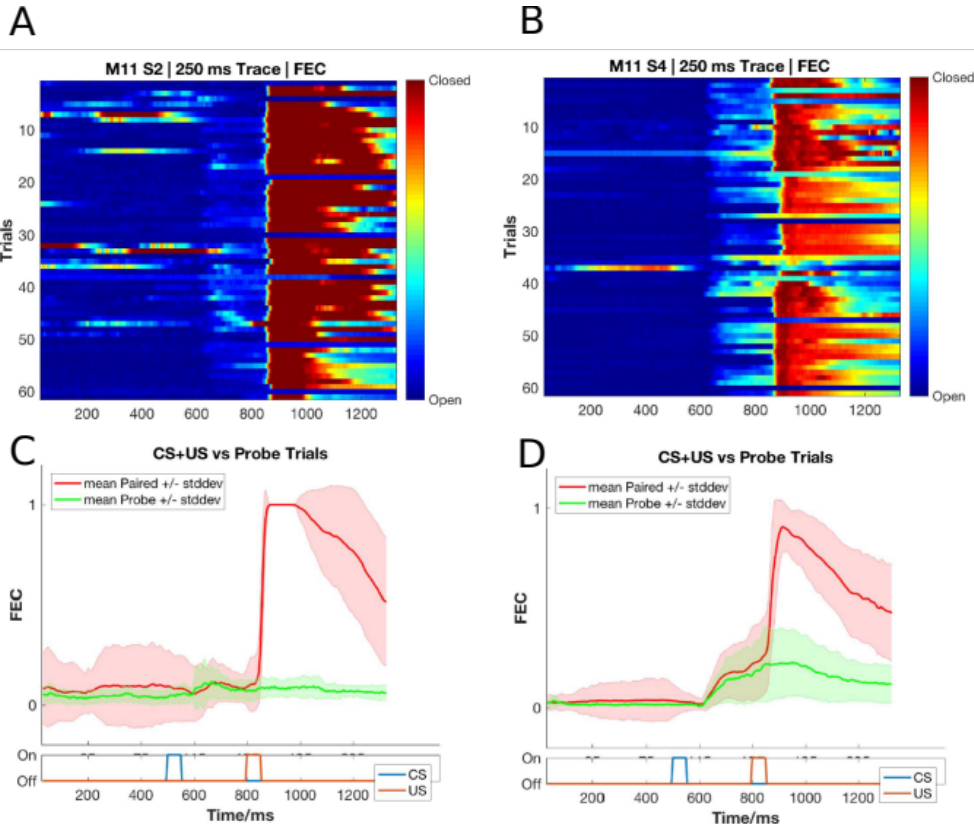


Figure 17: Conditioned Responses (CRs) are small amplitude eye-blanks triggered by the CS, and develop with multiple training sessions, while Unconditioned Responses (URs) are large eye-blinks to the US, typically consistent across sessions. (A,B) Trial-by-trial FEC traces for M11 (A) Session 2, and (B) Session 4. (C,D) Trial-averaged FEC traces for M11 (C) Session 2, and (D) Session 4, with paired (red) and probe (green) trials.

2642

2643 2. Most animals can pick up the task within 4-7 sessions (1
2644 session/day, 60 trials/session), even if on water deprivation.
2645 Animals can also be subsequently trained to different inter-
2646 stimulus intervals. Using the Conditioned Response (CR)
2647 amplitude, each trial can be binarized to whether a CR was
2648 elicited (Hit Trial) or not (Miss Trial), by thresholding at mean
2649 trial FEC + 2*Std. Dev.. Performance for the session is then

2650 estimated as the ratio of Hit Trials to Total Trials (Figure 18). We
 2651 additionally set a criterion that a performance of >70% be
 2652 considered “strong learning”, 30-60% be considered “weak
 2653 learning”, and “0-30%” be considered “non-learning”.

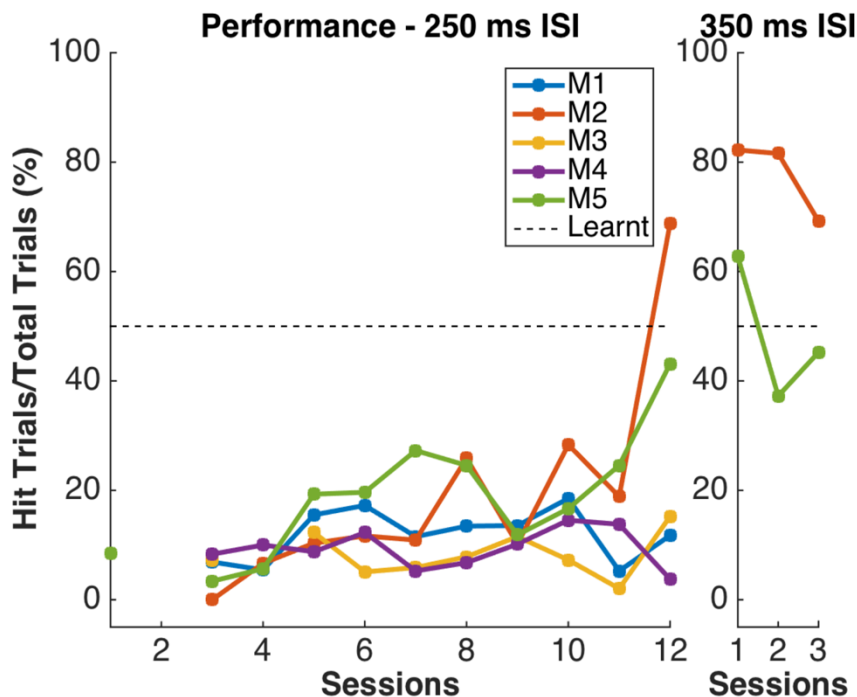


Figure 18: Performance in terms of the percentage of Hit Trials to total trials across sessions, including an ISI switch from 250 ms to 350 ms. Here, M2 is a strong learner (>60% hit trials/session) and M5 is a weak learner (30-60 % hit trials/session). M1, M3, and M4 did not learn the task.

2654
 2655 3. Animals that learn multiple ISIs, especially when the second ISI
 2656 is $\geq 2x$ the first ISI, showcase complex eye-blinks without
 2657 extinction of the previously learnt CRs. Once an animal
 2658 showcases the ability to produce Conditioned Responses (CRs)
 2659 to one inter-stimulus interval (ISI), this interval can be
 2660 elongated. In the example shown below we first trained the

2661 animal to a 250 ms ISI, and then switched to a 500 ms ISI
2662 (Figure 19).

2663

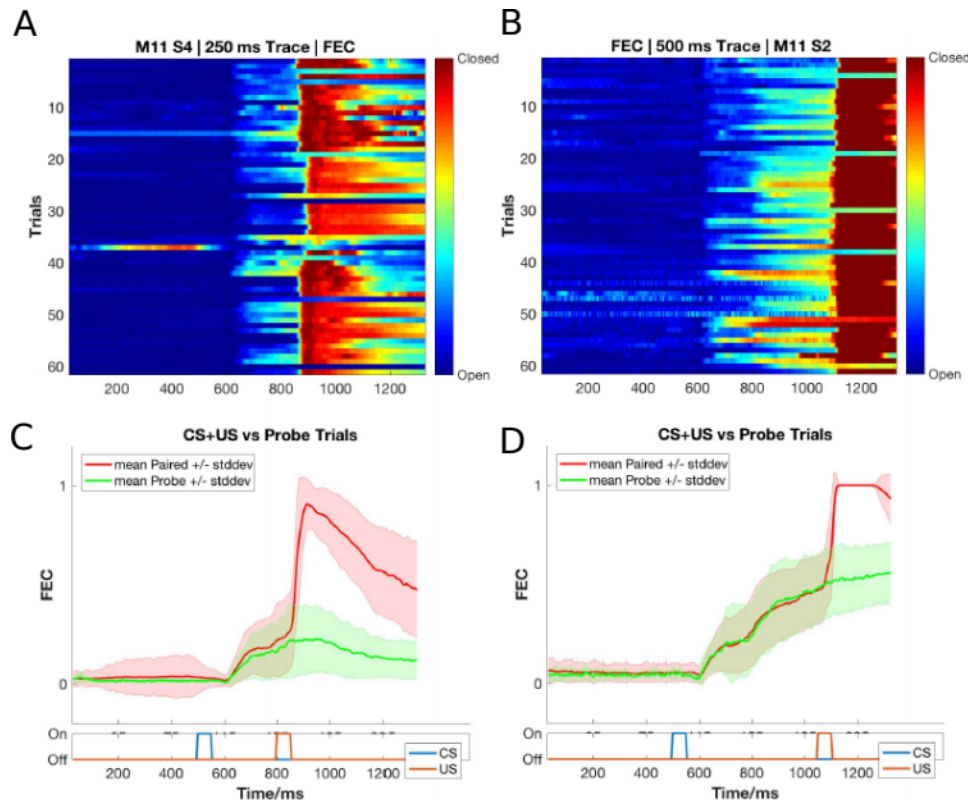


Figure 19: Conditioned Responses (CRs) are preserved for previously learnt ISIs, and switching the ISI to longer intervals results in Complex (multi-CR) eye-blink responses. (A,B) Trial-by-trial FEC scores for (A) 250 ms ISI (left) and (B) 500 ms ISI. (C,D) Trial-averaged FEC traces for (C) 250 ms ISI, and (D) 500 ms ISI, with paired (red) and probe (green) trials.

2664

2665 4. The onset of the Conditioned Response (CR) is not affected by
2666 the ISI switch, irrespective of how strongly the animals learn the
2667 task. CRs during paired and probe trials were near identical,
2668 showcasing that the animal (Figure 20; Figure 21).

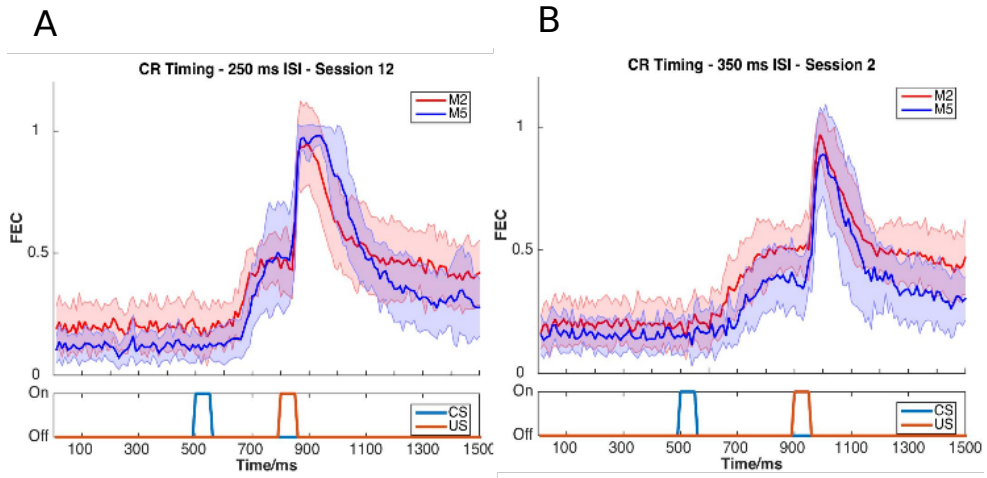


Figure 20: Conditioned Response (CR) onset timing is maintained across ISI switches. Representative examples from a short ISI switch from (A) 250 ms to (B) 350 ms (right).

2669

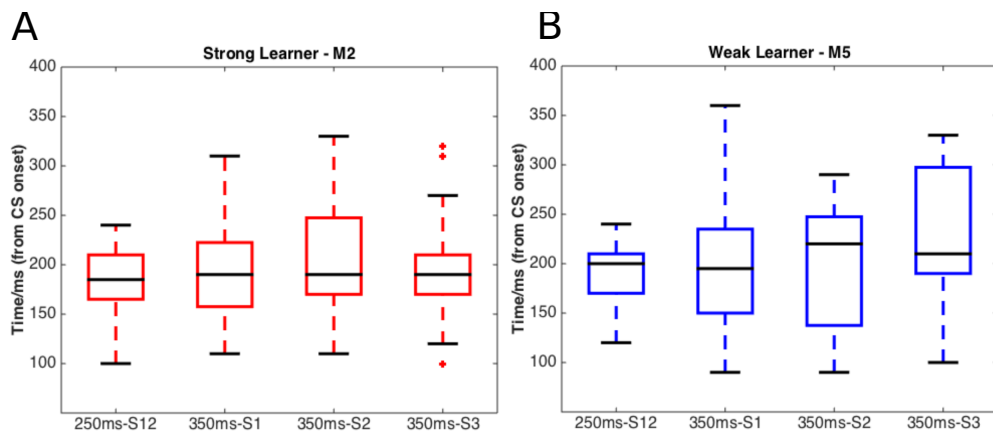


Figure 21: Bar plots for Conditioned Response (CR) onset across multiple sessions of training after ISI switch from 250 ms to 350 ms, irrespective of how strongly the animals learnt the task. (A) red, strong learner, and (B) blue, weak learner.

2670

2671 5. Animals can also be trained to very long ISIs from Session 1,
2672 with acquisition taking <10-14 days. Here we tried to train
2673 animals to either a 550 ms ISI or a 750 ms ISI. Note, however,

2674 that unless multiple ISIs are taught to the same animal, the CR
2675 eye-blink is singular (Figure 22).

2676

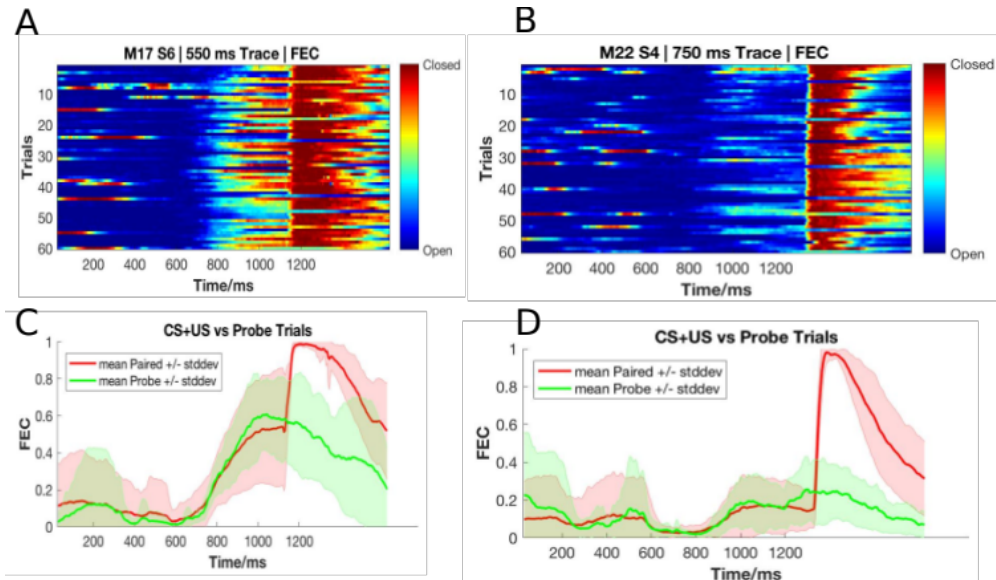


Figure 22: Representative example of mice trained to 550 ms ISI (Session 6) and 750 ms ISI (Session 4). (A,B) Trial-by-trial FEC responses for (A) 550 ms ISI (M17 Session 6), and (B) 750 ms ISI (M22 Session 4). (C,D) Trial-averaged FEC responses for (C) 550 ms ISI (M17 Session 6), and (D) 750 ms ISI (M22 Session 4), with paired (red) and probe trials (green).

2677

2678 **Total animals trained:** 18 [Conditioned Responses visible]

2679 **Conclusion:** Success

2680

2681 Ultimately, we were satisfied with the Trace Eye-Blink Conditioning
2682 paradigm since we could observe stable conditioned responses that
2683 developed over a reasonably short period of training time (<1 week),
2684 and adaptable conditioned responses to behaviour parameter
2685 modulations, in head-fixed mice that could be subjected to
2686 simultaneous 2-Photon calcium imaging.

Table 1: Summary table of behaviour protocols attempted and essential results.

NAME	PUNISHMENT TYPE	REMARKS
Operant Protocol 1.1 (Stimulus Detection)	No water reward for incorrect licks	Lack of water reward for incorrect licks not enough for behavioural discrimination at <1 week of training
Operant Protocol 1.2 (Stimulus Detection)	Air-puff punishment for incorrect licks	Strong punishment for incorrect licks not enough for behavioural discrimination at <1-2 weeks of training.
Operant Protocol 2 (Stimulus Detection)	Timeout (3s) punishment for incorrect licks	Alternate or weaker punishment attempted but not enough for behavioural discrimination at <1 week of training.
Operant Protocol 3 (DNMS)	Timeout (3s) punishment for incorrect licks	Alternate punishment attempted but not enough for behavioural discrimination at <1 week of training No obvious effect of adding delay intervals between stimulus presentations
Operant Protocol 4 (Go/No-Go)	Trial base repeat punishment for incorrect licks	Alternate punishment attempted but not enough for behavioural discrimination at <1 week of training
Aversive Protocol (Trace Eye-Blink Conditioning)	No punishment	Animals learn the task and produce stable, adaptable Conditioned Responses (CRs) within 1 week of training

2687 Bibliography

- 2688 Brown, G. D. (1998). Nonassociative learning processes affecting
2689 swimming probability in the seashell Tritonia diomedea:
2690 habituation, sensitization and inhibition. *Behavioural Brain
2691 Research*, 95(2), 151–165.
2692 [https://doi.org/https://doi.org/10.1016/S0166-4328\(98\)00072-2](https://doi.org/https://doi.org/10.1016/S0166-4328(98)00072-2)
- 2693 Chudasama, Y. (2010). Delayed (Non)Match-to-Sample Task. In I. P.
2694 Stolerman (Ed.), *Encyclopedia of Psychopharmacology* (p. 372).
2695 Springer Berlin Heidelberg. https://doi.org/10.1007/978-3-540-68706-1_1619
- 2696 Deshmukh, S. S., & Bhalla, U. S. (2003). Representation of odor
2697 habituation and timing in the hippocampus. *The Journal of
2698 Neuroscience : The Official Journal of the Society
2699 for Neuroscience*, 23(5), 1903–1915.
2700 <https://doi.org/10.1523/JNEUROSCI.23-05-01903.2003>
- 2701 Fyhn, M., Molden, S., Witter, M. P., Moser, E. I., & Moser, M.-B.
2702 (2004). Spatial representation in the entorhinal cortex. *Science
2703 (New York, N.Y.)*, 305(5688), 1258–1264.
2704 <https://doi.org/10.1126/science.1099901>
- 2705 Guo, Z. V., Hires, S. A., Li, N., O'Connor, D. H., Komiyama, T., Ophir,
2706 E., Huber, D., Bonardi, C., Morandell, K., Gutnisky, D., Peron, S.,
2707 Xu, N., Cox, J., & Svoboda, K. (2014). Procedures for Behavioral
2708 Experiments in Head-Fixed Mice. *PLOS ONE*, 9(2), e88678.
2709 <https://doi.org/10.1371/journal.pone.0088678>
- 2710 Hafting, T., Fyhn, M., Molden, S., Moser, M.-B., & Moser, E. I. (2005).
2711 Microstructure of a spatial map in the entorhinal cortex. *Nature*,
2712 436(7052), 801–806. <https://doi.org/10.1038/nature03721>
- 2713 Hubel, D. H., & Wiesel, T. N. (1962). Receptive fields, binocular
2714 interaction and functional architecture in the cat's visual cortex.
2715 *The Journal of Physiology*, 160(1), 106–154.
2716 <https://doi.org/10.1113/jphysiol.1962.sp006837>
- 2717 Jaramillo, S., & Zador, A. M. (2014). Mice and rats achieve similar
2718 levels of performance in an adaptive decision-making task . In
2719 *Frontiers in Systems Neuroscience* (Vol. 8).
2720 <https://www.frontiersin.org/articles/10.3389/fnsys.2014.00173>
- 2721 Modi, M. N., Dhawale, A. K., & Bhalla, U. S. (2014). CA1 cell activity
2722 sequences emerge after reorganization of network correlation
2723 structure during associative learning. *eLife*, 3, e01982–e01982.
2724 <https://doi.org/10.7554/eLife.01982>
- 2725 O'Keefe, J., & Dostrovsky, J. (1971). The hippocampus as a spatial
2726 map. Preliminary evidence from unit activity in the freely-moving
2727 rat. *Brain Research*, 34(1), 171–175. [https://doi.org/10.1016/0006-8993\(71\)90358-1](https://doi.org/10.1016/0006-8993(71)90358-1)

- 2730 Ranck, J. B. (1973). Studies on single neurons in dorsal hippocampal
2731 formation and septum in unrestrained rats: Part I. Behavioral
2732 correlates and firing repertoires. *Experimental Neurology*, 41(2),
2733 462–531. [https://doi.org/https://doi.org/10.1016/0014-4886\(73\)90290-2](https://doi.org/https://doi.org/10.1016/0014-4886(73)90290-2)
- 2734 Schreurs, B. G. (1989). Classical conditioning of model systems: A
2735 behavioral review. *Psychobiology*, 17(2), 145–155.
2736 <https://doi.org/10.3758/BF03337830>
- 2737 Siegel, J. J., Taylor, W., Gray, R., Kalmbach, B., Zemelman, B. V.,
2738 Desai, N. S., Johnston, D., & Chitwood, R. A. (2015). Trace
2739 Eyeblink Conditioning in Mice Is Dependent upon the Dorsal
2740 Medial Prefrontal Cortex, Cerebellum, and Amygdala: Behavioral
2741 Characterization and Functional Circuitry. *ENeuro*, 2(4),
2742 ENEURO.0051-14.2015. <https://doi.org/10.1523/ENEURO.0051-14.2015>
- 2743 Taube, J. S., Muller, R. U., & Ranck, J. B. J. (1990). Head-direction
2744 cells recorded from the postsubiculum in freely moving rats.
2745 I. Description and quantitative analysis. *The Journal of
2746 Neuroscience : The Official Journal of the Society
2747 for Neuroscience*, 10(2), 420–435.
2748 <https://doi.org/10.1523/JNEUROSCI.10-02-00420.1990>
- 2749 Tseng, W., Guan, R., Disterhoft, J. F., & Weiss, C. (2004). Trace
2750 eyeblink conditioning is hippocampally dependent in mice.
2751 *Hippocampus*, 14(1), 58–65. <https://doi.org/10.1002/hipo.10157>
- 2752
- 2753
- 2754

Chapter 3 – Imaging

2756

2757 The mammalian hippocampus is considered important in the formation
2758 of new memories about experienced events (episodic or
2759 autobiographical memory), general declarative memory (memories that
2760 can be explicitly verbalized), spatial memory and navigation, and
2761 associations between stimuli that are distinct in time, among other
2762 functions. To achieve this, the Hippocampus must integrate information
2763 from different areas of the cortex.

2764

2765 Much of the cortical information that enters the Hippocampus (at the
2766 Dentate Gyrus), comes through the Entorhinal Cortex, along the
2767 Perforant Path (Hjorth-Simonsen & Jeune, 1972). The Dentate Gyrus
2768 cell network then relays this information to the CA3 cell network
2769 through Mossy Fibers, which in turn relays the information to CA1
2770 cells, through the Schaffer Collateral Fibers. This is popularly known as
2771 the Trisynaptic Circuit or Pathway (Figure 1 from Chapter 1 -
2772 "Introduction") and there is scope and evidence for computation and
2773 information processing at every step (MacDonald et al., 2011, 2013;
2774 Modi et al., 2014; Nakashiba et al., 2008; Suh et al., 2011). Finally, the
2775 CA1 cells have their outputs to other brain regions. It is important to
2776 note, however, that regions like the CA1 are known to have access to
2777 information directly from other brain regions, as well (P. Andersen et
2778 al., 2006).

2779

2780 Literature in the field suggests that naïve animals may have some
2781 sensory gating of "Neutral" stimuli at the level of the CA1 (Abe et al.,
2782 2014; Bellistri et al., 2013; Kamondi, 1998). The source of this
2783 inhibition (at least the step before the local interneurons) seems to be

2784 the Medial Septum, through Fimbria-Fornix (Abe et al., 2014). Also,
2785 behavioural relevance allows the CA1 to elicit depolarizations that can
2786 be mapped to brain external stimuli (Dombeck et al., 2010; Harvey et
2787 al., 2009; P. M. Itskov et al., 2011; MacDonald et al., 2011, 2013; Modi
2788 et al., 2014; Pastalkova et al., 2008).

2789

2790 The Hippocampus consists of ventral and dorsal portions both of which
2791 are of similar composition but are parts of different neural circuits
2792 (Moser & Moser, 1998). The dorsal hippocampus performs primarily
2793 cognitive functions and in memory function, while the ventral
2794 hippocampus modulates emotional and affective processes (Fanselow
2795 & Dong, 2010).

2796

2797 **Physiology in the hippocampus**

2798

2799 The Hippocampus is located deep in the medial temporal lobe of
2800 mammals and is defined by several sub-structures, including the
2801 Dentate Gyrus (one site for information input to the hippocampus) and
2802 the Hippocampus Proper constituted by the CA1, CA2, CA3 and CA4
2803 cellular levels.

2804

2805 Using extracellular tungsten microelectrodes in naïve unanesthetized
2806 rabbits serially exposed to multimodal stimuli (Vinogradova, 2001), it
2807 was reported that in the CA1,

2808 1. A major fraction the reactive neurons have unimodal responses
2809 (41-44%)

2810 2. Multimodal neurons are modality-unspecific but have
2811 differentiated responses to stimuli of different modalities and even to
2812 various stimuli within a single modality
2813 3. Many neurons respond by Phasic (evoked responses last for the
2814 duration and as long as the stimulus) and Specific (stimulus-specific
2815 pattern) responses
2816 4. Neurons with inhibitory responses are encountered less
2817 frequently than those with various types of excitatory
2818 5. Habituation (non-responsiveness to repeatedly presented stimuli) is
2819 present though not among all the responsive cells (71-75%) and is
2820 often gradual

2821

2822 Imaging based activity studies have the advantage of being able to
2823 capture many more cells (>100 from the same animal) during
2824 experiments (Dombeck et al., 2010; Pachitariu et al., 2017; Peron et
2825 al., 2015; Sofroniew et al., 2016) as compared to typical
2826 electrophysiological measurements. Imaging provides an unambiguous
2827 method to identify cells that are not active during a period of interest.
2828 Another advantage is that it provides anatomical confirmation to help
2829 track the same cell over multiple days of recording, without ambiguity,
2830 for longitudinal studies. Finally, imaging techniques have gained
2831 momentum in the study of the hippocampal CA1 various spatial scales,
2832 from cellular resolution somatic studies (Dombeck et al., 2010; Modi et
2833 al., 2014), to dendrites (Mizrahi, 2004; Sheffield & Dombeck, 2014),
2834 axonic boutons terminating on the CA1 interneuron populations
2835 (Kaifosh et al., 2013; Lovett-Barron et al., 2014), as well as spines
2836 (Attardo et al., 2015), *in vivo*.

2837

2838 We designed our imaging studies (for this thesis), with the aim to
2839 understand the network and cellular mechanisms of the hippocampal
2840 CA1 that corresponded with behavioral learning induced changes. We
2841 started by looking for CA1 responses to neutral stimuli in naive
2842 animals, *in vivo*. Subsequently, we planned to subject these animals to
2843 behavioural training and study if and how the same cells would
2844 respond.

2845

2846 Depending on the intended duration of the imaging experiments, *viz.*, a
2847 few hours (single session) or a few days and weeks (multiple
2848 sessions), we were able to standardize both an Acute as well as a
2849 Chronic *in vivo* hippocampal preparation. We now discuss the *in vivo*
2850 hippocampal preparation, physiology recordings, and a brief summary
2851 of the results. An important perspective for our experiments was to
2852 study how sensory stimulus responses of hippocampal CA1 develop
2853 with associative learning.

2854

2855 **Methodology – Acute and chronic imaging**

2856 **[Projects I & II]**

2857

2858 The overall experiment deals with optically measuring the activity of
2859 the dorsal CA1 hippocampal neurons when different stimulus
2860 modalities are presented to a male C57BL/6 mouse. The thesis covers
2861 experiments conducted acutely (lasting <10 hours) using OGB-1 as a
2862 calcium sensor), as well as chronically (~7-21 days) using a genetically
2863 encoded calcium indicator, GCaMP6f).

2864

2865 The 2-Photon excitation wavelength for OGB-1 experiments was set to
 2866 810 nm (scattering coefficient: ~3 rad²/mm) and the same for
 2867 GCaMP6f was set to 910 nm (scattering coefficient: ~2 rad²/mm) to
 2868 image cell bodies (Min et al., 2017) in the CA1, *in vivo*. However,
 2869 despite the relatively low scattering of longer wavelengths, the
 2870 hippocampus cannot be imaged directly, through the cortex since the
 2871 layer of cortex is too thick (~1-1.5 mm) to allow proper excitation of the
 2872 sample. These infra-red (IR) photons are expected to be scattered
 2873 almost completely, well before the imaging depth of the CA1 layer.
 2874 These layers of cortex have to accordingly be carefully suctioned out to
 2875 allow the microscope objective to have optical access to the exposed
 2876 tissue (Figure 23).

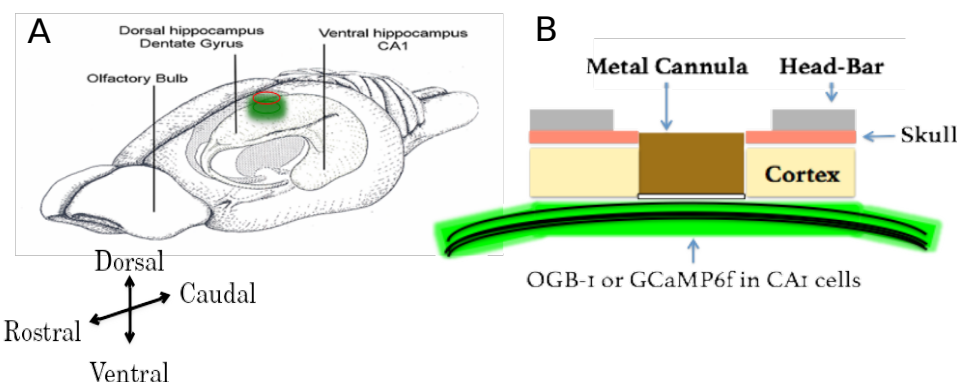


Figure 23: (A) A schematic of the rodent brain, showcasing the two hippocampi, one in each hemisphere. The hippocampi lie ~1 mm (mice) below the cortical surface. (B) The hippocampal preparation allows optical access to the deep lying hippocampal CA1 cells, relative to the skull/cortex. The CA1 cell bodies arrange in a laminar fashion as a tight cell body layer that can be visualized by fluorescence (using either OGB-1 or GCaMP).

2877
 2878 We first put the animal under anesthesia using a vapor chamber
 2879 saturated with 3% isoflurane. Next, the animal was cheek-clamped and
 2880 a light state of anesthesia was maintained using 1-2% isoflurane,

2881 provided directly to the nozzle of the animal, keeping track of ~1 Hz
2882 breathing rate and a body temperature of 35-37 °C (with heating pad).
2883 The animal was given a haircut and a circular incision of ~5 cm
2884 circumference was made on the scalp, revealing the skull below. We
2885 then affixed head-bars and skull screws with the help of dental cement,
2886 to be able to clamp the animal post surgery on the 2-Photon
2887 Microscope.

2888

2889 The left, dorsal hippocampus was targeted with a 3-5 mm circular
2890 craniotomy aimed at 1.5 mm left and 2.0 mm behind bregma, tearing
2891 and peeling out the Dura to reveal the cortex. We then carefully
2892 aspirated out the cortex (part of the somatosensory cortex) under
2893 repeated washes of Cortex Buffer (see table 1 for recipe), until the
2894 horizontal CC fibre layer was visible. Finally, we added a drop of low
2895 gelling agarose and a 5 mm coverslip (for acute preps); Kwik-Sil and
2896 inserted a 3 mm metal cannula with a coverslip attached at the bottom
2897 (for chronic preps). We used different sensors depending on the
2898 requirement for the preparation, *viz.*, acute (OGB-1) or chronic imaging
2899 (GCaMP6f). **We kept track of animals that showcase unusual gait or**
2900 **low/no mobility and avoid their use altogether for production datasets**
2901 **and experiments, in accordance with previously published protocols**
2902 **(Dombeck et al., 2010).** We refer to this series of steps as the
2903 hippocampal preparation.

2904 **Preparation of Cortex Buffer**

2905

2906 We prepared cortex buffer by weighing out the required amount of the
2907 salts, NaCL, KCl, Glucose and HEPES (see table 2 for recipe) and

2908 making up the volume of the solution with Milli Q Water to ~1000 ml.
2909 We then set the pH of the buffer using a calibrated pH meter to 7.35,
2910 using 1M NaOH_(aq). Next, we fill up the volume to 1000 ml and verify
2911 the pH (should not have changed). Finally, we filter the contents
2912 through a 0.22 um membrane using a vacuum filtration, and store at
2913 6 °C.

2914 Recipe for ready-to-use cortex buffer. The buffer is typically prepared
2915 and stored in aliquots to be used each week. The correct pH range of
2916 the buffer was often a crucial factor ensuring the success of the
2917 hippocampal preparation.

2918

Table 2: Recipe for ready-to-use cortex buffer. The buffer is typically prepared and stored in aliquots to be used each week. The correct pH range of the buffer was often a crucial factor ensuring the success of the hippocampal preparation.

INGREDIENT	CONCENTRATION (mM)	AMOUNT (g or ml) for 1000 ml]
NaCl (s)	125	7.31 g
KCl (s)	5	0.373 g
Glucose (s)	10	1.8 g
HEPES (s)	10	2.38 g
CaCl ₂ (aq)	2	1.6 ml of 1.25 M stock solution
MgCl ₂ (aq)	2	1.5 ml of 1.3 M stock solution

2919

2920 **Oregon Green Bapta-1 injections for acute
2921 imaging**

2922

2923 To prepare Oregon Green Bapta-1 (OGB-1) dye for microinjections, we
2924 first dissolve a 50 µg tube of OGB-1 in 5 µl of Pluronic Acid, and vortex
2925 the mix for 5 minutes. Separately, we dilute 20 µl of Phenol Red into

2926 500 μ l of cortex buffer, and transfer 45 μ l of this solution to the OGB-1
2927 mix. Next, we sonicate the 50 μ l solution for 20 mins., followed by
2928 centrifugation at 10000 RPM for 5 seconds. The remaining supernatant
2929 is split into 7 aliquots (7 μ l), and stored at -20 C for a maximum of one
2930 week (7 days).

2931

2932 For acute/single-day experiments, we injected OGB-1 using pulled,
2933 dye loaded micropipettes ($\sim 2 \text{ M}\Omega$ resistance, $\sim 2 \mu\text{m}$ diameter) at a
2934 depth of 100-150 μm (Figure 23) from the topmost layer of exposed
2935 tissue, till a slow but detectable pulse of dye (visualized as a red/pink
2936 solution) may be visible just below the tissue surface. This allows the
2937 dye to be soaked up by the basal dendrites of the CA1 and takes 30-
2938 60 mins for incorporation into the cytoplasm. We typically allow the
2939 animal 1-2 hours of respite before the subsequent imaging session.

2940 High pressure ejection of the dye into the tissue may damage the
2941 neuropil, while very low pressures or clogs in the pipette affect the
2942 spread of the dye across the tissue. We aimed to image $\sim 100 \times 100$
2943 μm^2 of the tissue in any particular ROI, and achieved this with 5 minute
2944 injections with each micropipette aiming to load the dye at 2-3, well
2945 separated positions spread across the entire exposed dorsal surface.

2946 We estimated that the dye volume was <1000 nl/injection. After the
2947 injection cycle with any micropipette, we left the tissue undisturbed for
2948 at least 5-10 mins before pulling the micropipette out of the tissue.

2949 Once all the injections were complete, the exposure was sealed using
2950 5% low gelling agarose making sure the temperature was cool enough
2951 to avoid heat-related tissue damage.

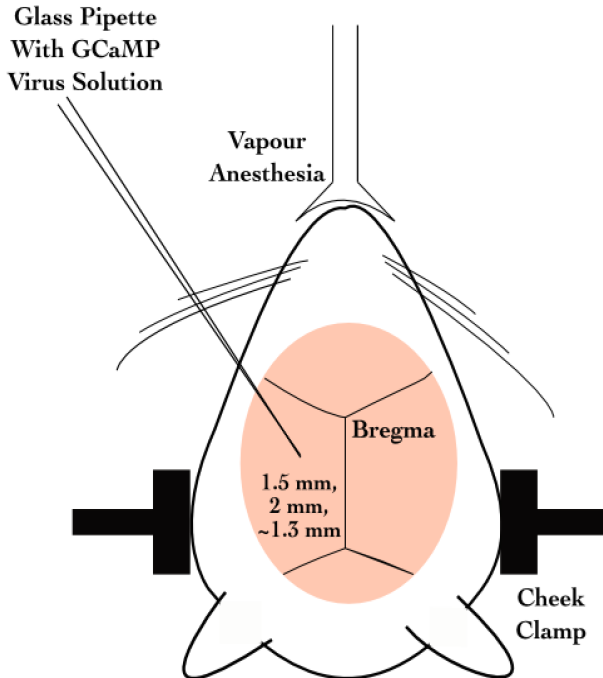
2952

2953 OGB-1 is eventually cleared from the cytoplasm but allows for a limited
2954 window for imaging studies (Stosiek et al., 2003). Reopening the

2955 agarose seal and re-injections were never attempted to prevent
2956 unnecessary damage to the underlying tissue. Additionally, the
2957 agarose plug itself was found to be unstable beyond 1-3 days. This
2958 resulted in the imaging possibility being limited to the same day as the
2959 surgery (acute imaging).
2960

2961 **GCaMP and chronic imaging**

2962
2963 For chronic/multi-day experiments, we standardized a stereotaxic viral
2964 injection step, where we inject the gene for GCaMP5 or GCaMP6f into
2965 the dorsal hippocampus at -1.5 mm lateral, 2 mm posterior, and 1.3
2966 mm dorsal from bregma on the skull surface (Figure 24).



2979

Figure 24: Figure 24: Schematic representation for stereotaxic viral injection.

2982

2983 Later on, we switched to directly using GCaMP6f transgenic mice
2984 (background: C56BL/6) which express GCaMP6f in the Hippocampus
2985 [Tg(Thy1-
2986 GCaMP6f)GP5.17Dkim JAX stock #025393]. This helped us
2987 circumvent the dye loading or viral injection steps, aiding in the
2988 potential success of the preparations, by way of tissue health and
2989 recording quality.

2990

2991 **Results - Imaging**

2992

2993 **2-Photon calcium imaging of hippocampal CA1, *in vivo***

2994

2995 The CA1 cell body layer is ~200 µm deep, in through the hippocampal
2996 surface. At these depths, scattering of excitation as well as emission
2997 light is significant. However, we are able to image at these depths with
2998 Two-Photon Imaging LASER Scanning Imaging (810 nm for OGB-1
2999 and 910 nm for GCaMP5/GCaMP6f), where a high intensity pulsed
3000 LASER allows for two photons to near instantaneously excite
3001 fluorophores in a thin z-slice plane which is the focal plane of the
3002 Objective. Our LASER, the Coherent Chameleon Ultra II emits ~3 W at
3003 810 nm, and ~2 W at 910 nm. At these depths, there is scattering of
3004 emitted photons. However, since only the focal plane is excited any
3005 and all emitted photons that we capture are part of the signal. We use
3006 a Nikon 16x water immersion, 0.8 NA, 3 mm working distance
3007 Objective (N16XLWD-PF), to get a large field of view.

3008

3009 **Acute Imaging of OGB-1 loaded hippocampal CA1, *in*
3010 *vivo***

3011

3012 We injected OGB-1 dye into brain tissue for our acute imaging
3013 experiments (see Methodology for details). OGB-1 spreads throughout
3014 the cytoplasm and neuropil, and infiltrates the cell nucleus, giving the
3015 cells the appearance of solid circles (cells). The cell body (soma)

3016 ranges from 10-15 μm depending on the orientation of the imaging
3017 layer in 3D tissue space (Figure 25A).
3018

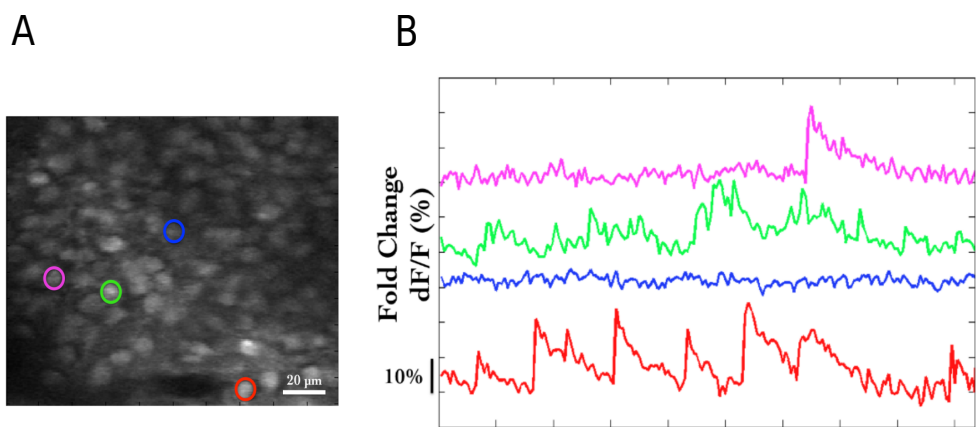


Figure 25: (A) Representative Two-Photon Calcium Image of a plane of Hippocampal CA1 cells, bolus loaded with Oregon Green Bapta-1 (OGB-1), at an instant in time. Example cells marked out post-hoc as pink, green, blue and red. Scale bar 20 μm . (B) Representative dF/F (%) traces for the calcium activity. Recorded in a single 10s video for example cells – pink, green, blue, and red. Scale bar 1 sec; 10% dF/F .

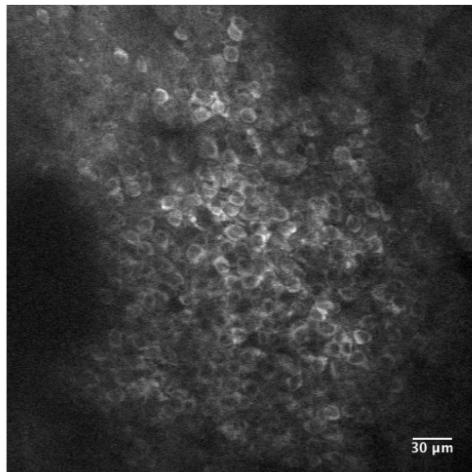
3019 Each cell in the recorded region of interest (ROI), is identified, marked
3020 out (in pixel identity), based on local activity of correlated pixels in the
3021 time series movies. The average intensity of the pixels corresponding
3022 to each cell for each frame in each recording video, is saved as the
3023 raw calcium fluorescence trace. Next, these raw calcium traces are
3024 baseline normalized to equate the baselines for each cell at 0, and
3025 describe the dynamic range of the intensity values as 0 to 1, or 1 to
3026 100%. The corresponding time series of baseline normalized dF/F for
3027 the representative example cells are shown (Figure 25B; Figure 28B).
3028

3029 **Chronic imaging of hippocampal CA1 using GCaMP**

3030

3031 For chronic imaging, tissue health was of paramount concern since it
3032 could easily degrade in time (Figure 26). With practice and
3033 standardization, we were able to get the preparations to survive for 2-4
3034 weeks at very good signal-to-noise. Preparations that resulted in very
3035 poor signal-to-noise were often recorded but have been filtered out of
3036 the data showcased in this thesis. While preparations can sometimes
3037 last even months, typically it is crucial to consider if the ROI for
3038 recording could provide >20 cells, to continue the experiment.
3039 GCaMP is typically designed to be cytosolic and does not typically
3040 cross into the cell nucleus. GCaMP labeled cell bodies appear as
3041 doughnuts in the imaging slice (Figure 26A; Figure 27).

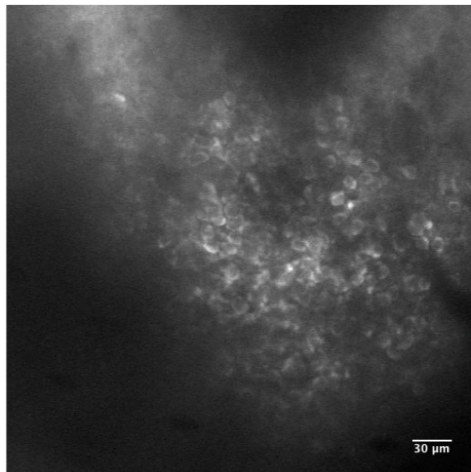
A



DAY 1

Laser Power (at 890 nm): ~50-60 mW
Supply Voltage to PMT: 13.5 V
Control Voltage to PMT: 0.5 V
Preamplifier Sensitivity: 200 nA/V

B



DAY 3

Laser Power (at 890 nm): ~150 mW (!!)
Supply Voltage to PMT: 12-13 V
Control Voltage to PMT: 0.5 V
Preamplifier Sensitivity: 200 nA/V

Figure 26: Tissue Degradation over time. Representative Two-Photon Calcium images of a snapshot in time of the Hippocampal CA1 cell body layer on (A) Day 1 after the surgery and (B) Day 3, after the surgery. Scale bar 30 μm.

3042

3043 Recordings with very good signal-to-noise, where the same chronically
3044 labeled CA1 cells could be anatomically identified on subsequent days
3045 even >2-3 weeks post surgery (Figure 27) were eventually acquired,
3046 and are featured in the data presented in Chapter 4.

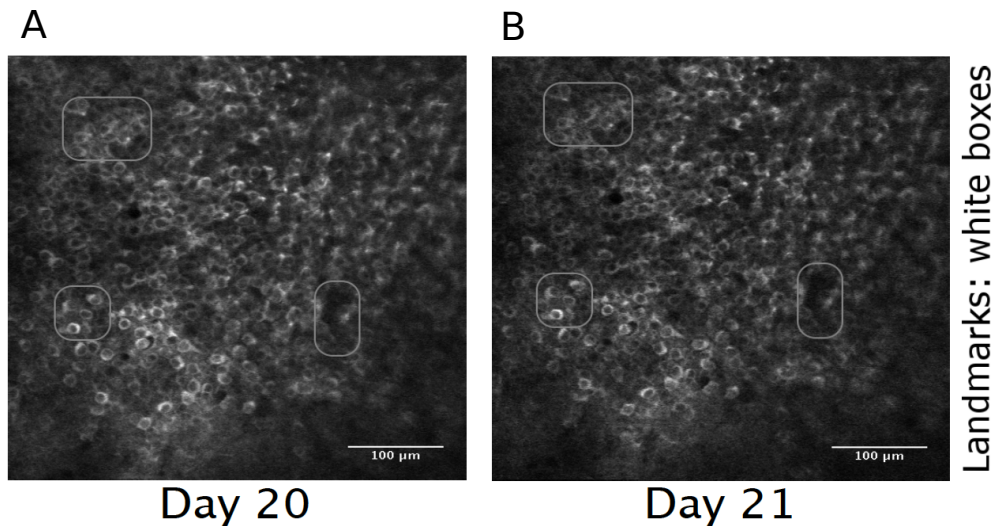


Figure 27: Chronic calcium imaging of the same Hippocampal CA1 cells over weeks. Representative 2-Photon images from (A) Day 20, and (B) Day 21, after surgery. Landmarks have been marked and were used to confirm frame registration and identify cells. Scale bar 100 μm .

3047
 3048 The magnification and resolution of the field of view are important
 3049 parameters to consider when balancing magnification for the resolution
 3050 and the maximization of the number of cells being simultaneously
 3051 recorded from (Figure 25A; Figure 28A).
 3052
 3053 While recording at high frame rates for live imaging, we captured a
 3054 relatively large number of cells (~100) in time-series imaging frames, at
 3055 frame rates of around 10-15 frames per second (FPS). Subsequently,
 3056 we subjected the animal to various stimuli across trials and saved
 3057 these images for analysis.

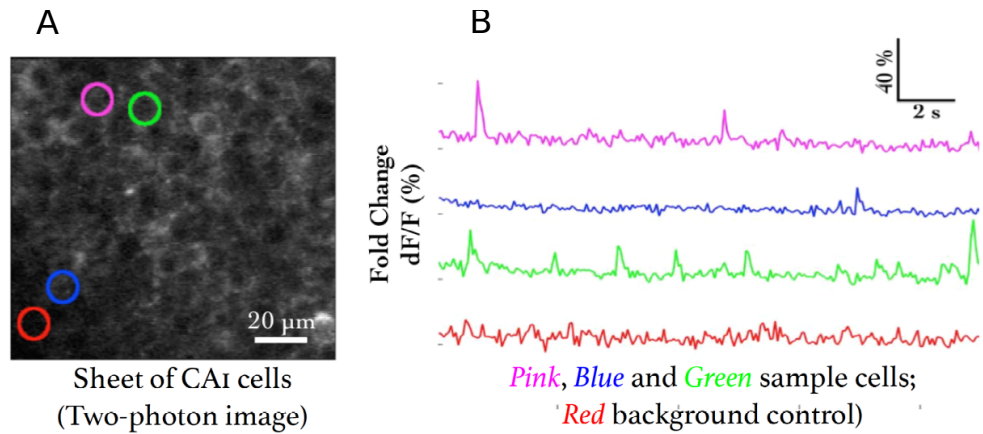


Figure 28: (A) Representative Two-Photon Calcium Image of a plane of Hippocampal CA1 cells expressing GCaMP6f at an instant in time. Example cells marked out post-hoc in pink, blue, and green, with no-cell background in red. Scale bar 20 μ m. (B) Representative dF/F (%) traces for the calcium activity recorded in a single 10s video for example cells – pink, blue, and green, with no-cell background in red. Scale bar 2 sec; 10% dF/F.

3058

3059 **Spontaneous activity during non-stimulus periods**

3060

3061 We recorded the calcium activity from a large number of hippocampal
 3062 CA1 cell bodies, while presenting various neutral and conditioning
 3063 stimuli, including fairly large periods of time before and after stimulus
 3064 presentation. Activity of cells, typically observed *in vivo*, in these
 3065 periods is termed spontaneous activity. Cells may showcase variable
 3066 rate (number of calcium events per sec) and timing. Given proper
 3067 signal isolation for identified cells in an ROI, each source or “cell” may
 3068 be considered independent, *i.e.* - there is minimized cross talk between
 3069 the fluorescence emitted by each cell body.

3070

3071 **Spatial organization of activity correlated cells during**
3072 **spontaneous activity**

3073

3074 As part of our Acute Imaging experiments using OGB-1, we studied the
3075 Pearson's Correlation Coefficient for the activity traces across all cell
3076 pairs, during bouts of spontaneous activity, viz., all frames from the
3077 beginning of the trial till the presentation of the stimulus, across all
3078 trials. Cell pairs showcased a range of correlation coefficients (Figure
3079 29) and we were able to cluster cells based on activity using Meta-K
3080 Means (unpublished data from Dhawale, 2013; Modi et al., 2014). We
3081 set the initial seed to $k = 3$, with 1000 bootstrap iterations (see Modi et
3082 al., 2014 for sensitivity analysis), distance as specified by pair-wise
3083 correlation coefficient (Figure 29A; Figure 31A; Figure 32A), and a
3084 threshold of 80% to bundle meta-groups.

3085

3086 Correlations were calculated for all frames post the whisker-puff
3087 (stimulus), which corresponds to ~8 s of network activity. It is across
3088 this period that the clustering was performed.

3089

3090 The correlation analysis was performed to check for consistency
3091 across previous recordings in the lab (Modi et al., 2014; Ashesh
3092 Dhawale's Thesis). The idea here is to be able to provide proof-of-
3093 principle results to confirm if the technique was working. Additionally,
3094 although the results are from 1 animal, the session consists of 60 trials
3095 for each of the >100 cells recorded. This very preliminary result has
3096 been studied and described in detail, previously (Modi et al., 2014).

3097

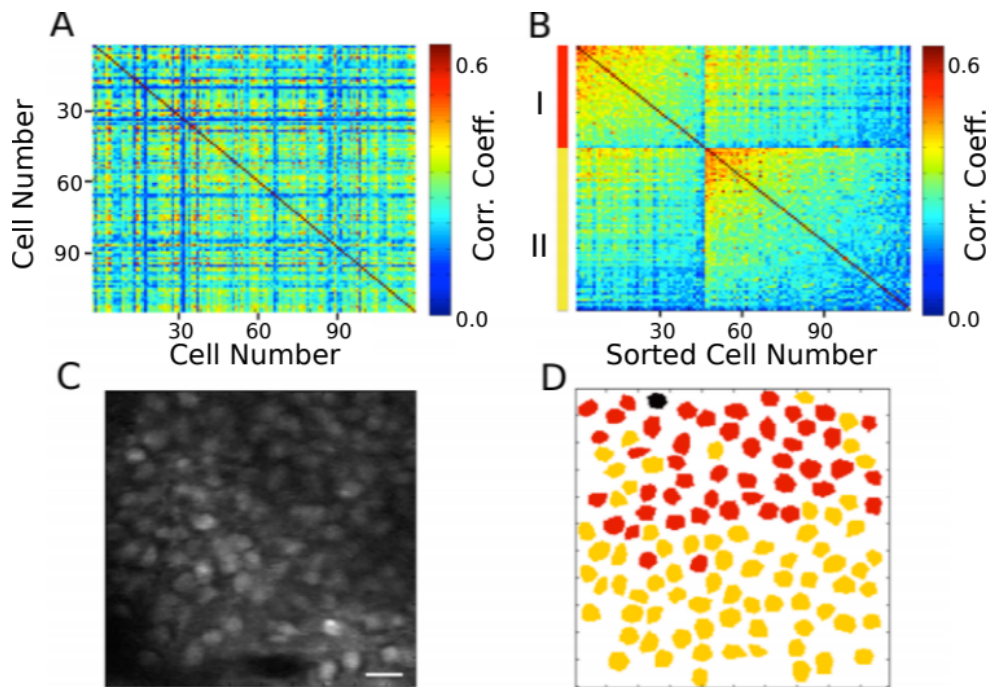


Figure 29: (A) Correlation Coefficients for cell pairs from an example two-photon recording. (B) Meta-K Means clustering with cell pairs using the heuristic that within group pairs would be more similar than between group pairs. In this example, the cells were clustered into two groups, I (red) and II (yellow). (C) Two-Photon image of the field of view of cells; same as Figure 25A. (D) Spatial organization of correlated cell pair groups during spontaneous activity (Modi et al., 2014).

3098 **Stimulus evoked responses**

3099

3100 We also recorded calcium activity from the same cells during
3101 presentation of various neutral stimuli to the animals. Here are the
3102 results of the auditory (tone) and somatosensory (whisker) stimulus
3103 experiments.

3104

3105 A neutral auditory tone at 5000 Hz (for 1 sec) was presented to the
3106 animals N= 6 animals; 25 trials). We observed no clear signs of cell
3107 activity modulation by neutral tones. Below, we show an example
3108 animal with trial-averaged calcium traces as dF/F (%), across all
3109 recorded cells with a 1 sec tone presentation (Figure 30A). We also
3110 presented animals to whisker stimulation by playing a 1s long air-puff
3111 (5 LPM) to the ipsilateral (left) whisker (N = 5 animals; 25 trials). In this
3112 case, we observed whisker-stimulation based cell activity modulation.
3113 Below, we show the trial-averaged calcium traces as dF/F (%) of the
3114 same example animal as above, presented with a 1 sec whisker-puff
3115 (Figure 30B).

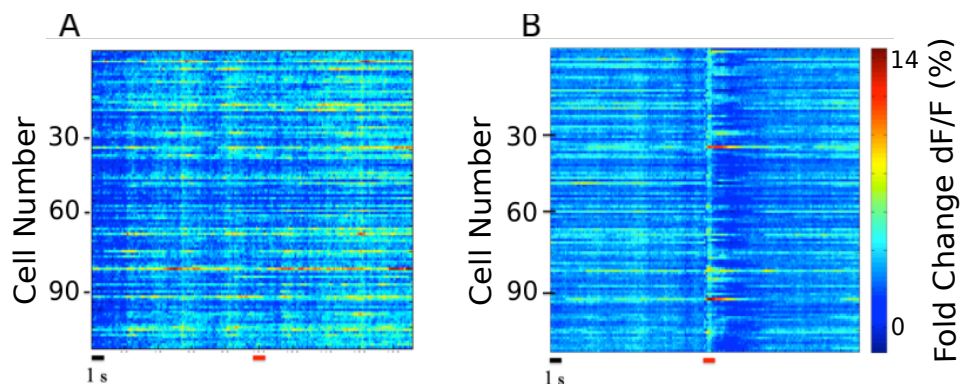


Figure 30: (A) Trial-averaged (25 trials) calcium activity from ~100 CA1 cells in trials where a 5000 Hz tone was presented (red bar). (B) Trial-averaged (18 trials) calcium activity from the same cells in trials where a 5 LPM air-puff to the ipsilateral whiskers was presented (red bar). Scale bar 1 sec (black bar).

3116
3117 The somatosensory cortex damage inflicted was only on one
3118 hemisphere. We presented somatosensory cortex to the ipsilateral
3119 whiskers, information that is expected to be processed on the
3120 contralateral hemisphere. In any case, we observed responses at the
3121 CA1 timed to the presentation of the whisker-puff, unlike trials with
3122 tone. We describe tuning modulations across days for the chronically

3123 tracked time cells in the last section of Chapter 3 – “Imaging”. It is very
3124 difficult to isolate and therefore comment on the effect of tissue
3125 recovery, since we did not directly measure this variable.

3126 **Spatial organization of activity correlated cells post whisker-puff
3127 stimulation**

3128

3129 We attempted the same clustering analysis using Meta-K-Means on
3130 the activity profiles of all the cells post presentation of the whisker-puff
3131 till the end of the trial, across all trials (~8 s). These functionally
3132 correlated cell pair groups were found distributed across the imaging
3133 plane with no clear sign of spatial clustering (Figure 31).

3134 Comparing Figure 29D and Figure 31C, we observe that the whisker-
3135 puff stimulation results in a change in the spatial map of correlated
3136 activity, in the same network of cells.

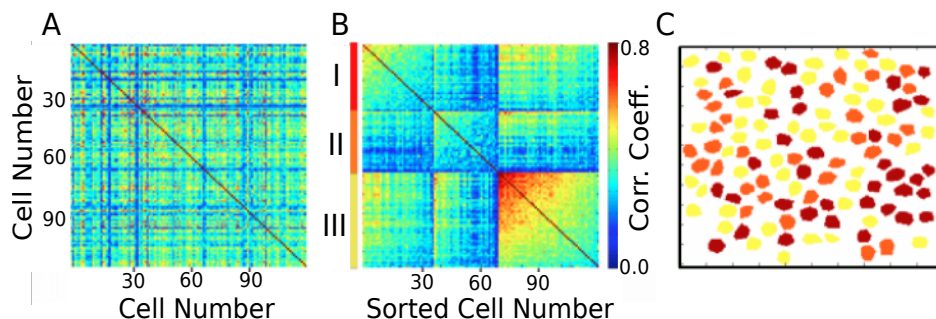


Figure 31: (A) Correlation Coefficients for cell pairs from post whisker-puff stimulation periods. (B) Meta-K Means clustering with cell pairs using the heuristic that within group pairs would be more similar than between group pairs. In this example, the cells were clustered into three groups I (red), II (orange), and III (yellow). (D) No clear spatial organization of correlated cell pair groups post whisker stimulation.

3137

3138 We don't have clear values for the exact duration of the persistence of
3139 the *in vivo*, hippocampal network state post US. This is actually a very
3140 interesting potential experiment, but we did not sub-divide the post-US
3141 period for this analysis. At the time, we only wished to see if our results
3142 were consistent with those previously published (Modi et al., 2014;
3143 Ashesh Dhawale's Thesis), as proof-of-principle for technique
3144 standardization.

3145

3146 As a control, we shuffled the trial time points for each cell
3147 pseudorandomly, to artificially break activity correlations. When we
3148 attempted the Meta-K-Means clustering on this surrogate dataset, we
3149 did not observe functional clustering (Figure 32).

3150

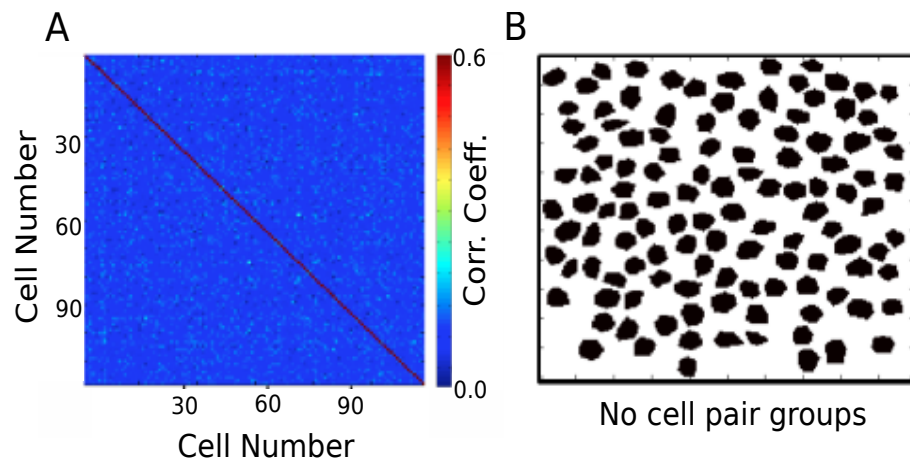


Figure 32: (A) Correlation Coefficients for cell pairs from a trial-shuffle control dataset (B) Meta-K Means clustering revealed that there were no cell pair groups identified.

3154 **Chronic imaging now possible for weeks with the same**
3155 **mouse**

3156

3157 The need for multi-day tracking was mandated for recordings through
3158 behavioural training, since the animals typically only learn Trace Eye-
3159 Blink Conditioning (TEC; Chapter 2) over the course of 3-7 days
3160 (Siegel et al., 2015). A different experiment design would have been to
3161 train animals and then perform the hippocampal preparation to record
3162 CA1 neural activity while the animal(s) exhibit learnt Conditioned
3163 Responses (CRs). However, we argued against this experimental
3164 design, on account of the following.

3165 1. The actual cellular and network mechanisms that allow for the
3166 animal to learn the behavioural task would be very difficult to study
3167 given that the learning period would have passed.

3168 2. The success rate of the hippocampal preparation is typically very
3169 low (estimated at ~33-50% based on the last 200 attempts), given
3170 potential sources of failures such as tissue decay, bleeding into the
3171 imaging window from damaged parts of the hippocampus, implant
3172 instability especially with stressed or unsettled experiment animals,
3173 and photobleaching from the 2-P excitation LASER over multiple
3174 imaging sessions. TEC is typically learnt by >50% animals (Modi et al.,
3175 2014; Siegel et al., 2015). We had argued for exposing the
3176 hippocampus for imaging before behavioural training since any
3177 successful preparations could then be subjected to the relatively more
3178 consistent behavioural training.

3179 3. Having the preparation performed before training minimizes the
3180 number of times the animal would be subjected to surgery (to just the
3181 once), improving chances of animal health through the experiment.

3182

3183 Next, we discuss some preliminary results from the chronic imaging
3184 datasets. A non-overlapping set of results that feature in “Chapter 4 -
3185 Analysis” of this thesis, have been skipped here for brevity.

3186

3187 **Preliminary analysis to identify time cells**

3188

3189 The analysis algorithm pertaining only to the results presented here in
3190 “Chapter 3 - Imaging”, was adapted from William Mau’s Temporal
3191 Information method (Mau et al., 2018; Chapter 4 – “Analysis”). This
3192 version of the algorithm is expected to be subject to some degree of
3193 Type I (false positives) and Type II (false negative) errors.

3194 Subsequently, the algorithm was developed to the extent of the
3195 Python/C++ implementation featured in “Chapter 4 – Analysis”, with
3196 much superior prediction performance.

3197

3198 1. We applied a filter to select for cells that had activity in >25% of
3199 trials (irrespective of tuning)
3200 2. We then develop Peri-stimulus Time Histograms (PSTH), using
3201 Area Under the Curve for a binsize of 3 frames, centering the “0
3202 ms” to the onset of the Conditioned Stimulus for visualization.
3203 3. Next, we estimate Temporal Information (TI), using

$$3204 \quad TI = 1/\lambda * \sum_j \lambda_j \log_2 (\lambda_j / \lambda) P_j$$

3205 where,

3206 λ : Average Transient rate for each cell

3207 λ_j : Average transient rate for each cell in bin “j”

3208 P_j : Probability that the mouse was in time bin “j”

3209 For every trial, we also random shuffled the frame points to develop a
3210 random activity model (1000 times) and ensure that $\lambda > \lambda_{\text{rand}}$ in more
3211 than 99% of the models. Filtering for cells active in >25% trials with a
3212 $\lambda > \lambda_{\text{rand}}$ in >99% shuffles along with the estimation of TI, provided us a
3213 handle on reliability.

3214

3215 We define time cells as cells with a higher probability of eliciting
3216 activation (tuning fields) to specific temporal landmarks across trials,
3217 rather than uniformly over the whole trial. For the results described in
3218 this chapter (Chapter 3 – “Imaging”), our temporal information
3219 calculation was used as a functional definition for time cells.

3220

3221 **Time Cells**

3222

3223 During the experience of temporally organized events or stimuli, in this
3224 case post training to Trace Eye-Blink Conditioning, a rough contingent
3225 of ~20% of the total cells recorded, were observed to showcase time-
3226 locked calcium activity mapping the Blue LED or Conditioned Stimulus
3227 (CS) to the air-puff or Unconditioned Stimulus (US). These cells were
3228 classified as time cells. Here are some example time cells (Figure 33).

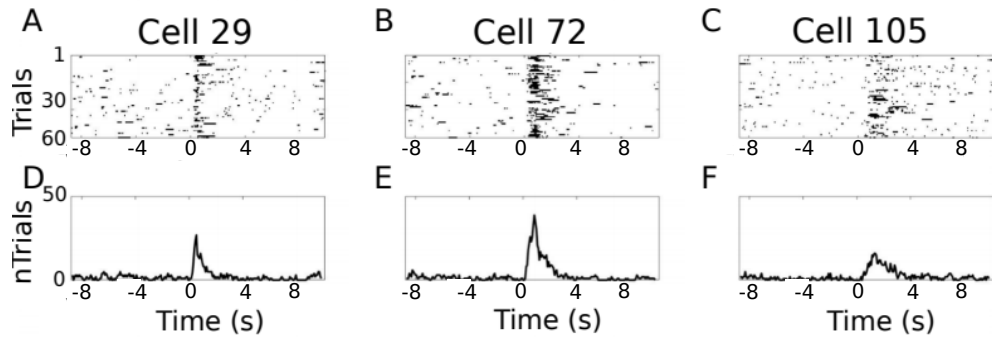


Figure 33: Example Time Cells visualized as event raster plots (A, B, C), along with the trial-summed activity profiles (D, E, F) suggesting ~50% hit trials, for cells 29 and 72 from Session 1 (session type 5) with mouse M26, and slightly lower reliability (~25% hit trials) from cell 105. **The Conditioned Stimulus (CS; blue LED) is presented at time 0 ms.**

3229

3230

3231 Other Cells

3232

3233 On the other hand, most cells did not clear our analysis algorithm

3234 checkpoints and were classified as other cells. Here are some example

3235 Other Cells (Figure 34) from the same session with mouse M26

3236 (Session 1; session type 5).

3237

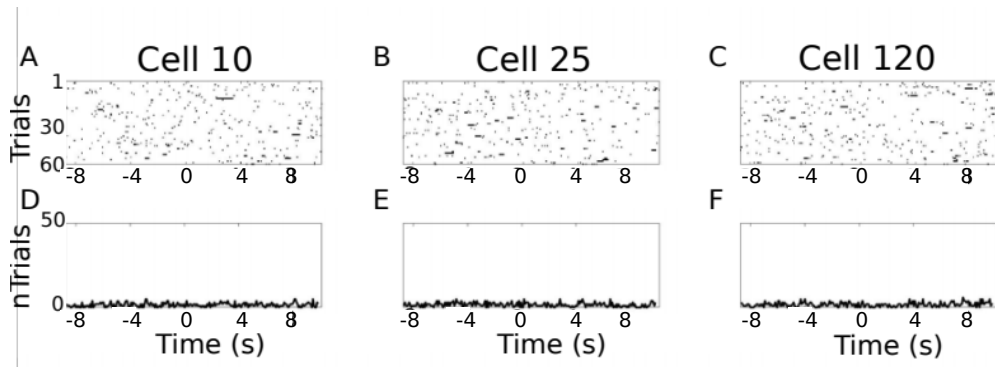


Figure 34: Example Other Cells visualized as event raster plots (A, B, C), along with the trial-summed activity profiles (D, E, F) for cells 10, 25, and 120 from Session 1 (session type 5) with mouse M26. **The Conditioned Stimulus (CS; blue LED) is presented at time 0 ms.**

3238

3239 Considering only the classified time cells, we sorted cells based on the
 3240 time of the peak of the trial-average activity and a spatiotemporal
 3241 sequence was visualized (Figure 35; also see “Chapter 4 - Analysis
 3242 Figure 7H”). **Peri-stimulus time histograms (PSTH) or event time**
 3243 **histograms (ETH)** were created by summing the number of threshold
 3244 crossing activity events per bin (bin size = 3 frames/bin or ~200 ms/bin
 3245 at 14.5 Hz) across trials. Different cells showcase different widths for
 3246 ETH or tuning curves (Figure 35A; Figure 35B).

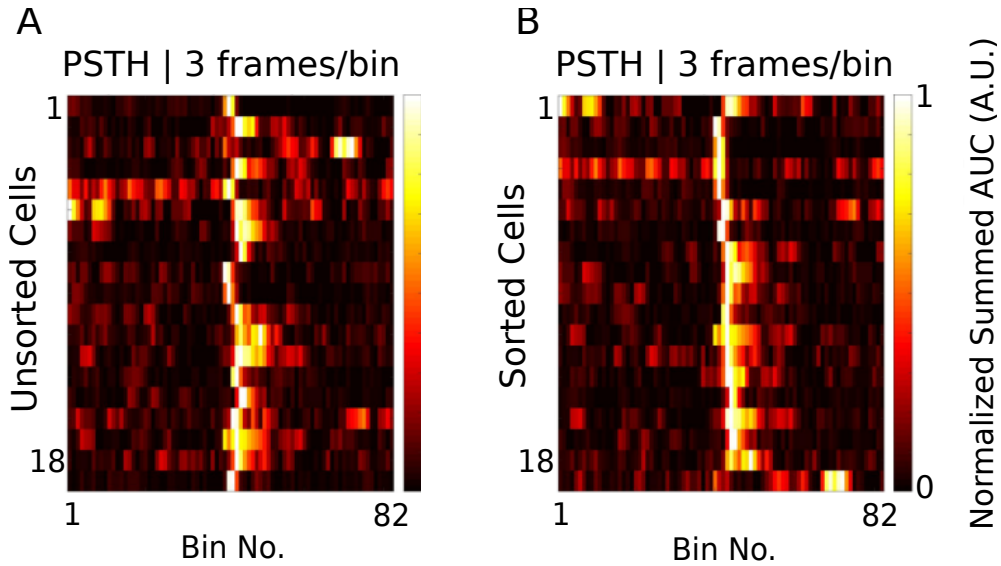


Figure 35: Event Time Histograms or tuning curves for Identified Time-Locked Cells with trial-summed peaks in session 4 of training (session type 5) with mouse M26. (A) Unsorted list of Time cells. (B) Peak-sorted list of the same cells. Here, 1 bin = 3 frames = ~210 ms (sampling rate 14.5 Hz without binning; ~5 Hz with binning). As per the (legacy) session type 5 protocol, the CS (50 ms Blue LED flash) was presented in frame bin 39, followed by a stimulus-free trace interval during frame bins 40 and 41, and then the US (50 ms airpuff to ipsilateral eye) was presented in frame bin 42.

3247

3248

3249 We did not observe any obvious trend in the temporal information of
3250 time cells with peak times. For the same cells (as in Figure 35), we
3251 now look at the actual Temporal Information estimates plotted against
3252 sorted time cells (Figure 36).

3253

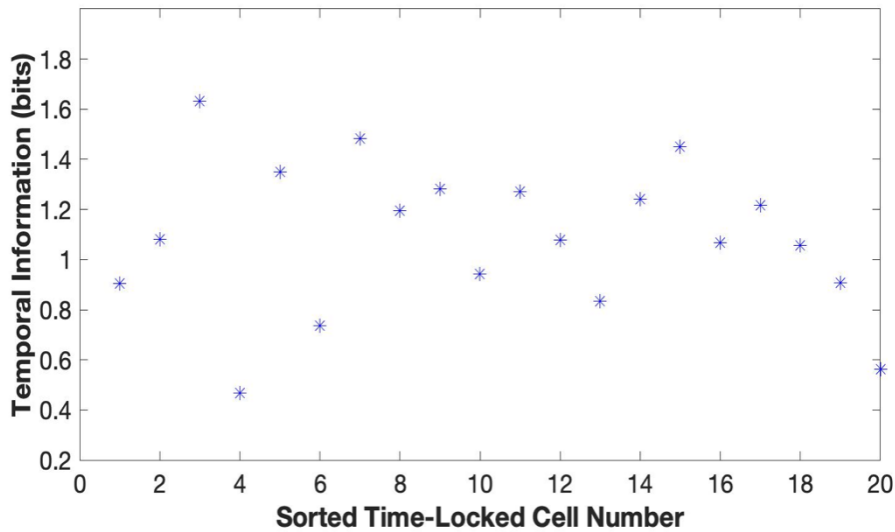


Figure 36: Temporal Information (bits) vs Sorted time cell number from the analytically identified Time Cells in Session 4 (session type 5) with mouse M26. No clear trend was observed.

3270 It has been observed in time cell literature as well as in our real
3271 physiology recordings that time cells with tuning to later time points in a
3272 trial, tend to have wider tuning curves (B. J. Kraus et al., 2015;
3273 MacDonald et al., 2011, 2013; Mau et al., 2018; Pastalkova et al.,
3274 2008). This is why no obvious trend in a graph of Temporal Information
3275 vs time of peak sorted time cells, seemed curious enough to mention in
3276 the thesis. However, while we report the observation, we made no
3277 attempts to delineate further detail, given a limited number of
3278 observations. This legacy adaptation of the temporal information
3279 calculation had not been benchmarked and thus the result was not
3280 certain, at the time. Subsequently, we have observed similar results in
3281 other lab colleague's recordings, and avoided further discussion, with
3282 regard to the scope of this thesis.

3283 **Tuning, re-tuning, and de-tuning of time cells across**
3284 **sessions**

3285
3286 A crucial advantage of the chronic preparation was that many
3287 anatomically aligned and classified cells (as cell ROIs), could be
3288 recorded from over several days and sessions, to look for possible
3289 changes in calcium activity profiles across sessions in the same set of
3290 cells.

3291
3292 We noticed some evidence for an expansion of the set of identified
3293 time cells with sessions, up to a reliable pool of ~20% time cells.
3294 Altogether, from the pool of chronically aligned cells (across sessions),
3295 there was an increase from 7.7% to 23.1% of time cells. Considering
3296 the full cohort cells (irrespective of tracking across multiple training
3297 sessions) the increase was from 7.2% to 21.1% time cells. Here are

3298 the classified time cells between two independent recording sessions,
3299 early in training (Figure 37).

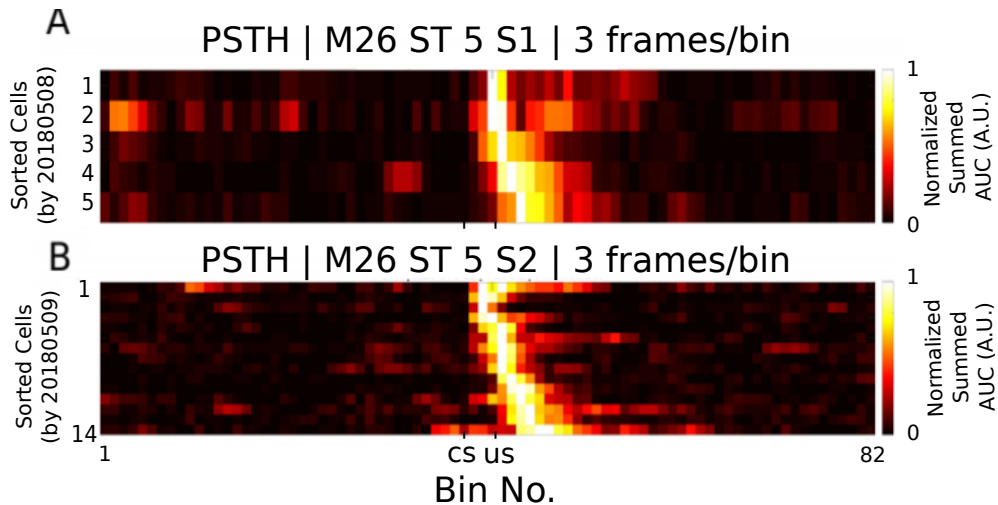


Figure 37: More time cells observed to attain tuning as training sessions. Event Time Histograms of the identified set of time cells between A) Sessions 1 and (B) Session 2, with mouse M26 (session type 5).

3300
3301 The same may also be visualized as trial-averaged calcium activity
3302 profiles for all recorded cells across independent recording sessions
3303 (Figure 38).

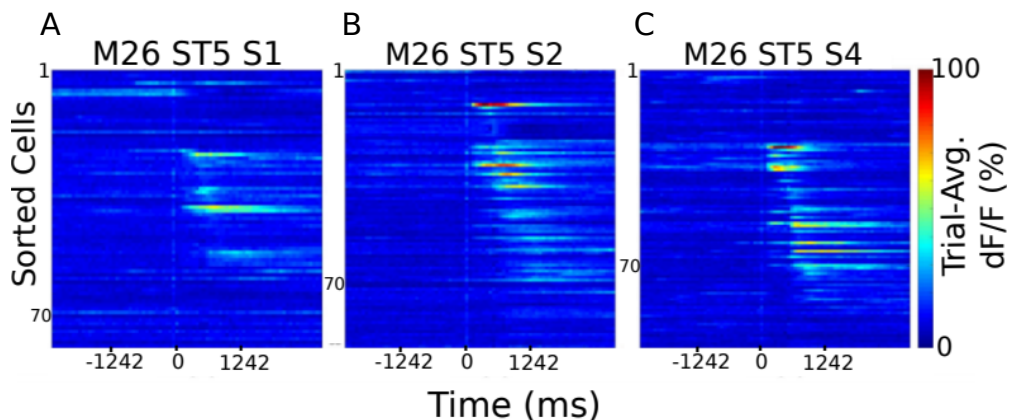


Figure 38: Sorted Time Cells form Sequences that develop with learning. Trial-Averaged calcium activity traces for all recorded cells across A) Session 1, B) Session 2, and C) Session 4, with mouse M26 (sessiontype 5). Time 0 ms was aligned to the CS. The CS + Trace + US interval lasted from 0-600 ms, here.

3304

3305 Chronically tracked time cells that showed reliable tuning across
 3306 sessions were then compared to look for any shifts in the peak tuning
 3307 bin. We observed examples of cells that maintained their tuning across
 3308 pairs of sessions (Figure 39).

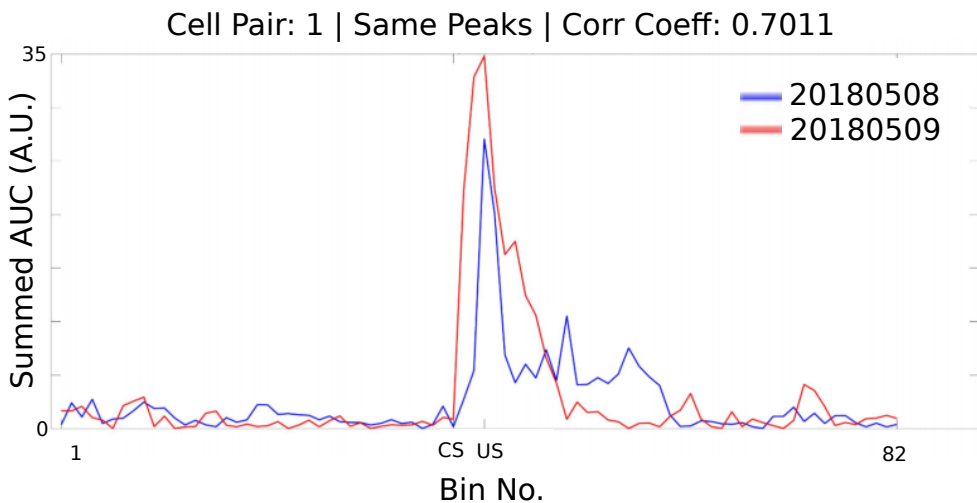


Figure 39: Same/similar tuning across session 1 and session 2 for this example time cell. Blue Event Time Histograms represent the tuning curve for the cell for session 1 (date: 20180508) and Red represent the same but for session 2 (date: 20180509). Pearson's correlation coefficient between the two session pairs was 0.7011.

3309

3310 Here are examples wherein the tuning curve peaks shift to earlier time
 3311 points, across sessions (Figure 40) for Mouse M26, session type 5,
 3312 session 1 vs 2.

3313

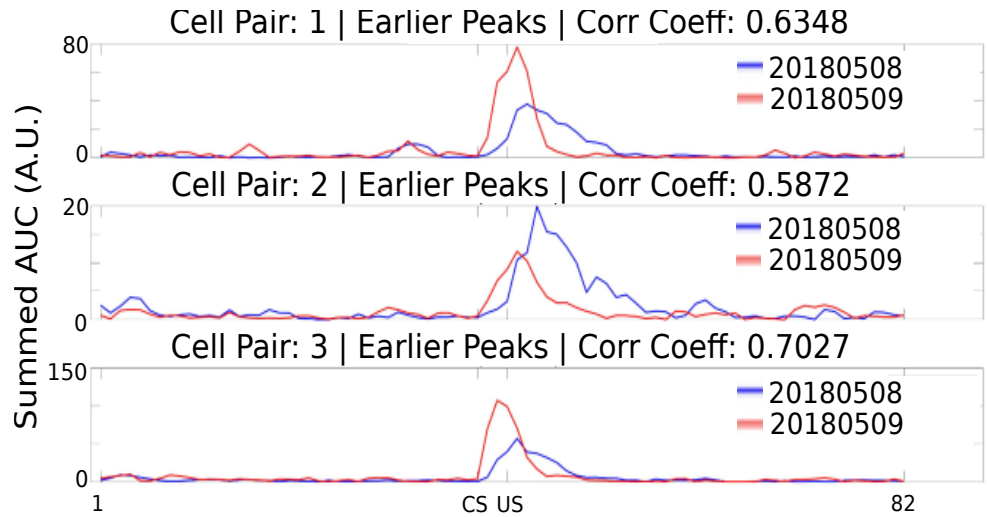


Figure 40: Three example chronically tracked cell pairs with tuning peaks arriving earlier with training sessions (rows). Blue Event Time Histograms represent the tuning curve for any cell for session 1 (date: 20180508) and Red represent the same but for session 2 (date: 20180509). Pearson's correlation coefficient between the session pairs was 0.6.348, 0.5872 and 0.7027 for A) cell pair 1, B) cell pair 2, and C) cell pair3, respectively.

3315 Here is an example of a cell showcasing de-tuning for the CS-US
3316 interval, across sessions (Figure 41), potentially with a new, delayed
3317 peak almost 100 frames later.

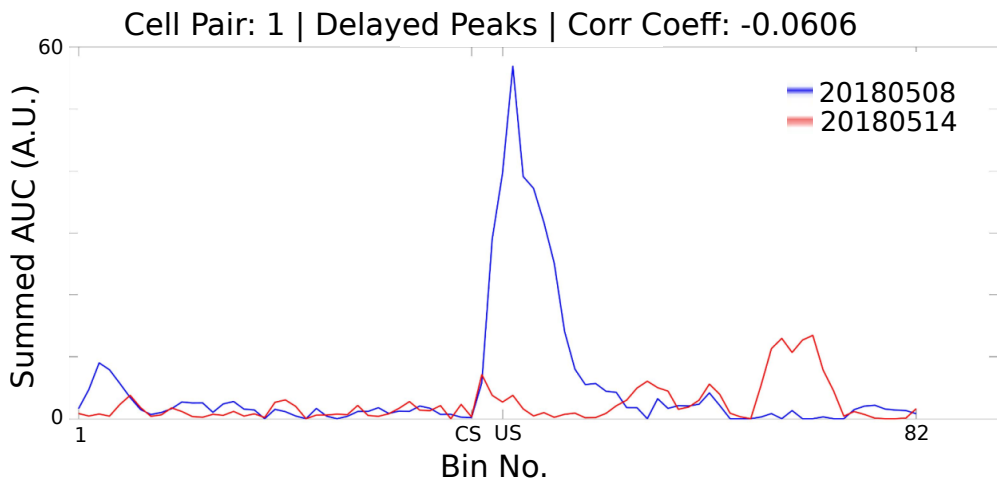


Figure 41: Example chronically tracked cell pair with de-tuning between session 1 and 4. Blue Event Time Histograms represent the tuning curve for the example cell for session 1 (date: 20180508) and Red represent the same but for session 4 (date: 20180514). Pearson's correlation coefficient between the two curves was -0.0606.

3318
3319 A full summary of the correlation based peak timing analysis for
3320 chronically identified time cells with mouse M26 is shown (Figure 42).
3321 Across all same cell pairs (~60% of all session-wise cells tracked; ~80
3322 cells), there was positive correlation (>0.2) in 71% of Time Cells
3323 (Figure 42A). Typically, we observed only at best a correlation
3324 coefficient of ~0.6-0.8 across cell pairs (please kindly refer to Figures
3325 29 and 31). Accordingly, we decided to choose 0.2 as the threshold.
3326
3327 Also a comparison of the tuning curve peaks between the same time
3328 cell pairs (Figure 42B) revealed that a majority of the re-tuned peaks
3329 occurred earlier in time, going across sessions (71%), with an equal

3330 proportion of cells without much re-tuning (14%) or de-tuning to later
3331 time points (14%).

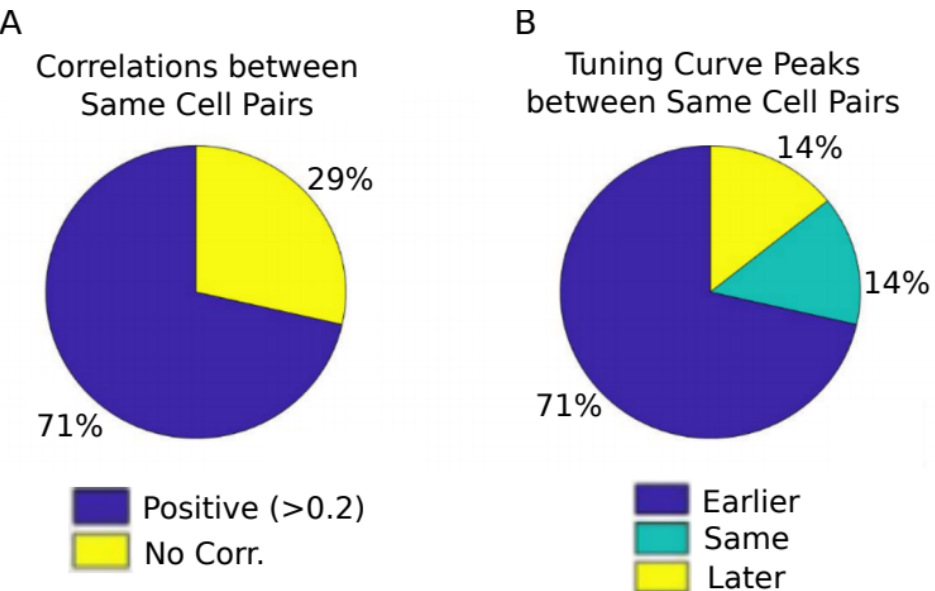


Figure 42: Comparing chronically tracked time cells across sessions for all matched cell pairs by (A) Correlation Analysis, and (B) Timing of peaks.

3332

3333 A summary of the key preliminary results observed using real
3334 physiology data is as follows.

3335 1. Time cell tuning curve peaks typically began only after the
3336 presentation of the CS.

3337 2. The width of the tuning curve peaks for time cells increased with
3338 tuning to later frame bins. This was consistent with the recordings
3339 presented in literature under physiological conditions (B. Kraus et al.,
3340 2013; B. J. Kraus et al., 2015; MacDonald et al., 2011, 2013; Mau et
3341 al., 2018; Pastalkova et al., 2008).

3342 3. Pairwise time cell tuning curves for different time cells may have
3343 some overlap in timing, but peaks were observed in all frame bins
3344 between the CS and the US. This particular observation is confounded

3345 by the short number of Trace period frames recorded and the
3346 requirement to consider 3 recording frames to every bin (Mau et al.,
3347 2018), decreasing the effective sampling rate even further (14.5 Hz
3348 without binning, to ~5 Hz with binning). However, the observation is still
3349 consistent with previous literature (B. Kraus et al., 2013; B. J. Kraus et
3350 al., 2015; MacDonald et al., 2011, 2013; Mau et al., 2018; Modi et al.,
3351 2014; Pastalkova et al., 2008).

3352 4. A surprisingly large number of time cells could be identified with
3353 tuning peaks for frame bins occurring after the termination of the US.
3354 Single cell measurements tend to define responses up to 200-1000 ms
3355 post US. Our own correlation based clustering analysis was across the
3356 whole post US phase (vs pre-stim phase), which corresponded to ~8s.
3357 It was surprising to us, to find the number of time cells even many
3358 frames after the US (>100-200 ms or 1-3 frames at 14.5 Hz).

3359 5. Considering all chronically tracked cells, the classified and sorted
3360 time cells formed sequences that were dynamic across learning
3361 sessions. Many time cells developed tuning curves with sessions while
3362 some time cells lost their tuning.

3363 6. For the majority of time cells, re-tuning occurred with initial tuning to
3364 the timing of the US in earlier sessions, followed by a shift to earlier
3365 time points for the tuning peak, as training progressed through
3366 sessions.

3367
3368 Our preliminary imaging and behaviour results describe neuronal
3369 sequence activations based on the emergence or re-tuning dynamics
3370 of temporal tuning by time cells, during early phases of behavioural
3371 acquisition, in a chronically tracked fashion. Future directions to be
3372 explored in the lab include studying the reliability of a larger pool of
3373 chronically tracked cells with switches in the inter-stimulus interval (ISI)

3374 between the CS and the US as well as with a larger palette of different
3375 stimuli testing out a battery of Conditioned Stimuli (CS1, CS2, etc.) and
3376 Unconditioned Stimuli (US1, US2, etc.). The goal is to understand how
3377 well the internal neural spatiotemporal CA1 sequence maps to the
3378 external behavioural protocol parameters, *in vivo*.

3379 **Bibliography**

- 3380 Abe, R., Sakaguchi, T., Matsumoto, N., Matsuki, N., & Ikegaya, Y.
3381 (2014). Sound-induced hyperpolarization of hippocampal neurons.
3382 *Neuroreport*, 25(13), 1013–1017.
3383 <https://doi.org/10.1097/WNR.0000000000000206>
- 3384 Andersen, P., Morris, R., Amaral, D., Bliss, T., & O'Keefe, J. (Eds.).
3385 (2006). *The Hippocampus Book*. Oxford University Press.
3386 <https://doi.org/10.1093/acprof:oso/9780195100273.001.0001>
- 3387 Attardo, A., Fitzgerald, J. E., & Schnitzer, M. J. (2015). Impermanence
3388 of dendritic spines in live adult CA1 hippocampus. *Nature*,
3389 523(7562), 592–596. <https://doi.org/10.1038/nature14467>
- 3390 Bellistri, E., Aguilar, J., Brotons-Mas, J. R., Foffani, G., & de la Prida, L.
3391 M. (2013). Basic properties of somatosensory-evoked responses
3392 in the dorsal hippocampus of the rat. *The Journal of Physiology*,
3393 591(10), 2667–2686. <https://doi.org/10.1113/jphysiol.2013.251892>
- 3394 Dhawale, A. K. (2013). *Temporal and spatial features of sensory*
3395 *coding in the olfactory bulb and hippocampus*. Tata Institute of
3396 Fundamental Research.
- 3397 Dombeck, D. A., Harvey, C. D., Tian, L., Looger, L. L., & Tank, D. W.
3398 (2010). Functional imaging of hippocampal place cells at cellular
3399 resolution during virtual navigation. *Nature Neuroscience*, 13(11),
3400 1433–1440. <https://doi.org/10.1038/nn.2648>
- 3401 Fanselow, M. S., & Dong, H.-W. (2010). Are the dorsal and ventral
3402 hippocampus functionally distinct structures? *Neuron*, 65(1), 7–19.
3403 <https://doi.org/10.1016/j.neuron.2009.11.031>
- 3404 Harvey, C. D., Collman, F., Dombeck, D. A., & Tank, D. W. (2009).
3405 Intracellular dynamics of hippocampal place cells during virtual
3406 navigation. *Nature*, 461(7266), 941–946.
3407 <https://doi.org/10.1038/nature08499>
- 3408 Hjorth-Simonsen, A., & Jeune, B. (1972). Origin and termination of the
3409 hippocampal perforant path in the rat studied by silver
3410 impregnation. *The Journal of Comparative Neurology*, 144(2),
3411 215–232. <https://doi.org/10.1002/cne.901440206>

- 3412 Itskov, P. M., Vinnik, E., & Diamond, M. E. (2011). Hippocampal
3413 representation of touch-guided behavior in rats: persistent and
3414 independent traces of stimulus and reward location. *PLoS One*,
3415 6(1), e16462. <https://doi.org/10.1371/journal.pone.0016462>
- 3416 Kaifosh, P., Lovett-Barron, M., Turi, G. F., Reardon, T. R., & Losonczy,
3417 A. (2013). Septo-hippocampal GABAergic signaling across
3418 multiple modalities in awake mice. *Nature Neuroscience*, 16(9),
3419 1182–1184. <https://doi.org/10.1038/nn.3482>
- 3420 Kamondi, A. (1998). *Theta Oscillations in Somata and Dendrites of
3421 Hippocampal Pyramidal Cells In Vivo: Activity-Dependent Phase-
3422 Precession of Action Potentials*. 261(March), 244–261.
- 3423 Kraus, B. J., Brandon, M. P., Robinson, R. J., Connerney, M. A.,
3424 Hasselmo, M. E., & Eichenbaum, H. (2015). During Running in
3425 Place, Grid Cells Integrate Elapsed Time and Distance Run.
3426 *Neuron*, 88(3), 578–589.
3427 <https://doi.org/10.1016/j.neuron.2015.09.031>
- 3428 Kraus, B., Robinson, R., White, J., Eichenbaum, H., & Hasselmo, M.
3429 (2013). Hippocampal “Time Cells”: Time versus Path Integration.
3430 *Neuron*, 78(6), 1090–1101.
3431 <https://doi.org/10.1016/j.neuron.2013.04.015>
- 3432 Lovett-Barron, M., Kaifosh, P., Kheirbek, M. A., Danielson, N.,
3433 Zaremba, J. D., Reardon, T. R., Turi, G. F., Hen, R., Zemelman, B.
3434 V, & Losonczy, A. (2014). Dendritic inhibition in the hippocampus
3435 supports fear learning. *Science (New York, N.Y.)*, 343(6173), 857–
3436 863. <https://doi.org/10.1126/science.1247485>
- 3437 MacDonald, C. J., Carrow, S., Place, R., & Eichenbaum, H. (2013).
3438 Distinct hippocampal time cell sequences represent odor
3439 memories in immobilized rats. *The Journal of Neuroscience : The
3440 Official Journal of the Society for Neuroscience*, 33(36), 14607–
3441 14616. <https://doi.org/10.1523/JNEUROSCI.1537-13.2013>
- 3442 MacDonald, C. J., Lepage, K. Q., Eden, U. T., & Eichenbaum, H.
3443 (2011). Hippocampal “time cells” bridge the gap in memory for
3444 discontiguous events. *Neuron*, 71(4), 737–749.
3445 <https://doi.org/10.1016/j.neuron.2011.07.012>
- 3446 Mau, W., Sullivan, D. W., Kinsky, N. R., Hasselmo, M. E., Howard, M.
3447 W., & Eichenbaum, H. (2018). The Same Hippocampal CA1
3448 Population Simultaneously Codes Temporal Information over
3449 Multiple Timescales. *Current Biology*, 28(10), 1499-1508.e4.
3450 <https://doi.org/10.1016/j.cub.2018.03.051>
- 3451 Modi, M. N., Dhawale, A. K., & Bhalla, U. S. (2014). CA1 cell activity
3452 sequences emerge after reorganization of network correlation
3453 structure during associative learning. *eLife*, 3, e01982–e01982.
3454 <https://doi.org/10.7554/eLife.01982>

- 3455 Moser, M.-B., & Moser, E. I. (1998). Distributed encoding and retrieval
3456 of spatial memory in the hippocampus. In *The Journal of*
3457 *Neuroscience* (Vol. 18, pp. 7535–7542). Society for Neuroscience.
- 3458 Nakashiba, T., Young, J. Z., McHugh, T. J., Buhl, D. L., & Tonegawa,
3459 S. (2008). Transgenic inhibition of synaptic transmission reveals
3460 role of CA3 output in hippocampal learning. *Science (New York,*
3461 *N.Y.*, 319(5867), 1260–1264.
3462 <https://doi.org/10.1126/science.1151120>
- 3463 Pachitariu, M., Stringer, C., Dipoppa, M., Schröder, S., Rossi, L. F.,
3464 Dalgleish, H., Carandini, M., & Harris, K. D. (2017). Suite2p:
3465 beyond 10,000 neurons with standard two-photon microscopy.
3466 *BioRxiv*, 61507. <https://doi.org/10.1101/061507>
- 3467 Pastalkova, E., Itskov, V., Amarasingham, A., & Buzsaki, G. (2008). Internally Generated Cell Assembly Sequences in the Rat
3468 Hippocampus. *Science*, 321(5894), 1322–1327.
3469 <https://doi.org/10.1126/science.1159775>
- 3470 Peron, S. P., Freeman, J., Iyer, V., Guo, C., & Svoboda, K. (2015). A
3471 Cellular Resolution Map of Barrel Cortex Activity during Tactile
3472 Behavior. *Neuron*, 86(3), 783–799.
3473 <https://doi.org/10.1016/j.neuron.2015.03.027>
- 3474 Siegel, J. J., Taylor, W., Gray, R., Kalmbach, B., Zemelman, B. V.,
3475 Desai, N. S., Johnston, D., & Chitwood, R. A. (2015). Trace
3476 Eyeblink Conditioning in Mice Is Dependent upon the Dorsal
3477 Medial Prefrontal Cortex, Cerebellum, and Amygdala: Behavioral
3478 Characterization and Functional Circuitry. *ENeuro*, 2(4),
3479 ENEURO.0051-14.2015. <https://doi.org/10.1523/ENEURO.0051-14.2015>
- 3480 Sofroniew, N. J., Flickinger, D., King, J., & Svoboda, K. (2016). A large
3481 field of view two-photon mesoscope with subcellular resolution for
3482 in vivo imaging. *eLife*, 5(JUN2016), 1–20.
3483 <https://doi.org/10.7554/eLife.14472>
- 3484 Stosiek, C., Garaschuk, O., Holthoff, K., & Konnerth, A. (2003). In vivo
3485 two-photon calcium imaging of neuronal networks. *Proceedings of*
3486 *the National Academy of Sciences of the United States of*
3487 *America*, 100(12), 7319–7324.
3488 <https://doi.org/10.1073/pnas.1232232100>
- 3489 Suh, J., Rivest, A. J., Nakashiba, T., Tominaga, T., & Tonegawa, S.
3490 (2011). Entorhinal cortex layer III input to the hippocampus is
3491 crucial for temporal association memory. *Science (New York,*
3492 *N.Y.*, 334(6061), 1415–1420.
3493 <https://doi.org/10.1126/science.1210125>
- 3494 Vinogradova, O. S. (2001). Hippocampus as comparator: Role of the
3495 two input and two output systems of the hippocampus in selection
- 3496

3498 and registration of information. *Hippocampus*, 11(5), 578–598.

3499 <https://doi.org/https://doi.org/10.1002/hipo.1073>

3500

3501

3502 **Chapter 4 – Analysis**

3503

3504

3505 Our efforts to identify the best use cases for the various implemented
3506 time cell analysis algorithms on the basis of a testbed of user-defined,
3507 categorically labeled synthetic data with known ground truth (Project
3508 III), have been consolidated into a publication. The early access
3509 version of our paper (along with supplementary figures) has been
3510 attached.

3511

Novel Tools and Methods

Synthetic Data Resource and Benchmarks for Time Cell Analysis and Detection Algorithms

Kambadur G. Ananthamurthy and Upinder S. Bhalla

<https://doi.org/10.1523/ENEURO.0007-22.2023>

National Centre for Biological Sciences - Tata Institute of Fundamental Research, Bellary Road, Bengaluru - 560065, Karnataka, India

Abstract

Hippocampal CA1 cells take part in reliable, time-locked activity sequences in tasks that involve an association between temporally separated stimuli, in a manner that tiles the interval between the stimuli. Such cells have been termed time cells. Here, we adopt a first-principles approach to comparing diverse analysis and detection algorithms for identifying time cells. We generated synthetic activity datasets using calcium signals recorded *in vivo* from the mouse hippocampus using two-photon (2-P) imaging, as template response waveforms. We assigned known, ground truth values to perturbations applied to perfect activity signals, including noise, calcium event width, timing imprecision, hit trial ratio and background (untuned) activity. We tested a range of published and new algorithms and their variants on this dataset. We find that most algorithms correctly classify over 80% of cells, but have different balances between true and false positives, and different sensitivity to the five categories of perturbation. Reassuringly, most methods are reasonably robust to perturbations, including background activity, and show good concordance in classification of time cells. The same algorithms were also used to analyze and identify time cells in experimental physiology datasets recorded *in vivo* and most show good concordance.

Significance Statement

Numerous approaches have been developed to analyze time cells and neuronal activity sequences, but it is not clear whether their classifications match, nor how sensitive they are to various sources of data variability. We provide two main contributions to address this: (1) a resource to generate ground truth labeled synthetic two-photon (2-P) calcium activity data with defined distributions for confounds such as noise and background activity, and (2) a survey of several methods for analyzing time cell data using our synthetic data as ground truth. As a further resource, we provide a library of efficient C++ implementations of several algorithms with a Python interface. The synthetic dataset and its generation code are useful for profiling future methods, testing analysis toolchains, and as input to computational and experimental models of sequence detection.

Introduction

The mammalian hippocampus is important for the formation of several kinds of memory, one of which is the association between stimuli occurring separately in time. Time cells were originally described using tuning curves from single-unit recordings of cellular activity when rats ran on a running wheel in between behavioral decisions (Pastalkova et al., 2008). These cells exhibited time tuning of the order of seconds. Several further studies have shown that small populations of hippocampal CA1 cells

fire in time-locked sequences, “bridging” the time gap between stimulus and response in temporal delay tasks lasting several seconds (Pastalkova et al., 2008; MacDonald et al., 2011, 2013; Kraus et al., 2013). Cellular calcium imaging studies have also been used to report time cells, albeit at slower sampling rate (Modi et al., 2014; Mau et al., 2018). For example, similar interval tiling properties of hippocampal CA1 neurons were observed on much shorter, 500 ms timescales in a Trace Eyeblink Conditioning (TEC) task (Modi et al., 2014). Spontaneous sequential activity

Received January 2, 2022; accepted February 9, 2023; First published February 23, 2023.

The authors declare no competing financial interests.

Author contributions: K.G.A. and U.S.B. designed research; K.G.A. performed research; K.G.A. and U.S.B. analyzed data; K.G.A. and U.S.B. wrote the paper.

has also been reported in free-running animals (Villette et al., 2015). Such cells with a well-defined temporal firing field are commonly termed time cells (MacDonald et al., 2011; Eichenbaum, 2017). However, there is a wide diversity of methods used to detect and characterize time cells, and it is not clear how consistent these methods are in classifying cells as time cells. It is also unclear how sensitive each method may be to a range of physiological sources of variability and noise. A consistent set of benchmarks of classification performance is necessary to draw accurate and comparable conclusions from real physiology data across different methods and different laboratories. Our approach in the current study is not prescriptive, but pragmatic: we ask how existing methods work when we already know exactly which cells are time cells, and we determine how well each method deals with imperfect data.

The major approaches used to identifying time cells are tuning curves (peristimulus time histograms), temporal information (TI), principal component analysis with time offset, support vector machines, and bootstrap analysis of activity peaks. Several studies have used a temporal delay task lasting several seconds, in which a rat runs on a treadmill during the delay period. A temporal information metric (Mau et al., 2018) has been used to find individual time cells in such tasks. A distinct task involves monitoring recurrent sequences of activity during free-running treadmill recordings. Such datasets have been analyzed using offset principal component analysis (Kaifosh et al., 2013; Villette et al., 2015; Malvache et al., 2016), to first denoise two-photon (2-P) data, establish correlation coefficients, and detect hippocampal CA1 sequences. Time cells have also been reported for much shorter duration tasks (~500 ms) such as hippocampus-dependent trace conditioning (Tseng et al., 2004; Modi et al., 2014). Time cells in these 2-P datasets were identified using yet another method, in which bootstrapping was used to determine whether peak activity at a given time was different from chance. This method was termed ratio of ridge/background (Modi et al., 2014). Yet other methods have utilized support vector machines to categorize time cells (Ahmed et al., 2020). Additionally, while the applicability of a variety of algorithms for place cell detection has been previously compared (Souza et al., 2018), we have

K.G.A. and the experiments received support from the Department of Biotechnology Grant BT/PR12255/MED/122/8/2016 (to U.S.B.). National Centre for Biological Sciences-Tata Institute of Fundamental Research (NCBS-TIFR) provided resources for analysis equipment and support to U.S.B. through intramural funds supported by the Department of Atomic Energy, Government of India, Project Identification No. TRI 4006.

Acknowledgments: We thank Daniel Dombeck for help with the chronic preparation for physiological 2-P calcium recording of hippocampal CA1 cells and William Mau for his Temporal Information calculation code. We also thank Vinu Varghese and Bhanu Priya Somashekhar for helpful comments on this manuscript.

Correspondence should be addressed to Upinder S. Bhalla at bhalla@ncbs.res.in.

<https://doi.org/10.1523/ENEURO.0007-22.2023>

Copyright © 2023 Ananthamurthy and Bhalla

This is an open-access article distributed under the terms of the Creative Commons Attribution 4.0 International license, which permits unrestricted use, distribution and reproduction in any medium provided that the original work is properly attributed.

focused on methods which are fully automatable and which scale well to large datasets, specifically comparing algorithms to detect time cells.

Time cell detection is closely related to sequence detection, which has been fraught with statistical challenges. For example, detection of synfire chains has been the subject of some debate (Ikegaya et al., 2004; Lee and Wilson, 2004; Mokeichev et al., 2007; Schrader et al., 2008). Time cell detection is usually easier, in that in most experiments there is a well-defined initiating stimulus and a known delay or trace phase (however, see Villette et al., 2015). For any cell identified as a time cell, it is desirable to define a score to measure quality or reliability along with decodable time. Hence it is also valuable to be able to compare the score of a time cell across recordings and even between groups, using well defined, analog measures. Each algorithm currently used in the literature implements a different scoring method and it is as yet unclear whether comparable results would be observed with other metrics.

In the current study, we compare these diverse methods by estimating their performance on synthetic test datasets where we controlled all features of the data, including the identity and timing of each time cell. The development of a synthetic dataset serves two purposes. First, it facilitates principled comparison of different methods, since the ground truth is known. Second, it facilitates an analysis over many dimensions of input variance, corresponding to very different experimental and neural circuit contexts. Richness in variety of input data allows for better sampling of the performance of the analyses under many potential conditions. We have explored variance along the key dimensions of noise, timing imprecision, signal widths, frequency of occurrence, as well as several others. To strengthen the applicability of this synthetic data resource to real data, our generated output uses sampled experimental data.

Our experimental data, synthetic dataset, and code base are intended to be a resource for algorithm testing and optimization.

Materials and Methods

Animals, chronic implants, and behavioral training

All animal procedures were performed in accordance with the National Centre for 114 Biological Sciences Institutional Animal Ethics Committee (project ID NCBS115 IAE-2016/20(M)), in accordance with the guidelines of the Government of India (Animal Facility CPCSEA registration number 109/1999/CPCSEA) and equivalent guidelines of the Society for Neuroscience.

To chronically monitor the activity of the same population of hippocampal CA1 cells, we implanted two- to four-month-old male and female GCaMP6f mice [Tg(Thy1-GCaMP6f)GP5.17Dkim JAX stock #025393] with an optical window and head-bar using a protocol adapted from previously published methods (Dombeck et al., 2010). Briefly, anesthesia was induced with 2–3% isoflurane in a chamber, and subsequently maintained (breathing rate of ~1 Hz) with 1–2% isoflurane, directly to the mouse's nose using an inverted pipette tip. Surgery was performed on a

temperature-controlled table, maintained at 36.5°C, while the anaesthetized animal was cheek-clamped. After a haircut, a ~5 cm piece of scalp was cut open to reveal the skull. A ~3 mm circular craniotomy was then performed at a position 2 mm caudal and ~1.5 mm lateral to bregma, on the left hemisphere. After gently tearing off the dura, the underlying cortex was carefully aspirated till the corpus callosum (CC) layer, clearing out any blood using repeated washes of cortex buffer (Modi et al., 2014). A small thickness of corpus callosum fibers were then carefully aspirated till horizontal CC fibers were sparse but visible. The cortex buffer was then carefully suctioned out to dry the exposure till tacky. The exposure was then quickly sealed using a thin layer of Kwik-Sil and a coverslip attached to the bottom of a 3 mm steel cannula. This preparation left the CA1 cell body layer ~200 μm below the most exposed tissue. Finally, an imaging head-bar was surgically implanted and fixed to the scalp, using dental cement and skull screws, before the animal was brought out of anesthesia.

The animals were allowed to recover for 1–5 d after implantation, with a further 3–4 d of habituation to the rig. Following this simultaneous behavioral training and 2-P *in vivo* imaging was conducted.

Trace Eyeblink Conditioning (TEC)

We standardized a multi-session Trace Eyeblink Conditioning (TEC) paradigm to train head-fixed mice, based on previous literature (Siegel et al., 2015). TEC involves an association between a previously neutral conditioned stimulus (CS) with an eyeblink inducing unconditioned stimulus (US), across an intervening, stimulus-free, trace interval. Training involved 60 trials per session, one session a day, for approximately two weeks. The CS was a 50 ms blue LED flash while the US was a 50 ms air-puff to the left eye. The stimulus-free trace interval was 250–750 ms long, depending on the session. Additionally, a pseudorandom 10% of the trials were CS-only probe trials (no US) to test for learning. All behavior routines were controlled by programmed Arduinos. Eyeblinks were measured for every trial, by video camera (Point Gray Chameleon3 1.3 MP Monochrome USB3.0) based detection.

The conditioned response (CR) is observed as a preemptive blink before the US is delivered, in animals that learn the task. The analysis of the behavioral data was performed using custom written MATLAB scripts. In brief, each frame for every trial was:

1. Cropped to get the eye;
2. Binarized to get the pixels defining just the eye, and finally;
3. Given an FEC score from 0 to 1 (see below).

Every trial was then scored as a hit or miss, using the result of a two-sample Kolmogorov-Smirnov test between the FEC during the trace and pre-CS period (1% significance). The performance of an animal for a session was then established as the percentage of hit trials/total trials.

Definitions:

FEC: The fraction of eye-closed is estimated by counting the pixels defining the eye in every image of a time series, normalized by the maximum number of pixels defining the eye, in that session. Thus, every frame was given an analog score from 0 to 1, where,

- 0: fully opened eye
- 1: fully closed eye

CR: The conditioned response is the eye-closing transition during the trace period.

UR: The unconditioned response is the eye-closing transition when the US is delivered.

Performance: Percentage of hit trials/total trials. This allowed us to observe how the animals perform during and across sessions.

Two-photon imaging

We used a custom-built two photon laser-scanning microscope (Modi et al., 2014) to record calcium activity from 100–150 hippocampal CA1 cell bodies *in vivo*, at cellular resolution. We performed galvo-scans through the imaging window, over a field of view of ~100 × 100 μm², at 14.5 Hz, during TEC (Fig. 1A). An Arduino microcontroller was used to control the behavior routines, and it additionally sent a TTL trigger to initiate the imaging trials. The behavior and imaging were conducted simultaneously to record calcium activity when the animal was learning the task.

Time-series fluorescence data for various cells was extracted using Suite2P (Pachitariu et al., 2017). All further analysis and code development was done on MATLAB R2017b and batch analysis runs were performed on MATLAB R2021a. The average of the fluorescence values for cell specific pixels is then converted into the fold change relative to the baseline (dF/F₀; F₀ as 10th percentile), for every marked cell, in every trial (Fig. 1B). These dF/F traces were used for the rest of the analysis.

Curating a library of calcium events

For all synthetic data experiments, we used one good quality 2-P recording session's worth of data from one animal. We mapped our imaging dataset into a matrix of dF/F values for all cells, trials, and frames. We then identified calcium events as signal deviations that were above a threshold (mean ± 2*SD) for more than four consecutive frames (frame rate: 14.5 Hz or ~70 ms per frame). Once identified, we curated a library for each event by a cell, and saved the respective start indices and widths. Using this library, we generated synthetic data by inserting experimental calcium events into the time series for each simulated cell. This approach just uses a time series of signal bins and amplitudes, hence is signal-agnostic and could be applied to other imaging and recording modalities. In the interests of data integrity, our synthetic datasets were watermarked to be distinguishable from real physiology datasets.

Generating synthetic data

Synthetic data were generated using a custom-written MATLAB function script “generateSyntheticData()” in the provided code repository. We preallocated and set up a 3-D matrix of zeros (as cells, trials, frames), and added

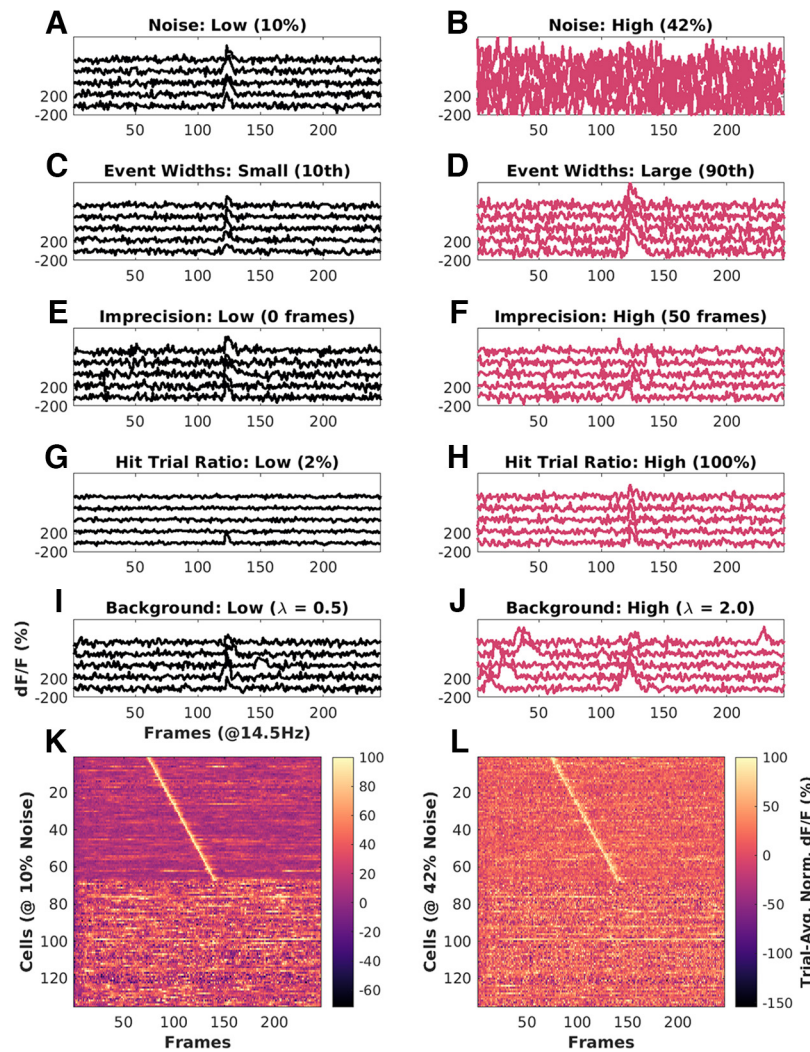


Figure 1. Key features of synthetic datasets. Left, Black panels, Low range of features. Right, Red panels, High range of features. **A**, Noise = 10%. **B**, Noise = 42%. **C**, Event width: 10th percentile ± 1 SD. **D**, Event width 90th percentile ± 1 SD. **E**, Imprecision at 0 frames FWHM. **F**, Imprecision at 50 frames FWHM. **G**, Hit trial ratio from 0% to 2%. **H**, Hit trial ratio from 0% to 100%. **I**, **J**, Background activity with the number of background spikes per background sampled from a Poisson distribution for with mean (λ), for **I**: $\lambda = 0.5$ (low), and **J**: $\lambda = 2.0$ (high). **K**, **L**, Trial-averaged Calcium traces from example synthetic datasets of 135 neurons, displayed as heatmap sorted by time of peak Ca signal. **K**, Baseline physiology synthetic data trial-average with 10% noise (low) and high background activity ($\lambda = 2$ to 3 events/trial). **L**, Same as **K** with 42% noise (high) and comparable background activity ($\lambda = 2$ to 3 events/trial). In both cases, 50% of the cells (top 67) are time cells and the remainder are not. Extended Data Figure 1-1 describes the most important parameters modulated for datasets in each of the three parameter regimes, “Unphysiological,” “Canonical,” and “Physiological,” along with the false positives and false negatives, for each of the 10 implemented algorithms.

calcium events sampled from the Calcium Event Library at frames (time) determined by the synthesis algorithm. The input parameters to this algorithm included timing, noise, imprecision, event width selection, hit trial ratio, background activity, and several others. We aimed to cover the most likely conditions to affect timing and other experiment design properties. In more detail, we generated synthetic datasets using the following control parameters:

- Time cell percent

Value: Number between 0 and 100. This sets the number of cells that are assigned tuned calcium activity as a

percentage of total cells, and controls the number of positive and negative class cells in the dataset.

- Cell order

Value: ‘basic’ or ‘random.’ In ‘basic’ mode, time cells are indexed lower than other cells. In ‘random’ mode, the indices of time cells and other cells are randomly selected. This should have no impact on algorithm detection but is useful for visualization.

- Max hit trial percent

Value: Number between 0 and 100. This sets the maximum possible fraction of total trials, during which a Time Cell will exhibit tuned calcium activity.

- Hit trial percent assignment

Value: ‘fixed’ or ‘random.’ In ‘fixed’ mode, the number of hit trials is set as defined by max hit trial percent. In ‘random’ mode, the number of hit trials is calculated by randomly picking a value from a range ($\frac{1}{2} \times \text{max hit trials}$, max hit trials).

- Trial order

Value: ‘basic’ or ‘random.’ In ‘basic’ mode, the hit trials are indexed lower than miss trials. In ‘random’ mode, the indices of hit and miss trials are randomly selected. Specific patterns of hit and miss trials for a session have not been reported in physiology, so this feature is not implemented.

- Event width

Value: {0–100 percentile value, Integer N}. For each cell, this defines the selection of events based on width in frames. The percentile value is estimated from the histogram of all event widths. The variance of this selection is set by “N,” which adds N^*SD to the selection. All synthetic cells exhibit a range of different calcium events. This is considered an important parameter.

- Event amplification factor

Value: Number from 0 to $+\infty$. This allows additional control to multiplicatively amplify any chosen calcium event, before incorporation. Our library was curated from physiologically recorded signals. The default value is 1.

- Event timing

Value: ‘sequential’ or ‘random.’ In ‘sequential’ mode, the time of peak calcium activity is reflected by the indexing of the time cells. In ‘random’ mode, the time of peak calcium activity is randomly dispersed over the trial frame points.

- Start frame

Value: Number from 0 to total number of frames. This sets the timing of the first cell in a time cell sequence.

- End frame

Value: Number from 0 to total number of frames. This sets the timing of the last cell in a time cell sequence.

- Imprecision full width at half max (FWHM)

Value: Number from 0 to total number of frames. This sets the lower and upper bounds for the difference in timing of calcium activity across trial pairs for a time cell. We use this parameter to model trial to trial variability and is considered an important parameter to test.

- Imprecision type

Value: ‘none,’ ‘uniform,’ or ‘normal.’ In ‘uniform’ and ‘normal’ modes, the trial pair Imprecision is picked from a normal and uniform distribution, respectively. In ‘none’ mode, the trial pair Imprecision defaults to 0.

- Noise

Value: ‘Gaussian’ or ‘none.’ In ‘Gaussian’ mode, the noise is sampled as a time-series vector with points from

a Gaussian distribution. In ‘none’ mode, the noise percent defaults to 0.

- Noise percent

Value: Number from 0 to 100. This allows scaling for any sample noise point, based on the max signal value for any cell.

- Add background spikes for time cells

Value: Boolean 0 or 1. This switch controls the incorporation of background (untuned) activity for putative time cells.

- Add background spikes for other cells

Value: Boolean 0 or 1. This switch controls the incorporation of background (untuned) activity for other (nontime) cells.

- Background distribution mean

Value: Number from 0 to $+\infty$. This sets the mean (λ) of the Poisson distribution to sample from when selecting how many background events to add per trial, for any given cell.

Implementation of a reference quality measure, Q

In order to compare the readouts from the various time-cell detection methods, we implemented a reference measure of quality (Q) of synthetic time cells that used the known inputs to the generation algorithm.

Based on preliminary analysis, we selected following five parameters as the most likely to affect the behavior and detection of time cells:

1. Noise
2. Event width
3. Imprecision
4. Hit trial ratio
5. Background activity

Accordingly, we were able to calculate a reference quality measure, using the following equation:

$$\text{RefQ} = \text{HTR} \times \exp - \{\alpha \times \text{MNP}/100 \times \text{EAF} + \beta \times \text{std. dev. EW}/\text{meanEW} + \gamma \times \text{std. dev. Imp}/\text{Stim Win}\}, \quad (1)$$

where HTR: hit trial ratio

MNP: max noise percent (%)

EAF: event amplification factor

EW: event widths (frames)

Imp: imprecision (frames)

Stim Win: stimulus window (frames)

α : 1

β : 1

γ : 10

The values of α , β , and γ , were set to have comparable effects of each of the terms inside the exponent. This reference Q was useful for debugging code and was the basis for a further metric for time cell classification discussed below. A representative synthetic activity trace for ‘low’ and ‘high’ values of each of these five parameters is shown in Figure 1.

All modulations for the datasets in this study along with the estimates for false positives and false negatives, across all algorithms are shown in Extended Data Figure 1-1.

Separate analysis modules were developed for three categories of analysis

We implemented three analysis modules: *ti*, *r2b*, and *peq*, shorthand for temporal information, ridge-to-background, and parametric equations. The *ti* module implements three algorithms from Mau et al. (2018). The *r2b* module implements two algorithms from Modi et al. (2014). The *peq* module computes estimates for noise, hit trial ratio, event width and imprecision, and estimates a Q score as above. All three methods were implemented in C++ with a PyBind11 interface to Python. This combination is fast and efficient in memory use, and also has the ease-of-use of Python. Thanks to the native MATLAB interface to Python, all three methods can also be called from MATLAB.

Synthetic datasets generated and analyzed in batch mode

We generated datasets pertaining to parameter sensitivity analysis by modulating one of the four main parameters and setting the others to noninterference levels. In this manner, we devised 99 cases to study in which one of the main parameters was varied. Note that in these cases the resultant activity was in an unphysiological regime because other sources of variation were kept to low levels so as not to interfere with the parameter of interest. With three randomized shuffles, we generated 297 unique datasets.

We wanted to use more realistic datasets, where we would modulate one of the four parameters while keeping the others to ranges typical of physiological data. We devised 12 canonical cases. With 10 randomized shuffles each, we generated 120 additional unique datasets in the canonical regime. Finally, we devised 12 physiological regime cases, identical to those in the canonical regime, with the addition of background (untuned) activity. This yielded another 150 datasets, with randomization.

Altogether, we had 567 unique datasets for our tests, each with 135 cells (total: 76,545 cells), 60 trials, and 246 frames/trial. Except when the percent time cells were modulated, all datasets featured 50% time cells.

We next implemented an analysis pipeline to run all the datasets through the time cell detection algorithms, yielding scores and predictions for each case. Finally, all the scores and predictions were collated for comparison and benchmarks as shown in the schematic (Fig. 2).

Metrics for time cell classification performance

Recall is inversely proportional to the number of false negatives (Type II error) and is the fraction of true positive class predictions over all positive class ground labels.

$$\text{Recall} = \text{TPR}/(\text{TPR} + \text{FNR}) \quad (2)$$

Precision is inversely proportional to the number of false positives (Type I error) and is the fraction of true positive class predictions over all positive class predictions.

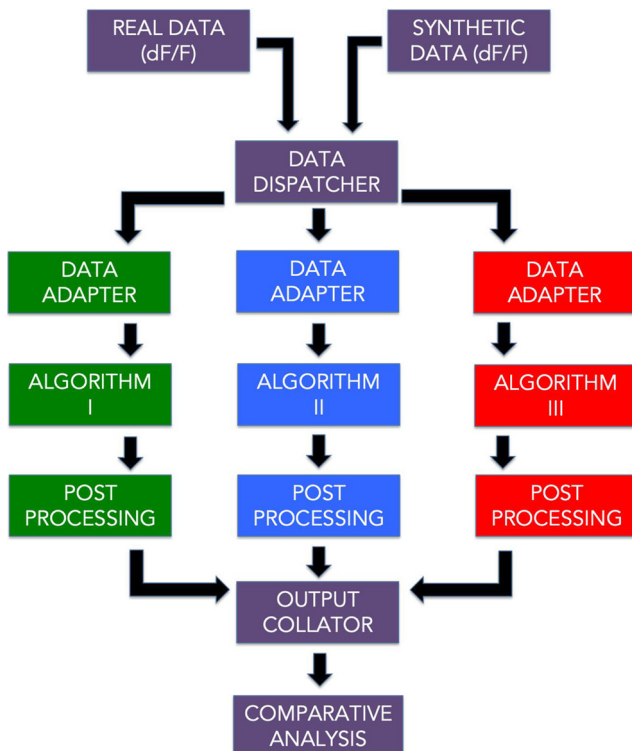


Figure 2. A schematic representation of the analysis pipeline. Physiology data as well as synthetic data were analyzed by 10 different implemented algorithms and the output was collated for comparative benchmarks.

$$\text{Precision} = \text{TPR}/(\text{TPR} + \text{FPR}). \quad (3)$$

F1 Score is the harmonic mean of recall and precision.

$$\text{F1 Score} = 2 * \text{Precision} * \text{Recall}/(\text{Precision} + \text{Recall}), \quad (4)$$

where

TPR: true positive rate

FNR: false negative rate

FPR: false positive rate

Here are the definitions for predictive/classification performance evaluation (Table 1).

Here are the important functions provided in the code base (Table 2).

Here are the MATLAB scripts running the comparative analysis and figure generation (Table 3).

Code and resource availability

The code/software described in the paper is freely available online at <https://github.com/BhallaLab/TimeCellAnalysis>. The code is available as Extended Data 1.

Results

We developed a pipeline (Fig. 2) with 10 different algorithm implementations for time cell detection, which involve scoring and then classifying cells.

Here, we describe the implementation of each of the methods.

Table 1: Definitions for predictive/classification performance evaluation

Ground truth	Prediction/classification	Remark
0/false/other cell	0/false	True negative (TN)
0/false/other cell	1/true	False positive (FP)
1/true/time cell	0/false	False negative (FN)
1/true/time cell	1/true	True positive (TP)

For each detection algorithm, the classification results were compared with known ground truth values to get the total number of true positive (TP), true negative (TN), false positive (FP), and false negative (FN) cases.

Time cell scoring methods and classification

Temporal information: *tiBoot*, *tiMean*, *tiBoth*, *tiMean-O*, *tiBase-O* (Mau et al., 2018)

Here, we used the algorithm from Mau et al. (2018) as follows. There was an initial criterion of cells to have activity in at least 25% of trials. Their activity was summed into event time histograms with a bin size of three frames. The temporal information (TI) was estimated using Equation 5,

$$TI = 1 \times \lambda j \times \log_2 \lambda j \times P_j, \quad (5)$$

where, λ is the average transient rate for each cell;

λj is the average transient rate for each cell in bin “j”; P_j is the probability that the mouse was in time bin “j.”

Bootstrapping was used to determine whether each cell had a TI greater than chance. We circularly randomized the frame points to develop a random activity model (1000 iterations) and classified cells as time cells if $\lambda > \lambda_{rand}$ in >99% of the models for at least two consecutive bins. We implemented the activity filter from Mau et al. (2018); by considering the trial-averaged peak of the calcium traces for each of the cells, and testing for significance using bootstrapping (*tiMean*). A logical AND operation between the prediction lists for *tiBoot* and *tiMean*, provided us with the full Mau et al., 2018 Temporal Information based detection algorithm (*tiBoth*).

Additionally, we used Otsu’s threshold (Otsu, 1979) on the temporal information scores as well as the trial-averaged peaks to get *tiBase-O* and *tiMean-O* using the MATLAB function “graythresh()” (<https://in.mathworks.com/help/images/ref/graythresh.html>). The purpose of adding the Otsu’s threshold-based classification step was to study how well the scores could be classified with a fast thresholding method, rather than the computationally expensive bootstrap.

Table 2: List of important functions provided in the code base

Name	Description	Command line	Location	Language
synthesis Demo.m	Command line demo, output to file: “synthData-demo.mat”. Generates a synthetic 2-P time cell dataset file	\$ cd TimeCellAnalysis/rho-matlab/demos && matlab -nodisplay -nosplash -r “synthesisDemo; quit”	rho-matlab/demos	MATLAB
ti_demo.py	Command-line demo, output to console.	\$ python TcPy(ti_demo.py sampleData/sample_synth_data.mat	TcPy	Python interface and C++ numerics
r2b_demo.py	Command-line demo, output to console. Runs Ridge-to-Background analysis from Modi et al. (2014). Reports R2B Mean and R2B Bootstrap classifications	\$ python TcPy(r2b_demo.py sampleData/sample_synth_data.mat	TcPy	Python interface and C++ numerics
peq_demo.py	Command-line demo, output to console. Runs parametric equation analysis from current study. Reports PEQ threshold classification, and estimates for noise, event width, imprecision, and hit trial ratio for dataset	\$ python TcPy(peq_demo.py sampleData/sample_synth_data.mat	TcPy	Python interface and C++ numerics
ground_truth_check.py	Command-line demo, output to console. Uses synthetic data files to assess accuracy of classification by the various Mau and Modi algorithms	\$ python TcPy/ground-truth_check.py sampleData/sample_synth_data.mat	TcPy	Python interface and C++ numerics
Benchmark.py	Command-line demo, output to console. Simple time and memory benchmarks for the Mau, Modi, or PEQ algorithms	\$ python TcPy/run_batch_analysis.py sampleData/sample_synth_data.mat	TcPy	Python interface and C++ numerics
run_batch_analysis.py	Command-line production script, output to CSV files. Runs a batch analysis using all methods on a data file. Generates .csv files for TI, R2B, PEQ, and ground truth classifications	\$ python TcPy(ti_demo.py sampleData/sample_synth_data.mat	TcPy	Python interface and C++ numerics
pyBindMap.py	Provides an interface for MATLAB programmers, to the python/C__ fuctions using two wrapper functions: runTlanalysis and runR2Banalysis	Utility function, not run from command line	TcPy	Python
dodFbF.m	Utility function to convert experimental raw 2p calcium activity data from Suite2P to df/F form.	Utility function, not run from command line	rho-matlab/CustomFunctions	MATLAB

All these functions should be run from the cloned repository, TimeCellAnalysis.

Table 3: List of paper figure generating scripts

Name	Description	Command line
paperFigures	Plots all figures estimating algorithm performance for synthetic data analysis (paper Figs. 1, 4–6, and 8)	\$ matlab -r "paperFiguresSynth"
Synth.m		
paperFigures	Plots all figures estimating algorithm performance for real physiology data analysis (paper Fig. 7)	\$ matlab -r "paperFiguresReal"
Real.m		
paperFigures	For diagnostics; plots figures estimating algorithm performance over all the regimes (unphysiological, canonical, and physiologic)	\$ cd .. /src && matlab -r "paperFiguresSplits"
Splits.m		

All these functions should be run from the cloned repository, TimeCellAnalysis/p-matlab/paperFigures.

Ratio of ridge/background, *r2bMean*, *r2bBoot*, *r2bBase-O* (Modi et al., 2014)

Here, we re-implemented the algorithm from Modi et al., 2014. The time of peak response for each cell was identified in averaged, nonoverlapping trials' worth of $\Delta F/F$ traces, in the CS-onset to US-onset period, or as specified. The rest of the trials were averaged and the summed area under the time of peak was estimated. The ridge was then defined to be a 200 ms window centered at the peak. Next, we calculated the summed area in the ridge window as well as the background (non-ridge frames) to get the ridge to background ratio. As a control condition, these traces were given random time-offsets and then averaged. An independent time of peak was identified for each random-offset, averaged trace and ridge to background ratio calculated for it. This bootstrapping was repeated 1000 times for each cell's data and averaged. The reliability score was then calculated individually, for each cell, as the ratio of the ridge to background ratio for aligned traces to the mean of that of the random-offset traces (*r2bMean*).

We also studied the significance of each cell's raw *r2b* values by comparing them to each of the *r2b* values of the randomized datasets, thresholding significance at the 99th percentile (*r2bBoot*). Finally, the raw *r2b* values were also thresholding using Otsu's Thresholding (*r2bBase-O*; Otsu 1979).

Parametric equations, *peqBase* and *peqBase-O* (in-house)

We developed this method to score cells in a manner similar to the reference quality, which uses the known ground truth of the input parameters given to the generator functions for the synthetic dataset. Rather than using the known inputs, this method computes the corresponding parameters read out or estimated from the dataset, whether synthetic or real. It is applicable to labeled or unlabeled datasets. It is defined as:

$$Q = \text{HTR} \times \exp - \{\alpha \times N/S + \beta \times \text{std. dev. EW} / \text{mean EW} + \gamma \times \text{std. dev. Imp/Stim Win}\}, \quad (6)$$

where HTR: hit trial ratio

N/S: estimated noise/signal

EW: read out event widths (frames)

Imp: estimated imprecision (frames)

Stim Wind: stimulus window (frames)

$\alpha: 10$

$\beta: 1$

$\gamma: 10$

While $10 \times \alpha$ was required, β , and γ , were inspired by the same used for reference Q. Classification was then performed using Bootstrapping (as described above) as well as Otsu's threshold.

All of these implemented algorithms can handle unlabeled (real) or ground truth labeled (synthetic) data.

A schematic to describe the steps involved in each algorithm is shown (Fig. 3). We were then able to run all our synthetically generated datasets through each of the 10 implemented algorithms and perform comparative benchmarks.

Good predictive power in time cell quality scores despite different distributions

We ran each of the analysis methods on our synthetic datasets to assess how they scored the (known) time cells. There were four methods that provided a scoring function for time-cell classification: *tIMean*, *tIBase*, *r2bBase*, and *peqBase* (Fig. 4A–D). By inspection, these methods appeared to have distinct distributions. Below we describe how we compare the distributions using correlation analysis. In subsequent sections we describe other methods in our study that used these scores to generate a categorization through thresholding or bootstrap.

In these synthetic experiments, time cells were generated with a single calcium event per hit trial. Event insertions into the synthetic datasets were subject to noise, variable selection of event widths, trial-pair or timing imprecision, and hit trial ratio. We generated 99 unique unphysiological combinations (3 \times randomized shuffles) 12 unique canonical regime combinations (10 \times randomized shuffles), as well as 15 unique physiological regime combinations featuring background activity (10 \times randomized shuffles). In all, we performed our comparative analysis studies using 567 datasets, each with 135 cells, 60 trials/session, and 246 frames/trial at 14.5 Hz). We found that only *tIMean* and *tIBase* had a correlation coefficient of ~ 0.6 , whereas other pairs were correlated below 0.4 (Fig. 4E).

Generalized linear regression (GLM) models were generated to look for the ideal thresholding value for the best classification predictions by each method. We used the MATLAB implementation of GLMs (*fitglm*); <https://in.mathworks.com/help/stats/fitglm.html>). This is a linear model assuming a binomial distribution of categories (0 or 1, i.e., other cell or time cell; Collett, 2002). We obtained good predictive power for the four methods that provided a scoring function for time-cell classification. We generated Receiver Operating Characteristic (ROC) curves by going over the full range of thresholds for the range of scores for each method

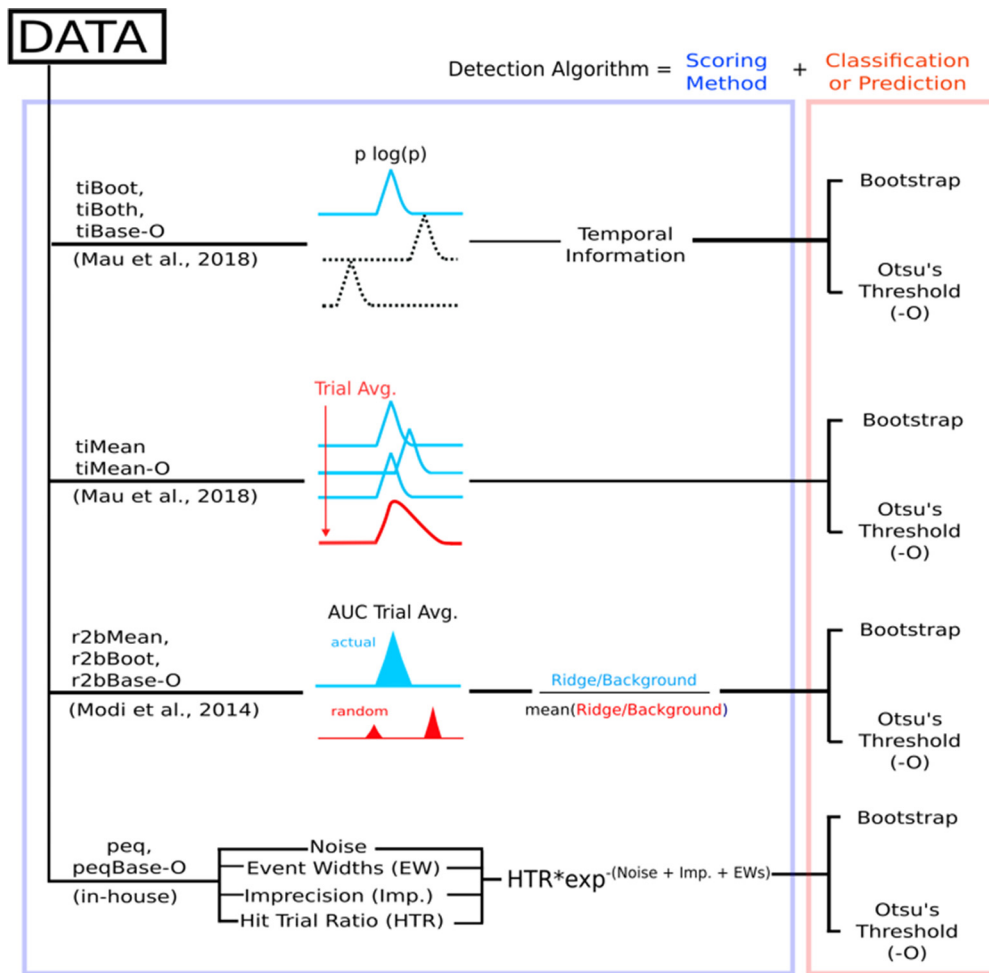


Figure 3. Schematic representation of the implemented algorithms, involving four different scoring methods followed by a classification step (bootstrapping or Otsu's automatic threshold) to have 10 complete time cell detection algorithms.

(ROC curves; Fig. 4F). We found that each distribution of scores had good predictive power, since ideal thresholds could be found to maximize TPR/FPR in all cases. We used the *tiBoth* categorization to distinguish time cells (Fig. 4G) from other cells (Fig. 4H), and plotted trial-averaged calcium traces to visually assess quality of classification as seen from raw data. Overall, each of our methods had distinct distributions of their base scores, but all had good predictive power for classification. The outcome of the classification steps is described in the next sections.

All algorithms exhibit near perfect precision with good recall

Next, we used the scores to classify the cells in our synthetic datasets, compared the predictions to ground truth, and established summaries for true and false cases. Confusion matrices were estimated to compare the predictions (classifications) for each algorithm, with reference to ground truth, and are shown (Fig. 5A,B). All methods exhibit very good precision (true positive classifications over the sum of all positive classifications), suggesting low false positive rates (Type I error; Fig. 5C). Most algorithms also generate good values for recall (true positive

classifications over ground-truth positives). We observed F1 scores (harmonic mean of recall and precision) >0.75 , all the way to 1 (perfect score), for most of the algorithms, as shown (Fig. 5C), suggesting overall usability.

We noticed moderate to strong correlation (>0.8) between the Boolean prediction lists for *tiMean*, *tiBoot*, *tiBoth*, *r2bMean*, and *r2bBoot* (Fig. 5D), but only weak to moderate correlation (<0.6) between the other pairs of predictions. The *tiMean-O* method does slightly better (correlation ~ 0.7 with the first five methods).

Algorithms differ in memory use and speed

Hardware and runtime requirements are a secondary, but practical concern when designing analysis of large datasets, and are specially relevant for experiment designs that require online analysis. We therefore looked at how memory use and runtime scaled on a per dataset basis when considering 67 or 135 cells per dataset ($2\times$).

We ran the memory usage and runtime experiments on a gaming laptop (Lenovo Ideapad 3 Gaming) with a 6 core AMD Ryzen 5 4600H, 16 GB DDR4 RAM (3200 MHz) running MATLAB R2021a on Ubuntu 20.04. Note, however, that we have implemented all the time cell algorithms in

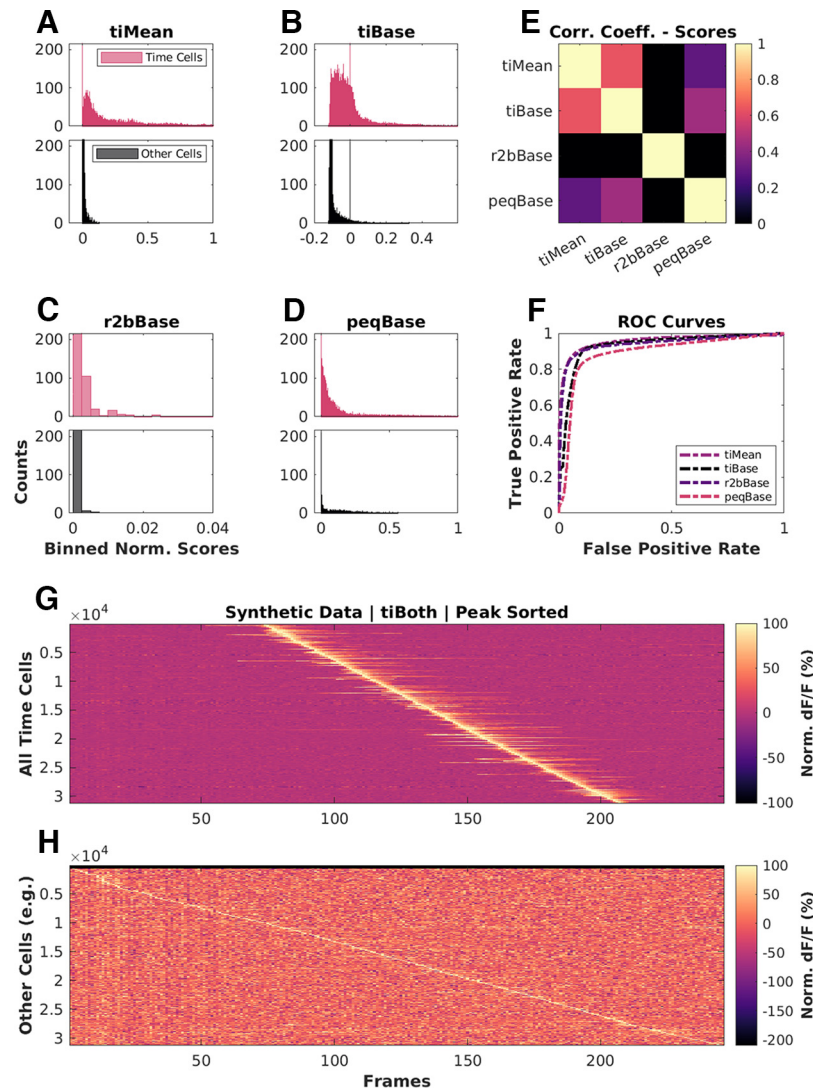


Figure 4. Base scores for different methods differ in their distributions but all have good predictive power. Scores for top (blue): time cells; bottom (red): other cells, across **A**, **tiMean**; **B**, **tiBase**; **C**, **r2bBase**; **D**, **peqBase**. **E**, Pairwise correlation coefficients between the distributions of analog scores (pooling time cells and other cells) by each of the four scoring methods. **F**, Receiver-operator characteristic (ROC) curves after generalized linear regression using the respective distributions of scores and comparisons with known ground truth. **G**, **H**, Trial-averaged calcium activity traces for cells classified as **G**, time cells; **H**, other cells.

serial and these do not use the additional cores. We found that most algorithms ran to completion requiring \sim 15 MB/dataset at a rate of \sim 1–4 s/dataset (135 cells/dataset). With 67 cells/dataset, the memory requirement and runtimes are approximately halved, suggesting that computational costs in memory and time were roughly linear with dataset size. We note that the analysis algorithms work independently for each cell. Thus, in principle, the analysis could be run in an embarrassingly parallel manner and should scale well on multicore architectures.

The synthesis of the main benchmarking datasets ($N=567$ datasets or 76,545 total cells) required a more powerful analysis machine, running a 6 core AMD Ryzen 5 3600, 32GB of DDR4 RAM, running MATLAB R2021a on Ubuntu 20.04. Dataset batches up to \sim 30 datasets ($N=40,500$ cells), however, could be easily handled by a less powerful laptop. The memory usage and runtime for

135 cells per dataset were accordingly, \sim 30 MB/dataset requiring \sim 1 s to complete. Thus, the methods scale readily to handle large datasets on modern hardware.

Physiologic range tests show sensitivity to noise but not to other features of the dataset

We next set out to see how these methods would work in estimated physiological ranges of signal confounds. Given our categorical labels on the synthetic data, we were able to split the datasets to look for the effects of the five main parameters: noise, event widths, imprecision, hit trial ratio, and background activity. We first computed the baseline physiology readouts keeping noise to 10%, event widths to the 60th percentile (± 1 SD), imprecision to 0 frames, hit trial ratios to a range of 33–66%, and background activity to 0.9–1.2 events/trial for time cells

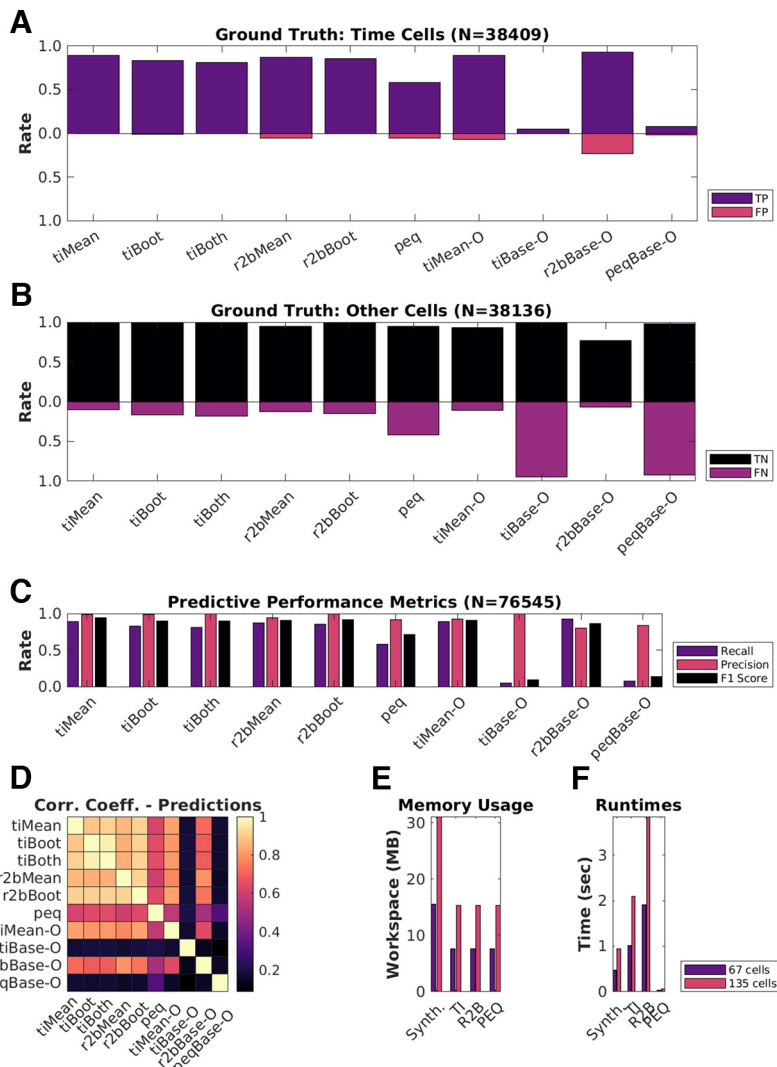


Figure 5. Good predictive performance by all algorithms. **A, B,** Classification performance of each of the 10 implemented detection algorithms. **A,** True positives (TP; purple), false positives (FP; red). **B,** True negatives (TN; black), false negatives (FN; purple). **C,** Predictive performance metrics [Recall = TP/(TP + FN), Precision = TP/(TP + FP), and F1 Score = Harmonic mean of Recall and Precision] to consolidate the confusion matrices. **D,** Pairwise correlation coefficients between the Boolean prediction lists by each of the 10 detection algorithms. Note that the first six methods correlate strongly. **E,** Average memory usage per dataset by the implemented algorithms on datasets with either 67 cells (purple) or 135 cells (red). **F,** Average runtimes per dataset by the implemented algorithms on datasets with either 67 cells (purple) or 135 cells (red).

(~50% of all synthetically generated cells, $N=50$ baseline datasets, 135 cells/dataset, 60 trials/dataset). Next, we established dependency slopes for each of the algorithms, based on their predictions ($N=10$ randomized shuffles for each case; Fig. 6B–F; Extended Data Figs. 6-1, 6-2).

Most methods exhibited a negative dependence of noise (range: 10% to 70%) on prediction F1 score (Fig. 6B). Although many methods are designed with some form of denoising strategy (trial-averaging, etc.), as expected all algorithms ran into classification difficulties at higher Noise levels. This reinforces the value of relatively high signal-to-noise recordings.

The relative insensitivity to event widths (Fig. 6C) is potentially useful for calcium imaging datasets where events may be slow, and in cases where slower tuning curves are

expected. However, this criterion may need to be stringent for analyses that need to precisely identify fine differences in cell responses.

We observed that most algorithms were insensitive to how frequently time cells were active across trials in a session (HTR). This is possibly the reason for the potential confusion among physiologists with regard to how many time cells were expected in a recorded dataset.

We found that the first six algorithms (tiMean, tiBoot, tiBoth, r2bMean, r2bBoot, and peq) gave equivalent predictions in ~66% of cases (Extended Data Fig. 6-1A). Next, we considered the various prediction lists across these top six algorithms and looked for consensus in time cell predictions from the most lenient threshold (“ ≥ 1 ” algorithm), incrementally through the most stringent threshold (“ $=10$ ” algorithms). We thus established a

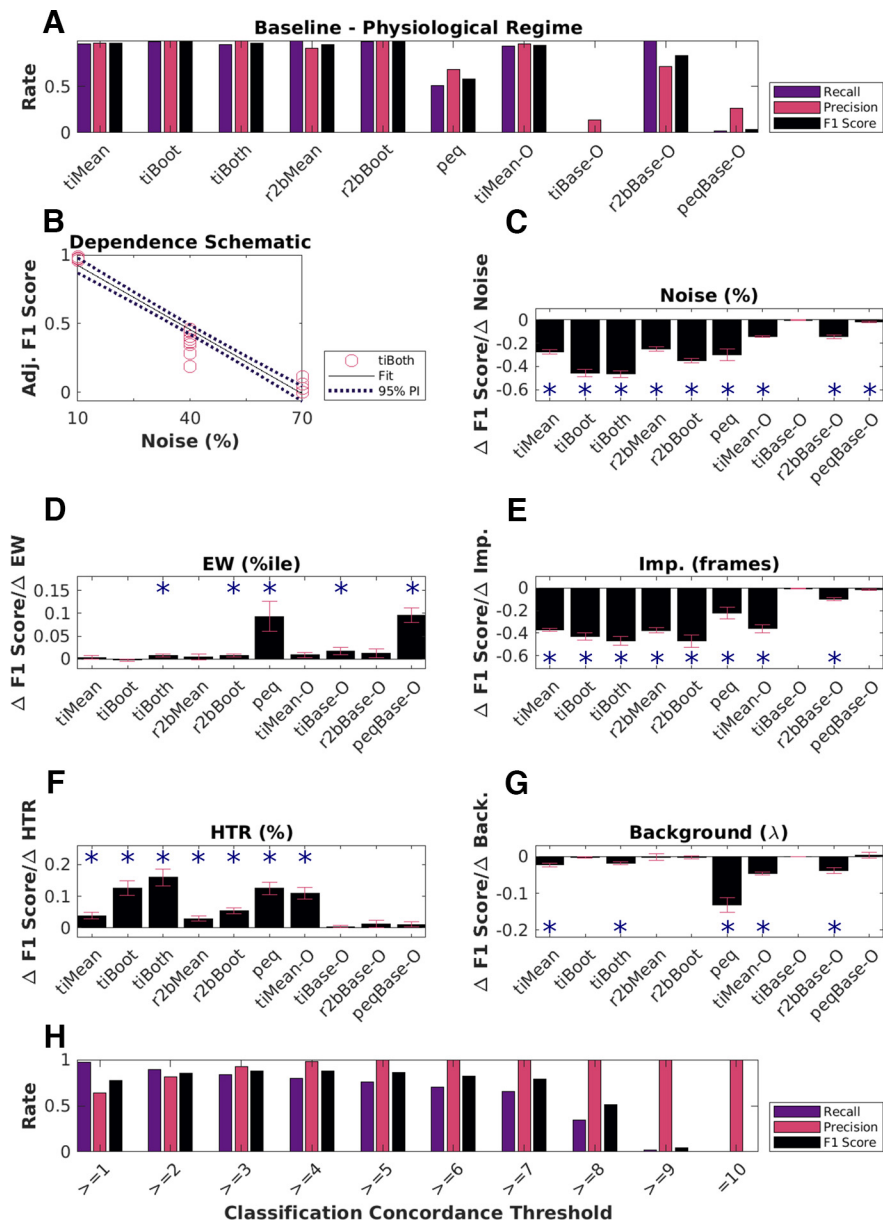


Figure 6. Physiological sensitivity analysis and concordance. **A**, Classification performance scores for all algorithms with the baseline physiology synthetic datasets ($N=6750$ cells). The first five methods perform well. Peq does poorly by all measures when confronted with physiology-range activity variability. Otsu's threshold method for score classification also does not work well for any method under physiological conditions. **B**, Dependence of F1 score on noise as a schematic. This has an overall negative slope (dashed line) which was used for panel **C**, TI-both. A similar calculation was performed for each method. Panels **C–G**, Parameters were systematically modulated one at a time with respect to baseline and the impact on classification score for each algorithm was estimated by computing the slope, using repeats over 10 datasets each with an independent random seed. Significant dependence on the perturbing parameter was determined by testing whether the slope differed from 0 at $p < 0.01$, indicated by asterisks using the MATLAB function `coeffTest()`. Plotted here are bar graphs with mean and error as RMSE normalized by the square root of N ($N=10$ datasets). **C**, Dependence on noise %. **D**, Dependence on event width percentiles. **E**, Dependence on imprecision frames. **F**, Dependence on hit trial ratio (HTR; %). **G**, Background activity (Poisson distribution mean, λ). **H**, Classification performance using concordance for a range of classification thresholds. Extended Data Figure 6-1 describes the three-point line plot dependency curves for the F1 score for each of the implemented algorithms against each of the five main parameters modulated, as the mean of $N=10$ datasets for each case, with error bars as SD. Extended Data Figure 6-2 showcases the linear regression fits for the same, with 95% prediction intervals (PIs), used to estimate the slopes of the various dependency curves.

Concordance based metric for time cell classification. We tested the predictive power of this Concordance based metric, which considers time cells based on consensus among the predictions from all the 10 implemented algorithms.

We identified differences in the classification performance, across the full range of concordance thresholds (Fig. 6H). With lower threshold values (“ $>=4$ ” and below), we notice a slight drop in the Precision, indicating an

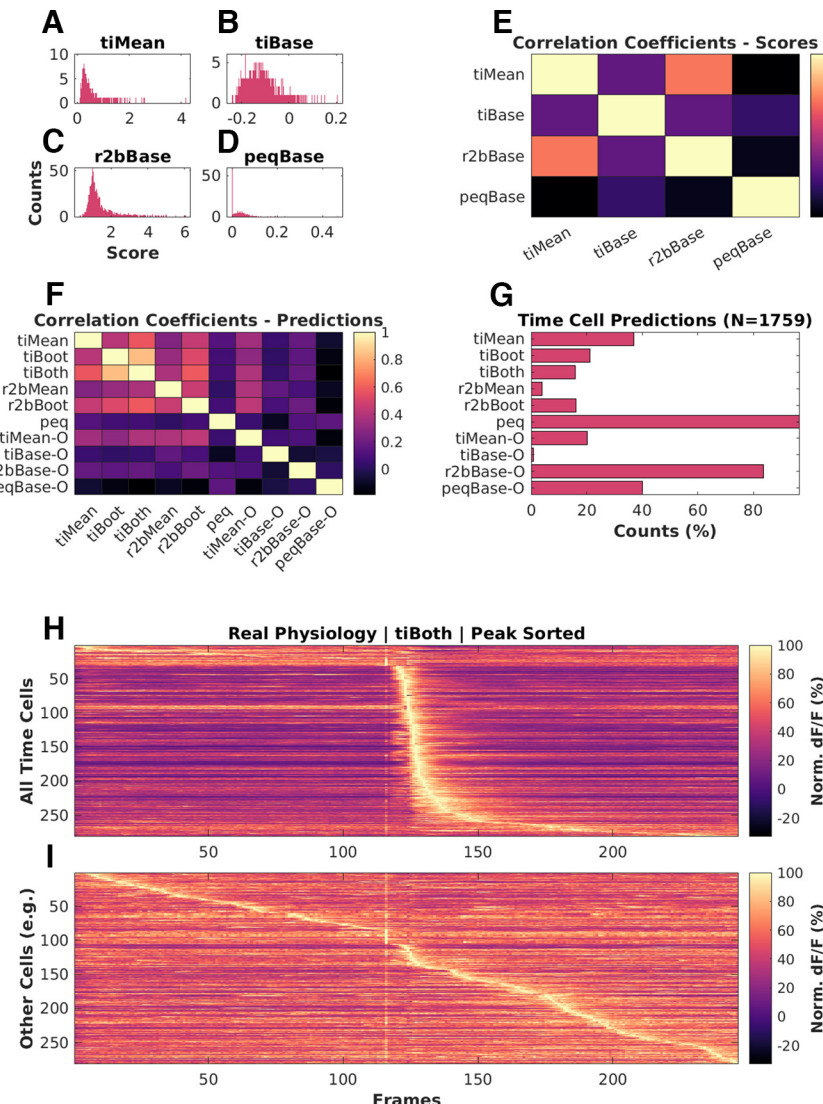


Figure 7. Analysis of experimental 2-P recordings of Ca^{2+} signals. **A–D**, Histograms of scores for physiologically recorded *in vivo* calcium activity from hippocampal CA1 cells (total $N = 1759$), by (A) tiMean, (B) tiBase, (C) r2bBase, and (D) peqBase. **E**, Pairwise correlation coefficients between the distributions of analog scores by the four scoring methods. **F**, Pairwise correlation coefficients between the Boolean prediction lists by the 10 detection algorithms. **G**, Numbers of positive class (time cell) predictions by each of the detection algorithms. **H, I**, Trial-averaged calcium activity traces for (H) time cells and (I) other cells. LED conditioned stimulus (CS) is presented at frame number 116, as seen by the bright band of the stimulus artifact. Most cells classified as time cells are active just after the stimulus. There is a characteristic broadening of the activity peak for classified time cells at longer intervals after the stimulus. Some of the cells at the top of panel **H** may be false positives because their tuning curve is very wide or because of picking up the stimulus transient. Similarly, some of the cells in the middle of panel **I** may be false negatives because of stringent cutoffs, although they appear to be responsive to the stimulus.

increase in false positive rate (Type I error). On the other hand, with increasing threshold values it is the Recall that drops, suggesting a higher false negative rate (Type II error). We find that a concordance threshold of “ $>=4$ ” achieves the best recall, precision, and F1 scores, for time cell prediction (Fig. 6F). The utility of this approach is subject to the availability of resources to apply multiple algorithms to each dataset.

Time cells identified in real physiology recordings

We used the 10 different implemented algorithms on *in vivo* 2-P calcium recordings ($N = 13$ datasets, namely,

1759 isolated cells from three animals across chronically recorded datasets), to compare time cell classification between the algorithms. As we observed for the synthetic data, experimental 2-P Ca traces also yielded different base scores from the four different methods (Fig. 7A–D). Again, consistent with the synthetic data, the pairwise correlation was weak to moderate (Fig. 7E). When we consider the boolean prediction lists (Fig. 7F), we observed moderate pairwise correlation between tiMean, tiBoot, tiBoth, r2bMean, and r2bBoot (>0.5), and low or weak correlation between the other pairs (<0.5). This was consistent with observations for the synthetic data but the correlations were overall slightly

weaker. The total number of time cells predicted were also different across the implemented algorithms (Fig. 7G). Algorithms such as *r2bBase-O* and *peq*, which had more false positives (Fig. 5B) also had more cells classified as time cells. The converse was not true. *r2bMean*, which had moderate false negatives as well as false positives on the synthetic dataset, classified very few of the experimental set as time cells. The trial-averaged activity of the detected time cells (Fig. 7H; including false positives) and other cells (Fig. 7I), based on the predictions by *tiBoth*, are shown. The experimentally recorded time cells exhibited a characteristic widening of tuning curves (Pastalkova et al., 2008; MacDonald et al., 2011, 2013; Kraus et al., 2013; Mau et al., 2018) with tuning to later time points (Fig. 7H).

Overall, four of the algorithms from the literature seemed consistent in their classifications as well as having reasonable numbers of classified time cells. These were the three algorithms from Mau et al. (2018; *tiMean*, *tiBoot*, and *tiBoth*), and the *r2bBoot* method derived from Modi et al. (2014). This is broadly in agreement with their performance on the synthetic datasets.

Discussion

We have developed a full pipeline for comparing time cell detection algorithms. This starts with synthetic datasets for benchmarking, in which we program in the ground truth of cell identity and timed activity, and a range of perturbations characteristic of experiments. These include noise, event widths, trial-pair timing imprecision, hit trial ratio, and background activity. This resource is, in itself, a key outcome of the current study, and though it is designed for 2-P calcium imaging data it can be extended to rate-averaged single-unit recordings. We built a pipeline for running and comparing the outcome from five methods derived from two previous studies, and one from the current work. These algorithms were applied to synthetic and experimental datasets and compared against each other and, where possible, against ground truth. We observed that most algorithms perform well and substantially agree in their time cell classification, but there were different degrees of sensitivity to different forms of signal variability, notably noise and imprecision.

The value of synthetic data in experimental science

Synthetic neural activity datasets are valuable in at least two main ways: evaluating algorithms for detection of important activity features, and for delivering stimuli to *in vitro* and simulated neurons, so as to provide a more physiological context in which to study input-output properties (Abbasi et al., 2020). While we have deployed our synthetic dataset for the specific purpose of comparing time cell detection algorithms, we suggest that it could also be useful for evaluating sequence analysis algorithms (Ikegaya et al., 2004; Foster and Wilson, 2006; Villette et al., 2015). Beyond the domain of neuronal data analysis, such synthetic datasets act as a test-bed for critique and development of analysis algorithms meant for deployment on real-world or typical use case data. They have been used previously to benchmark unsupervised outlier detection

(Steinbuss and Bohm, 2020), explainable machine learning (Liu et al., 2021), intrusion detection systems (Iannucci et al., 2017), 3D reconstruction algorithms (Koch et al., 2021), among several others. We report the first use of synthetic data pertaining to cellular physiology in the context of identifying time cells from network recordings. Moreover, our experiments study important operational differences across several previously published and new detection algorithms.

Our dataset may also be valuable for the second use case, stimulus delivery. There is a growing body of work on network detection of sequences (Ikegaya et al., 2004; Foster and Wilson, 2006; Csicsvari et al., 2007; Jadhav et al., 2012; Villette et al., 2015; Malvache et al., 2016) or even single-neuron sequence selectivity (Branco et al., 2010; Bhalla, 2017). More realistic input activity patterns with a range of physiological perturbations may be useful probes for such experimental and theoretical studies. Further, experimenter-defined neural activity inputs through optogenetic stimulation has already begun to use more complex temporal patterns than static or periodic illumination (Schrader et al., 2008; Dhawale et al., 2010; Bhatia et al., 2021). Our approaches to synthetic sequential neuronal activity generation may be useful to add more physiological dimensions to the sequential activity employed in such studies.

Further dimensions of time cell modulation

Our experiments allowed us to probe for parametric dependence systematically across published and new algorithms. We observed little or no dependence of the predictive performance (F1 score) of the various algorithms to event widths, hit trial ratios, and background activity. We did observe the F1 scores for most algorithms to be negatively dependent on noise and imprecision. On the one hand, this is a useful outcome in that different methods yield similar time-cell classification. It is a limitation, however, if the network uses such response features for coding, since it means that these methods are insensitive to relevant response changes. Further potential coding dimensions were not explored. Thus, several potential behavioral correlates of tuned cells (Ranck, 1973), could not be studied in our experiments. Such correlates include but are not limited to measurements of spatial navigation (O'Keefe and Dostrovsky, 1971; O'Keefe and Nadel, 1978; Wilson and McNaughton, 1993) and decision-making (Foster and Wilson, 2006; Csicsvari et al., 2007; Diba and Buzsáki, 2007; Davidson et al., 2009; Karlsson and Frank, 2009; Gupta et al., 2010; MacDonald et al., 2013; Villette et al., 2015), as well as navigation across tone frequencies (Aronov and Tank, 2014). While each of these further inputs would be interesting to incorporate into synthetic datasets, this requires that the time cell generation algorithm itself incorporate some form of simulation of the neural context. This is beyond the scope of the current study.

A specific limitation of our dataset is that it assumes that time is encoded by individual neurons. This leaves out population encoding schemes in which no one cell responds with the level of precision or consistency that would clear the criteria we use. For example, many of the same studies that use the methods tested here also use

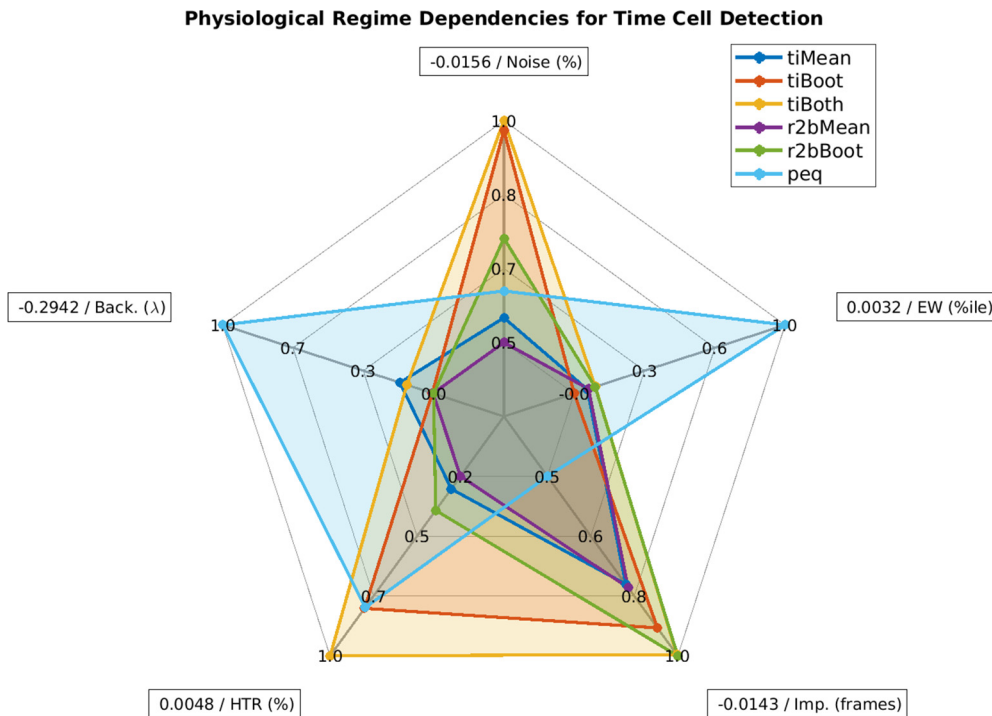


Figure 8. Spider plot summary. Relative sensitivity of the six best detection algorithms (*tiMean*, *tiBoot*, *tiBoth*, *r2bMean*, *r2bBoth*, and *peq*) to the five main parameters for data variability, noise (%), event widths (%ile), imprecision (frames), hit trial ratio (%), and background activity (λ). A perfect algorithm would have very small values (i.e., low sensitivity) for each of the parameters and, thus, occupy only the smallest pentagon in the middle. Note that even the maximal absolute value of sensitivity for most parameters (outer perimeter) is quite small, indicated in boxes at the points of the spider plot.

neural network decoders to report time (Mau et al., 2018). Such decoders might detect time encoding without time cells. A similar situation of individual versus network coding appears for the closely related problem of sequence representation. Place cell replay sequences have been shown to be modulated by the prevalence of location specific aversive (Wu et al., 2017) as well as appetitive stimuli (Bhattarai et al., 2020). Such physiological findings have been the subject of theoretical models of behavior planning (Foster, 2017; Mattar and Daw, 2018), and have been reported to improve performance on multiple Atari games by artificial neural networks (Mnih et al., 2015) featuring salience detection and experience mapping. We suggest that synthetic data for such higher-order encoding schemes might be a useful tool, and could draw on the approaches in the current study.

Comparative analysis benchmarks and concordance

A particularly challenging time cell classification problem is when the same cells may play different timing roles, such as forward and reverse replay. This is made more difficult because of the relative rarity of forward replay sequences over the more typical reverse replay (Diba and Buzsáki, 2007; Foster, 2017). Preplay is also a topic of some debate (Dragoi and Tonegawa, 2013; Foster, 2017). At least one possible problem in such debates is the degree of consistency between time cell or sequence classifiers. Our pipeline allows for (1) error correction in case of nonconcordant classifications, (2) suggest candidate algorithms

with a dependence on dataset features like event widths, imprecision, and hit trial ratio, as well as (3) the possibility to expand the detection regime in more realistic physiological datasets using concordance.

Which algorithms to use?

We did not set out to rank algorithms, but our analysis does yield suggestions for possible use domains based on sensitivity to experimental perturbations (Fig. 8). In cases where runtime and compute resource use is a concern, we recommend using the temporal information method with Bootstrap along with the activity filter (*tiBoth*). Combinations of *tiBoth* with *r2bBoth* may be useful where there are rare and potentially multimodally tuned time cells (Pastalkova et al., 2008; Villette et al., 2015), either to combine their classification for stringent time cell identification, or to pool their classified cells. While it is tempting to use Otsu's threshold as a very fast alternative to bootstrapping, we found that none of the Otsu variants of these methods did a good job of classification. Ultimately, five of our algorithms *tiMean*, *tiBoot*, *tiBoth*, *r2bMean*, and *r2bBoth*: all based on either Mau et al. (2018) or Modi et al. (2014), have very good Precision, and classify with very few false positives (low Type I error). Many methods are susceptible to classification errors if the dataset has high noise.

Here we also implemented the parametric equation (*peq*) algorithm. It is not very good for time cell classification per se, as it is prone to false positives and is susceptible to noise and low hit trial ratios. However, it generates useful

additional estimates of the four key parameters of real data, namely, noise, hit trial ratio, event width and imprecision. This is useful for a first-pass characterization of the properties of the dataset.

Sequence detection in large-scale recordings and scaling of analysis runs

The discovery of replay over the past two decades, has benefitted from the technological advances made in increasing the cellular yield of network recordings and has been reviewed previously (Foster, 2017). Further advances such as with the large scale recordings of $\sim 10^3$ single units by electrical recording using Neuropixels (Jun et al., 2017), fast volumetric fluorescence scanning with up to $\sim 10^4$ cells using resonant electro-optic imaging (Poort et al., 2015; Pachitariu et al., 2017; Bowman and Kasevich, 2021), $\sim 10^3$ mesoscopes (Sofroniew et al., 2016), as well as advances in automated cell region of interest (ROI) detection, denoising, and neuropil subtraction (Pachitariu et al., 2017; Pnevmatikakis et al., 2016) only increase the scale and size of datasets, likely leading to longer analysis runtimes. In addition to our recommendations above for the temporal information/boot method for scalable time-cell analysis, our C++/Python implementations may also be useful in further optimizing these methods. Our implementations allow for relatively fast analysis of the same datasets with multiple algorithms.

References

- Abbasi S, Maran S, Jaeger D (2020) A general method to generate artificial spike train populations matching recorded neurons. *J Comput Neurosci* 48:47–63.
- Ahmed MS, Priestley JB, Castro A, Stefanini F, Solis Canales AS, Balough EM, Lavoie E, Mazzucato L, Fusi S, Losonczy A (2020) Hippocampal network reorganization underlies the formation of a temporal association memory. *Neuron* 107:283–291.e6.
- Aronov D, Tank DW (2014) Engagement of neural circuits underlying 2D spatial navigation in a rodent virtual reality system. *Neuron* 84:442–456.
- Bhalla US (2017) Synaptic input sequence discrimination on behavioral timescales mediated by reaction-diffusion chemistry in dendrites. *Elife* 6:e25827.
- Bhatia A, Moza S, Bhalla US (2021) Patterned optogenetic stimulation using a DMD projector. *Methods Mol Biol* 2191:173–188.
- Bhattarai B, Lee JW, Jung MW (2020) Distinct effects of reward and navigation history on hippocampal forward and reverse replays. *Proc Natl Acad Sci U S A* 117:689–697.
- Bowman AJ, Kasevich MA (2021) Resonant electro-optic imaging for microscopy at nanosecond resolution. *ACS Nano* 15:16043–16054.
- Branco T, Clark BA, Häusser M (2010) Dendritic discrimination of temporal input sequences in cortical neurons. *Science* 329:1671–1675.
- Collett D (2002) Modeling binary data. London: Chapman and Hall.
- Csicsvari J, O'Neill J, Allen K, Senior T (2007) Place-selective firing contributes to the reverse-order reactivation of CA1 pyramidal cells during sharp waves in open-field exploration. *Eur J Neurosci* 26:704–716.
- Davidson TJ, Kloosterman F, Wilson MA (2009) Hippocampal replay of extended experience. *Neuron* 63:497–507.
- Dhawale AK, Hagiwara A, Bhalla US, Murthy VN, Albeau DF (2010) Non-redundant odor coding by sister mitral cells revealed by light addressable glomeruli in the mouse. *Nat Neurosci* 13:1404–1412.
- Diba K, Buzsáki G (2007) Forward and reverse hippocampal place-cell sequences during ripples. *Nat Neurosci* 10:1241–1242.
- Dombeck DA, Harvey CD, Tian L, Looger LL, Tank DW (2010) Functional imaging of hippocampal place cells at cellular resolution during virtual navigation. *Nat Neurosci* 13:1433–1440.
- Dragoi G, Tonegawa S (2013) Distinct preplay of multiple novel spatial experiences in the rat. *Proc Natl Acad Sci U S A* 110:9100–9105.
- Eichenbaum H (2017) On the integration of space, time, and memory. *Neuron* 95:1007–1018.
- Foster DJ (2017) Replay comes of age. *Annu Rev Neurosci* 40:581–602.
- Foster DJ, Wilson MA (2006) Reverse replay of behavioural sequences in hippocampal place cells during the awake state. *Nature* 440:680–683.
- Gupta AS, van der Meer MAA, Touretzky DS, Redish AD (2010) Hippocampal replay is not a simple function of experience. *Neuron* 65:695–705.
- Iannucci S, Kholidy HA, Ghimire AD, Jia R, Abdelwahed S, Banicescu I (2017) A comparison of graph-based synthetic data generators for benchmarking next-generation intrusion detection systems. 2017 IEEE International Conference on Cluster Computing (CLUSTER), Honolulu, HI, pp. 278–289, <https://doi.org/10.1109/CLUSTER.2017.54>.
- Ikegaya Y, Aaron G, Cossart R, Aronov D, Lampl I, Ferster D, Yuste R (2004) Synfire chains and cortical songs: temporal modules of cortical activity. *Science* 304:559–564.
- Jadhav SP, Kemere C, German PW, Frank LM (2012) Awake hippocampal sharp-wave ripples support spatial memory. *Science* 336:1454–1458.
- Jun JJ, et al. (2017) Fully integrated silicon probes for high-density recording of neural activity. *Nature* 551:232–236.
- Kaifosh P, Lovett-Barron M, Turi GF, Reardon TR, Losonczy A (2013) Septo-hippocampal GABAergic signaling across multiple modalities in awake mice. *Nat Neurosci* 16:1182–1184.
- Karlsson MP, Frank LM (2009) Awake replay of remote experiences in the hippocampus. *Nat Neurosci* 12:913–918.
- Koch S, Worcel M, Silva C, Alexa M (2021) Hardware Design and Accurate Simulation of Structured-Light Scanning for Benchmarking of 3D Reconstruction Algorithms (Vol. 2021). Proceedings of the Neural Information Processing Systems Track on Datasets and Benchmarks 1 (NeurIPS Datasets and Benchmarks 2021). Retrieved from <https://openreview.net/forum?id=bNL5VfTe3p>.
- Kraus B, Robinson R, White J, Eichenbaum H, Hasselmo M (2013) Hippocampal “time cells”: time versus path integration. *Neuron* 78:1090–1101.
- Lee AK, Wilson MA (2004) A combinatorial method for analyzing sequential firing patterns involving an arbitrary number of neurons based on relative time order. *J Neurophysiol* 92:2555–2573.
- Liu Y, Khandagale S, White C, Neiswanger W (2021) Synthetic benchmarks for scientific research in explainable machine learning. <https://github.com/abacusai/xai-bench>.
- MacDonald CJ, Lepage KQ, Eden UT, Eichenbaum H (2011) Hippocampal “time cells” bridge the gap in memory for discontinuous events. *Neuron* 71:737–749.
- MacDonald CJ, Carrow S, Place R, Eichenbaum H (2013) Distinct hippocampal time cell sequences represent odor memories in immobilized rats. *J Neurosci* 33:14607–14616.
- Malvache A, Reichinnek S, Villette V, Haimerl C (2016) Awake hippocampal reactivations project onto orthogonal neuronal assemblies. *353:1280–1283*.
- Mattar MG, Daw ND (2018) Prioritized memory access explains planning and hippocampal replay. *Nat Neurosci* 21:1609–1617.
- Mau W, Sullivan DW, Kinsky NR, Hasselmo ME, Howard MW, Eichenbaum H (2018) The same hippocampal CA1 population simultaneously codes temporal information over multiple time-scales. *Curr Biol* 28:1499–1508.e4.
- Mnih V, Kavukcuoglu K, Silver D, Rusu AA, Veness J, Bellemare MG, Graves A, Riedmiller M, Fidjeland AK, Ostrovski G, Petersen S, Beattie C, Sadik A, Antonoglou I, King H, Kumaran D, Wierstra D,

- Legg S, Hassabis D (2015) Human-level control through deep reinforcement learning. *Nature* 518:529–533.
- Modi MN, Dhawale AK, Bhalla US (2014) CA1 cell activity sequences emerge after reorganization of network correlation structure during associative learning. *Elife* 3:e01982.
- Mokeichev A, Okun M, Barak O, Katz Y, Ben-Shahar O, Lampl I (2007) Stochastic emergence of repeating cortical motifs in spontaneous membrane potential fluctuations in vivo. *Neuron* 53:413–425.
- O'Keefe J, Dostrovsky J (1971) The hippocampus as a spatial map. Preliminary evidence from unit activity in the freely-moving rat. *Brain Res* 34:171–175.
- O'Keefe J, Nadel L (1978) The hippocampus as a cognitive map. Oxford: Clarendon Press.
- Otsu N (1979) A threshold selection method from gray level histograms. *IEEE Trans Syst Man Cyber* 9:62–66.
- Pachitariu M, Stringer C, Dipoppa M, Schröder S, Rossi LF (2017) Suite2p: beyond 10,000 neurons with standard two-photon microscopy. *BioRxiv* 061507. <https://doi.org/https://doi.org/10.1101/061507>.
- Pastalkova E, Itskov V, Amarasingham A, Buzsáki G (2008) Internally generated cell assembly sequences in the rat hippocampus. *Science* 321:1322–1327.
- Pnevmatikakis EA, Soudry D, Gao Y, Machado TA, Merel J, Pfau D, Reardon T, Mu Y, Lacefield C, Yang W, Ahrens M, Bruno R, Jessell TM, Peterka DS, Yuste R, Paninski L (2016) Simultaneous denoising, deconvolution, and demixing of calcium imaging data. *Neuron* 89:285–299.
- Poort J, Khan AG, Pachitariu M, Nemri A, Orsolic I, Krupic J, Bauza M, Sahani M, Keller GB, Mrsic-Flogel TD, Hofer SB (2015) Learning enhances sensory and multiple non-sensory representations in primary visual cortex. *Neuron* 86:1478–1490.
- Ranck JB, J (1973) Studies on single neurons in dorsal hippocampal formation and septum in unrestrained rats. I. Behavioral correlates and firing repertoires. *Exp Neurol* 41:461–531.
- Schrader S, Grün S, Diesmann M, Gerstein GL (2008) Detecting synfire chain activity using massively parallel spike train recording. *J Neurophysiol* 100:2165–2176.
- Siegel JJ, Taylor W, Gray R, Kalmbach B, Zemelman BV, Desai NS, Johnston D, Chitwood RA (2015) Trace eyeblink conditioning in mice is dependent upon the dorsal medial prefrontal cortex, cerebellum, and amygdala: behavioral characterization and functional circuitry. *eNeuro* 2:ENEURO.0051-14.2015.
- Sofroniew NJ, Flickinger D, King J, Svoboda K (2016) A large field of view two-photon mesoscope with subcellular resolution for in vivo imaging. *Elife* 5:e14472.
- Souza BC, Pavão R, Belchior H, Tort ABL (2018) On information metrics for spatial coding. *Neuroscience* 375:62–73.
- Steinbuss G, Bohm K (2020) Generating artificial outliers in the absence of genuine ones—a survey. *arXiv*. <https://doi.org/10.48550/arXiv.2006.03646>.
- Tseng W, Guan R, Disterhoft JF, Weiss C (2004) Trace eyeblink conditioning is hippocampally dependent in mice. *Hippocampus* 14:58–65.
- Villette V, Malvache A, Tressard T, Dupuy N, Cossart R (2015) Internally recurring hippocampal sequences as a population template of spatiotemporal information. *Neuron* 88:357–366.
- Wilson MA, McNaughton BL (1993) Dynamics of the hippocampal ensemble code for space. *Science* 261:1055–1058.
- Wu CT, Haggerty D, Kemere C, Ji D (2017) Hippocampal awake replay in fear memory retrieval. *Nat Neurosci* 20:571–580.

3675 specific frequency “landmarks” during the auditory sequence (Aronov
3676 et al., 2017). The CA1 were, thus, argued to be capable of tuning to
3677 abstract variables and were designed to map out sequences of
3678 events/stimuli in their own spatiotemporal patterns of activity.

3679

3680 The ubiquity of neural sequences in a wide variety of systems has
3681 been discussed previously (Bhalla, 2019; Conen & Desrochers, 2022;
3682 S. Zhou et al., 2020) and over a century of research has discovered
3683 remarkable physiological features that may be used to identify neurons
3684 that participate in these sequences. However, research is still required
3685 to carefully dissect out the contribution that each participant neuron
3686 has to behaviour, an important goal in neuroscience (Ranck, 1973,
3687 1975).

3688

3689 The use of user-configurable, categorically labeled synthetic calcium
3690 activity profiles allowed us to probe and compare a range of different
3691 time cell detection algorithms, identifying strategies to best classify
3692 time cells. We were able to identify Temporal Information as a strong
3693 contender for the choice of algorithm for such classification
3694 (Ananthamurthy & Bhalla, 2023). The algorithms developed along the
3695 way were tested within the time scales of ~100 ms, that correspond to
3696 Replay Sequences or other behaviour timescale sequences. We
3697 expect the analysis routines to be useful in a variety of different
3698 experiments that could potentially help describe the neural code in
3699 more detail.

3700 **Better temporal resolution requires new**
3701 **techniques**

3702
3703 There are many other techniques that experimenters in the field have
3704 employed to record activity. Many of these techniques do, in fact,
3705 achieve much better temporal resolution. Here are some examples:

3706 1) Resonant Scanning based 2p calcium imaging can achieve even up
3707 to 30 Hz for 4x larger fields of view, or more frame rates for smaller
3708 fields of view (Bonin et al., 2011; Leybaert et al., 2005; Nguyen et al.,
3709 2001; Rochefort et al., 2009). At the time when we started the
3710 experiments for the thesis, Resonant scanning microscopes required a
3711 lot of additional, expensive components to be purchased. Towards this,
3712 we co-wrote a sanctioned DBT grant application
3713 (BT/PR12255/MED/122/8/2016) and began setting up the new
3714 microscope. However, we did not have this technology available for
3715 experiments before 2020.

3716 2) High-density tetrodes can be used to perform electrical recordings
3717 at >=20 kHz, as compared to ~14.5 Hz for our galvo-scanning 2p
3718 calcium imaging experiments. This technique typically achieves yields
3719 of ~40 cells for hippocampal recordings, and we argued that we could
3720 achieve a higher yield (>100 cells) with galvo-scanning 2p calcium
3721 imaging. The relative sparsity of the hippocampal neural code in terms
3722 of cells participating in any engram, mandates high-yield recordings to
3723 identify the full temporal sequence of CA1 activations (Foster, 2017).

3724 3) Neuropixels (Jun et al., 2017) can be used to perform electrical
3725 recordings at >=20 kHz. At the time when we started the experiments
3726 for the thesis, these sorts of electrical probes had yet to be
3727 successfully deployed in published literature.

3728

3729 We discuss all of these techniques while comparing electrical vs
3730 imaging based recording strategies in Chapter 1 – “Introduction”.
3731 Fundamentally, given the technological constraints at the time, we had
3732 devised combined behaviour with galvo-scanning 2p calcium imaging as
3733 the principle for the experiments described in this thesis.

3734 Does the brain create or predict?

3735 An important directive to neuroscience research is to understand the
3736 brain and nervous system, in how these structures allow animals to
3737 interact meaningfully with their environment. More humbly, however,
3738 the ultimate goal of this thesis was to help provide a multi-disciplinary
3739 toolkit to study time cells in the hippocampus. Predictive coding has
3740 been considered as a way for the brain to ultimately use external
3741 sensory information to minimize prediction errors during tasks (Doya et
3742 al., 2007; Rao & Ballard, 1999). One of the core ideas of Bayesian
3743 approaches to neurophysiology and behaviour is that the brain could
3744 be modeled as a prediction machine that is constantly modeling the
3745 change of variables. These variables may be external or internal yet
3746 salient concepts to any experimental animal, arguably expressed in
3747 neurophysiology as the dynamics of engrams. The ability of the
3748 mammalian hippocampus to bind both information streams to create
3749 new, more elaborate engrams, is likely crucial to the learning of new
3750 concepts behaviourally (N. J. Cohen & Eichenbaum, 1993;
3751 Eichenbaum, 2017).

3752

3753 Attentional states have been shown to have a bidirectional relationship
3754 with the expression of memory and learning (Chun & Johnson, 2011;

3755 Hutchinson & Turk-Browne, 2012; Uncapher et al., 2011). Specifically,
3756 Trace Eye-Blink Conditioning (TEC) performance has been suggested
3757 to be positively correlated with attention (Manns et al., 2000). The
3758 question of the effect of attentional states on the dynamics of the
3759 associated engram motivated an important milestone for the Thesis,
3760 *viz.*, to combine stable, adaptable behaviour studies with large-scale
3761 neurophysiology.

3762

3763 We were able to train head-fixed mice to TEC and confirm adaptable
3764 conditioned responses to task variables. We were also able to
3765 simultaneous record from ~100 hippocampal CA1 cell bodies as the
3766 animals acquired top behavioural performance. We observed in our
3767 preliminary results that many identified time cells showcased the ability
3768 to tune to different time points across sessions or days, as has been
3769 previously reported (Mau et al., 2018). This standardization of
3770 simultaneous behaviour and imaging ensured that colleagues from our
3771 lab were able to generate production quality data, quickly.

3772

3773 Several more high quality recordings and behaviour modulations would
3774 be required to conclusively describe time cells physiology and engram
3775 dynamics, at least at the level of a sub-population of hippocampal CA1.
3776 However, progress has been made to suggest the best time cell
3777 detection algorithm(s) based on their sensitivity to different recording
3778 parameters (Ananthamurthy & Bhalla, 2023). We hope that the Thesis
3779 is of aid to future research on the neural mechanisms of Learning and
3780 Memory by the nervous system.

3781

3782 Bibliography

- 3783 Ananthamurthy, K. G., & Bhalla, U. S. (2023). Synthetic Data Resource
3784 and Benchmarks for Time Cell Analysis and Detection Algorithms.
3785 *ENeuro*, ENEURO.0007-22.2023.
3786 <https://doi.org/10.1523/ENEURO.0007-22.2023>
- 3787 Aronov, D., Nevers, R., & Tank, D. W. (2017). Mapping of a non-spatial
3788 dimension by the hippocampal-entorhinal circuit. *Nature*,
3789 543(7647), 719–722. <https://doi.org/10.1038/nature21692>
- 3790 Bhalla, U. S. (2019). Dendrites, deep learning, and sequences in the
3791 hippocampus. *Hippocampus*, 29(3), 239–251.
3792 <https://doi.org/https://doi.org/10.1002/hipo.22806>
- 3793 Bonin, V., Histed, M. H., Yurgenson, S., & Reid, R. C. (2011). Local
3794 Diversity and Fine-Scale Organization of Receptive Fields in
3795 Mouse Visual Cortex. *The Journal of Neuroscience*, 31(50),
3796 18506. <https://doi.org/10.1523/JNEUROSCI.2974-11.2011>
- 3797 Chun, M. M., & Johnson, M. K. (2011). Memory: enduring traces of
3798 perceptual and reflective attention. *Neuron*, 72(4), 520–535.
3799 <https://doi.org/10.1016/j.neuron.2011.10.026>
- 3800 Cohen, N. J., & Eichenbaum, H. (1993). *Memory, amnesia, and the*
3801 *hippocampal system*.
- 3802 Conen, K. E., & Desrochers, T. M. (2022). *The Neural Basis of*
3803 *Behavioral Sequences in Cortical and Subcortical Circuits*. Oxford
3804 University Press.
3805 <https://doi.org/10.1093/acrefore/9780190264086.013.421>
- 3806 Davidson, T. J., Kloosterman, F., & Wilson, M. A. (2009). Hippocampal
3807 replay of extended experience. *Neuron*, 63(4), 497–507.
3808 <https://doi.org/10.1016/j.neuron.2009.07.027>
- 3809 Dhawale, A. K. (2013). *Temporal and spatial features of sensory*
3810 *coding in the olfactory bulb and hippocampus*. Tata Institute of
3811 Fundamental Research.
- 3812 Doya, K., Ishii, S., Pouget, A., & Rao, R. P. N. (2007). Bayesian brain:
3813 Probabilistic approaches to neural coding. In K. Doya, S. Ishii, A.
3814 Pouget, & R. P. N. Rao (Eds.), *Bayesian brain: Probabilistic*
3815 *approaches to neural coding*. MIT Press.
- 3816 Eichenbaum, H. (2017). On the Integration of Space, Time, and
3817 Memory. *Neuron*, 95(5), 1007–1018.
3818 <https://doi.org/10.1016/j.neuron.2017.06.036>
- 3819 Foster, D. J. (2017). Replay Comes of Age. *Annual Review of*
3820 *Neuroscience*, 40, 581–602. <https://doi.org/10.1146/annurev-neuro-072116-031538>
- 3822 Hutchinson, J. B., & Turk-Browne, N. B. (2012). Memory-guided
3823 attention: control from multiple memory systems. *Trends in*

- 3824 Cognitive Sciences, 16(12), 576–579.
3825 <https://doi.org/10.1016/j.tics.2012.10.003>
- 3826 Jun, J. J., Steinmetz, N. A., Siegle, J. H., Denman, D. J., Bauza, M.,
3827 Barbarits, B., Lee, A. K., Anastassiou, C. A., Andrei, A., Aydin, Ç.,
3828 Barbic, M., Blanche, T. J., Bonin, V., Couto, J., Dutta, B., Gratiy,
3829 S. L., Gutnisky, D. A., Häusser, M., Karsh, B., ... Harris, T. D.
3830 (2017). Fully integrated silicon probes for high-density recording of
3831 neural activity. *Nature*, 551(7679), 232–236.
3832 <https://doi.org/10.1038/nature24636>
- 3833 Leybaert, L., de Meyer, A., Mabilde, C., & Sanderson, M. J. (2005). A
3834 simple and practical method to acquire geometrically correct
3835 images with resonant scanning-based line scanning in a custom-
3836 built video-rate laser scanning microscope. *Journal of Microscopy*,
3837 219(3), 133–140. <https://doi.org/10.1111/j.1365-2818.2005.01502.x>
- 3838 Manns, J. R., Clark, R. E., & Squire, L. R. (2000). Parallel acquisition
3839 of awareness and trace eyeblink classical conditioning. *Learning &*
3840 *Memory (Cold Spring Harbor, N.Y.)*, 7(5), 267–272.
3841 <https://doi.org/10.1101/lm.33400>
- 3842 Mau, W., Sullivan, D. W., Kinsky, N. R., Hasselmo, M. E., Howard, M.
3843 W., & Eichenbaum, H. (2018). The Same Hippocampal CA1
3844 Population Simultaneously Codes Temporal Information over
3845 Multiple Timescales. *Current Biology*, 28(10), 1499-1508.e4.
3846 <https://doi.org/10.1016/j.cub.2018.03.051>
- 3847 Modi, M. N., Dhawale, A. K., & Bhalla, U. S. (2014). CA1 cell activity
3848 sequences emerge after reorganization of network correlation
3849 structure during associative learning. *eLife*, 3, e01982–e01982.
3850 <https://doi.org/10.7554/eLife.01982>
- 3851 Nguyen, Q.-T., Callamaras, N., Hsieh, C., & Parker, I. (2001).
3852 Construction of a two-photon microscope for video-rate Ca²⁺
3853 imaging. *Cell Calcium*, 30(6), 383–393.
3854 <https://doi.org/https://doi.org/10.1054/ceca.2001.0246>
- 3855 Ranck, J. B. (1973). Studies on single neurons in dorsal hippocampal
3856 formation and septum in unrestrained rats: Part I. Behavioral
3857 correlates and firing repertoires. *Experimental Neurology*, 41(2),
3858 462–531. [https://doi.org/https://doi.org/10.1016/0014-4886\(73\)90290-2](https://doi.org/https://doi.org/10.1016/0014-4886(73)90290-2)
- 3859 Ranck, J. B. (1975). *Behavioral Correlates and Firing Repertoires of*
3860 *Neurons in the Dorsal Hippocampal Formation and Septum of*
3861 *Unrestrained Rats BT - The Hippocampus: Volume 2:*
3862 *Neurophysiology and Behavior* (R. L. Isaacson & K. H. Pribram,
3863 Eds.; pp. 207–244). Springer US. https://doi.org/10.1007/978-1-4684-2979-4_7

- 3867 Rao, R. P. N., & Ballard, D. H. (1999). Predictive coding in the visual
3868 cortex: a functional interpretation of some extra-classical
3869 receptive-field effects. *Nature Neuroscience*, 2(1), 79–87.
3870 <https://doi.org/10.1038/4580>
- 3871 Rochefort, N. L., Garaschuk, O., Milos, R.-I., Narushima, M., Marandi,
3872 N., Pichler, B., Kovalchuk, Y., & Konnerth, A. (2009).
3873 Sparsification of neuronal activity in the visual cortex at eye-
3874 opening. *Proceedings of the National Academy of Sciences of the*
3875 *United States of America*, 106(35), 15049–15054.
3876 <https://doi.org/10.1073/pnas.0907660106>
- 3877 Siegel, J. J., Taylor, W., Gray, R., Kalmbach, B., Zemelman, B. V.,
3878 Desai, N. S., Johnston, D., & Chitwood, R. A. (2015). Trace
3879 Eyeblink Conditioning in Mice Is Dependent upon the Dorsal
3880 Medial Prefrontal Cortex, Cerebellum, and Amygdala: Behavioral
3881 Characterization and Functional Circuitry. *ENeuro*, 2(4),
3882 ENEURO.0051-14.2015. <https://doi.org/10.1523/ENEURO.0051-14.2015>
- 3883 Uncapher, M. R., Hutchinson, J. B., & Wagner, A. D. (2011).
3884 Dissociable effects of top-down and bottom-up attention during
3885 episodic encoding. *The Journal of Neuroscience : The Official*
3886 *Journal of the Society for Neuroscience*, 31(35), 12613–12628.
3887 <https://doi.org/10.1523/JNEUROSCI.0152-11.2011>
- 3888 Zhang, S., & Manahan-Vaughan, D. (2015). Spatial olfactory learning
3889 contributes to place field formation in the hippocampus. *Cerebral*
3890 *Cortex (New York, N.Y. : 1991)*, 25(2), 423–432.
3891 <https://doi.org/10.1093/cercor/bht239>
- 3892 Zhou, S., Masmanidis, S. C., & Buonomano, D. V. (2020). Neural
3893 Sequences as an Optimal Dynamical Regime for the Readout of
3894 Time. *Neuron*, 108(4), 651-658.e5.
3895 <https://doi.org/https://doi.org/10.1016/j.neuron.2020.08.020>
- 3896
- 3897

All Bibliography

- 3898 Abe, R., Sakaguchi, T., Matsumoto, N., Matsuki, N., & Ikegaya, Y.
3899 (2014). Sound-induced hyperpolarization of hippocampal neurons.
3900 *Neuroreport*, 25(13), 1013–1017.
3901 <https://doi.org/10.1097/WNR.0000000000000206>
3902 Abeles, M. (1982). *Local Cortical Circuits: An Electrophysiological Study*. Springer-Verlag.
3903 <https://books.google.co.in/books?id=s25lwwEACAAJ>
3904 Abeles, M. (1991). *Corticonics: Neural Circuits of the Cerebral Cortex*.
3905 Cambridge University Press. <https://doi.org/DOI:10.1017/CBO9780511574566>
3906 Abeles, M. (2004). Time Is Precious. *Science*, 304(5670), 523–524.
3907 <https://doi.org/10.1126/science.1097725>
3908 Abeles, M. (2009). *Synfire Chains* (L. R. B. T.-E. of N. Squire, Ed.; pp. 829–832). Academic Press.
3909 <https://doi.org/https://doi.org/10.1016/B978-008045046-9.01437-6>
3910 Abeles, M., Hayon, G., & Lehmann, D. (2004). Modeling
3911 compositionality by dynamic binding of synfire chains. *Journal of Computational Neuroscience*, 17(2), 179–201.
3912 <https://doi.org/10.1023/B:JCNS.0000037682.18051.5f>
3913 Ananthamurthy, K. G., & Bhalla, U. S. (2023). Synthetic Data Resource
3914 and Benchmarks for Time Cell Analysis and Detection Algorithms.
3915 *ENeuro*, ENEURO.0007-22.2023.
3916 <https://doi.org/10.1523/ENEURO.0007-22.2023>
3917 Andermann, M. L., Gilfoy, N. B., Goldey, G. J., Sachdev, R. N. S.,
3918 Wölfel, M., McCormick, D. A., Reid, R. C., & Levene, M. J. (2013).
3919 Chronic Cellular Imaging of Entire Cortical Columns in Awake
3920 Mice Using Microprisms. *Neuron*, 80(4), 900–913.
3921 <https://doi.org/10.1016/j.neuron.2013.07.052>
3922 Andersen, P., Morris, R., Amaral, D., Bliss, T., & O'Keefe, J. (Eds.).
3923 (2006). *The Hippocampus Book*. Oxford University Press.
3924 <https://doi.org/10.1093/acprof:oso/9780195100273.001.0001>
3925 Andersen, R. A., Snyder, L. H., Li, C.-S., & Stricanne, B. (1993).
3926 Coordinate transformations in the representation of spatial
3927 information. *Current Opinion in Neurobiology*, 3(2), 171–176.
3928 [https://doi.org/https://doi.org/10.1016/0959-4388\(93\)90206-E](https://doi.org/https://doi.org/10.1016/0959-4388(93)90206-E)
3929 Aronov, D., Nevers, R., & Tank, D. W. (2017). Mapping of a non-spatial
3930 dimension by the hippocampal-entorhinal circuit. *Nature*,
3931 543(7647), 719–722. <https://doi.org/10.1038/nature21692>
3932 Attardo, A., Fitzgerald, J. E., & Schnitzer, M. J. (2015). Impermanence
3933 of dendritic spines in live adult CA1 hippocampus. *Nature*,
3934 523(7562), 592–596. <https://doi.org/10.1038/nature14467>

- 3940 Ballard, I. C., Wagner, A. D., & McClure, S. M. (2019). Hippocampal
3941 pattern separation supports reinforcement learning. *Nature*
3942 *Communications*, 10(1), 1073. <https://doi.org/10.1038/s41467-019-08998-1>
- 3943 Barreto, R. P. J., Messerschmidt, B., & Schnitzer, M. J. (2009). In vivo
3944 fluorescence imaging with high-resolution microlenses. *Nature*
3945 *Methods*, 6(7), 511–512. <https://doi.org/10.1038/nmeth.1339>
- 3946 Barreto, R. P. J., & Schnitzer, M. J. (2012). In vivo optical
3947 microendoscopy for imaging cells lying deep within live tissue.
3948 *Cold Spring Harbor Protocols*, 2012(10), 1029–1034.
3949 <https://doi.org/10.1101/pdb.top071464>
- 3950 Baudry, M., & Lynch, G. (1981). Hippocampal glutamate receptors.
3951 *Molecular and Cellular Biochemistry*, 38(1), 5–18.
3952 <https://doi.org/10.1007/BF00235685>
- 3953 Bellistri, E., Aguilar, J., Brotons-Mas, J. R., Foffani, G., & de la Prida, L.
3954 M. (2013). Basic properties of somatosensory-evoked responses
3955 in the dorsal hippocampus of the rat. *The Journal of Physiology*,
3956 591(10), 2667–2686. <https://doi.org/10.1113/jphysiol.2013.251892>
- 3957 Bhalla, U. S. (2019). Dendrites, deep learning, and sequences in the
3958 hippocampus. *Hippocampus*, 29(3), 239–251.
3959 <https://doi.org/https://doi.org/10.1002/hipo.22806>
- 3960 Bialek, W., Callan, C. G., & Strong, S. P. (1996). Field Theories for
3961 Learning Probability Distributions. *Physical Review Letters*,
3962 77(23), 4693–4697. <https://doi.org/10.1103/physrevlett.77.4693>
- 3963 Bialek, W., Nemenman, I., & Tishby, N. (2001). Predictability,
3964 Complexity, and Learning. *Neural Comput.*, 13(11), 2409–2463.
3965 <https://doi.org/10.1162/089976601753195969>
- 3966 Bienenstock, E. (1995). A model of neocortex. *Network: Computation*
3967 *in Neural Systems*, 6(2), 179–224. https://doi.org/10.1088/0954-898X_6_2_004
- 3968 Bjerknes, T. L., Moser, E. I., & Moser, M.-B. (2014). Representation of
3969 Geometric Borders in the Developing Rat. *Neuron*, 82(1), 71–78.
3970 <https://doi.org/10.1016/j.neuron.2014.02.014>
- 3971 Bonin, V., Histed, M. H., Yurgenson, S., & Reid, R. C. (2011). Local
3972 Diversity and Fine-Scale Organization of Receptive Fields in
3973 Mouse Visual Cortex. *The Journal of Neuroscience*, 31(50),
3974 18506. <https://doi.org/10.1523/JNEUROSCI.2974-11.2011>
- 3975 Brown, G. D. (1998). Nonassociative learning processes affecting
3976 swimming probability in the seashell Tritonia diomedea:
3977 habituation, sensitization and inhibition. *Behavioural Brain*
3978 *Research*, 95(2), 151–165.
3979 [https://doi.org/https://doi.org/10.1016/S0166-4328\(98\)00072-2](https://doi.org/https://doi.org/10.1016/S0166-4328(98)00072-2)
- 3980 Buccino, A. P., Garcia, S., & Yger, P. (2022). Spike sorting: new trends

- 3983 and challenges of the era of high-density probes. *Progress in*
3984 *Biomedical Engineering*, 4(2), 022005.
3985 <https://doi.org/10.1088/2516-1091/ac6b96>
- 3986 Buzsáki, G., & Llinás, R. (2017). Space and time in the brain. *Science*
3987 (*New York, N.Y.*), 358(6362), 482–485.
3988 <https://doi.org/10.1126/science.aan8869>
- 3989 Cai, D. J., Aharoni, D., Shuman, T., Shobe, J., Biane, J., Song, W.,
3990 Wei, B., Veshkini, M., La-Vu, M., Lou, J., Flores, S. E., Kim, I.,
3991 Sano, Y., Zhou, M., Baumgaertel, K., Lavi, A., Kamata, M.,
3992 Tuszyński, M., Mayford, M., ... Silva, A. J. (2016). A shared neural
3993 ensemble links distinct contextual memories encoded close in
3994 time. *Nature*, 534(7605), 115–118.
3995 <https://doi.org/10.1038/nature17955>
- 3996 Caporale, N., & Dan, Y. (2008). Spike timing-dependent plasticity: a
3997 Hebbian learning rule. *Annual Review of Neuroscience*, 31, 25–
3998 46. <https://doi.org/10.1146/annurev.neuro.31.060407.125639>
- 3999 Carew, T. J., Castellucci, V. F., & Kandel, E. R. (1971). An Analysis of
4000 Dishabituation and Sensitization of The Gill-Withdrawal Reflex In
4001 Aplysia. *International Journal of Neuroscience*, 2(2), 79–98.
4002 <https://doi.org/10.3109/00207457109146995>
- 4003 Chen, T.-W., Wardill, T. J., Sun, Y., Pulver, S. R., Renninger, S. L.,
4004 Baohan, A., Schreiter, E. R., Kerr, R. A., Orger, M. B., Jayaraman,
4005 V., Looger, L. L., Svoboda, K., & Kim, D. S. (2013). Ultrasensitive
4006 fluorescent proteins for imaging neuronal activity. *Nature*,
4007 499(7458), 295–300. <https://doi.org/10.1038/nature12354>
- 4008 Chigirev, D., & Bialek, W. (2004, January). Optimal manifold
4009 representation of data: An information theoretic approach.
4010 *Advances in Neural Information Processing Systems 16 -*
4011 *Proceedings of the 2003 Conference, NIPS 2003*.
- 4012 Chudasama, Y. (2010). Delayed (Non)Match-to-Sample Task. In I. P.
4013 Stolerman (Ed.), *Encyclopedia of Psychopharmacology* (p. 372).
4014 Springer Berlin Heidelberg. https://doi.org/10.1007/978-3-540-68706-1_1619
- 4016 Chun, M. M., & Johnson, M. K. (2011). Memory: enduring traces of
4017 perceptual and reflective attention. *Neuron*, 72(4), 520–535.
4018 <https://doi.org/10.1016/j.neuron.2011.10.026>
- 4019 Clayton, N. S., Salwiczek, L. H., & Dickinson, A. (2007). Episodic
4020 memory. *Current Biology*, 17(6), R189–R191.
4021 <https://doi.org/10.1016/j.cub.2007.01.011>
- 4022 Cohen, M. R., & Kohn, A. (2011). Measuring and interpreting neuronal
4023 correlations. *Nature Neuroscience*, 14(7), 811–819.
4024 <https://doi.org/10.1038/nn.2842>
- 4025 Cohen, N. J., & Eichenbaum, H. (1993). *Memory, amnesia, and the*

- 4026 *hippocampal system.*
- 4027 Conen, K. E., & Desrochers, T. M. (2022). *The Neural Basis of*
4028 *Behavioral Sequences in Cortical and Subcortical Circuits*. Oxford
4029 University Press.
4030 <https://doi.org/10.1093/acrefore/9780190264086.013.421>
- 4031 Csicsvari, J., O'Neill, J., Allen, K., & Senior, T. (2007). Place-selective
4032 firing contributes to the reverse-order reactivation of
4033 CA1 pyramidal cells during sharp waves in open-field exploration.
4034 *The European Journal of Neuroscience*, 26(3), 704–716.
4035 <https://doi.org/10.1111/j.1460-9568.2007.05684.x>
- 4036 Davidson, T. J., Kloosterman, F., & Wilson, M. A. (2009). Hippocampal
4037 replay of extended experience. *Neuron*, 63(4), 497–507.
4038 <https://doi.org/10.1016/j.neuron.2009.07.027>
- 4039 Denk, W., Strickler, J. H., & Webb, W. W. (1990). Two-photon laser
4040 scanning fluorescence microscopy. *Science (New York, N.Y.)*,
4041 248(4951), 73–76. <https://doi.org/10.1126/science.2321027>
- 4042 Deshmukh, S. S., & Bhalla, U. S. (2003). Representation of odor
4043 habituation and timing in the hippocampus. *The Journal of*
4044 *Neuroscience : The Official Journal of the Society*
4045 *for Neuroscience*, 23(5), 1903–1915.
4046 <https://doi.org/10.1523/JNEUROSCI.23-05-01903.2003>
- 4047 Dhawale, A. K. (2013). *Temporal and spatial features of sensory*
4048 *coding in the olfactory bulb and hippocampus*. Tata Institute of
4049 Fundamental Research.
- 4050 Dhawale, A. K., Poddar, R., Wolff, S. B. E., Normand, V. A.,
4051 Kopelowitz, E., & Ölveczky, B. P. (2017). Automated long-term
4052 recording and analysis of neural activity in behaving animals.
4053 *eLife*, 6, e27702. <https://doi.org/10.7554/eLife.27702>
- 4054 Diba, K., & Buzsáki, G. (2007). Forward and reverse hippocampal
4055 place-cell sequences during ripples. *Nature Neuroscience*, 10(10),
4056 1241–1242. <https://doi.org/10.1038/nn1961>
- 4057 Dickinson, A., Nicholas, D. J., & Mackintosh, N. J. (1983). A re-
4058 examination of one-trial blocking in conditioned suppression. *The*
4059 *Quarterly Journal of Experimental Psychology B: Comparative and*
4060 *Physiological Psychology*, 35, 67–79.
4061 <https://doi.org/10.1080/14640748308400914>
- 4062 Disterhoft, J. F., & Weiss, C. (2017). Eyeblink Conditioning – A
4063 Behavioral Model of Procedural and Declarative Learning. In J. H.
4064 Byrne (Ed.), *Learning and Memory: A Comprehensive Reference*
4065 (*Second Edition*) (pp. 327–355). Academic Press.
4066 <https://doi.org/https://doi.org/10.1016/B978-0-12-809324-5.21087-0>
- 4067 Dombeck, D. A., Graziano, M. S., & Tank, D. W. (2009). Functional

- 4069 Clustering of Neurons in Motor Cortex Determined by Cellular
4070 Resolution Imaging in Awake Behaving Mice. *The Journal of*
4071 *Neuroscience*, 29(44), 13751 LP – 13760.
4072 <https://doi.org/10.1523/JNEUROSCI.2985-09.2009>
- 4073 Dombeck, D. A., Harvey, C. D., Tian, L., Looger, L. L., & Tank, D. W.
4074 (2010). Functional imaging of hippocampal place cells at cellular
4075 resolution during virtual navigation. *Nature Neuroscience*, 13(11),
4076 1433–1440. <https://doi.org/10.1038/nn.2648>
- 4077 Doya, K., Ishii, S., Pouget, A., & Rao, R. P. N. (2007). Bayesian brain:
4078 Probabilistic approaches to neural coding. In K. Doya, S. Ishii, A.
4079 Pouget, & R. P. N. Rao (Eds.), *Bayesian brain: Probabilistic*
4080 *approaches to neural coding*. MIT Press.
- 4081 Dragoi, G. (2013). Internal operations in the hippocampus: single cell
4082 and ensemble temporal coding. *Frontiers in Systems*
4083 *Neuroscience*, 7, 46. <https://doi.org/10.3389/fnsys.2013.00046>
- 4084 Dragoi, G., & Buzsáki, G. (2006). Temporal encoding of place
4085 sequences by hippocampal cell assemblies. *Neuron*, 50(1), 145–
4086 157. <https://doi.org/10.1016/j.neuron.2006.02.023>
- 4087 Dragoi, G., Carpi, D., Recce, M., Csicsvari, J., & Buzsáki, G. (1999).
4088 Interactions between hippocampus and medial septum during
4089 sharp waves and theta oscillation in the behaving rat. *The Journal*
4090 *of Neuroscience : The Official Journal of the Society for*
4091 *Neuroscience*, 19(14), 6191–6199.
4092 <http://www.ncbi.nlm.nih.gov/pubmed/10407055>
- 4093 Dragoi, G., & Tonegawa, S. (2011). Preplay of future place cell
4094 sequences by hippocampal cellular assemblies. *Nature*,
4095 469(7330), 397–401. <https://doi.org/10.1038/nature09633>
- 4096 Eichenbaum, H. (2004). Hippocampus: Cognitive processes and
4097 neural representations that underlie declarative memory. *Neuron*,
4098 44(1), 109–120. <https://doi.org/10.1016/j.neuron.2004.08.028>
- 4099 Eichenbaum, H. (2017). On the Integration of Space, Time, and
4100 Memory. *Neuron*, 95(5), 1007–1018.
4101 <https://doi.org/10.1016/j.neuron.2017.06.036>
- 4102 Ekstrom, A. D., & Ranganath, C. (2018). Space, time, and episodic
4103 memory: The hippocampus is all over the cognitive map.
4104 *Hippocampus*, 28(9), 680–687.
4105 <https://doi.org/https://doi.org/10.1002/hipo.22750>
- 4106 Fanselow, M. S., & Dong, H.-W. (2010). Are the dorsal and ventral
4107 hippocampus functionally distinct structures? *Neuron*, 65(1), 7–19.
4108 <https://doi.org/10.1016/j.neuron.2009.11.031>
- 4109 Fassihi, A., Akrami, A., Pulecchi, F., Schönfelder, V., & Diamond, M. E.
4110 (2017). Transformation of Perception from Sensory to Motor
4111 Cortex. *Current Biology : CB*, 27(11), 1585-1596.e6.

- 4112 <https://doi.org/10.1016/j.cub.2017.05.011>
- 4113 Ferbinteanu, J., & Shapiro, M. L. (2003). Prospective and retrospective
4114 memory coding in the hippocampus. *Neuron*, 40(6), 1227–1239.
4115 [https://doi.org/10.1016/s0896-6273\(03\)00752-9](https://doi.org/10.1016/s0896-6273(03)00752-9)
- 4116 Ferbinteanu, J., Shirvalkar, P., & Shapiro, M. L. (2011). Memory
4117 Modulates Journey-Dependent Coding in the Rat Hippocampus.
4118 *The Journal of Neuroscience*, 31(25), 9135 LP – 9146.
4119 <https://doi.org/10.1523/JNEUROSCI.1241-11.2011>
- 4120 Foster, D. J. (2017). Replay Comes of Age. *Annual Review of
4121 Neuroscience*, 40, 581–602. <https://doi.org/10.1146/annurev-neuro-072116-031538>
- 4123 Foster, D. J., & Wilson, M. A. (2006). Reverse replay of behavioural
4124 sequences in hippocampal place cells during the awake state.
4125 *Nature*, 440(7084), 680–683. <https://doi.org/10.1038/nature04587>
- 4126 Foster, D. J., & Wilson, M. A. (2007). Hippocampal theta sequences.
4127 *Hippocampus*, 17(11), 1093–1099.
4128 <https://doi.org/10.1002/hipo.20345>
- 4129 Francis, M., Qian, X., Charbel, C., Ledoux, J., Parker, J. C., & Taylor,
4130 M. S. (2012). Automated region of interest analysis of dynamic
4131 Ca²⁺ signals in image sequences. *American Journal of
4132 Physiology. Cell Physiology*, 303(3), C236-43.
4133 <https://doi.org/10.1152/ajpcell.00016.2012>
- 4134 Frank, L. M., Brown, E. N., & Wilson, M. (2000). Trajectory encoding in
4135 the hippocampus and entorhinal cortex. *Neuron*, 27(1), 169–178.
4136 [https://doi.org/10.1016/s0896-6273\(00\)00018-0](https://doi.org/10.1016/s0896-6273(00)00018-0)
- 4137 Fyhn, M., Molden, S., Witter, M. P., Moser, E. I., & Moser, M.-B.
4138 (2004). Spatial representation in the entorhinal cortex. *Science
4139 (New York, N.Y.)*, 305(5688), 1258–1264.
4140 <https://doi.org/10.1126/science.1099901>
- 4141 Giovannucci, A., Badura, A., Deverett, B., Najafi, F., Pereira, T. D.,
4142 Gao, Z., Ozden, I., Kloth, A. D., Pnevmatikakis, E., Paninski, L.,
4143 De Zeeuw, C. I., Medina, J. F., & Wang, S. S.-H. (2017).
4144 Cerebellar granule cells acquire a widespread predictive feedback
4145 signal during motor learning. *Nature Neuroscience*, 20(5), 727–
4146 734. <https://doi.org/10.1038/nn.4531>
- 4147 Grün, S. (2009). Data-Driven Significance Estimation for Precise Spike
4148 Correlation. *Journal of Neurophysiology*, 101(3), 1126–1140.
4149 <https://doi.org/10.1152/jn.00093.2008>
- 4150 Guo, Z. V., Hires, S. A., Li, N., O'Connor, D. H., Komiyama, T., Ophir,
4151 E., Huber, D., Bonardi, C., Morandell, K., Gutnisky, D., Peron, S.,
4152 Xu, N., Cox, J., & Svoboda, K. (2014). Procedures for Behavioral
4153 Experiments in Head-Fixed Mice. *PLOS ONE*, 9(2), e88678.
4154 <https://doi.org/10.1371/journal.pone.0088678>

- 4155 Gupta, A. S., van der Meer, M. A. A., Touretzky, D. S., & Redish, A. D.
4156 (2010). Hippocampal Replay Is Not a Simple Function of
4157 Experience. *Neuron*, 65(5), 695–705.
4158 <https://doi.org/https://doi.org/10.1016/j.neuron.2010.01.034>
- 4159 Hafting, T., Fyhn, M., Molden, S., Moser, M.-B., & Moser, E. I. (2005).
4160 Microstructure of a spatial map in the entorhinal cortex. *Nature*,
4161 436(7052), 801–806. <https://doi.org/10.1038/nature03721>
- 4162 Hamme, L. J. Van, & Wasserman, E. A. (1993). Cue Competition in
4163 Causality Judgments: The Role of Manner of Information
4164 Presentation. *Bulletin of the Psychonomic Society*, 31(5), 457–
4165 460. <https://doi.org/10.3758/bf03334962>
- 4166 Han, J.-H., Kushner, S. A., Yiu, A. P., Hsiang, H.-L. L., Buch, T.,
4167 Waisman, A., Bontempi, B., Neve, R. L., Frankland, P. W., &
4168 Josselyn, S. A. (2009). Selective erasure of a fear memory.
4169 *Science (New York, N.Y.)*, 323(5920), 1492–1496.
4170 <https://doi.org/10.1126/science.1164139>
- 4171 Harvey, C. D., Collman, F., Dombeck, D. A., & Tank, D. W. (2009).
4172 Intracellular dynamics of hippocampal place cells during virtual
4173 navigation. *Nature*, 461(7266), 941–946.
4174 <https://doi.org/10.1038/nature08499>
- 4175 Hebb, D. O. (1949). The organization of behavior; a
4176 neuropsychological theory. In *The organization of behavior; a*
4177 *neuropsychological theory*. Wiley.
- 4178 Helmchen, F., & Denk, W. (2005). Deep tissue two-photon microscopy.
4179 2(12), 9. <https://doi.org/10.1038/nmeth818>
- 4180 Heys, J. G., Rangarajan, K. V., & Dombeck, D. A. (2014). The
4181 Functional Micro-organization of Grid Cells Revealed by Cellular-
4182 Resolution Imaging. *Neuron*, 84(5), 1079–1090.
4183 <https://doi.org/10.1016/j.neuron.2014.10.048>
- 4184 Hjorth-Simonsen, A., & Jeune, B. (1972). Origin and termination of the
4185 hippocampal perforant path in the rat studied by silver
4186 impregnation. *The Journal of Comparative Neurology*, 144(2),
4187 215–232. <https://doi.org/10.1002/cne.901440206>
- 4188 Hubel, D. H., & Wiesel, T. N. (1962). Receptive fields, binocular
4189 interaction and functional architecture in the cat's visual cortex.
4190 *The Journal of Physiology*, 160(1), 106–154.
4191 <https://doi.org/10.1113/jphysiol.1962.sp006837>
- 4192 Hutchinson, J. B., & Turk-Browne, N. B. (2012). Memory-guided
4193 attention: control from multiple memory systems. *Trends in*
4194 *Cognitive Sciences*, 16(12), 576–579.
4195 <https://doi.org/10.1016/j.tics.2012.10.003>
- 4196 Hyde, R. A., & Strowbridge, B. W. (2012). Mnemonic representations
4197 of transient stimuli and temporal sequences in the rodent

- 4198 hippocampus in vitro. *Nature Neuroscience*, 15(10), 1430–1438.
4199 <https://doi.org/10.1038/nn.3208>
- 4200 Ikegaya, Y., Aaron, G., Cossart, R., Aronov, D., Lampl, I., Ferster, D.,
4201 & Yuste, R. (2004). Synfire chains and cortical songs: temporal
4202 modules of cortical activity. *Science (New York, N.Y.)*, 304(5670),
4203 559–564. <https://doi.org/10.1126/science.1093173>
- 4204 Itskov, P. M., Vinnik, E., & Diamond, M. E. (2011). Hippocampal
4205 representation of touch-guided behavior in rats: persistent and
4206 independent traces of stimulus and reward location. *PloS One*,
4207 6(1), e16462. <https://doi.org/10.1371/journal.pone.0016462>
- 4208 Itskov, V., Pastalkova, E., Mizuseki, K., Buzsaki, G., & Harris, K. D.
4209 (2008). Theta-mediated dynamics of spatial information in
4210 hippocampus. *The Journal of Neuroscience : The Official Journal
4211 of the Society for Neuroscience*, 28(23), 5959–5964.
4212 <https://doi.org/10.1523/JNEUROSCI.5262-07.2008>
- 4213 Jadhav, S. P., Kemere, C., German, P. W., & Frank, L. M. (2012).
4214 Awake hippocampal sharp-wave ripples support spatial memory.
4215 *Science (New York, N.Y.)*, 336(6087), 1454–1458.
4216 <https://doi.org/10.1126/science.1217230>
- 4217 Jaramillo, S., & Zador, A. M. (2014). Mice and rats achieve similar
4218 levels of performance in an adaptive decision-making task . In
4219 *Frontiers in Systems Neuroscience* (Vol. 8).
4220 <https://www.frontiersin.org/articles/10.3389/fnsys.2014.00173>
- 4221 Josselyn, S. A., & Tonegawa, S. (2020). Memory engrams: Recalling
4222 the past and imagining the future. *Science (New York, N.Y.)*,
4223 367(6473). <https://doi.org/10.1126/science.aaw4325>
- 4224 Jun, J. J., Steinmetz, N. A., Siegle, J. H., Denman, D. J., Bauza, M.,
4225 Barbarits, B., Lee, A. K., Anastassiou, C. A., Andrei, A., Aydin, Ç.,
4226 Barbic, M., Blanche, T. J., Bonin, V., Couto, J., Dutta, B., Gratiy,
4227 S. L., Gutnisky, D. A., Häusser, M., Karsh, B., ... Harris, T. D.
4228 (2017). Fully integrated silicon probes for high-density recording of
4229 neural activity. *Nature*, 551(7679), 232–236.
4230 <https://doi.org/10.1038/nature24636>
- 4231 Kaifosh, P., Lovett-Barron, M., Turi, G. F., Reardon, T. R., & Losonczy,
4232 A. (2013). Septo-hippocampal GABAergic signaling across
4233 multiple modalities in awake mice. *Nature Neuroscience*, 16(9),
4234 1182–1184. <https://doi.org/10.1038/nn.3482>
- 4235 Kalmbach, B. E., Davis, T., Ohyama, T., Riusech, F., Nores, W. L., &
4236 Mauk, M. D. (2010). Cerebellar Cortex Contributions to the
4237 Expression and Timing of Conditioned Eyelid Responses. *Journal
4238 of Neurophysiology*, 103(4), 2039–2049.
4239 <https://doi.org/10.1152/jn.00033.2010>
- 4240 Kalmbach, B. E., Ohyama, T., & Mauk, M. D. (2010). Temporal

- 4241 Patterns of Inputs to Cerebellum Necessary and Sufficient for
4242 Trace Eyelid Conditioning. *Journal of Neurophysiology*, 104(2),
4243 627–640. <https://doi.org/10.1152/jn.00169.2010>
- 4244 Kamondi, A. (1998). *Theta Oscillations in Somata and Dendrites of*
4245 *Hippocampal Pyramidal Cells In Vivo: Activity-Dependent Phase-*
4246 *Precession of Action Potentials*. 261(March), 244–261.
- 4247 Khan, A. G., Parthasarathy, K., & Bhalla, U. S. (2010). Odor
4248 representations in the mammalian olfactory bulb. *Wiley*
4249 *Interdisciplinary Reviews. Systems Biology and Medicine*, 2(5),
4250 603–611. <https://doi.org/10.1002/wsbm.85>
- 4251 Kim, S., & Lee, I. (2012). The hippocampus is required for visually
4252 cued contextual response selection, but not for visual
4253 discrimination of contexts. *Frontiers in Behavioral Neuroscience*,
4254 6. <https://doi.org/10.3389/fnbeh.2012.00066>
- 4255 Kraus, B. J., Brandon, M. P., Robinson, R. J., Connerney, M. A.,
4256 Hasselmo, M. E., & Eichenbaum, H. (2015). During Running in
4257 Place, Grid Cells Integrate Elapsed Time and Distance Run.
4258 *Neuron*, 88(3), 578–589.
4259 <https://doi.org/10.1016/j.neuron.2015.09.031>
- 4260 Kraus, B., Robinson, R., White, J., Eichenbaum, H., & Hasselmo, M.
4261 (2013). Hippocampal “Time Cells”: Time versus Path Integration.
4262 *Neuron*, 78(6), 1090–1101.
4263 <https://doi.org/10.1016/j.neuron.2013.04.015>
- 4264 Kropff, E., Carmichael, J. E., Moser, M.-B., & Moser, E. I. (2015).
4265 Speed cells in the medial entorhinal cortex. *Nature*, 523(7561),
4266 419–424. <https://doi.org/10.1038/nature14622>
- 4267 Krupa, D., & Thompson, R. (2003). Inhibiting the Expression of a
4268 Classically Conditioned Behavior Prevents Its Extinction. *The*
4269 *Journal of Neuroscience : The Official Journal of the Society for*
4270 *Neuroscience*, 23, 10577–10584.
4271 <https://doi.org/10.1523/JNEUROSCI.23-33-10577.2003>
- 4272 Lever, C., Burton, S., Jeewajee, A., O'Keefe, J., & Burgess, N.
4273 (2009). Boundary Vector Cells in the Subiculum of the
4274 Hippocampal Formation. *The Journal of Neuroscience*, 29(31),
4275 9771 LP – 9777. <https://doi.org/10.1523/JNEUROSCI.1319-09.2009>
- 4277 Leybaert, L., de Meyer, A., Mabilde, C., & Sanderson, M. J. (2005). A
4278 simple and practical method to acquire geometrically correct
4279 images with resonant scanning-based line scanning in a custom-
4280 built video-rate laser scanning microscope. *Journal of Microscopy*,
4281 219(3), 133–140. <https://doi.org/https://doi.org/10.1111/j.1365-2818.2005.01502.x>
- 4283 Lovett-Barron, M., Kaifosh, P., Kheirbek, M. A., Danielson, N.,

- 4284 Zaremba, J. D., Reardon, T. R., Turi, G. F., Hen, R., Zemelman,
4285 B. V., & Losonczy, A. (2014). Dendritic inhibition in the
4286 hippocampus supports fear learning. *Science (New York, N.Y.)*,
4287 343(6173), 857–863. <https://doi.org/10.1126/science.1247485>
- 4288 Luo, L., Callaway, E. M., & Svoboda, K. (2018). Genetic Dissection of
4289 Neural Circuits: A Decade of Progress. *Neuron*, 98(2), 256–281.
4290 <https://doi.org/https://doi.org/10.1016/j.neuron.2018.03.040>
- 4291 MacDonald, C. J., Carrow, S., Place, R., & Eichenbaum, H. (2013).
4292 Distinct hippocampal time cell sequences represent odor
4293 memories in immobilized rats. *The Journal of Neuroscience : The
4294 Official Journal of the Society for Neuroscience*, 33(36), 14607–
4295 14616. <https://doi.org/10.1523/JNEUROSCI.1537-13.2013>
- 4296 MacDonald, C. J., Lepage, K. Q., Eden, U. T., & Eichenbaum, H.
4297 (2011). Hippocampal “time cells” bridge the gap in memory for
4298 discontiguous events. *Neuron*, 71(4), 737–749.
4299 <https://doi.org/10.1016/j.neuron.2011.07.012>
- 4300 Manns, J. R., Clark, R. E., & Squire, L. R. (2000). Parallel acquisition
4301 of awareness and trace eyeblink classical conditioning. *Learning &
4302 Memory (Cold Spring Harbor, N.Y.)*, 7(5), 267–272.
4303 <https://doi.org/10.1101/lm.33400>
- 4304 Maruyama, R., Maeda, K., Moroda, H., Kato, I., Inoue, M., Miyakawa,
4305 H., & Aonishi, T. (2014). Detecting cells using non-negative matrix
4306 factorization on calcium imaging data. *Neural Networks : The
4307 Official Journal of the International Neural Network Society*, 55,
4308 11–19. <https://doi.org/10.1016/j.neunet.2014.03.007>
- 4309 Mau, W., Sullivan, D. W., Kinsky, N. R., Hasselmo, M. E., Howard, M.
4310 W., & Eichenbaum, H. (2018). The Same Hippocampal CA1
4311 Population Simultaneously Codes Temporal Information over
4312 Multiple Timescales. *Current Biology*, 28(10), 1499-1508.e4.
4313 <https://doi.org/10.1016/j.cub.2018.03.051>
- 4314 McLelland, D., & Paulsen, O. (2007). Cortical Songs Revisited: A
4315 Lesson in Statistics. *Neuron*, 53(3), 319–321.
4316 <https://doi.org/https://doi.org/10.1016/j.neuron.2007.01.020>
- 4317 McNaughton, N., & Gray, J. A. (2000). Anxiolytic action on the
4318 behavioural inhibition system implies multiple types of arousal
4319 contribute to anxiety. *Journal of Affective Disorders*, 61(3), 161–
4320 176. [https://doi.org/10.1016/s0165-0327\(00\)00344-x](https://doi.org/10.1016/s0165-0327(00)00344-x)
- 4321 Medina, J. F., Garcia, K. S., Nores, W. L., Taylor, N. M., & Mauk, M. D.
4322 (2000). Timing mechanisms in the cerebellum: testing predictions
4323 of a large-scale computer simulation. *The Journal of
4324 Neuroscience : The Official Journal of the Society
4325 for Neuroscience*, 20(14), 5516–5525.
4326 <https://doi.org/10.1523/JNEUROSCI.20-14-05516.2000>

- 4327 Meeks, J. P., Arnson, H. A., & Holy, T. E. (2010). Representation and
4328 transformation of sensory information in the mouse
4329 accessory olfactory system. *Nature Neuroscience*, 13(6), 723–
4330 730. <https://doi.org/10.1038/nn.2546>
- 4331 Miller, A. M. P., Jacob, A. D., Ramsaran, A. I., De Snoo, M. L.,
4332 Josselyn, S. A., & Frankland, P. W. (2023). Emergence of a
4333 predictive model in the hippocampus. *Neuron*.
4334 <https://doi.org/10.1016/j.neuron.2023.03.011>
- 4335 Modi, M. N., Dhawale, A. K., & Bhalla, U. S. (2014). CA1 cell activity
4336 sequences emerge after reorganization of network correlation
4337 structure during associative learning. *eLife*, 3, e01982–e01982.
4338 <https://doi.org/10.7554/eLife.01982>
- 4339 Mokeichev, A., Okun, M., Barak, O., Katz, Y., Ben-Shahar, O., &
4340 Lampl, I. (2007). Stochastic Emergence of Repeating Cortical
4341 Motifs in Spontaneous Membrane Potential Fluctuations In Vivo.
4342 *Neuron*, 53, 413–425.
4343 <https://doi.org/10.1016/j.neuron.2007.01.017>
- 4344 Mollinedo-Gajate, I., Song, C., & Knöpfel, T. (2021). Genetically
4345 Encoded Voltage Indicators. *Advances in Experimental Medicine
and Biology*, 1293, 209–224. https://doi.org/10.1007/978-981-15-8763-4_12
- 4348 Morris, R. G. M., Garrud, P., Rawlins, J. N. P., & O'Keefe, J. (1982).
4349 Place navigation impaired in rats with hippocampal lesions.
4350 *Nature*, 297(5868), 681–683. <https://doi.org/10.1038/297681a0>
- 4351 Moscovitch, M., Cabeza, R., Winocur, G., & Nadel, L. (2016). Episodic
4352 Memory and Beyond: The Hippocampus and Neocortex in
4353 Transformation. *Annual Review of Psychology*, 67(1), 105–134.
4354 <https://doi.org/10.1146/annurev-psych-113011-143733>
- 4355 Moser, M.-B., & Moser, E. I. (1998). Distributed encoding and retrieval
4356 of spatial memory in the hippocampus. In *The Journal of
4357 Neuroscience* (Vol. 18, pp. 7535–7542). Society for Neuroscience.
- 4358 Moyer, J. R. J., Thompson, L. T., & Disterhoft, J. F. (1996). Trace
4359 eyeblink conditioning increases CA1 excitability in a transient
4360 and learning-specific manner. *The Journal of Neuroscience : The
4361 Official Journal of the Society for Neuroscience*, 16(17), 5536–
4362 5546. <https://doi.org/10.1523/JNEUROSCI.16-17-05536.1996>
- 4363 Mukamel, E. A., Nimmerjahn, A., & Schnitzer, M. J. (2009). Automated
4364 analysis of cellular signals from large-scale calcium imaging data.
4365 *Neuron*, 63(6), 747–760.
4366 <https://doi.org/10.1016/j.neuron.2009.08.009>
- 4367 Muller, R. U., & Kubie, J. L. (1989). The firing of hippocampal place
4368 cells predicts the future position of freely moving rats. *The Journal
4369 of Neuroscience : The Official Journal of the Society*

- 4370 for *Neuroscience*, 9(12), 4101–4110.
4371 <https://doi.org/10.1523/JNEUROSCI.09-12-04101.1989>
- 4372 Murray, T. A., & Levene, M. J. (2012). Singlet gradient index lens for
4373 deep in vivo multiphoton microscopy. *Journal of Biomedical
4374 Optics*, 17(2), 021106. <https://doi.org/10.1117/1.JBO.17.2.021106>
- 4375 Nakashiba, T., Young, J. Z., McHugh, T. J., Buhl, D. L., & Tonegawa,
4376 S. (2008). Transgenic inhibition of synaptic transmission reveals
4377 role of CA3 output in hippocampal learning. *Science (New York,
4378 N.Y.)*, 319(5867), 1260–1264.
4379 <https://doi.org/10.1126/science.1151120>
- 4380 Nguyen, Q.-T., Callamaras, N., Hsieh, C., & Parker, I. (2001).
4381 Construction of a two-photon microscope for video-rate Ca²⁺
4382 imaging. *Cell Calcium*, 30(6), 383–393.
4383 <https://doi.org/https://doi.org/10.1054/ceca.2001.0246>
- 4384 Ohyama, T., Nores, W. L., Murphy, M., & Mauk, M. D. (2003). What
4385 the cerebellum computes. *Trends in Neurosciences*, 26(4), 222–
4386 227. [https://doi.org/10.1016/S0166-2236\(03\)00054-7](https://doi.org/10.1016/S0166-2236(03)00054-7)
- 4387 O'Keefe, J., & Burgess, N. (1996). Geometric determinants of the
4388 place fields of hippocampal neurons. *Nature*, 381(6581), 425–428.
4389 <https://doi.org/10.1038/381425a0>
- 4390 O'Keefe, J., & Dostrovsky, J. (1971). The hippocampus as a spatial
4391 map. Preliminary evidence from unit activity in the freely-moving
4392 rat. *Brain Research*, 34(1), 171–175. [https://doi.org/10.1016/0006-8993\(71\)90358-1](https://doi.org/10.1016/0006-8993(71)90358-1)
- 4393 O'Keefe, J., & Nadel, L. (1978). The Hippocampus as a Cognitive Map.
4394 In *Philosophical Studies* (Vol. 27).
4395 <https://doi.org/10.5840/philstudies19802725>
- 4396 O'Keefe, J., & Recce, M. L. (1993). Phase relationship between
4397 hippocampal place units and the EEG theta rhythm.
4398 *Hippocampus*, 3(3), 317–330.
4399 <https://doi.org/10.1002/hipo.450030307>
- 4400 Ozden, I., Lee, H. M., Sullivan, M. R., & Wang, S. S.-H. (2008).
4401 Identification and Clustering of Event Patterns From In Vivo
4402 Multiphoton Optical Recordings of Neuronal Ensembles. *Journal
4403 of Neurophysiology*, 100(1), 495–503.
4404 <https://doi.org/10.1152/jn.01310.2007>
- 4405 Pachitariu, M., Stringer, C., Dipoppa, M., Schröder, S., Rossi, L. F.,
4406 Dalgleish, H., Carandini, M., & Harris, K. D. (2017). Suite2p:
4407 beyond 10,000 neurons with standard two-photon microscopy.
4408 *BioRxiv*, 61507. <https://doi.org/10.1101/061507>
- 4409 Paredes, R. M., Etzler, J. C., Watts, L. T., Zheng, W., & Lechleiter, J.
4410 D. (2008). Chemical calcium indicators. *Methods (San Diego,
4411 Calif.)*, 46(3), 143–151.
4412

- 4413 https://doi.org/10.1016/j.ymeth.2008.09.025
- 4414 Pastalkova, E., Itskov, V., Amarasingham, A., & Buzsaki, G. (2008).
4415 Internally Generated Cell Assembly Sequences in the Rat
4416 Hippocampus. *Science*, 321(5894), 1322–1327.
4417 https://doi.org/10.1126/science.1159775
- 4418 Pavlov, I. P. (1927). Conditioned reflexes: an investigation of the
4419 physiological activity of the cerebral cortex. In *Conditioned*
4420 *reflexes: an investigation of the physiological activity of the*
4421 *cerebral cortex*. Oxford Univ. Press.
- 4422 Peron, S. P., Freeman, J., Iyer, V., Guo, C., & Svoboda, K. (2015). A
4423 Cellular Resolution Map of Barrel Cortex Activity during Tactile
4424 Behavior. *Neuron*, 86(3), 783–799.
4425 https://doi.org/10.1016/j.neuron.2015.03.027
- 4426 Petersen, C. C. H. (2019). Sensorimotor processing in the rodent
4427 barrel cortex. *Nature Reviews. Neuroscience*, 20(9), 533–546.
4428 https://doi.org/10.1038/s41583-019-0200-y
- 4429 Pfeiffer, B. E., & Foster, D. J. (2013). Hippocampal place-cell
4430 sequences depict future paths to remembered goals. *Nature*,
4431 497(7447), 74–79. https://doi.org/10.1038/nature12112
- 4432 Pnevmatikakis, E. A., Soudry, D., Gao, Y., Machado, T. A., Merel, J.,
4433 Pfau, D., Reardon, T., Mu, Y., Lacefield, C., Yang, W., Ahrens, M.,
4434 Bruno, R., Jessell, T. M., Peterka, D. S., Yuste, R., & Paninski, L.
4435 (2016). Simultaneous Denoising, Deconvolution, and Demixing of
4436 Calcium Imaging Data. *Neuron*, 89(2), 285–299.
4437 https://doi.org/https://doi.org/10.1016/j.neuron.2015.11.037
- 4438 Poort, J., Khan, A. G., Pachitariu, M., Nemri, A., Orsolic, I., Krupic, J.,
4439 Bauza, M., Sahani, M., Keller, G. B., Mrsic-Flogel, T. D., & Hofer,
4440 S. B. (2015). Learning Enhances Sensory and Multiple Non-
4441 sensory Representations in Primary Visual Cortex. *Neuron*, 86(6),
4442 1478–1490. https://doi.org/10.1016/j.neuron.2015.05.037
- 4443 Poppenk, J., Evensmoen, H. R., Moscovitch, M., & Nadel, L. (2013).
4444 Long-axis specialization of the human hippocampus. *Trends in*
4445 *Cognitive Sciences*, 17(5), 230–240.
4446 https://doi.org/10.1016/j.tics.2013.03.005
- 4447 Pudil, P., & Novovičová, J. (1998). Novel Methods for Feature Subset
4448 Selection with Respect to Problem Knowledge. In H. Liu & H.
4449 Motoda (Eds.), *Feature Extraction, Construction and Selection: A*
4450 *Data Mining Perspective* (pp. 101–116). Springer US.
4451 https://doi.org/10.1007/978-1-4615-5725-8_7
- 4452 Ranck, J. B. (1973). Studies on single neurons in dorsal hippocampal
4453 formation and septum in unrestrained rats: Part I. Behavioral
4454 correlates and firing repertoires. *Experimental Neurology*, 41(2),
4455 462–531. https://doi.org/https://doi.org/10.1016/0014-

- 4456 4886(73)90290-2
- 4457 Ranck, J. B. (1975). *Behavioral Correlates and Firing Repertoires of*
4458 *Neurons in the Dorsal Hippocampal Formation and Septum of*
4459 *Unrestrained Rats BT - The Hippocampus: Volume 2:*
4460 *Neurophysiology and Behavior* (R. L. Isaacson & K. H. Pribram,
4461 Eds.; pp. 207–244). Springer US. https://doi.org/10.1007/978-1-4684-2979-4_7
- 4463 Rao, R. P. N., & Ballard, D. H. (1999). Predictive coding in the visual
4464 cortex: a functional interpretation of some extra-classical
4465 receptive-field effects. *Nature Neuroscience*, 2(1), 79–87.
4466 <https://doi.org/10.1038/4580>
- 4467 Rescorla, R. A., & Wagner, A. (1972). A theory of Pavlovian
4468 conditioning: Variations in the effectiveness of reinforcement and
4469 nonreinforcement. In *Classical Conditioning II: Current Research*
4470 *and Theory: Vol. Vol. 2.*
- 4471 Reyes, A. D. (2003). Synchrony-dependent propagation of firing rate in
4472 iteratively constructed networks in vitro. *Nature Neuroscience*,
4473 6(6), 593–599. <https://doi.org/10.1038/nn1056>
- 4474 Robbins, M., Christensen, C. N., Kaminski, C. F., & Zlatic, M. (2021).
4475 Calcium imaging analysis - how far have we come?
4476 *F1000Research*, 10, 258.
- 4477 Rochefort, N. L., Garaschuk, O., Milos, R.-I., Narushima, M., Marandi,
4478 N., Pichler, B., Kovalchuk, Y., & Konnerth, A. (2009).
4479 Sparsification of neuronal activity in the visual cortex at eye-
4480 opening. *Proceedings of the National Academy of Sciences of the*
4481 *United States of America*, 106(35), 15049–15054.
4482 <https://doi.org/10.1073/pnas.0907660106>
- 4483 Rogerson, T., Cai, D. J., Frank, A., Sano, Y., Shobe, J., Lopez-Aranda,
4484 M. F., & Silva, A. J. (2014). Synaptic tagging during memory
4485 allocation. *Nature Reviews Neuroscience*, 15(3), 157–169.
4486 <https://doi.org/10.1038/nrn3667>
- 4487 Savelli, F., Yoganarasimha, D., & Knierim, J. J. (2008). Influence of
4488 boundary removal on the spatial representations of the
4489 medial entorhinal cortex. *Hippocampus*, 18(12), 1270–1282.
4490 <https://doi.org/10.1002/hipo.20511>
- 4491 Schreurs, B. G. (1989). Classical conditioning of model systems: A
4492 behavioral review. *Psychobiology*, 17(2), 145–155.
4493 <https://doi.org/10.3758/BF03337830>
- 4494 Scoville, W. B., & Milner, B. (1957). Loss of recent memory after
4495 bilateral hippocampal lesions. In *Journal of Neurology,*
4496 *Neurosurgery & Psychiatry* (Vol. 20, pp. 11–21). BMJ Publishing
4497 Group. <https://doi.org/10.1136/jnnp.20.1.11>
- 4498 Shannon, C. E. (1948). A Mathematical Theory of Communication. *Bell*

- 4499 *System Technical Journal*, 27(3), 379–423.
4500 <https://doi.org/https://doi.org/10.1002/j.1538-7305.1948.tb01338.x>
- 4501 Siegel, J. J., & Mauk, M. D. (2013). Persistent Activity in Prefrontal
4502 Cortex during Trace Eyelid Conditioning: Dissociating Responses
4503 That Reflect Cerebellar Output from Those That Do Not. *The*
4504 *Journal of Neuroscience*, 33(38), 15272 LP – 15284.
4505 <https://doi.org/10.1523/JNEUROSCI.1238-13.2013>
- 4506 Siegel, J. J., Taylor, W., Gray, R., Kalmbach, B., Zemelman, B. V.,
4507 Desai, N. S., Johnston, D., & Chitwood, R. A. (2015). Trace
4508 Eyeblink Conditioning in Mice Is Dependent upon the Dorsal
4509 Medial Prefrontal Cortex, Cerebellum, and Amygdala: Behavioral
4510 Characterization and Functional Circuitry. *ENeuro*, 2(4),
4511 ENEURO.0051-14.2015. <https://doi.org/10.1523/ENEURO.0051-14.2015>
- 4512 Silva, A. J., Zhou, Y., Rogerson, T., Shobe, J., & Balaji, J. (2009).
4513 Molecular and cellular approaches to memory allocation in neural
4514 circuits. *Science (New York, N.Y.)*, 326(5951), 391–395.
4515 <https://doi.org/10.1126/science.1174519>
- 4516 Skaggs, W., McNaughton, B., Gothard, K., & Markus, E. (1996). An
4517 Information-Theoretic Approach to Deciphering the Hippocampal
4518 Code. *Neural Inf. Process Syst.*, 5.
- 4519 Sofroniew, N. J., Flickinger, D., King, J., & Svoboda, K. (2016). A large
4520 field of view two-photon mesoscope with subcellular resolution for
4521 in vivo imaging. *eLife*, 5(JUN2016), 1–20.
4522 <https://doi.org/10.7554/eLife.14472>
- 4523 Solstad, T., Boccara, C. N., Kropff, E., Moser, M.-B., & Moser, E. I.
4524 (2008). Representation of Geometric Borders in the Entorhinal
4525 Cortex. *Science*, 322(5909), 1865–1868.
4526 <https://doi.org/10.1126/science.1166466>
- 4527 Souza, B. C., Pavão, R., Belchior, H., & Tort, A. B. L. (2018). On
4528 Information Metrics for Spatial Coding. *Neuroscience*, 375, 62–73.
4529 <https://doi.org/10.1016/j.neuroscience.2018.01.066>
- 4530 Stosiek, C., Garaschuk, O., Holthoff, K., & Konnerth, A. (2003). In vivo
4531 two-photon calcium imaging of neuronal networks. *Proceedings of*
4532 *the National Academy of Sciences of the United States of*
4533 *America*, 100(12), 7319–7324.
4534 <https://doi.org/10.1073/pnas.1232232100>
- 4535 Suh, J., Rivest, A. J., Nakashiba, T., Tominaga, T., & Tonegawa, S.
4536 (2011). Entorhinal cortex layer III input to the hippocampus is
4537 crucial for temporal association memory. *Science (New York,*
4538 *N.Y.)*, 334(6061), 1415–1420.
4539 <https://doi.org/10.1126/science.1210125>
- 4540 Takehara, K., Kawahara, S., Takatsuki, K., & Kirino, Y. (2002). Time-

- 4542 limited role of the hippocampus in the memory for trace eyeblink
4543 conditioning in mice. *Brain Research*, 951(2), 183–190.
4544 [https://doi.org/10.1016/s0006-8993\(02\)03159-1](https://doi.org/10.1016/s0006-8993(02)03159-1)
- 4545 Tao, S., Wang, Y., Peng, J., Zhao, Y., He, X., Yu, X., Liu, Q., Jin, S., &
4546 Xu, F. (2021). Whole-Brain Mapping the Direct Inputs of Dorsal
4547 and Ventral CA1 Projection Neurons. *Frontiers in Neural Circuits*,
4548 15. <https://doi.org/10.3389/fncir.2021.643230>
- 4549 Taube, J. S., Muller, R. U., & Ranck, J. B. J. (1990). Head-direction
4550 cells recorded from the postsubiculum in freely moving rats.
4551 I. Description and quantitative analysis. *The Journal of
4552 Neuroscience : The Official Journal of the Society
4553 for Neuroscience*, 10(2), 420–435.
4554 <https://doi.org/10.1523/JNEUROSCI.10-02-00420.1990>
- 4555 Thompson, R. F. (2004). In Search of Memory Traces. *Annual Review
4556 of Psychology*, 56(1), 1–23.
4557 <https://doi.org/10.1146/annurev.psych.56.091103.070239>
- 4558 Tishby, N., Pereira, F. C., & Bialek, W. (1999). The information
4559 bottleneck method. *Proc. of the 37-Th Annual Allerton Conference
4560 on Communication, Control and Computing*, 368–377.
4561 <https://arxiv.org/abs/physics/0004057>
- 4562 Tseng, W., Guan, R., Disterhoft, J. F., & Weiss, C. (2004). Trace
4563 eyeblink conditioning is hippocampally dependent in mice.
4564 *Hippocampus*, 14(1), 58–65. <https://doi.org/10.1002/hipo.10157>
- 4565 Uncapher, M. R., Hutchinson, J. B., & Wagner, A. D. (2011).
4566 Dissociable effects of top-down and bottom-up attention during
4567 episodic encoding. *The Journal of Neuroscience : The Official
4568 Journal of the Society for Neuroscience*, 31(35), 12613–12628.
4569 <https://doi.org/10.1523/JNEUROSCI.0152-11.2011>
- 4570 Valero, M., Cid, E., Averkin, R. G., Aguilar, J., Sanchez-Aguilera, A.,
4571 Viney, T. J., Gomez-Dominguez, D., Bellistri, E., & de la Prida, L.
4572 M. (2015). Determinants of different deep and superficial CA1
4573 pyramidal cell dynamics during sharp-wave ripples. *Nature
4574 Neuroscience*. <https://doi.org/10.1038/nn.4074>
- 4575 van der Maaten, L., Postma, E., & van den Herik, H. (2009).
4576 Dimensionality reduction: a comparative review. *Journal of
4577 Machine Learning Research*, 66–71.
- 4578 Velasco, M. G. M., & Levene, M. J. (2014). In vivo two-photon
4579 microscopy of the hippocampus using glass plugs. *Biomedical
4580 Optics Express*, 5(6), 1700–1708.
4581 <https://doi.org/10.1364/BOE.5.001700>
- 4582 Vinogradova, O. S. (2001). Hippocampus as comparator: Role of the
4583 two input and two output systems of the hippocampus in selection
4584 and registration of information. *Hippocampus*, 11(5), 578–598.

- 4585 https://doi.org/https://doi.org/10.1002/hipo.1073
4586 Voelcker, B., Pancholi, R., & Peron, S. (2022). Transformation of
4587 primary sensory cortical representations from layer 4 to layer 2.
4588 *Nature Communications*, 13(1), 5484.
4589 https://doi.org/10.1038/s41467-022-33249-1
4590 Wood, E. R., Dudchenko, P. A., Robitsek, R. J., & Eichenbaum, H.
4591 (2000). Hippocampal Neurons Encode Information about Different
4592 Types of Memory Episodes Occurring in the Same Location.
4593 *Neuron*, 27(3), 623–633.
4594 https://doi.org/https://doi.org/10.1016/S0896-6273(00)00071-4
4595 Yiu, A. P., Mercaldo, V., Yan, C., Richards, B., Rashid, A. J., Hsiang,
4596 H.-L. L., Pressey, J., Mahadevan, V., Tran, M. M., Kushner, S. A.,
4597 Woodin, M. A., Frankland, P. W., & Josselyn, S. A. (2014).
4598 Neurons are recruited to a memory trace based on relative
4599 neuronal excitability immediately before training. *Neuron*, 83(3),
4600 722–735. https://doi.org/10.1016/j.neuron.2014.07.017
4601 Zhang, S., & Manahan-Vaughan, D. (2015). Spatial olfactory learning
4602 contributes to place field formation in the hippocampus. *Cerebral
4603 Cortex (New York, N.Y. : 1991)*, 25(2), 423–432.
4604 https://doi.org/10.1093/cercor/bht239
4605 Zhou, S., Masmanidis, S. C., & Buonomano, D. V. (2020). Neural
4606 Sequences as an Optimal Dynamical Regime for the Readout of
4607 Time. *Neuron*, 108(4), 651-658.e5.
4608 https://doi.org/https://doi.org/10.1016/j.neuron.2020.08.020
4609 Zhou, Y., Won, J., Karlsson, M. G., Zhou, M., Rogerson, T., Balaji, J.,
4610 Neve, R., Poirazi, P., & Silva, A. J. (2009). CREB regulates
4611 excitability and the allocation of memory to subsets of neurons
4612 in the amygdala. *Nature Neuroscience*, 12(11), 1438–1443.
4613 https://doi.org/10.1038/nn.2405
4614 Ziv, Y., Burns, L. D., Cocker, E. D., Hamel, E. O., Ghosh, K. K., Kitch,
4615 L. J., El Gamal, A., & Schnitzer, M. J. (2013). Long-term dynamics
4616 of CA1 hippocampal place codes. *Nature Neuroscience*, 16(3),
4617 264–266. https://doi.org/10.1038/nn.3329
4618